Assessment of the impact of climate change on an instrumented embankment: an unsaturated soil mechanics approach

MENDES, JOAO

Durham University

Assessment of the impact of climate change on an instrumented embankment:

an unsaturated soil mechanics approach

João Paulo Duarte Pereira da Conceição Mendes

Ph.D. Thesis

2011

In memory of:

Manuel da Conceição Mendes
(1942-2010)

Ricardo Duarte Pereira de Almeida
(1977-2010)

Abstract

Climate change has the potential to affect any transportation network that comprises embankments and cuttings built with soil material in an unsaturated state that is exposed to the climate. The BIONICS project (BIOlogical and eNgineering Impacts of Climate change on Slopes) aims to investigate how climate change will affect the serviceability and safety of earth structures. Part of the BIONICS project was to build a full-scale highly instrumented embankment combined with an automated climate control system.

Studies on the fill material used in the construction of the BIONICS embankment were carried out to understand the hydro-mechanical behaviour of the material, which is a sandy clay of medium plasticity. This involved the determination of the soil water retention behaviour and the mechanical behaviour under unsaturated conditions. Soil water retention curves (SWRC) were determined by a series of tests performed on compacted samples comprising various techniques (filter paper, psychrometer, high capacity suction probe and pressure plate). Total and matric suction SWRC following primary drying paths from 25% of water content were determined. In addition, a series of tests with the filter paper on samples at lower water contents (15%, 20% and 22%) was also performed. The SWRC following drying paths showed behavior similar to scanning curves intercepting the primary curve around 3000 kPa (11% water content). However, SWRCs that followed wetting paths showed atypical behaviour by intercepting the primary drying curve.

For the investigation of the mechanical behaviour a series of constant water content triaxial tests were carried out in double cell triaxial cells on as-compacted samples, and also samples wetted and dried from as-compacted conditions of 15%, 20% and 22%. A test series of samples tested in a saturated state was also performed to provide a reference state for the unsaturated tests. The

unsaturated test series showed that the slope of the critical state line (CSL) in deviatoric stress space (*M*) was found to be similar for all water contents. The slope of the CSL in v-ln(p-u_w) space (λ) was found to be similar for all water contents, however the CSL shifted position due to variation in the intercept, Γ. Since specimens were at high degrees of saturation, calculations based on effective stress showed a reasonable interpretation of the data. However, a better agreement was achieved using the Bishop's average stress assumption.

A new field measurement system to continuously measure pore water pressure at different depths using high capacity suction probes has been developed. This system was installed at the BIONICS embankment in two different panels (well and poorly compacted). In the well compacted panel pore water pressure behaviour had the tendency to increase with depth, always recording values that were slightly negative at shallower depths and positive at greater depths, showing profiles roughly parallel to the hydrostatic line suggesting that the material was close to saturation. In the poorly compacted panel the behaviour was found to be more variable showing abrupt reactions from the probes to weather events.

The differences in behaviour between the well compacted and poorly compacted panels could be related to the laboratory investigations. The well compacted panel was more homogeneous and less permeable (10^{-11} m/s). The poorly compacted panel was more heterogenic, more permeable and hence, during monitoring, showed more dramatic changes in pore pressure compared to the well compacted panel.

Acknowledgements

I would like to acknowledge my supervisors Dr. David G. Toll, Dr. Charles E. Augarde and Dr. Domenico Gallipoli (Glasgow University) for their untiring support, friendship and sharing of knowledge. I am particularly thankful for all the opportunities given such as the participation in the various MUSE encounters that allowed the broadening of my knowledge of unsaturated soils. Dr. Gabriela M. Medero (Heriot-Watt University) provided guidance during the first year of the PhD.

The laboratory work in Durham and installation of the equipment at BIONICS embankment was conducted with the assistance of Mr. Charles McEleavy and Mr. Stephen Richardson. But also I would like to refer to the sharing of knowledge on soils testing and discussion of test results during the tiny coffee breaks.

This work could not have been possible without the help given by the mechanical and electronic workshops and computer support available at School of Engineering and Computing Sciences of Durham University. Thanks to Mr Colin Wintrip and Mr. Kevan Longley, from the mechanical workshop, for the assistance given with design and construction of the heavily-insulated box for the transistor psychrometer, the borehole probe locators and for that screw that was always missing from the equipment. To Mr. Ian Hutchinson and Mr. Colin Dart for their assistance with electronic problems with the various equipments and the assembly of cables necessary to run the triaxial frames. To Mr. Michael Wilson, from computer support, for responding promptly whenever computer problems occurred. To Mr. Fred Evans from Wykeham Farrance Division (Controls Testing) for its support with the field high capacity suction probes and double cell triaxial cells.

This thesis strongly benefitted from discussion and work done by other colleagues in Durham: discussions on the high capacity suction probes, soil water retention behaviour and about the double cell triaxial cells with Dr. Sérgio Lourenço (PhD 2008); Dr. Zulfhami Ali Rahman (PhD 2008) introduced triaxial testing on unsaturated soils and calibration of the double cell triaxial cells; Dr. Wojciech Solowski (PhD 2008), Ms Sarah Hidayat (MSc 2006), Mr. Vincent Vercraeije and Mr. Phillip Wallbridge (MEng 2007), Mr Juan Fernandez (ERASMUS project) with the pressure plate assembly, Ms Teiko Noguchi (MEng 2009) with the soil suction measurements, Dr. Paul Jaquin (PhD 2008) and Dr. Cathy Dowding (PhD 2008).

During these years in Durham this work could only be finished with the close friendship given by Dr. João Pires (PhD 2010), Dr. Vasco Fernandes (PhD 2009), Dr. Farhan Chak (PhD 2007), Dr. Francisco Aguiar (PhD 2009) and more recently with the friendship of Ms. Paula Lopes (ongoing PhD) and Mr Rui Campos (ongoing PhD). To my sister Ms Sara Mendes (ongoing PhD) and my parents. And more importantly the emotional support given by Ms. Chrysoula Toufexi.

Finally I would like to acknowledge the financial support from the Engineering and Physical Sciences Research Council (EPSRC) of the United Kingdom.

Table of contents

List of figures

List of tables

Statement of Copyright

1 Introduction

1.1 **Climate change**

In recent years much research has been directed towards climate change and its impacts. The recognition of global warming has led to a series of studies, in various disciplines, to understand its direct and indirect implications for the World in which we live. Social, political and economical problems related to climate change have been the focus of the majority of governments, recognizing climate change as a key factor of global change.

One of the factors that can shape climate change is the variations on greenhouse gas emissions. Evidence of global warming derived from the increase in production of greenhouse gas since the Industrial Era has been presented in the IPCC 4th Assessment Report (IPCC, 2007), where it states that "Continued greenhouse gas emissions at or above current rates would cause further warming and induce many changes in the global climate system during the 21st century that would *very likely* be larger than those observed during the 20th century".

Different scenarios related with greenhouse gas emissions have been presented by Hulme et al (2001) of possible changes in weather variables for the UK. Hulme at al used a scale from low emissions to high emissions. A "low" scenario would involve reducing the amount of emissions being produced at the present time whereas "high" would imply a continued increase in gas emissions. Shown in Figure 1.1 are visual presentations of predictions of climate change suggested by Hulme et al for two weather variables: temperature and precipitation.

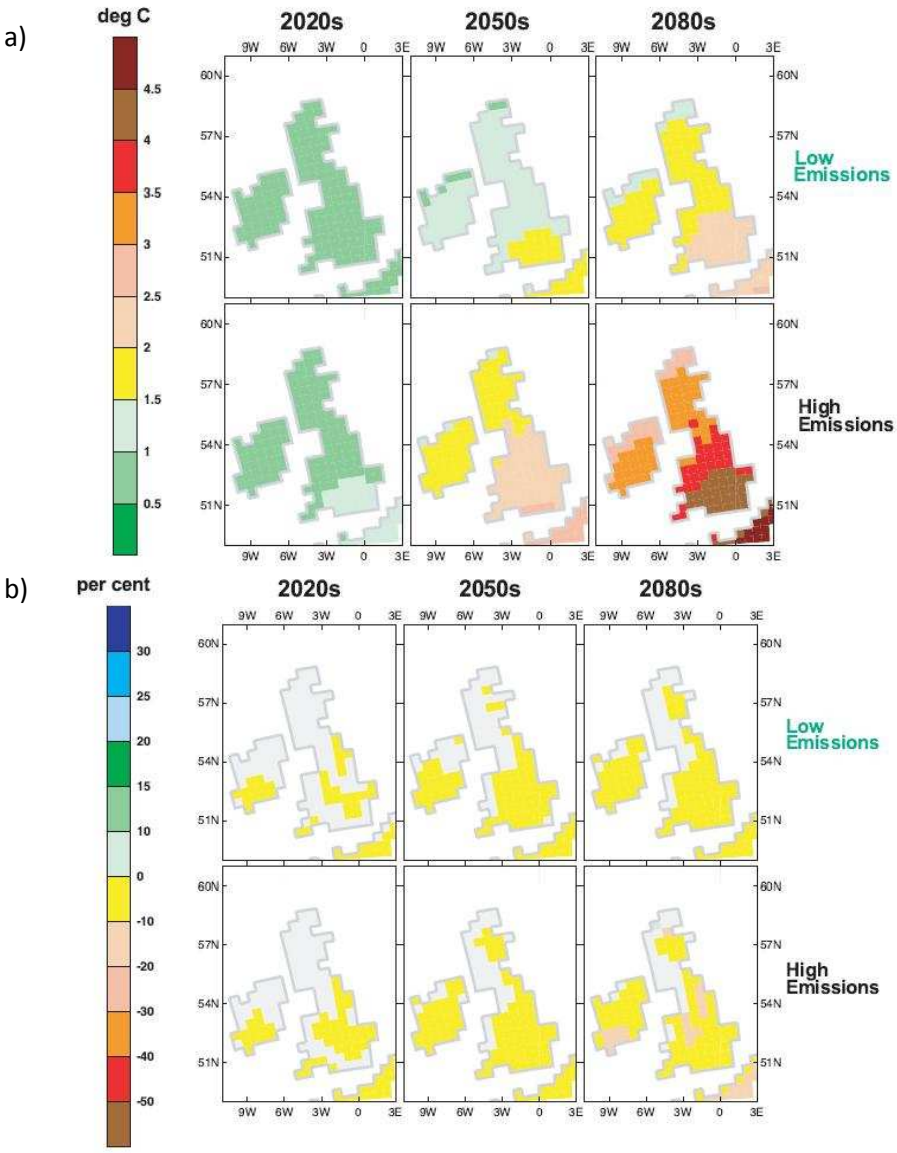

Figure 1.1 – Climate change predictions for annual values of **a)** temperature and **b)** precipitation for the UK (After Hulme et al, 2001).

It is important to understand in climate change that not only do predictions suggest that we will experience temperature changes but that we are also going to experience changes in the weather patterns. The seasonal behaviour will vary with climate change. For the UK it is expected that we will experience stronger winters with intense rain showers and dry summers with longer drying periods. The role of climate change can be already observed in the UK with the recent events

of flooding (Carlisle in 2005 or Gloucestershire, Worcestershire and Yorkshire in 2007) where extreme rain events affected the population.

In Civil Engineering there is the need to understand the impact of climate changes on the infrastructure for the built environment such as embankments and cuttings. These comprises a large part of any transportation network. To avoid social and economical losses, there is the need to ensure that the infrastructure can cope with future climate events.

In order to study the implications of climate change on slopes the BIONICS project was instigated. BIONICS is an acronym for BIOlogical and eNgineering Impacts of Climate change on Slopes, funded by the Engineering and Physical Sciences Research Council. This aims to investigate the serviceability and safety of earth structures (embankments, cuttings). It involves various institutions; the project partners are the universities of Newcastle upon Tyne, Durham, Dundee, Nottingham Trent, Loughborough and Bristol, together with industrial stakeholders: British Waterways, Cementation Foundations, Skanska Ltd, CIRIA, Highways Agency, Geotechnical Observations Limited, Metronet Rail SSL Ltd, Mott McDonald, Network Rail, Rail Research UK, Rail Safety and Standards Board and the Scottish Crop Research Institute.

The part of the study involving Durham University under the BIONICS project had the following objectives:

- To perform unsaturated laboratory testing for the characterization of the hydro mechanical behaviour of the fill material;

- To develop a multi measurement system for continuous monitoring of pore water pressure to install in the BIONICS embankment.

1.2 Thesis structure

The thesis is divided into 10 chapters. Chapter 2 introduces the background to the work contained in subsequent chapters. Chapter 2 starts by introducing unsaturated soils and their general behaviour, followed by the experimental techniques available to study the water retention behaviour of unsaturated soils, for both laboratory and field environments. Some field investigations of unsaturated soils carried out throughout the world are also presented. The chapter continues with the most commonly used techniques for the mechanical testing of unsaturated soils, concluding with the available constitutive models for unsaturated soils.

Chapter 3 presents the BIONICS embankment and the characteristics of the fill material followed by the instrumentation installed in the embankment and a climate control system. Chapter 4 presents the sample preparation method procedures used for the BIONICS fill material to prepare samples for laboratory investigations. Assessment of the sample preparation methods at different conditions (as-compacted, wetted and dried conditions) is also presented in Chapter 4.

The characterisation of the BIONICS fill material is divided into two chapters Chapter 5 and 6. Chapter 5 describes the techniques used to determine the soil water retention curve (SWRC) of the BIONICS fill material in more detail. Total and matric suction SWRC are presented and an assessment of the quality of the measurement is made by comparing measurements obtained from

different techniques. The SWRC for the BIONICS fill material is presented and a description of the behaviour of the material is given. A study at lower water contents is also presented.

Chapter 6 describes the mechanical behaviour of the BIONICS fill material in saturated and unsaturated conditions. The mechanical testing was carried out in a new double cell triaxial system involved constant water content triaxial tests at different confining pressures on samples at different initial conditions, prepared from as-compacted conditions (following the sample preparation method procedures described in Chapter 4) and subject to drying and wetting before testing. The results obtained were used to examine the mechanical behaviour of the BIONICS fill material within the critical state framework and comparisons are made with the results obtained from saturated tests.

Chapter 7 and 8 are dedicated to the field study at the BIONICS embankment itself. Chapter 7 presents in detail the continuous monitoring system for pore water pressure measurement at different depths developed, including the installation and *modus operandi* of the system at the BIONICS site (with installations in a well compacted panel and a second in a poorly compacted panel). Chapter 8 presents the field monitoring over 2 two years of continuous measurements in both panels. The influence of the weather behaviour during this time is compared with the pore water pressure measurements. A comparison between the measurements obtained from the different panels is discussed. Conditions of the fill material from samples obtained during installation were also analysed in the laboratory and compared with the previous measurements.

Chapter 9 correlates the data gathered in the previous chapters relating field and laboratory measurements in order to identify the hydro-mechanical behaviour. Chapter 10 summarizes the conclusions drawn from various parts of the thesis and recommendations for future work are given.

2 Literature review

2.1 Introduction

The literature review in this thesis forms the background of information to all subsequent work. The topics include: understanding the behaviour of unsaturated soils, the different methodologies that can be implemented to study unsaturated soils, mechanical and hydraulic properties, and some of the available frameworks found in literature for presenting and explaining such information.

2.2 Unsaturated soils

Unsaturated soils are wide spread and are present in most engineered earth structures: earth dams, flood defences, railroad and road embankments, etc. While in saturated soils, the mechanical behaviour can be described by Terzaghi's law for effective stress, in unsaturated soils, where the voids are filled with both air and water, the mechanical behaviour is much more complicated to understand. In unsaturated soils only recently has there been some agreement on the most acceptable stress state variables to use in practice (Fredlund and Rahardjo 1993). Fredlund and Morgenstern (1977) concluded that net normal stress and soil matric suction are the stress state variables appropriate for unsaturated soils.

2.3 Phases of unsaturated soils

In saturated soils the soil is composed of soil particles with voids filled with water and thus only two phases: solid and water need to be considered. In unsaturated soils the voids, are filled with water and air, therefore three recognisable phases exist: solid, water and air. A fourth phase, the air-water interface, can also be considered due to its unique properties

(Fredlund and Morgenstern 1977). The most distinctive property of the air-water interface, also known as the contractile skin, is its ability to exert a tensile pull, or surface tension. Within a soil the contractile skin can act like a thin rubber membrane pulling soil particles together, leading to volumetric shrinkage under no changes of total stress while the soil specimen undergoes drying (Fredlund and Rahardjo, 1993).

2.4 Soil suction

Soil suction can be defined as the attraction that the soil exerts on free water if the two are placed in contact. This attraction can be stronger if the water inside the voids starts to evaporate. Soil suction, or total suction, has two components: matric suction and osmotic suction.

Total suction can be expressed by the following equation:

$$\psi = (u_a - u_w) + \pi \tag{2.1}$$

where:

ψ – total suction;

$(u_a - u_w)$ – matric suction, i.e. difference between pore air pressure (u_a) and pore water pressure (u_w):

u_a – pore-air pressure;

u_w – pore-water pressure;

π – osmotic suction, i.e. equivalent suction associated with the osmotic potential of the pore water.

The matric suction is generated by the capillarity phenomenon associated with the existence of surface tension between water and air phases within the soil pores. Matric suction is thus dependent on the soil structure as it is affected by the pore size distribution of the soil. A finer grain size soil is capable of supporting a higher value of matric suction than a coarse grain size material. The water content of the soil also plays its role where the matric suction increases with the decrease of the water content within the soil.

The osmotic suction is associated with salt concentration in the pore water. Changes in osmotic suction are generally less significant than changes in matric suction for most engineering problems although volume change behaviour (shrinkage and swelling) can be strongly influenced by osmotic suction.

The total suction of the soil water can also be related to the partial saturated vapour pressure in equilibrium with the soil water (Richards, 1965), by the following equation:

$$\psi = - \frac{RT}{\nu_{wo}\omega_v} \ln \left(\frac{\bar{u}_v}{\bar{u}_{v0}} \right) \qquad (2.2)$$

ψ – total suction (kPa);

R – universal gas constant (8.31432 $m^3.Pa.K^{-1}.mol^{-1}$);

T – absolute temperature (273.16 + t) (K):

t – temperature (^oC)

ν_{wo} – specific volume of water ($1/\rho_w$) ($m^3.kg^{-1}$):

ρ_w – density of water ($kg.m^{-3}$)

ω_v – molecular mass of water vapour ($kg.mol^{-1}$);

$\bar{u}_v / \bar{u}_{v0}$ – RH - relative humidity:

$\bar{u}_v$ – partial pressure of water vapour (kPa);

$\bar{u}_{v0}$ – saturation pressure of water vapour over a flat surface of pure water at same temperature (kPa).

2.5 Soil water retention curve

The ability of a soil to attract and retain water is an important property for each soil. A soil water retention curve (SWRC) is defined from the relationship between water content and suction. The water content can be expressed in various terms as gravimetric water content, w, volumetric water content, θ or even degree of saturation, Sr. These are intimately related as presented in Equation 2.3.

$$\theta = \frac{w.Gs}{1+e} = \frac{Sr.e}{1+e} \tag{2.3}$$

Where:

θ – volumetric water content

w – gravimetric water content

Sr – degree of saturation

Gs – specific gravity of the soil

e – void ratio

The SWRC is dependent on various factors such as soil type, soil structure and mineralogy. The typical behaviour of a SWRC following a drying path is presented in Figure 2.1. Initially the suction increases while still maintaining a degree of saturation close to 100% (the boundary effect zone). The increase of suction does not change the saturation value

significantly since the magnitude of the suction value is not sufficient to drain the pores (Blight, 1967). When the value of suction is sufficient to start draining the pores the air entry value (AEV) of the soil is reached. After the AEV is reached bulk water starts to be pulled from the largest pores and air starts to fill the pores. After this point is reached the soil is considered as being desaturated and the magnitude of suction necessary to pull water out of the pores may not need to increase significantly until a residual degree of saturation is reached (transition zone). By this point the bulk water has been drained and it is necessary to increase significantly the value of suction in order to change the degree of saturation (residual zone).

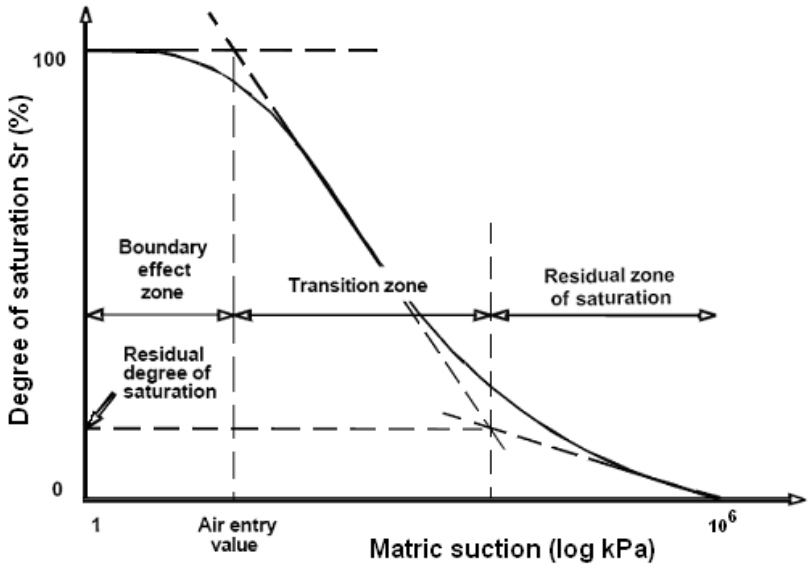

Figure 2.1 – Schematic of a Soil Water Retention Curve (SWRC), Vanapalli et al. (1999).

The shape of the SWRC is also dependent on the process by which it is obtained. If the soil is subject to drying or wetting paths, the obtained curves show different curves. This hysteretic behaviour is normally attributed to hydraulic hysteresis (Croney, 1952). The hydraulic hysteresis is often explained by the effects of pore entrapment (ink-bottle pores).

Clayey soils present an additional problem related with the shrink and swell behaviour that is characteristic of these materials. The observed hysteresis is even more complex due to rearrangement of the pores including pore size changes.

A soil may not follow a continuous path from a totally dried or totally wetted state. It is very common to find soils in an intermediate stage in which the direction of water content change is reversed. SWRC obtained at intermediate stages are known as scanning curves. In Figure 2.2 two kinds of scanning curves are presented as simple examples: ascending scanning curve where the initial condition was reached while following a drying path and was subsequently wetted and a descending scanning curve where the intermediate stage starts on the wetting path of the SWRC and the material gradually dries until the drying path of the SWRC is reached. In reality any point between the wetting and drying paths can be obtained and by following wetting or drying the curve will eventually converge with one of the primary paths of the SWRC.

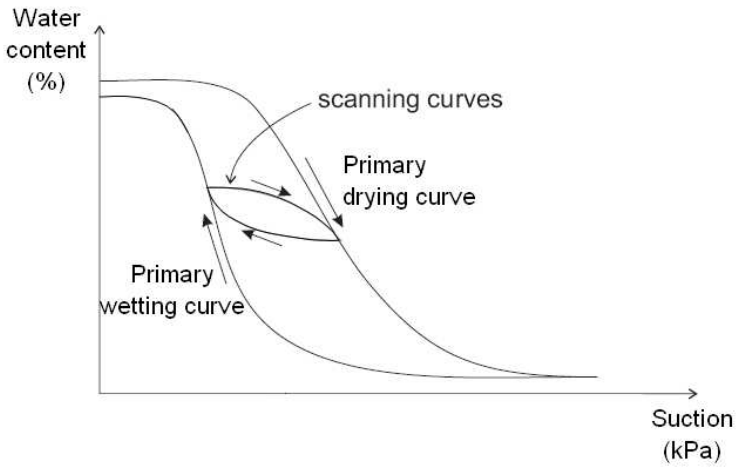

Figure 2.2 - Hysteretic characteristics of SWRC (after Lourenço 2008)

The importance of the SWRC can be seen from studies where it can be used to estimate various properties such as shear strength, permeability and thermal coefficient (Barbour, 1998).

2.6 Soil suction determination

Soil suction can be determined using various techniques; an overview of the various methods can be found in: Fredlund and Rahardjo (1993), Lee and Wray (1995), Ridley and Wray (1996), Rahardjo and Leong (2006), Bulut and Leong (2008), Delage et al. (2008) among others. A wide range of systems and methods to measure suction are available in the market. However, only the methodologies used to produce this research are presented, namely: filter paper, psychrometer transistor and high capacity tensiometer (also known as suction probe) and the pressure plate technique. The measuring ranges of the most common techniques to determine the SWRC is presented in Table 2.1.

Table 2.1 – Suction component, suction range and equilibration time for presented methodologies to determine SWRCs (adapted from Bulut and Leong, 2005).

Suction Component	Methodology	Suction Range (kPa)	Equilibration Time
Total Suction	Thermocouple Psychrometer	300 – 7000	1 hour
	Transistor Psychrometer	100 – 18000	1 hour
	Non-contact Filter Paper	400 – 30000	5 – 14 days
Matric Suction	Contact Filter Paper	30 – 30000	5 – 14 days
	Pressure Plate	0 – 1500	Days
	Tensiometer	0 – 1600	Hours

2.6.1 Filter paper technique

Marinho (1994) notes that the concept of the filter paper technique dates back to 1916. Shull (1916) observed that by allowing dried seeds to absorb vapour at different

concentrations of sulphuric acid at known vapour pressures, after an equalisation period, it was possible to relate the weight of the seeds with the vapour pressure. A calibration relating the water content of the seeds with vapour pressure permitted the determination of soil suction.

The concept of the seeds was replicated by Gardner (1937) who was the first to use dried filter papers. The introduction of an industrial process to produce the absorption method was the great innovation by Gardner which gave the technique more credibility (Marinho, 1994). If the process of creating the filter paper was the same then filter papers would have unique properties.

This technique is widely used nowadays in different laboratories. The major advantages of this technique are the ability to measure total and matric suction, low cost and the fact that it is one of the simpler techniques available. The wide range of measurement as presented in Table 2.1, is by far the greatest of the advantages in the filter paper technique.

In the market there are two filter papers that are commonly used by different researchers: the Whatman 42 filter paper (e.g. Fawcett and Collis-George 1967; Hamlin 1981; Chandler and Gutierrez 1986; Chandler et al. 1991; Harrison and Blight 1998) and the Scheicher & Schuell No. 589 (e.g. McQueen and Miller 1968; Al-Khafaf and Hanks 1974; McKeen 1980; Harrison and Blight 1998).

The principal of the filter paper technique is to measure suction indirectly by relating the water absorbed (by matric or by water vapour transfer) by the filter paper with suction by means of a calibration curve. Therefore the total suction is measured if the transfer is by water vapour and matric suction is measured if there is matric flow.

One of the procedures for the measurement of suction using filter paper was presented by Bulut et al. (2001). In this procedure the matric suction is determined by the middle filter paper (contact filter paper) of a sandwich of 3 filter papers which is placed in direct contact in the middle of the sample. For the total suction a single filter paper is placed at the top of the sample in a non-contact position, this is to allow the filter paper to absorb the water vapour that evaporates from the sample. This system is placed in a container to avoid influence from external humidity. After a period of equalisation, for both measurements, the water contents of the filter papers are determined and the value of suction is taken from a calibration curve. The equalisation time is dependent on the calibration curve. Bulut et al. (2001) mention the fact that the container should be placed in a temperature controlled environment at 25^{o}C for the duration of the equalisation.

In the literature different calibration curves can be found; an overview of most of the calibration curves in existence was presented by Leong et al. (2002), where the authors compare different calibration curves with known data from the literature. An agreement of which calibration curve(s) to use has not been reached, some authors such as Leong et al. (2002) claiming that the responses of filter papers exposed to total suction and matric suction are different, while others claim that if enough time is given for the equilibrium period both total and matric calibration curves converge. In either case it is highly important to respect the guidance (such as equilibrium time) of each calibration curve when performing filter paper tests.

There are some noticeable disadvantages in this technique since it is highly dependent on the operator input and the longer testing period (up to 14 days depending on the calibration curve). Adding the fact that it is an indirect measurement, where it is dependent on a calibration curve, makes it one of the least reliable techniques available.

2.6.2 Transistor psychrometer

The transistor psychrometer measures total suction indirectly from the relative humidity (RH) generated by the soil sample inside a confined space.

In the case of the SMI Psychrometer (Woodburn and Lucas, 1995) there are 12 probes and each probe has 2 transistors, one wet and one dry, see Figure 2.3. When a sample is placed inside the probe the RH of the air above the sample starts to change until it reaches an equilibrium with the soil. As water evaporates from the water drop on the wet transistor, this creates a variation in the output voltage between the 2 transistors, which relates to the RH.

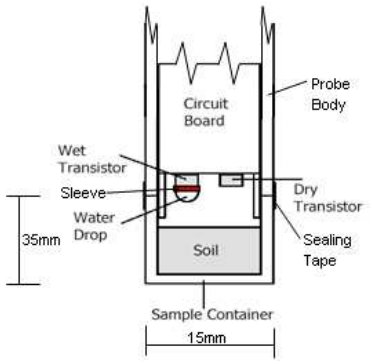

Figure 2.3 - Transistor psychrometer probe (after Bulut and Leong 2005).

The RH relates to suction by means of a calibration. The calibration is performed on each probe by using different salt solutions at known total suction values. Usually NaCl is the most common salt; however, other salts can be used.

As a system for measure total suction it is an improvement on the filter paper technique for total suction, since the operator has less direct effect on the measurement process and the measurement is obtained relatively fast (1 hour). However, the technique is more laborious, more costly and most importantly, it is extremely sensitive to temperature

changes. It presents the same disadvantage as the filter paper since it is still an indirect measurement of suction.

2.6.3 High capacity suction probe

The terminology of high capacity suction probe can differ; authors refer to this equipment variously as a suction probe or tensiometer. The terminology of "high capacity" marks it out as different from other tensiometers available, which are limited to measuring suctions below the normal cavitation limit of 100 kPa.

The first high capacity suction probe was designed by Ridley and Burland (1993) at Imperial College London. This high capacity suction probe comprised a 1.5 MPa ceramic disc as a filter between the measuring device and the soil sample, followed by small water reservoir (3 mm^3) and an Entran Ltd EPX series electronic pressure transducer (3.5 MPa capacity) as the measuring device. When fully saturated, ceramic high air entry disc and water reservoir, the pressure transducer measured zero suction. When in contact with a soil sample with a certain value of suction, the water in the high capacity suction probe starts to be drawn towards the soil until equilibrium is reached. This induces a deflection on the pressure transducer due to the matric suction of the soil.

Since then, various high capacity suction probes have been reported, where the working principle is generally the same, with variations in the ceramic disc, the water reservoir, the pressure transducer or size. A general overview from Delage et al. (2008) presented most of the high capacity suction probes in existence shown in Table 2.2.

The high capacity suction probe used in this project was the Durham University – Wykeham Farrance (DU-WF) high capacity suction probe. This probe differs from the Ridley and Burland (1993) probe in the fabrication process and some internal changes: the water reservoir is 5 mm^3 in volume and it uses a ceramic pressure transducer that is soldered to a 1.5 MPa high AEV ceramic disc of 10mm thickness, see Figure 2.4, resulting in the dimensions of the high capacity suction probe being 35mm by Ø14mm.

Table 2.2 - Effect of the pre-pressurisation pressure on the maximum sustained tension (after Delage et al, 2008).

Authors	Ceramic AEV (MPa)	Max positive pressure (MPa)	Max tension water (MPa)
Ridley and Burland (1993)	1.5	6	1.37
	0.1	4	0.164
Ridley and Burland (1995)	0.5	4	0.74
	1.5	4	1.8
Guan and Fredlund (1997)	1.5	12	1.25
Meilani et al. (2002)	0.5	0.8	0.495
Tarantino and Mongiovi (2002)	1.5	4	2.06
Take and Bolton (2003)	0.3	1	0.53
Chiu et al. (2005)	0.5	0.7	0.47
Lourenco et al. (2006)	1.5	1	1.23
He et al. (2006)	0.5	2	0.55
Mahler and Diene (2007)	0.5	0.6	0.8
	1.5	0.6	1.4

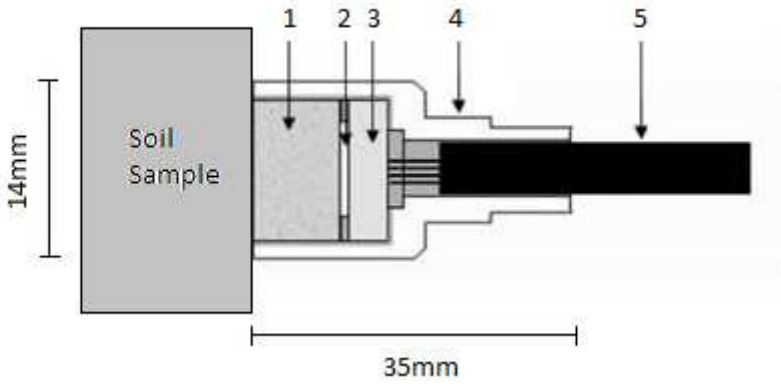

1 – Saturated 1.5 MPa porous ceramic disc
2 – Water reservoir
3 – Pressure transducer
4 – Stainless steel casing
5 – Four core screened cable

Figure 2.4 – Schematic of the DU-WF high capacity suction probe (after Lourenço, 2008).

Increasing the measuring range and the stability of the measurement has been the greatest concern in the development of these devices, however, in all devices the saturation process of these probes is the key factor towards a reliable measurement.

2.6.3.1 Saturation

The saturation process of the DU-WF high capacity suction as reported by Lourenço (2008) from initial dry conditions was by water infiltration under vacuum and subsequently pressurization of 1.5 MPa inside a saturation manifold developed by Donohgue (2006). This process of saturation is common to most high capacity suction probes.

From non-dry conditions, if the probe has desaturated by cavitation, a 24 hours period should be sufficient for the re-saturation process.

2.6.3.2 Calibration

In these kind of probes the calibration of the pressure transducers is normally carried in the positive range and extrapolated to the negative range; however, it is suction that is the desired measured value i.e. negative pore water pressure. Tarantino and Mongiovi (2003) reported that extrapolating the positive to the negative range generated an error of the measurement of 1 to 1.5%, which was assumed to be satisfactory.

The extrapolation from positive to the negative range for the DU-WF high capacity suction probe was studied by Lourenço (2008). Calibrations by extrapolation where made against a normal pressure transducer. In his work he showed that accuracy was dependent on the method in which the probe was calibrated. When calibrations were preformed inside the

saturation manifold the external forces from the holding system for the probe influenced the calibration. He concluded that for a more accurate calibration by extrapolation the calibration should be performed under the same conditions as the expected conditions of use.

Lourenço et al. (2008) validated the extrapolated calibrations against known values of suction imposed by soil samples by axis translation technique and isotropic unloading. Good agreements were observed for both techniques; however better agreement was obtained with the isotropic unloading. He also obtained a good agreement for the calibrations when using a vacuum pump, where negative pore water pressures were applied down to -100 kPa.

2.6.3.3 Advantages and disadvantages

The advantages on using high capacity suction probes can be summarised as: direct measurement of matric suction, small size of equipment and short time of measurement (less than an hour). With a good system to saturate and good calibrations the measurement obtained from the probes are reliable and accurate. Also important, the device has the ability to measure in both the negative and positive range.

The main disadvantages of these probes are cavitation and zero suction value. Drifting of the zero suction value are normally observed in these probes when used for a long period in the negative pressure range. With the DU-WF high capacity suction probe the observed variations have been small, ranging up to 5 kPa; when working in the small suction range this can induce some errors.

2.6.4 Pressure Plate

The pressure plate differs from the remaining techniques since it does not measure but imposes suction to the soil sample, but is commonly used to determine SWRCs. Suction is imposed to the soil samples by controlling both pore air pressure and pore water pressure, the difference between the pressures defines the matric suction.

The pressure plate apparatus consists of a pressure chamber, inside of which is a saturated high air entry value (HAEV) porous ceramic disc (Figure 2.5). The soil sample is placed on top of the HAEV during testing.

The maximum differential pressure attainable by this kind of apparatus is dependent on the AEV of the HAEV porous ceramic disc inside the chamber. The AEV value is the maximum value of air pressure that can be applied to the camber before air entry (or "bubbling") occurs (when air starts to flow through the HAEV porous ceramic disc). The most common ceramic discs have AEV values of 500 kPa or 1500 kPa.

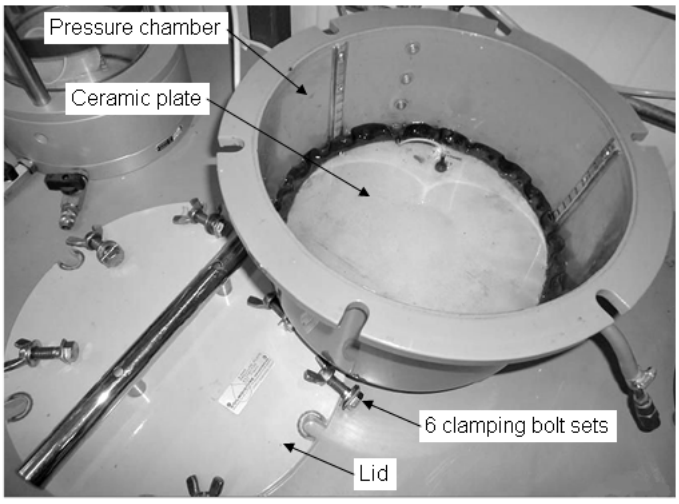

Figure 2.5 – 5bar pressure plate apparatus (Lid open).

The common methodology applied in this technique is, once the chamber is sealed, he pore water pressure is maintained at atmospheric values and the pore air pressure is increased

to imposing values above atmospheric pressure. When the desired values of both pore pressures (air and water) are achieved the soil sample is left to attain equilibrium. Water is expelled from the soil sample pores, passes through the HAEV porous disc and flows to a burette. The burette in this case is used to observe the amount of water that flows out of the sample which can be related back to the water content at this particular value of suction. Equilibrium is only achieved water flow stops. This process is repeated, imposing different values of suction (increasing the pore air pressure), to generate the SWRC. After the final suction stage the final water content can be determined and can be used to verify the indirect measurements of water content observed with the burette.

At Durham University a different methodology was developed for this technique by Vaquero (2007) from an existing pressure plate apparatus manufactured by Soil Moisture Corp. of Santa Barbara, California. The normal single HAEV porous disc of 1500 kPa (AEV value) was replaced by 4 independent porous discs (100mm in diameter) of the same AEV value, enabling multi sample testing. The second modification related to the burette, where the measurement was performed by independent volume gauges (one volume gauge for each porous disc). A transducer is attached to the volume gauge and is connected to the automatic data acquisition system, which is then connected to a computer for scanning and recording of measurements (Figure 2.6).

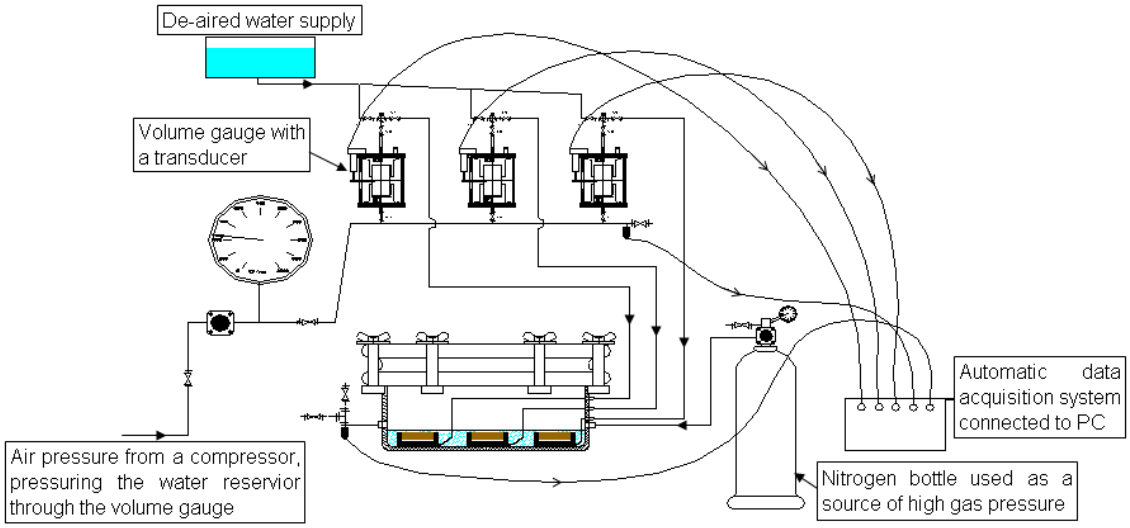

Figure 2.6 - Setup of the pressure plate apparatus (After Vaquero 2007).

2.7 Field testing

All the techniques to measure soil suction presented in this literature review, apart from the pressure plate, have been suggested for use in field conditions. However, the high capacity suction probe or common tensiometers, which, measure suction continuously, directly and in a short time makes them most suitable and preferred for field measurement. The usage of these devices has been reported by a number of researchers. Field observations using high capacity suction probes (Ridley et al., 2003) have used “spot” measurements where the suction probe has been placed in contact with the soil to take a suction reading at a particular time; the suction probe was not left in place to take continuous readings with time. Cui et al (2008) have used high capacity suction probes for the continuous measurement of suction at an experimental embankment. Common tensiometers (capable of measuring to 100 kPa suction) have also been reported in the literature for continuous monitoring; some of these reports are mention in the subsequent section.

2.8 Rainfall induced landslides

Many slopes exist in soil where suctions are present. An increase in pore water pressure (loss of suction) within the soil leads to a decrease of strength and hence reduction in stability of the slope and ultimately failure.

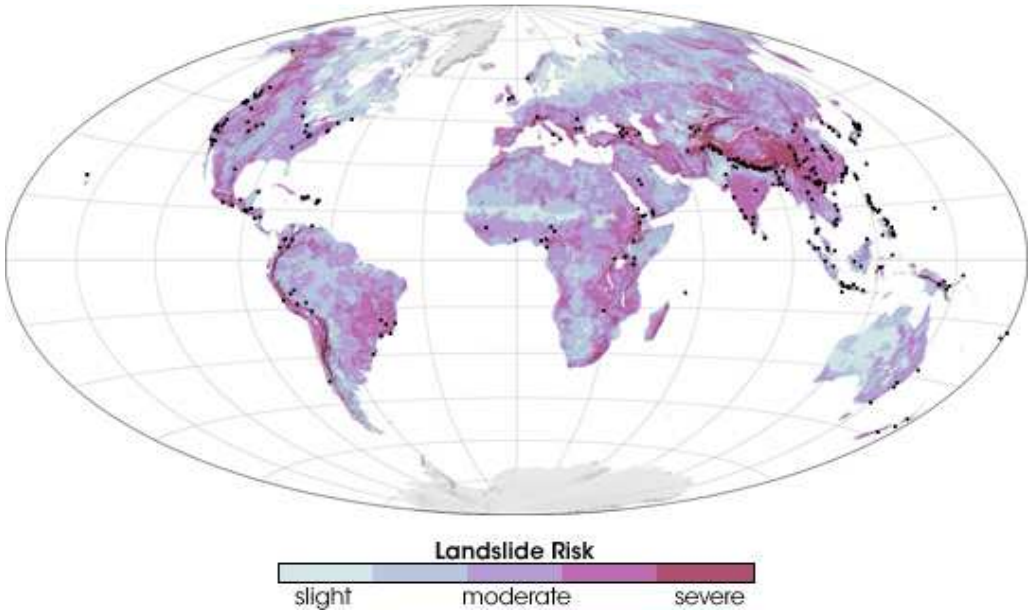

Figure 2.7 – Landslide risk world map overlaid by major landslides during 2003-2006 as the black dots (NASA map adapted from Hong et al., 2006, by Simmon, 2007).

Hong et al. (2006) using data gathered by the Tropical Rainfall Measuring Mission (TRMM) satellite coupled with general information on topographic data, land cover classifications and soil types generated a rainfall induced landslide susceptibility world map where, the risk was quantified from slight to severe. The generated landslide risk map, shown in Figure 2.7, shows that landslides are prone to occur in most regions, with more impact in tropical regions such as the South East Asia.

In the Hong Kong region various studies have been reported over the years on the monitoring of soil suction in various slopes. In this area the normal depth of the water table is greater than 10 metres; this is an important factor since at these depths the influence of the

water table on suction at shallower depths can be almost neglected and suctions become controlled entirely by environmental conditions (rainfall/evaportation) at the surface. The studies performed by Sweeney (1982), Chipp et al (1982), The Geotechnical Control Office (1982) and Ching et al (1984) shown that in dry seasons suctions greater than 80 kPa were recorded at shallow depths (in the cases where suction was 80 kPa the real value was possibly higher due to the use of conventional tensiometers with max range below 100 kPa) while fading to lower values in wet seasons. The major difference between the chosen sites reported by the authors was the existence or lack of cover. When coverage of the slope was present suction values tended to reduce less culminating in the observation of Au (1998) in which the difference in suction between exposed and covered slopes can explain why many covered steep slopes have remained stable.

In Singapore similar studies have been conducted at shallow depths by Pitts and Cy (1987), Chatterjea (1989), Chatterjea (1994), Lim (1995), Lim et al (1996), Gasmo (1997), etc. The results obtained were similar in behaviour to the results obtained in Hong Kong. The measurements were obtained using conventional tensiometers with a range of 100 kPa. The measurements obtained show values as great as 80 kPa during the drier periods and a decrease in suction during wetter periods (intensive rainfall) even reaching small positive values of pore water pressure. Some studies were performed considering the coverage of the slope: Pitts and Cy (1987), Lim (1995) and Lim et al. (1996), Gasmo (1997). A general consensus was reached: vegetation accelerates the recovery of suction when compared to a bare surface while under a canvas covered surface small suctions can be maintained even during wetter periods.

For all studies reported, in both Hong Kong and Singapore, the changes in suction due to rainfall infiltration has been observed as a gradual change from top to bottom, changes are

gradual and more noticeable at shallower depths. In Singapore, in particularly, the type of soil in the study showed that small amounts of rainfall were sufficient to reduce the suction to a value of zero, and those changes were almost immediate.

Rainfall as failure trigger for landslides occurrence in Singapore, was analysed by Toll (2001), see Figure 2.8. Toll (2001) compared the rainfall data on the day of the landslide plotted against the antecedent rainfall over a five day period. From this it was observed that failure could occur in 1 day event but also due to an accumulation of rainfall, suggesting that the total rainfall over a period dictated the minimum conditions for failure, in this case 100 mm.

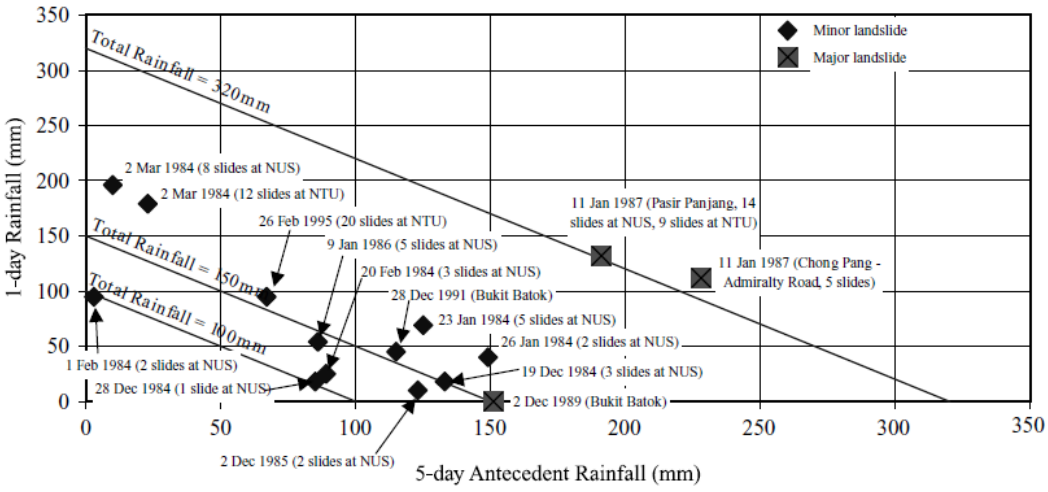

Figure 2.8 – Rainfall events leading to landslides in Singapore (after Toll, 2001).

In Europe some studies have also been carried out. In problematic regions, such as the area surrounding the Vesuvius volcano in Naples, rainfall induced landslides of pyroclastic material is very frequent. Evangelista et al. (2008) monitored a site in the Naples region using conventional tensiometers at different depths. In their observations, in the cover layer, suction was affected by singular rainfall events usually maintaining higher suctions of 60-70 kPa (topping the range of the tensiometers in use) in summer (dry season) and dissipating during

the wetter periods (autumn and winter) (see tensiometers TL1 and TL2 in Figure 2.9). An interesting remark from the authors was that below the cover layer the suction variations followed the usual seasonal trend but were unaffected by singular rainfall events (see tensiometers TL3 and TL4 in Figure 2.9). Their continuous monitoring is still in use to understand the mechanisms of landslides in the region, where some assumptions point out for the occurrence of landslides in the layers below the cover (Papa et al., 2008).

Apart from studies of the current behaviour of slopes some researchers started new investigations of landslides related with climate change. The general predictions for climate change are an increase of temperature globally. This means that glaciers will melt and the soils beneath the glacier will suffer from two different effects: the release of pressure from the disappearing glacier but also different regimes of infiltration caused by the melting of the ice. This has generated interest in areas such as Switzerland. Apart from the monitoring itself, the concern of the researchers were to achieve an installation system that would allow the monitoring in such climate conditions. Information on monitoring of suction in Alpine and Pre-alpine regions can be found in Springman and Teysserie (2001) and Springman et al. (2003).

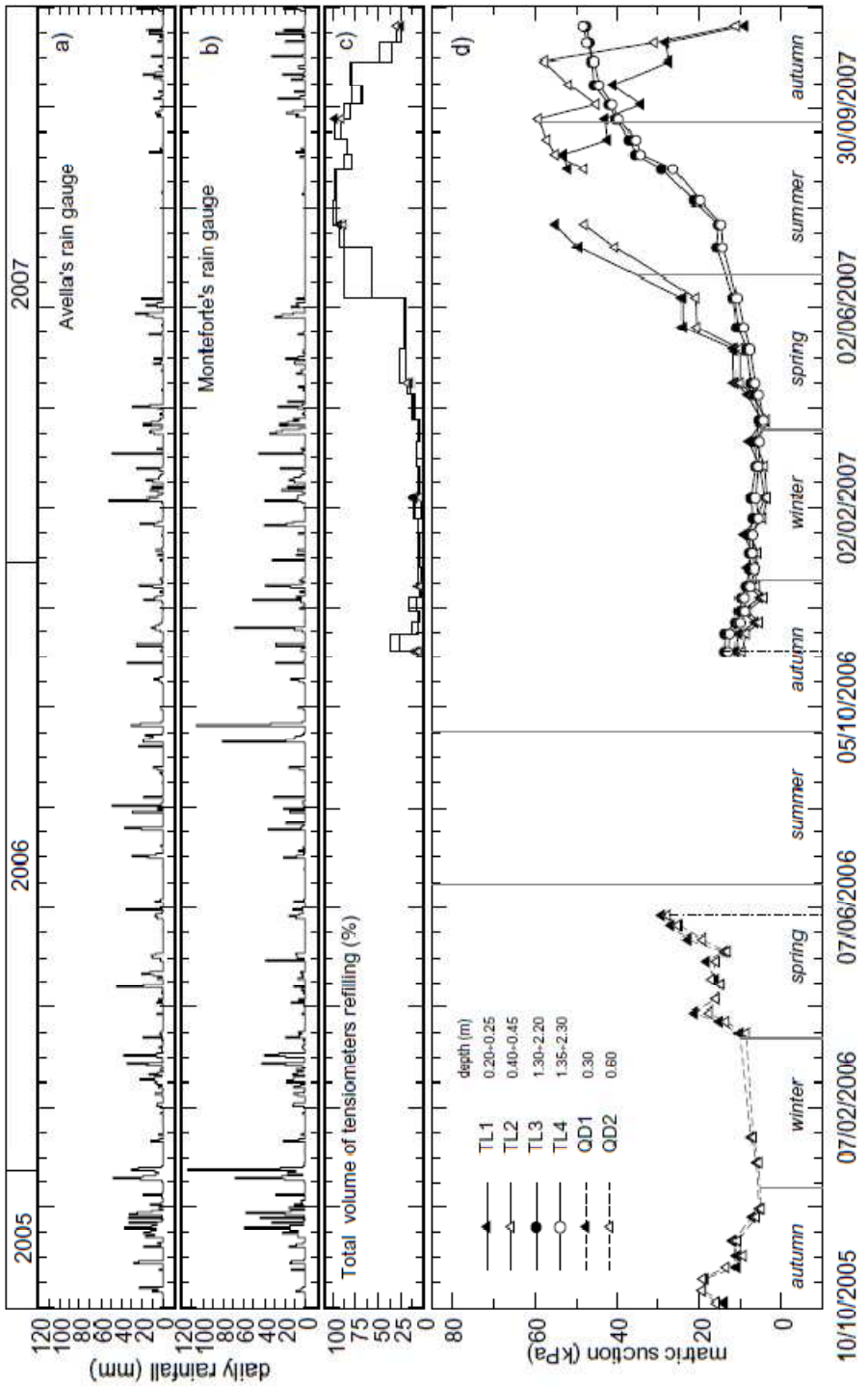

Figure 2.9 - Main monitoring results: a) Avella rain gauge readings; b) Monteforte rain gauge readings; c) total volume of tensiometer refilling; d) mean matric suction. After Evangelista et al. (2008).

Another effect of climate change is in the annual weather pattern. The changes in the weather behaviour can cause a multitude of problems for earth structures. Climate regions in which an almost homogeneous weather behaviour exists, for example the UK where only small variations of the weather throughout the seasons is noticeable, a change in the annual pattern can change the behaviour of slopes. The predictions for climate change, for the UK, suggest longer dry seasons and intense bursts of precipitation during the wet seasons. The possibility of volumetric changes during the different seasons topped by loss of stability due to rainfall infiltration that is higher than the current expectations can provoke serious reductions in serviceability for slopes that form the backbone of the transport network.

2.9 Mechanical testing of unsaturated soils

To understand the strength changes that can lead to the occurrence of landslides it is necessary to understand the mechanical behaviour of unsaturated soils. The mechanical behaviour of unsaturated soils has been studied by investigating different types of soil samples including compacted samples (Toll, 1990; Wheeler and Sivakumar, 1995), reconstituted samples (Cunningham et al., 2003) and intact samples (Futai and Almeida, 2005). Techniques usually employed in association with known techniques for saturated soils, such as the triaxial apparatus, for the study of the mechanical behaviour in unsaturated conditions are axis translation (e.g. Toll, 1990, Wheeler and Sivakumar, 1995), relative humidity (e.g. Oldecop and Alonso, 2000), osmotic (e.g. Dineen and Burland, 1995) and more recently a computer controlled technique based on the use of high capacity suction probes (e.g. Jotisankasa, 2005).

The axis translation technique has been one of the techniques most widely used by researchers to study the mechanical behaviour of unsaturated soils using a triaxial cell. The origins of the Axis Translation Technique date from 1935 by Schofield and Hilf i(1956) in which,

providing that there are no changes in water content and suction, if the air pressure is raised subsequently the pore water pressure rises by the same amount. If the increase of pore air pressure is raised enough, to a value greater than the initial negative value of pore water pressure, then the pore water pressure becomes positive, enabling the reading of pore water pressure using conventional pressure transducers. Bishop and Donald (1961) developed a double wall triaxial cell capable of controlling independently both air pressure and water pressure, which enabled the control of suction during the test. In the axis translation technique the maximum value of suction attainable is dependent on different parts of the triaxial apparatus: the cell robustness, the air entry value of the porous stone (that separates the sample from the pore water pressure mechanism) and the achievable air pressure. There are other limitations for this technique: the long duration of the test and the possibility of air diffusion through the porous stone.

The relative humidity control system is a technique adapted by Al Mukhtaret et al (1993) to geotechnics, particularly for testing soils at suctions above 1 MPa. It began as a soil science system, essentially based on controlling the relative humidity of the air surrounding the soil sample. By doing so, the total suction can also be controlled through its relationship with relative humidity, although an independent suction measurement is needed to guarantee the suction equilibrium. Advances in this independent suction measurement have been presented by Blatz and Graham (2003): whilst testing a high plasticity clay, they incorporated a thermocouple psychometer to measure suction.

The Osmotic system was developed by Zur (1966) and has been widely used ever since in works such as Cui and Delage (1996), Dineen (1997), Colmenares (2002) among others. In the osmotic system, a semi permeable membrane is used to separate the sample from a solution of a large molecular weight substance (usually Polyethylene Glycol, PEG). Since this

membrane is permeable to water but not to PEG, by osmosis, the water flows from the soil across the membrane to the PEG solution until the osmotic potential of the PEG solution is equalled by the soil suction. The suction applied is therefore a function of the concentration of the PEG solution; this means that when the concentration of the PEG solution increases so does the suction and vice-versa.

More recently, Cunningham (2000) at Imperial College developed a technique for suction measurement that encompasses the flow of dry air across the surface of the soil sample. This air-regulated system comprises suction probes for independent suction measurement and uses the flow of dry air across the base of the soil sample, drying the soil sample and, in consequence, causing an increase in suction. Cunningham used this system in situations in which suction usually decreases (loading and shearing stages of tests); his objective was to keep a constant suction value, so the measurements from the suction probes were used to control the flow of air and, by that means, keep a constant suction value.

2.10 **Constitutive models**

Based on such experimental investigation, constitutive models have been proposed to describe the mechanical behaviour of unsaturated soils. Bishop (1959) tried to describe the mechanical behaviour of unsaturated soils using a single effective stress variable, as an extension to the saturated effective stress, incorporating pore air pressure and pore water pressure as in equation 2.4. Bishop included a parameter in the formulation, X, related to the degree of saturation representing the contribution made by either water or air in the voids.

$$\sigma' = \sigma - X.u_w - (1 - X).u_a \tag{2.4}$$

Describing the behaviour of unsaturated soils by a single stress variable was discouraged by Jennings and Burland in 1962. The problem of using a single stress variable is that it was incapable of reproducing the behaviour of collapsible soils. Jennings and Burland showed this by experimenting on silt samples at constant applied stress during inundation where samples reduced in volume while pore water pressure was still increasing.

To overcome the limitation of a single stress variable more recent constitutive models use two or more variables to describe the behaviour of unsaturated soils. These separated stress variables are net stress, in the two possible forms of ($\sigma - u_a$) and ($\sigma - u_w$), and matric suction ($u_a - u_w$). To describe satisfactorily the volumetric response of unsaturated soils two of the variables are sufficient (Fredlund and Morgenstern, 1978). The net stress is a tensorial variable, expressed as:

$$\bar{\sigma} = \begin{bmatrix} (\sigma_x - u_a) & \tau_{yx} & \tau_{zx} \\ \tau_{xy} & (\sigma_y - u_a) & \tau_{zy} \\ \tau_{xz} & \tau_{yz} & (\sigma_z - u_a) \end{bmatrix} \quad (2.5)$$

The matric suction is, instead, a scalar variable, expressed as:

$$s = u_a - u_w \quad (2.6)$$

The most common and recent constitutive models for unsaturated soils are described below.

2.10.1 Critical state framework for saturated soils

Most recent constitutive models to describe the mechanical behaviour of unsaturated soils derive from the critical state framework for saturated soils.

The critical state theory underlines the principle that a soil under stress ultimately reaches a state of plastic behaviour characterized by continuous deformation without any further increase in stress, idealizing the limits of possible states at which the soil can exist. The critical state framework can explain the behaviour of shear and volume changes of saturated soils under external loading.

The first elasto-plastic critical state model was Cam clay (Schofield and Wroth, 1968), although later a second model emerged, named Modified Cam clay (Roscoe and Burland, 1968).

The elasto-plastic critical state models are simplified by a certain number of assumptions that helps explaining the stress-strain behaviour and considers the complex nature of soils (Kurtay and Reece, 1970):

- Soil is considered to be homogeneous and isotropic;
- The mechanical behaviour can be expressed in terms of appropriate stress states variables,
- The mechanical behaviour is described by a macroscopic continuum mechanics model;
- There are no time dependent aspects for the mechanical behaviour;
- And finally, the soil is not viscous.

Assuming the assumptions presented, the sate variables to describe the mechanical behaviour are effective mean effective stress (p'), deviatoric stress (q) and specific volume (ν) which can be defined as:

$$p' = \frac{\sigma_1 + \sigma_2 + \sigma_3}{3} - u_w = \frac{\sigma'_1 + \sigma'_2 + \sigma'_3}{3} = p - u_w \tag{2.7}$$

$$q = \sigma_1 - \sigma_3 = \sigma'_1 - \sigma'_3 \tag{2.8}$$

$$\nu = 1 + e \tag{2.9}$$

Where

p – mean stress
e – void ratio
$\sigma_1,\sigma_2,\sigma_3$ – principal stresses
$\sigma'_1,\sigma'_2,\sigma'_3$ – principal effective stresses

Under triaxial conditions where σ_2 is equal to σ_3, equation 2.7 takes the form of equation 2.10.

$$p' = \frac{\sigma_1 + 2\sigma_3}{3} - u_w \tag{2.10}$$

Or in terms of principal effective stresses:

$$p' = \frac{\sigma'_1 + 2\sigma'_3}{3} \tag{2.11}$$

The critical state can be defined by unique lines in two two-dimensional planes, one line is defined in the q-p' plane, stress plane (plane where no volume changes occur) and the second unique line is defined in the specific volume – effective stress plane, ν-p' plane (plane without the shear stresses).

From the two-dimensional planes new parameters to describe the critical state line can be obtained:

$$\nu = \Gamma - \lambda \ln p' \qquad \text{in the ν-p' plane} \qquad (2.12)$$

$$q = Mp' \qquad \text{in the q-p' plane} \qquad (2.13)$$

Where,

λ – slope of critical state line on the ν-p' plane;

Γ – intercept of the critical state line on the ν axis;

M - slope of critical state line on the q-p' plane.

M can be seen as a friction parameter, from M the internal friction angle at the critical state can be determined from equation 2.16.

The internal effective friction angle ($\emptyset'$) can be determined from:

$$\sin \emptyset' = \frac{\sigma'_1 - \sigma'3}{\sigma'_1 + \sigma'3} \qquad (2.14)$$

Following the derivation from equation 2.14, where:

$$\frac{\sigma'_1 - \sigma'_3}{\sigma'_1 + \sigma'_3} = \frac{3(\sigma'_1 - \sigma'_3)}{3(\sigma'_1 + \sigma'_3)} = \frac{3(\sigma'_1 - \sigma'_3)}{(\sigma'_1 - \sigma'_3) + 2(\sigma'_1 + 2\sigma'_3)} = \frac{3}{3} \times \frac{3(\sigma'_1 - \sigma'_3)/(\sigma'_1 + 2\sigma'_3)}{(\sigma'_1 - \sigma'_3)/(\sigma'_1 + 2\sigma'_3) + 2}$$

$$= \frac{3M}{M + 6} \qquad (2.15)$$

This provides the possibility of determining the critical state friction angle using equation 2.16:

$$\emptyset' = \arcsin\left(\frac{3M}{M + 6}\right) \qquad (2.16)$$

2.10.2 The Barcelona Basic Model

The Barcelona Basic Model (BBM) was presented by Alonso et al (1990) as an extension of the Modified Cam Clay (MCC) framework (Burland, 1965a; Roscoe and Burland, 1968) for the partly saturated case. There are a few main stress variables involved in this model, namely:

Mean net stress(tensor) $$p" = p - u_a = \frac{1}{3}(\sigma_1 + 2\sigma_3) - u_a \quad (2.17)$$

Deviatoric stress (tensor) $$q = (\sigma_1 - u_a) - (\sigma_3 - u_a) = \sigma_1 - \sigma_3 \quad (2.18)$$

Matric suction (scalar) $$s = (u_a - u_w) \quad (2.19)$$

In the BBM, along the s - p'' space, a yield line (also known as the Load Collapse (LC) yield curve) separates a zone of quasi-elastic behaviour from a zone where plastic compression occurs, representing the locus of volumetric yield points in the s : p'' plane. According to this model, yield can either occur due to an increase in the mean net stress or a decrease in matric suction. The yield line itself describes the onset of irreversible compressive phenomena, no matter which stress path causes them, but the mechanical response of the soil is basically the same when inducing yield by wetting or loading. The BBM also states that, within the quasi-elastic region, any path will lead to recoverable elastic volumetric strains.

The BBM is a strain hardening type of model, and states that plastic deformations result in an expansion of the quasi-elastic region, i.e. pushing the LC yield line to the right in the s : p'' space. However, no matter what causes the LC yield line to move (wetting or loading), its movement represents the same value of volumetric strains.

The model also implies that a soil is saturated when matric suction equals zero, which, in reality, might not be true. Saturated soil can display suction values and, on the other hand, it has also been shown that partly saturated soils can have null matric suction. This is one of the main reasons why some researchers have been trying to improve this model, taking the fact that it represents basic concepts on partly saturated soils mechanical behaviour, namely:

- the increasing magnitude of the collapse strains with constant increasing load
- the collapse on wetting under constant load
- the increasing yield stress with increasing suction when loading at constant suction.

To overcome the questions that arose from BBM, new types of elasto-plastic models have been presented (Gallipoli et al. (2003a), Wheeler et al. (2003)), using two independent modified stress variables. These last two models, which will be described below, have successfully reproduced important concepts of the behaviour of partly saturated soils (that were not reproduced by earlier models such as BBM). Apart from accounting for irreversible changes of void ratio during the wetting-drying cycle, these models also encompass the history of suction (meaning that a soil response to compression at constant suction will depend on the previous history of suction) and present smooth transitions from fully saturated to partly saturated behaviours.

The main idea behind these models is to separate the two mechanical effects that a partly saturated soil experiences, an influence of both the degree of saturation of the soil and the distribution of water in it – these will affect the two stress variables used for the Wheeler and Gallipoli models.

The first variable, related to the distribution of water in soil, is a function of the effective stress, imposed on the soil skeleton and the bulk water in soil - Bishop's average skeleton stress (Jommi, 2000) in the form of equation 2.20 which is based on equation 2.4.

$$p^* = p - [\, Sr.u_w + (\, 1 - Sr\,).u_a] \qquad (2.20)$$

Where,

p^* - Bishop's average stress skeleton

p – total stress

Sr – degree of saturation

u_w – pore water pressure

u_a – pore air pressure

The second variable, although interpreted differently by Wheeler and Gallipoli, is related to the water menisci, more precisely, to the stabilisation that these water menisci provide at the inter-particle contacts of the soil. This effect ends up as being accounted for as a function of suction, porosity and degree of saturation.

Below, the models proposed by Wheeler and Gallipoli are presented, due to their capability of incorporating important effects in soil behaviour and their realistic approaches in modelling partly saturated soils.

2.10.3 Wheeler model

Wheeler et al (2003) present a model that assumes that soil stability reflects the variation of stabilising forces at interpaticle contacts, taking into consideration the phenomenon of hydraulic hysteresis. The phenomenon of hydraulic hysteresis (that can be

represented by a Soil Water Retention Curve – SWRC) explains how two soils can present similar values of matric suction and yet contain different amounts of fluid within the soil's pores. Wheeler was able to incorporate this effect (and the influence it has on soil mechanical behaviour) by distinguishing bulk and meniscus pore fluid. Soil behaviour is, then, dependent on the proportion of meniscus and pore fluid within the soil skeleton, or, in other words, the degree of saturation of the soil – so it is possible to say that two samples with similar values of matric suction, dry densities and subjected to the same external load, but presenting different degrees of saturation, represent two different states of a soil. The influence of the degree of saturation on soil behaviour is due to differences in the contact forces that result from fluid filled pores as opposed to samples where only menisci are present. When menisci are present, an additional stabilising force is present at interparticle contacts. The position of the SWRC can also be affected by volumetric deformations. During compression, when voids become smaller, higher values of suction are required to maintain the saturation degree – this will shift the SWRC to the right.

The Wheeler et al model is, therefore, able to couple hydraulic and mechanical processes, using elasto-pastic processes for both cases. This coupling is possible due to two separate phenomena:

- elasto-plastic deformation of the soil skeleton by loading
- elasto-plastic inflow and outflow of fluid from interparticle pores.

The behaviour of the soil is said to be controlled by two independent stress variables: p^*, also known as Bishop's stress (which represents total stress, pore fluid pressure and gas pressure effect on the soil skeleton) and s^*, also known as modified suction (which represents the stabilizing effect of menisci at interparticle contacts). As for strain variables, Wheeler et al

present two conjugate strain variables: volumetric strains ($d\varepsilon_v$) and the degree of saturation ($-dSr$).

As in Alonso et al (1990) model, plastic volumetric deformations can be modelled using a Load Collapse (LC) yield line. However, Wheeler considers this line to be straight and vertical in the s*:p* plane, stating that the reason for this is that the stabilizing force present on the menisci is constant and independent of suction. Soil stability is a result of the number of interparticle contacts presenting menisci and not a result of the matric suction value. When, during loading, the LC yield line is crossed, the soil sample experiences compressive plastic volumetric strains, which lead to a shifting in position of the LC yield line. Wetting or drying the soil sample to the point where plastic changes in the degree of saturation occur also changes the number of menisci at interparticle contacts and, as a consequence, the LC yield line will also shift (to the right, expanding the yield locus, on drying or to the left, contracting the yield locus, on wetting). Irreversible changes in the degree of saturation occur when either a Suction Decrease (SD) or a Suction Increase (SI) line are crossed, which is when the scanning curve meets the main branches of the SWRC (see Figure 2.10).

If, during loading, the LC yield line is crossed and plastic volumetric strains occur, the SWRC position shifts, and the SI and SD yield lines will also move in a coupled way (Figure 2.10).

According to this model, elastic behaviour is the one enclosed within the SI, SD and LC lines in the s*:p* space; any path that crosses any of these three lines will result in either plastic volumetric strains or irreversible changes in the degree of saturation.

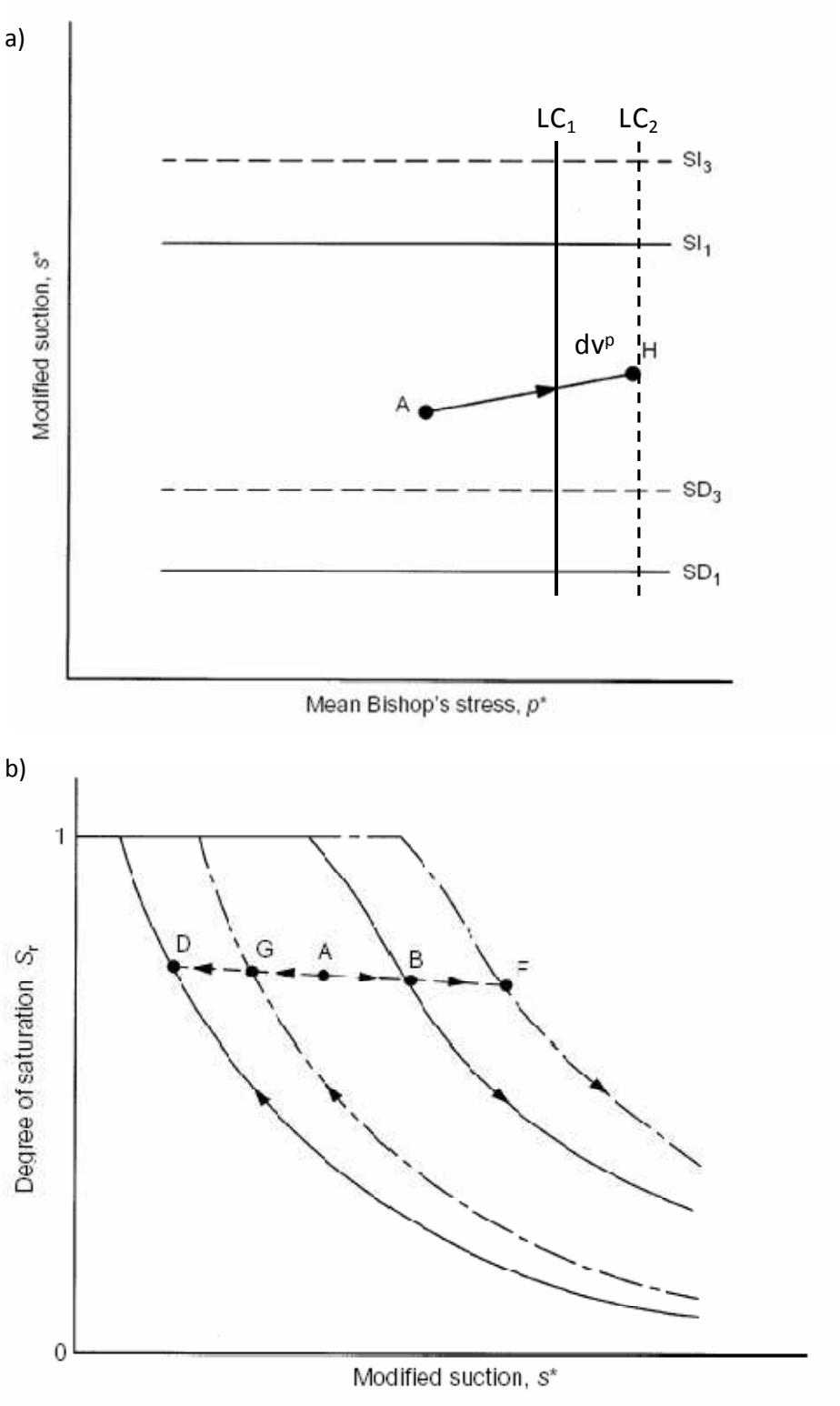

Figure 2.10 – Coupled movement of the SI and SD caused by plastic volumetric yielding:

a) Stress path **b)** SWRC (after Wheeler et al., 2003).

Wheeler et al model is, then, capable of reproducing a series of important aspects of soil behaviour, being able of modelling particular phenomena such as:

- the swelling or collapse on wetting
- the transition between the saturated and partly-saturated states of a soil
- plastic compression during drying on a wetting-drying cycle
- changes in degree of saturation due to hydraulic hysteresis
- the influence of wetting-drying cycles on subsequent mechanical responses of a soil during loading.

Most of the above aspects cannot be modelled by a single LC yield line (or curve) or excluding the effect of hydraulic hysteresis. The model presented by Wheeler also has the advantage of allowing the prediction of a smooth transition from unsaturated to saturated behaviour. However, only qualitative predictions have been attained so far, and some assumptions in the model still require experimental verification and validation.

2.10.4 Gallipoli model

Whilst the Wheeler et al (2003) model focuses on the different behaviour of fluid and gas filled pores, a slightly different approach is used by Gallipoli et al (2003a), focusing on soil variables in terms of stress, pore gas pressure, pore fluid pressure and degree of saturation.

Gallipoli et al (2003a) present a model that also encompasses two independent stress variables, but this model explicitly accounts for the effects of plastic changes in degree of saturation on the stress-strain behaviour of partly saturated soils. The stress variables used on the model by Gallipoli are:

σ^*, known as the average skeleton stress, which is equivalent to Bishop's stress

ξ, is the bonding variable that accounts for the menisci bonding effect at interparticle contacts.

Gallipoli suggested that the presence of menisci and the bonding effect provided by these are the main reason for void ratio increase with increasing suction of samples that yield along a normal compression line. Comparing the normal compression lines at constant suction of soil samples with different values of matric suction (Figure 2.11a)), Gallipoli observed a relationship between the void ratio of the partly saturated samples (e) and the saturated samples (e_s) yielding along a normal compression line of constant suction and subjected to the same skeleton stress (Figure 2.11b)). This relationship is related to the bonding effect of menisci and, therefore, with the bonding variable ξ.

Although the authors have found the relationship between the ratio e/e_s and the bonding variable ξ holds true both on isotropic and anisotropic loading, the mathematical formulation has only been given for the isotropic stress space so far. According to this, a normal compression state surface is defined in the e: p*: ξ space, modeling plastic volumetric compression. Similarly to the models described above, the normal compression state surface represents states of yielding, where paths below it are related to entirely elastic processes and paths along it represent elasto-plastic changes in void ratio.

Since the ratio e/e_s is constant, for a given value of ξ, the normal compression lines for different values of ξ are straight (Figure 2.12a)). Elastic changes in void ratio depend on changes on p* and are not influenced by ξ.

To include the effects of hydraulic hysteresis and plastic changes in void ratio on the variation of the degree of saturation, Gallipoli suggested that the mechanical formulation he had attained should be used together with models such as the ones by Vaunat el al (2000) or Gallipoli et al (2003b), although this latter work does not specifically cover hydraulic hysteresis but only changes in the SWRC due to void ratio variations. In addition, the model presented by Gallipoli does not distinguish expansive from non-expansive soils.

Still, it allows a prediction of important aspects of soil behaviour, namely partly saturated soil behaviour and both expansive and non-expansive soils. Some of these aspects, which cannot be reproduced with a single LC yield line as previous models advocate, include the development of plastic compressive strains on drying (during a wetting-drying cycle) and also the importance of suction history on stress-strain behaviour during isotropic loading at constant matric suction along the normal compression line.

a)

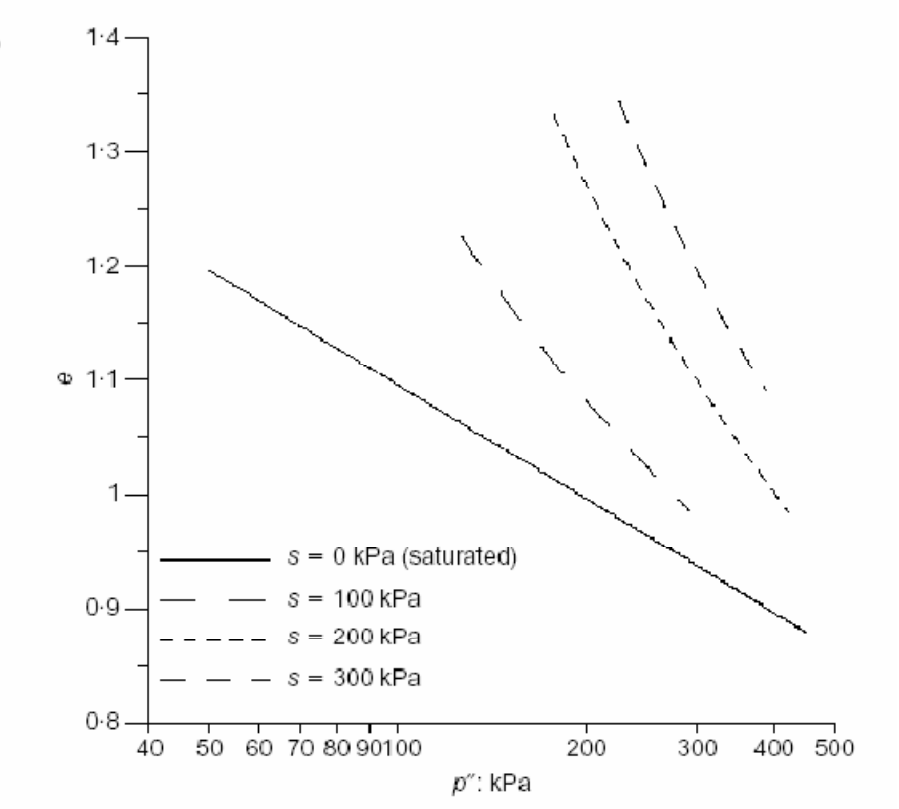

b)

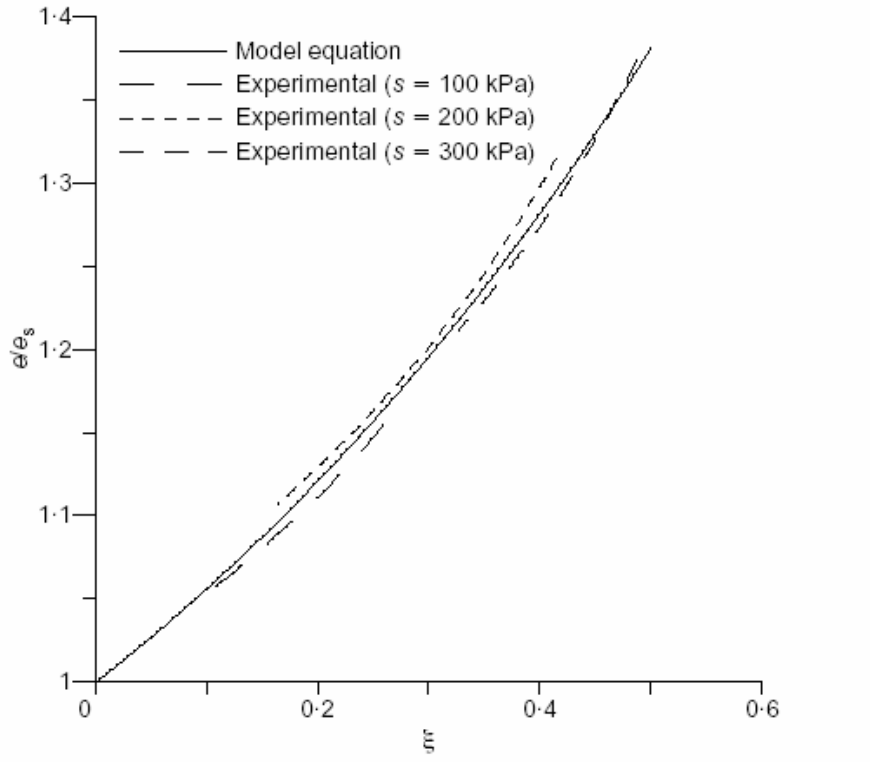

Figure 2.11 - a) Normal Compression Line at constant suction **b)** Relationship between ratio e/e_s and bonding factor ξ during isotropic virgin loading at constant suction (Gallipoli et al., 2003a, experimental data from Sharma, 1998).

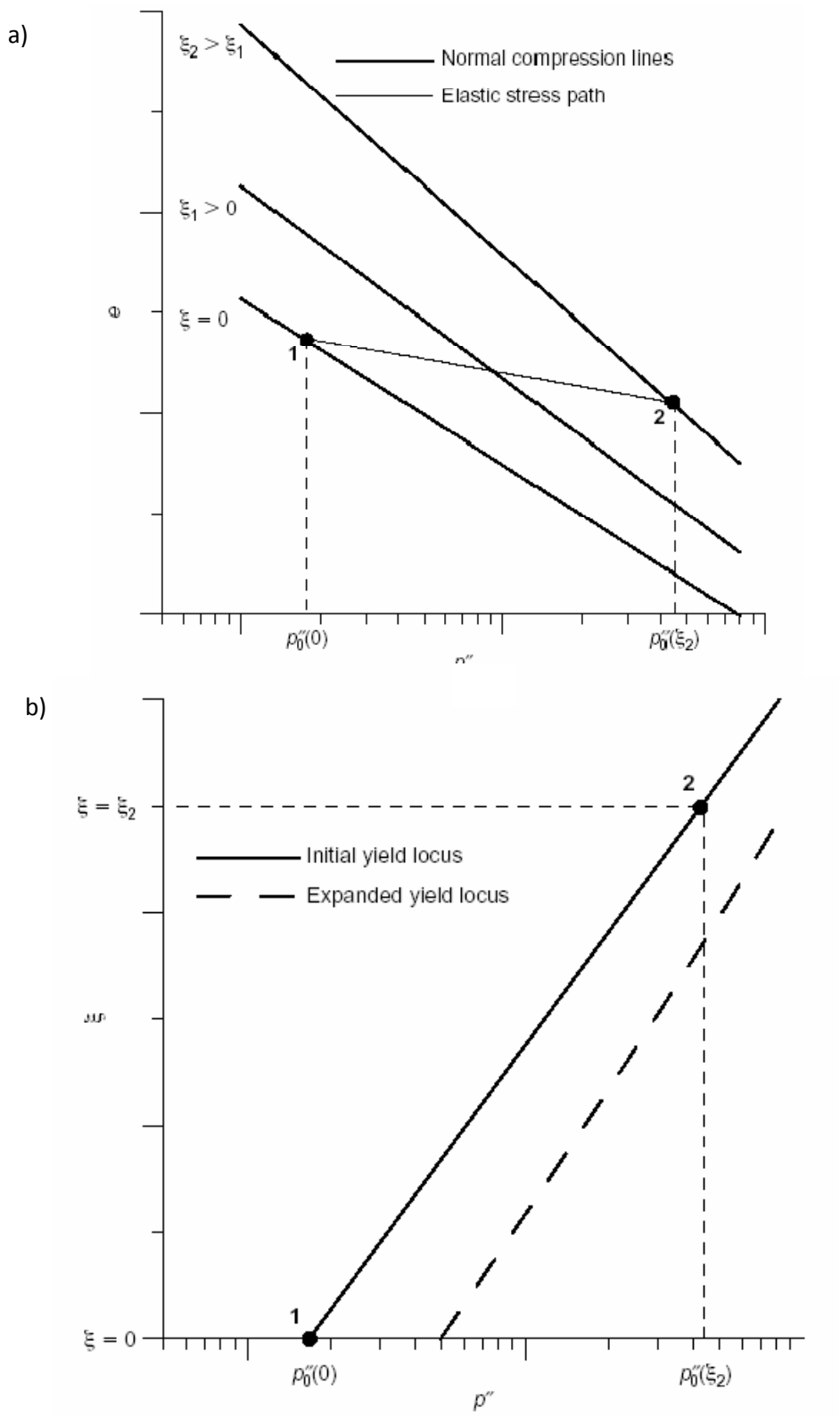

Figure 2.12 - Yield locus derivation in the isotropic plane for the Gallipoli et al. (2003a) model:

a) change of void ratio; **b)** stress path (Gallipoli et al., 2003a).

2.10.5 Toll framework for unsaturated soil behaviour

Toll (1990) put forward a framework that tried to explain the behaviour of unsaturated soils in terms of total stresses and suction acting within compacted soils, while testing the framework on Kiunyu gravel (a lateritic gravel). Like in the BBM, this framework was based on the critical state model for saturated soils with total stresses and suction considered separately to describe the unsaturated behaviour. Toll's approach differed to the BBM by giving importance to soil fabric in which the contributions of total stress and suction to shear strength are expressed as two individual stress ratios heavily dependent on the degree of saturation.

The importance of the soil fabric in compacted clays is discussed in Toll (1990) reporting the observation of Croney et al (1958) which describes the fabric of compacted clays as being composed by aggregates of clay particles (or clays plackets) separated by comparatively large air voids. Brackley (1973, 1975) suggested that within the clay aggregates the voids are saturated while the voids between the aggregates are filled with air. The distribution and the size of the clay aggregates influences the inter aggregate void space, which in turn, influences the behaviour of a compacted soil. If suction was large enough in the inter aggregates voids the aggregates of clay particles could behave as individual larger particles, behaving similarly to soils with coarser grading. On the other hand, if the suction was reduced the aggregates could become unstable, with possibilities in the reduction in volume (collapse).

The proposed framework by Toll describes the behaviour of unsaturated compacted soils at the critical state is expressed as:

$$q = M_a(p - u_a) + M_w(u_a - u_w) \tag{2.21}$$

$$\nu = \Gamma_{aw} - \lambda_a \ln(p - u_a) - \lambda_w \ln (u_a - u_w) \quad (2.22)$$

where,

q – deviator stress

p – total stress

u_a - u_w – matric suction

u_a – pore air pressure

u_w – pore water pressure

M_a – total stress ratio

M_w – suction ratio

ν – specific volume

Γ_{aw} – intercept in the ν space

λ_a – slope of the critical state derived from the total stress

λ_w – slope of the critical state derived from suction

In equations 2.21 and 2.22 the parameters M_a, M_w, λ_a, λ_w, and Γ_{aw} are functions of the degree of saturation and fabric of the soil. The dependence of these parameters on the degree of saturation has to be determined experimentally. In this framework the degree of saturation is used as an indicator, although with some limitations, of the fabric.

To fully describe the unsaturated soil behaviour at the critical state using this framework it is required 5 dimensions: p-u_a, u_a – u_w, q, ν and Sr (degree of saturation).

Toll and Ong (2003) also applied this framework to a residual sandy clay soil from Singapore and found that the functions that related M_a and M_w to degree of saturation, when normalised, were similar to that for the lateritic gravel.

2.11 Chapter summary

The literature review presented in this chapter focused on topics that are relevant for the subsequent work presented in the following chapters. The topics include: understanding the behaviour of unsaturated soils, the different methodologies that can be implemented to study unsaturated soils, mechanical and hydraulic properties, and some of the available frameworks found in literature for presenting and explaining such information.

To understand the behaviour of unsaturated soils it is imperative to understand the basic concepts presented in the first sections of this chapter: the nature of unsaturated soils; the phases of unsaturated soils (soil, water, air and air-water), soil suction and water retention behaviour.

Soil suction can be determined using various techniques; however, only the methodologies used to produce this research were presented, namely: filter paper, psychrometer transistor, high capacity suction probe and the pressure plate technique. For each technique the concept behind the measurement, advantages and disadvantages were presented. Since part of this research was also to monitor suction outside a controlled environment the work carried out by other researchers including methodologies and major findings were presented.

Importance was given to the hydro-mechanical testing of unsaturated soils in which the available methodologies found in the literature: axis translation, relative humidity, osmotic and a computer controlled technique based on the use of high capacity suction probes were presented.

This chapter finishes by presenting some of the available frameworks found in literature for presenting and explaining the behaviour of unsaturated soils: the Barcelona basic model or BBM, the Gallipoli model, the Wheeler model and the Toll framework for unsaturated soil behaviour.

3 The BIONICS embankment

3.1 Introduction

The BIONICS project (BIOlogical and eNgineering Impacts of Climate change on Slopes), funded by the Engineering and Physical Sciences Research Council, aims to investigate the serviceability and safety of earth structures (embankments, cuttings). The rationale for the project is that future climate scenarios for the UK (UK Climate Impacts Program, UKCP09) present concerns for engineers about the performance of earth structures that form the transportation network. Intense rainfall and longer drier periods, as are predicted for the UK, might greatly affect the stability of slopes and foundations that are the base of the complex and extended transportation network throughout the UK. Problems such as shrinkage settlements of foundations due to drought and failure of slopes due to intense rainfall are experienced to some extent nowadays, but are more likely to occurr with future climate change.

The BIONICS project involves various institutions; the project partners are the universities of Newcastle upon Tyne, Durham, Dundee, Nottingham Trent, Loughborough and Bristol, together with industrial stakeholders: British Waterways, Cementation Foundations, Skanska Ltd, CIRIA, Highways Agency, Geotechnical Observations Limited, Metronet Rail SSL Ltd, Mott McDonald, Network Rail, Rail Research UK, Rail Safety and Standards Board and the Scottish Crop Research Institute.

Part of the BIONICS project was to build a full-scale test embankment, the BIONICS embankment, where a climate control system backed by extensive instrumentation and laboratory testing would generate information on the effects of climate change on earth structures. The

gathered information could, subsequently, be used to validate analytical methodologies that would enable assessment of other earth structures.

3.2 The embankment

The BIONICS embankment is an experimental embankment that was built with the intention of providing some insight into the consequences of climate change on earth structures. The embankment was built in 2005 at Nafferton farm, near Newcastle upon Tyne (Marker A in Figure 3.1). The embankment physical dimensions are of moderate scale: 90 metres long by 6 metres high and 29 metres wide at the base (Figure 3.2) with side slopes of 1 in 2 and a 5m width crest. The end slopes of the embankment were constructed with reinforced soil with an inclination of 45^0.

Figure 3.1 – Location of the embankment (Google maps, 2009).

The embankment was divided into six different panels (not accounting for the end slopes) for the multidisciplinary tests that were proposed in the BIONICS project plan. Figure 3.2 shows the 6

panels, where the outermost panels are used for biological studies; panels of 4 metres in length. The four central panels with 18 metres length represent two different types of constructions methods commonly found throughout the UK, differing in the compaction method applied.

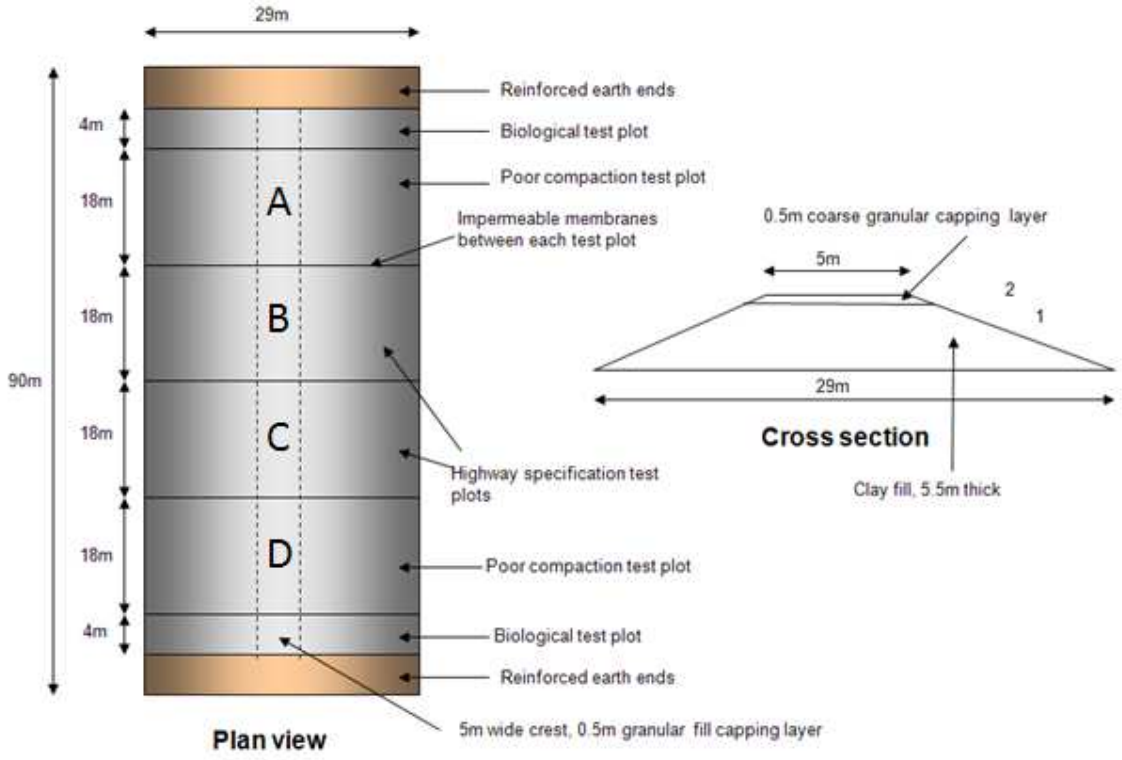

Figure 3.2 – BIONICS embankment plan view and cross section.

Panels A and D in Figure 3.2 (known as poorly compacted panels, PCP) represent the railway embankments resembling existing old structures from Victorian times In this kind of embankment, compaction was not controlled during construction and they frequently do not incorporate any drainage measures. These panels were built in layers of up to 1 metre and simply compacted using a JCB digger to resemble the commonly-used poor compaction methods, see Figure 3.3. This kind of embankment is still present nowadays throughout the UK and ageing is one of the more noticeable problems presented to engineers due to its heterogeneous evolution.

Figure 3.3 – Construction of a poorly compacted panel using a JCB, (Hughes, 2005).

Panels B and C in Figure 3.2 (known as well compacted panels, WCP) represent modern highway embankments, different to the Victorian embankments by being more uniform and better compacted. Layers in panel B and C were compacted according to Method 3 as set out in the Highways Agency Specification for Highway Works (Highways Agency, 1998). The fill was placed in 300mm layers and was subjected to 9 passes by a self propelled vibrating smooth drum roller, see Figure 3.4.

Figure 3.4 - Construction of a well compacted panel using a self propelled vibrating smooth drum roller, (Hughes, 2005).

Vertical impermeable membranes were placed between panels and end slopes to ensure engineering and hydraulic isolation as shown in Figures 3.3 and 3.5.

At the top of the embankment a 0.5 metres thickness of coarse material was built. The coarse, free draining material was placed in order to simplify boundary conditions by preventing surface cracking along the crest of the embankment but still to allow water access to the crest of the embankment, Figure 3.5. Mainly composed of basalt it was proposed due to its qualities as being mineralogically inert and not reactive with the underlying fill so as not to alter the fill material properties.

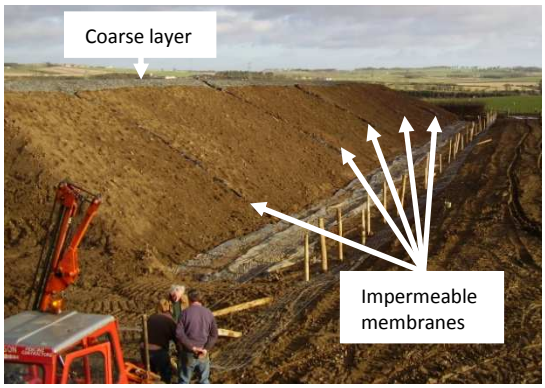

Figure 3.5 – Perspective of the BIONICS embankment at the end of construction, (Hughes, 2005).

3.2.1 The fill material

The fill material used to build the BIONICS embankment was a glacial till, a very common material spread throughout the Northeast of England, normally widely graded and heterogeneous sediments of glacial origin with no stratification.

The material that was selected for the construction of the BIONICS embankment was a single sourced material from a stock pile in County Durham (Hughes et al., 2005) with the general particle size distribution (PSD) curve shown in Figure 3.6 where the material was found to be composed by 12% of gravel, 16% of sand, 35% of silt and 37% of clay. The high percentage of clay minerals lead to the classification of the material as a sandy clay soil.

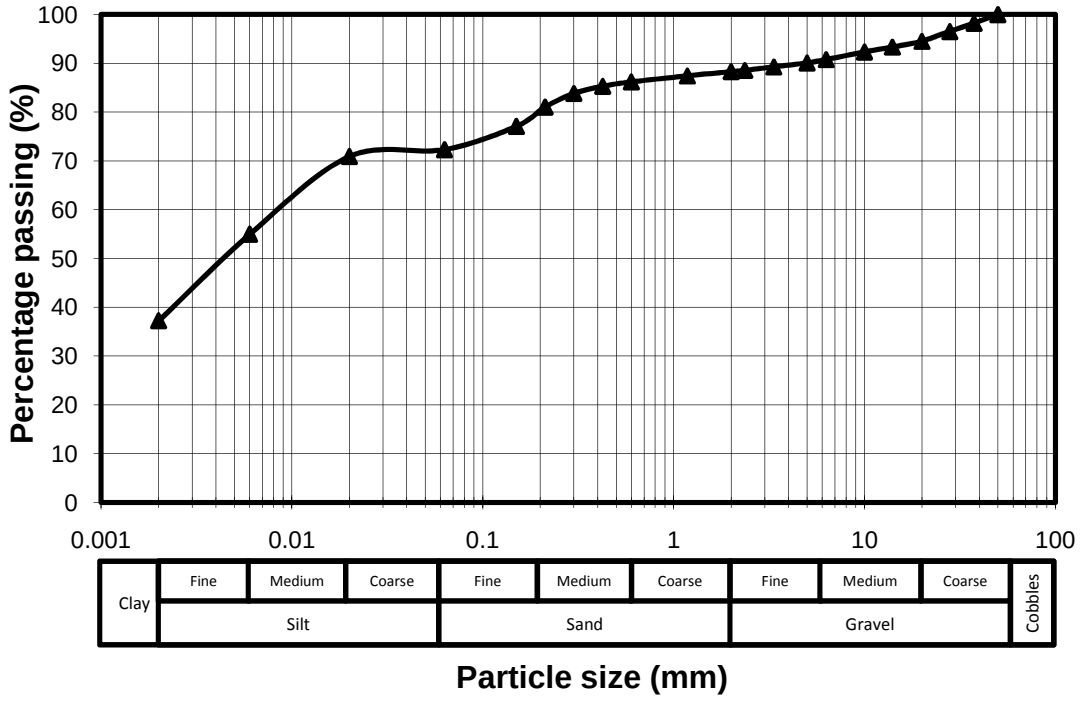

Figure 3.6 – Particle size distribution of the BIONICS fill material.

From the PSD in Figure 3.6 the effective size (d_{10}) was smaller than 0.002mm and d_{60} (60% of material passed) is around 0.02mm resulting on an estimated uniformity coefficient c_u higher than 10. This classifies the material as well graded.

The Atterberg limits obtained by cone penetrometer test for the Liquid Limit (LL) and the rolled thread for the Plastic Limit (PL) (BS 1377, 1990: Tests 4.3 and 5.3) are shown in Table 3.1,

which classifies the fill material as being of intermediate plasticity according to the Casagrande plasticity chart (BS 1377, 1990).

Table 3.1 – Atterberg Limits for the BIONICS fill material.

Natural water content Wn (%)	Liquid limit LL (%)	Plastic Limit PL (%)	Plasticity Index PI	Liquidity Index LI
22.6	43.3	23.7	19.6	-0.05

The Activity (A) of clay minerals of fill material can be determined by dividing the PI by the percentage of clay material (Skempton, 1953). In this case the clay minerals of the fill material are considered to be inactive, since A=0.53, smaller than 0.75 in accordance with Skempton's classification.

Two compaction curves were obtained for the BIONICS soil by the BS light 2.5 kg hammer (Proctor) compaction test and by the BS heavy 4.5 kg hammer (Modified Proctor) compaction test (BS1377, 1990: Tests 3.3 and 3.5), using a mechanical compaction machine. They were performed with the objective of determining the maximum dry density for the material, and hence, the correspondent (optimum) water content. Samples were tested under different water contents (10%, 13%, 15%, 20 and 22%) and compaction curves defined by plotting water content against dry density. In practical engineering, compaction of earth structures should be performed close to W_{opt}, given that at these values the material presents the best performance.

In the case of the fill material at the BIONICS embankment, presented in Figure 3.7, it was determined that for the normal Proctor test the maximum dry density of 1.71 Mg/m^3 was achieved at W_{opt} of 15.5%. For the modified test a higher maximum dry density was achieved of 1.80 Mg/m^3 at W_{opt} of 13%.

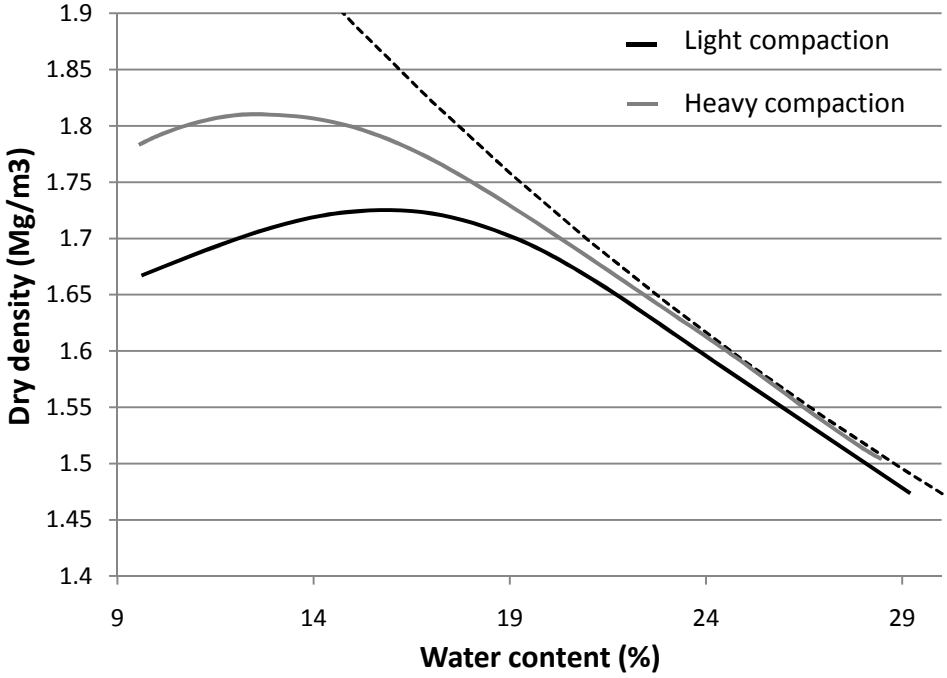

Figure 3.7 – BIONICS fill material - light and heavy compaction curves.

During construction some values were taken to assess each layer compaction level (Hughes et al., 2007) and are presented in Figure 3.8. It is shown that most of the construction was performed in the wet part of the compaction curve, with water contents ranging from 15% to 24%. It can be observed also that for the well compacted panels built using modern construction techniques the achieved density is close to the curve of the Proctor compaction test, while the densities achieved for the poorly compacted panels the densities were generally smaller. Average values of the in-site densities for both construction techniques are presented in Table 3.2. Table 3.2 also shows the average values of percentage of air voids and degree of saturation during construction.

Table 3.2 – Average values for various properties of both poor and well compacted panels (After Hughes et al., 2007).

	Bulk Density (Mg/M^3)	Water Content (%)	Dry Density (Mg/M^3)	Air voids (%)	Degree of saturation (%)
"Poor" compaction	1.93	20.7	1.6	6.0	85.3
Good compaction	2.01	20.1	1.7	3.2	91.4

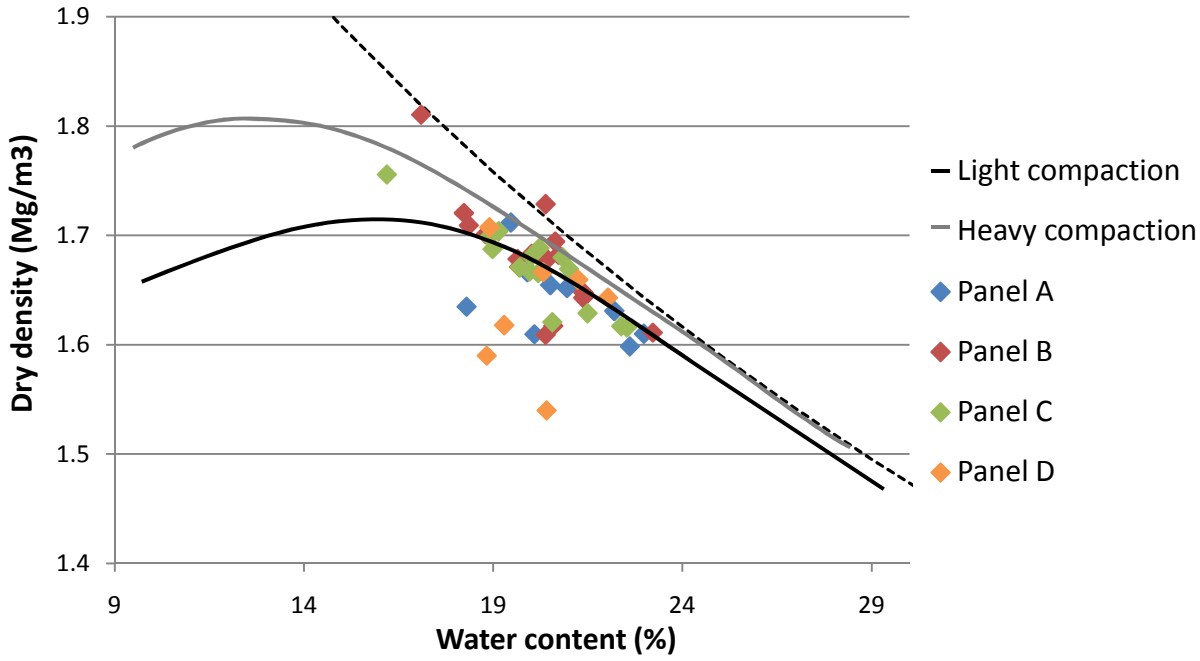

Figure 3.8 – Compaction curves versus field measurements (Panels A&D – Poorly compacted; B&C – Well compacted).

Higher achieved density means a lesser permeable material, this is noticeable on the results from laboratory permeability tests performed at Newcastle University showing the well compacted panels as having permeability of 8.77×10^{-11} m/s in comparison with the poorly compacted panels of 1.6×10^{-10} m/s, (Hughes, 2007). However, in both cases the material presents quite low values of permeability.

3.3 Instrumentation

As an experimental embankment the BIONICS embankment was intended to be used in the future as a platform for new testing methodologies that can help the investigation and determination of soil properties.

At present, the instrumentation at the BIONICS embankment can be divided into two major groups, a general description of the instrumentation throughout of the embankment is shown in Table 3.3.

Table 3.3 – Summary of the embankment instrumentation, after (Hughes et al., 2009).

	Parameter measured	Typical usage	Primary information on failure mode(s)
Flushable piezometers	Positive and negative pore pressure, continuous measurement	Geotechnical monitoring	Shrink–swell, re-wetting
Durham tensiometers	High values of positive and negative pore pressure continuous measurement	Experimental, under development by Durham University	Shrink–swell, re-wetting
GEO observations, tensiometers	High values of negative pore pressure, point measurement	Geotechnical monitoring	Shrink–swell, re-wetting
Standpipe piezometers	Piezometric surface, point measurement	Geotechnical monitoring	Shrink–swell, re-wetting
In-place inclinometers	Slope movement, continuous monitoring	Geotechnical monitoring	Progressive failure
Probe inclinometers	Slope movement, point measurement	Geotechnical monitoring	Progressive failure
Magnetic extensometers	Settlement/heave, point measurement	Geotechnical monitoring	Shrink–swell, surface creep
Acoustic waveguides	Slope movement, continuous measurement	Experimental, under development by Loughborough University	Progressive failure
Theta probes	Volumetric soil water content, continuous measurement	Agriculture irrigation control and geotechnical monitoring.	Shrink–swell, re-wetting
Water content profile probes	Volumetric water content, point measurement	Agriculture irrigation control	Shrink–swell, re-wetting
Temperature probes	Soil temperature, continuous measure-ment	Agriculture, biology, hydrology, meteorology	Shrink–swell, re-wetting
Weather stations	Rainfall, wind speed/direction, pressure, humidity, air temperature, sunlight (inputs to potential evapo-transpiration calculation; indirect, requires calculation)	Meteorology, agriculture, hydrology, biology	Shrink–swell, re-wetting
Remote methods: Lidar, terres-trial laser scanner, GPS	Movement, condition of vegetation	Remote ground surface monitoring	Progressive failure, surface creep

The first group includes the general instrumentation commonly found in most instrumented embankments and are validated equipment. The second group comprises all the newly developed technologies. Both groups of instrumentation are widely distributed through the embankment in all kind of panels, as it can be observed in the Instrumentation Plan for the well compacted panel B in (Figure 3.9).

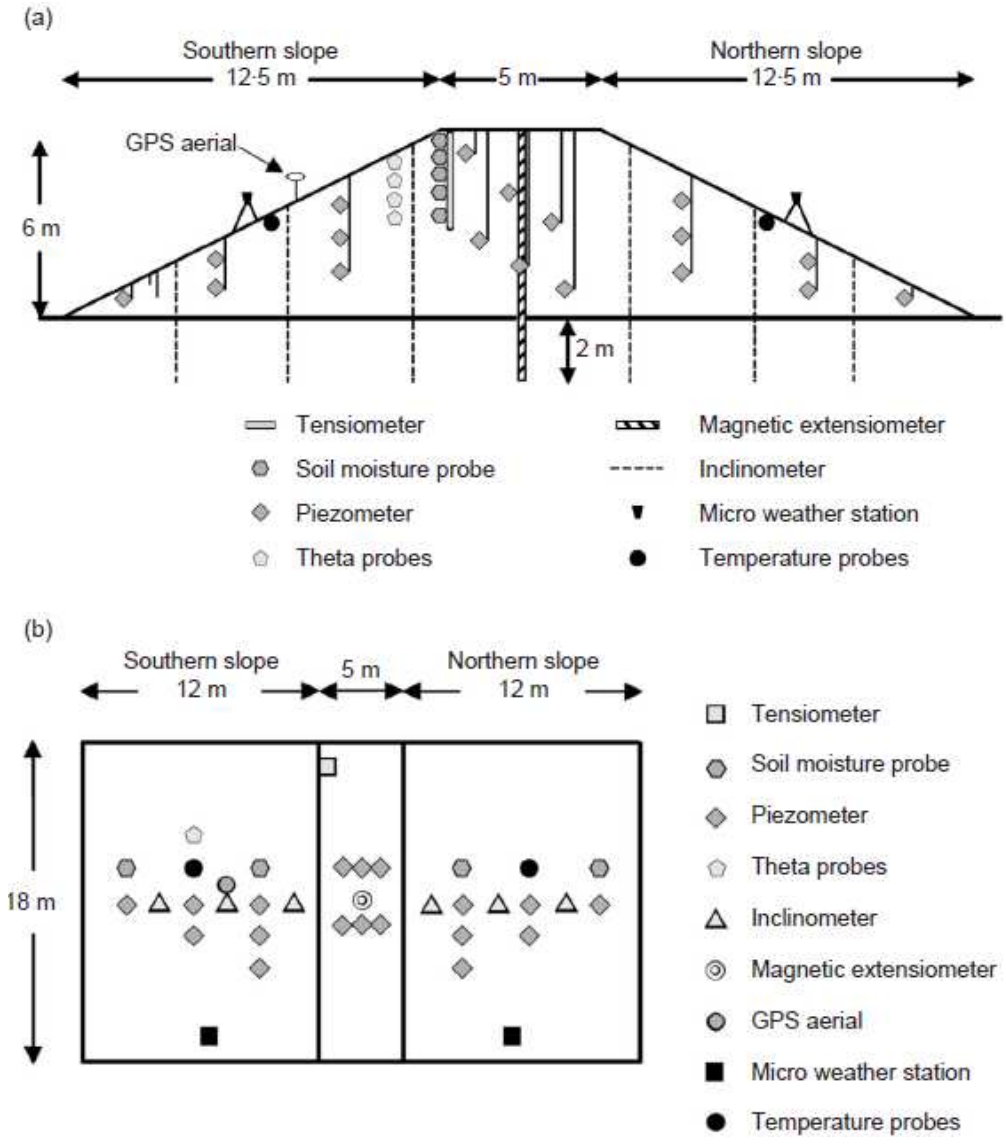

Figure 3.9 – Instrumentation plan for panel B: a) cross section and b) plan view. (After Hughes et al., 2009).

The general instrumentation can be divided into two subgroups; the classical instrumentation composed of extensometers, at the centre of the crest in each panel, various inclinometers in both North and South slopes with a total of six per panel and standpipe piezometers spread out through the embankment to measure pore water pressure. Adding to the classical instrumentation, the specialised equipment group such as collecting points to determine the surface runoff and flushable piezometers, from GEOobservations, to measure negative pore water pressure (suction) were also installed. Due to limitations of the range in flushable piezometers, around -100 kPa, four high capacity suction probes from GEOobservations were used in dry vertical boreholes, with a greater range than the flushable piezometer of -2000 kPa. Also in this group is included the Theta probes that measure volumetric water content at different shallow depths ranging up to 600mm.

Three different weather stations were used to monitor the climate at the embankment. One of the weather stations is located 300 metres from the embankment and monitors the annual weather pattern (i.e. rainfall, air speed, etc), also belonging to the Nafferton Ecological Farming Group of Newcastle University. The other two weather stations (micro weather stations) were installed on top of the North and South slopes of the embankment. The latter two weather stations were used to monitor the climate effects when the climate control system is in operation.

The newly developed techniques group comprises the acoustic waveguide system from project ALARMS (Assessment of Landslides using an Acoustic Real Time Monitoring System), developed by Loughborough University, intended to “listen” to the formation of shear surfaces inside the embankment and the Durham University-Wykenham Farrance Ltd. field high capacity suction measurement system to monitor the evolution of pore water pressure both with depth and

in time at a single location enabling the creations of continuous suction profiles. The latter equipment is part of this study and will be described later in this work.

3.3.1 Climate control system

A climate control system was developed at the embankment to be able to impose different scenarios predicted for climate change. A major concern that engineers face with assessing earth structures, is whether structures can deal with the actual climate patterns and maintain their serviceability when facing different climate patterns (intense rainfall and longer dry periods).

The system employed at the BIONICS embankment can recreate extreme scenarios; designed to reproduce intense rainfall and dry events. To reproduce dry events segments of the embankment were covered with transparent flexible roofing, see Figure 3.10. This system features the possibility of pulling back the cover if desired. This special roofing system was expensive, therefore it was only installed on the south slope of panels C (well compacted) and D (poorly compacted). With this design, precipitation from natural climate events can be prevented from reaching the embankment. Due to its proximity to the surface, 1 metre high, temperature loss is also greatly reduced. By reducing infiltration and by reducing the temperature loss higher rates of evaporation are generated resulting in drying on panels C and D.

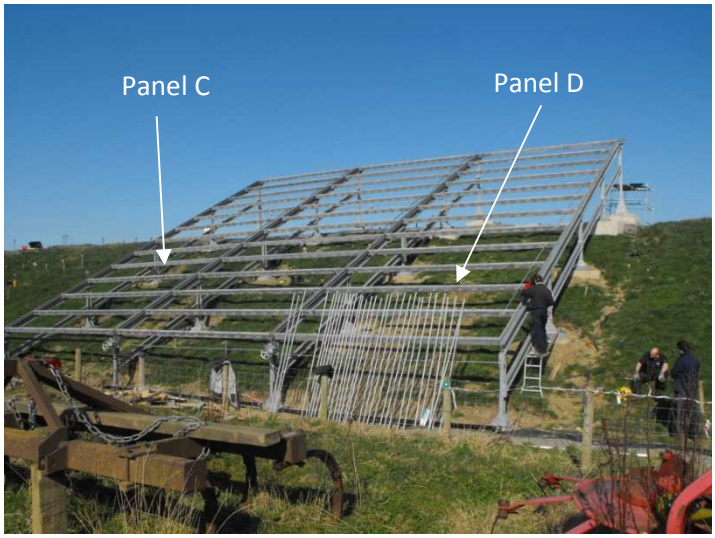

Figure 3.10 – Construction of the covering system during spring of 2009.

To reproduce extreme rainfall events, rainfall sprinklers mounted in poles were installed on panels A and B (see Figure 3.11), as shown in Figure 2.8. The position of the sprinklers on the embankment ensured a spatially uniform rainfall at the ground surface with appropriate droplet sizes.

Figure 3.11 – Sprinkler system (after Hughes 2007).

Both systems are remotely controlled by computer, making the climate control system completely autonomous.

3.4 **Final remarks**

With the predicted changes to the climate in the future the behaviour of old and modern earth structures can change. The change in weather patterns is the biggest concern. The changes in pore water pressure due to these processes (longer dry periods and short bursts of intense rainfall) could greatly affect the stability of earth structures.

The BIONICS embankment is a highly valuable potential tool to study the effect of climate change. Built with material that is present in various earth structures throughout the UK and resembling different structures (old and modern), with its disposition of panels, it can be related to other existing structures. The climate control system backed by a wide range of instrumentation can be used to generate a clear view of the behaviour of the embankment through different climate events. It also enables the testing of new field methodologies that can help future design of earth structures.

The end result of the BIONICS project is to generate enough data to help the development of new or existing analytical methodologies so that the stability and serviceability of existing and future earth structures can be predicted.

4. Laboratory sample preparation methodology

4.1 Introduction

This chapter presents the methodology necessary to perform testing to describe the hydro-mechanical behaviour of the BIONICS fill material. In addition to describing the methodology utilised, the problems encountered throughout the testing programme and their solutions are also outlined.

One of the most important features of testing soils is to have good and reliable sample preparation procedures. This enables replication and confidence in the obtained results. Consideration was given to performing the testing on samples obtained from the BIONICS embankment after construction. However, the difficulty in obtaining sufficient specimens and in ensuring reproducibility between specimens precluded this approach. Therefore, dynamic (drop-hammer) compaction was adopted.

To attempt to describe the mechanical behaviour and have some understanding of the hydraulic behaviour, constant water content tests were performed in the triaxial cell apparatus. Suctions were measured during testing using high capacity suction probes.

4.2 Sample preparation

Samples were compacted using drop-hammer (dynamic) compaction to obtain densities resembling construction conditions (as will be demonstrated later). For normal compaction testing a mould of 115 mm high by 105mm diameter was used (BS 1377: Part 4, 1990). For triaxial testing, specimens with a height:diameter ratio of 2:1 are required. To attempt a better representation of

field conditions a sample size of 100mm diameter was decided on, so the sample height needed to be 200mm. The level of compaction was maintained as equivalent to BS Light (Proctor) compaction, but a 100mm diameter by 200mm high split mould was used. Therefore, the soil was compacted in 6 layers of approximately 33mm each (compared to 3 layers of 38mm for conventional compaction testing).

Table 4.1 – Compaction procedure

	BS1377-4 Light (Proctor) compaction	**BS1377-4 Heavy (Proctor) compaction**	**Compaction procedure adopted**
Height (mm)	115	115	200
Diameter (mm)	105	105	100
Nr. of blows per layer	27	27	27
Nr. of layers	3	3	6
Ram weight (kg)	2.5	4.5	2.5

Table 4.2 shows the results of compaction tests carried out in the 200mm high mould using the compactive effort described in Table 4.1. The material tested was the original material taken from the BIONICS site used without any sieving prior to testing. Repeat tests were performed for two water contents (15% and 20%). The obtained results for dry density at 15% water content for the original material show a variation of 0.075 Mg/m^3 but at the wetter level, 20%, the difference was smaller (0.016Mg/m^3).

Table 4.2 – Comparison of dry density for samples at the same water content.

	Compaction Curve BSL 200	**Repeat tests**	
Water content %	**Dry density values for different samples Mg/m^3**		
10	1.716		
13	1.721		
15	1.745	1.805	1.820
20	1.681	1.689	1.697
22	1.635		

The variation in density of 0.075 Mg/m^3 (equivalent to 4%) was thought to be too high and was attributed to the presence of larger particles. To suppress this variation in the obtained densities the material was sieved through a 2.8mm sieve to remove the larger particles corresponding to 11.5% of the total material. The results of compaction tests on this sieved material are shown in Table 4.3. Better results were obtained with a variation of 0.019Mg/m^3 (1%). Therefore, all further testing was carried out on material sieved through a 2.8mm sieve.

Table 4.3 - Comparison of dry density for sieved samples

Water content %	BSL 200 S Dry density values for different samples Mg/m^3	Repeat tests	
10	1.666		
13	1.698		
15	1.719	1.715	1.734
16	1.697		
20	1.667		
22	1.626		

The sample preparation methodology used concluded as following:

- The soil was dried to atmosphere;
- The soil was sieved through a 2.80 mm mesh to remove larger particles;
- The soil was oven drying for a minimum period of 24 hours;
- 4 bags each with 1000 g of soil were prepared, to simplify calculations for the amount of water needed;
- Water was added to achieve the desired water content;
- The bags were left to equalise for 24 hours for homogenisation of the water content within the soil;
- The soil was compacted using a drop-hammer compaction machine.

4.3 **BIONICS laboratory soil**

As noted in the previous section the original material was sieved through a 2.80mm mesh to reduce variation in density. Therefore, the material used for testing would present different behaviour to that obtained for the original material reported in Chapter 3.

The particle size distribution for the sieved soil is presented in Figure 4.1. Four particle size distribution curves were obtained. The initial part of all curves in Figure 4.1 was obtained from one test of dry sieving 3000g of material through sieves from 2.80mm down to the size of 0.063 mm sieve in accordance with BS1377 Part 2 (1990). The material passing this sieve was subjected to pipette sedimentation analysis using the pipette method. Sedimentation analysis tests were performed on four independent samples resulting in the four particle size distributions curves obtained in Figure 4.1.

Since the Atterberg limits (liquid limit, plastic limit, plasticity index and liquidity index) and specific gravity are obtained on material passing 425μm, these test results will have the same values as for the non sieved material.

Clay activity (A) for the sieved material is 1.3, calculated as PI/Clay fraction, classifying the BIONICS laboratory material according to activity as normal. When compared with the unsieved material this increase on the activity resulted from the increase in percentage of the clay material of the sieved material.

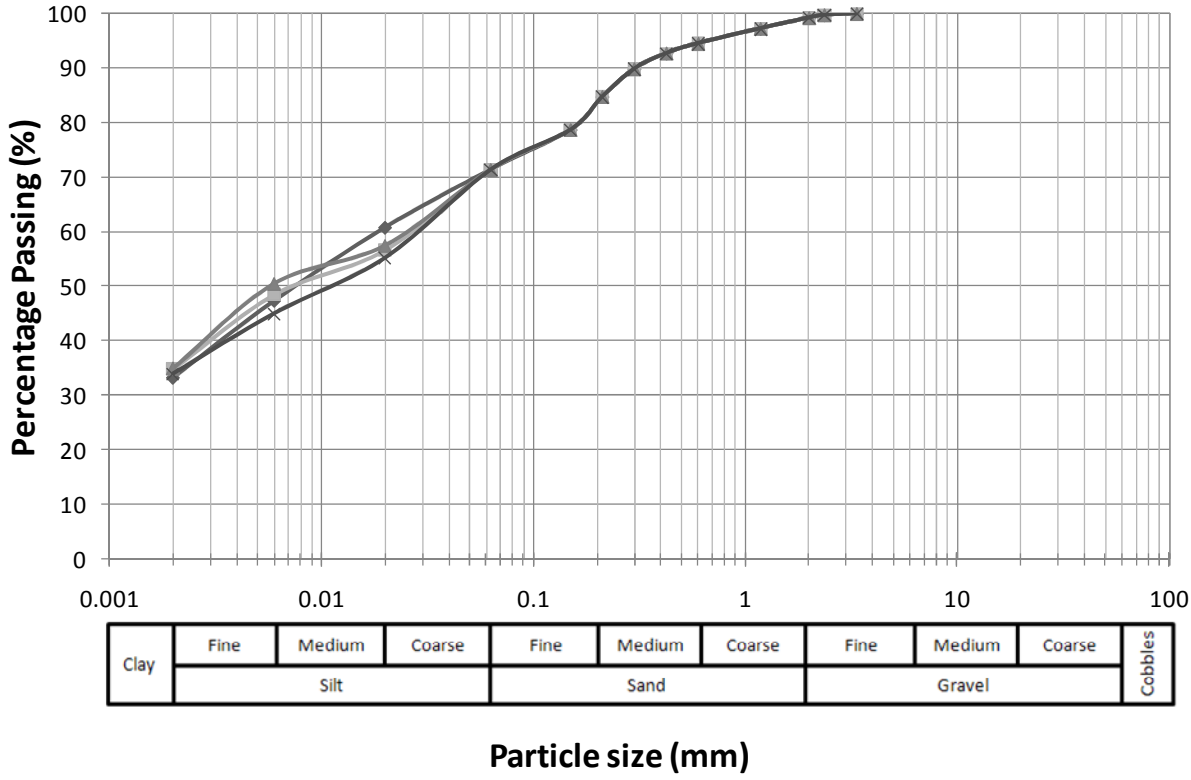

Figure 4.1 – Particle distribution curves for the sieved material.

Another change to the material is in the reference compaction curve. Different compaction curves were obtained for different samples and for different compactive efforts. Each compaction curve was labelled in accordance to the employed compactive effort followed by the height of the sample compacted. Where BS stands for British standard, L (light) or H (heavy) represents the compactive effort while the number 100 and 200 refers to the height of the sample compacted. For the compaction curve obtained for the sieved material the letter S was added at the end of the label. Compaction curves for the original material, using the BS1377 procedure (BSL100 and BSH100) and the modified procedure for the 200mm high mould (BSL200 and BSH200) are presented in Figure 4.2. A test on the sieved material is also shown (BSL200 S). A noticeable reduction in the dry density is clearly observed when comparing the compaction curves obtained for the original material (BSL200) and that obtained for the sieved material (BSL200 S). For the BSL200 S test the optimum water content and maximum dry density were W_{opt} =15% and $\gamma_{d\ max}$ = 1.719 Mg/m^3. Another

observation is the close proximity of BSL200 S with the light proctor compaction curve BSL100. In any case, the compaction curve BSL200 S was the reference compaction curve for all subsequent testing.

The compaction curves BSL200 S and BSL100 demonstrate a good comparison with measurements obtained during the construction of the BIONICS embankment (Hughes, 2005) as shown in Figure 4.3. Therefore, the sample preparation procedures lead to material of very similar density as was found to be present in the BIONICS embankment.

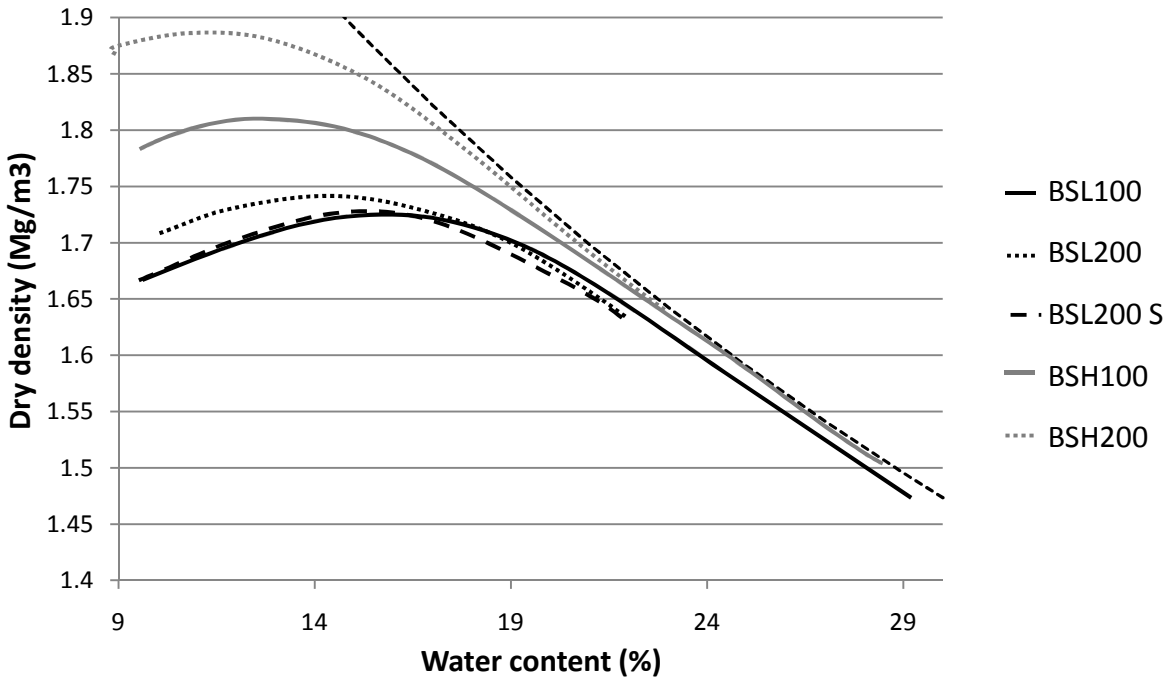

Figure 4.2 – Results obtained for the compaction curves defined

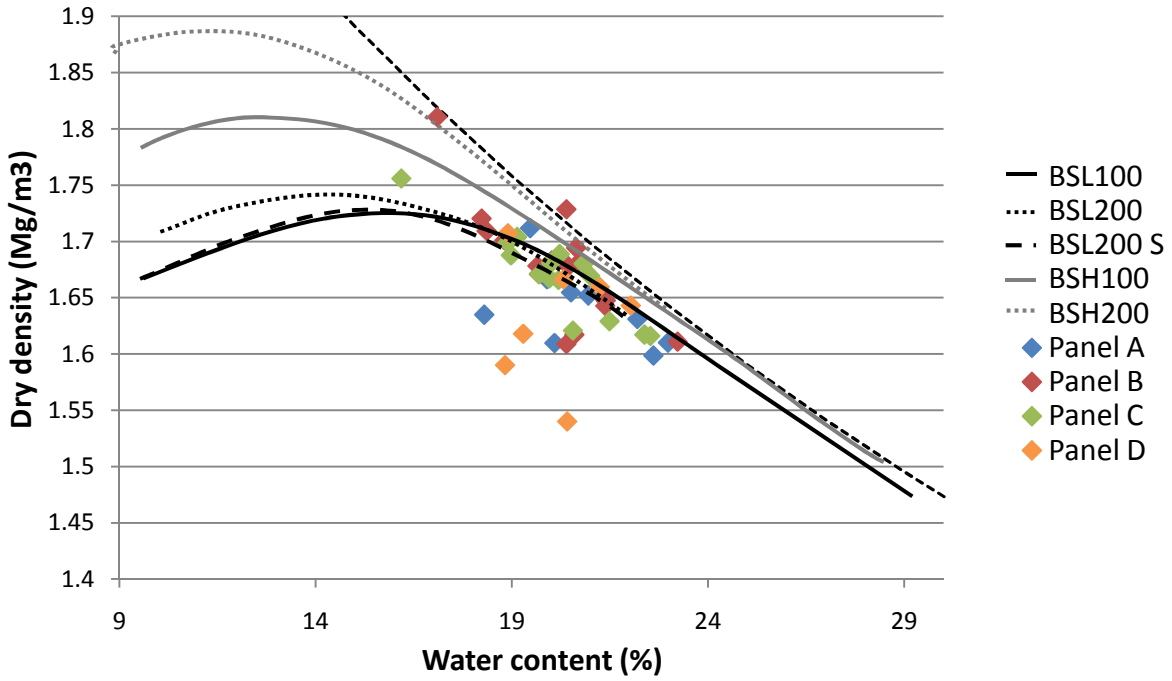

Figure 4.3 – Different compaction curves related with field measurements obtained for each panel of the BIONICS embankment.

4.4 Drying and wetting procedures

To study the performance of the soil when subjected to various climate conditions it was decided to perform constant water triaxial tests on samples with different water contents for the same initial conditions. In other words, subsequently to compaction, samples with similar water content would be subjected to drying or wetting procedures, prior to the triaxial testing, in order to replicate different climate conditions.

The drying and wetting procedures were implemented to attain precise target water content. To determine the target water content a simple calculation was preformed prior to the desired procedure:

$$m = m_d(1 + w) \quad (4.1)$$

Where, m is the total mass, m_d is the dry mass and w the water content of the sample.

After compaction the total mass ($m_{initial}$) was determined by weighting the sample on a balance while the water content ($w_{initial}$) was determined from the leftovers from the compaction. During wetting or drying the value of the dry mass remains constant while trying to achieve the target water content (w_{final}). Combining the two stages, after compaction and after drying or wetting, with the E.q. 4.1 E.q 4.2 can be obtained.

$$m_{final} = \frac{m_{initial} \times (1 + w_{final})}{(1 + w_{initial})} \quad (4.2)$$

Drying and wetting procedures were defined to achieve the target mass calculated according to Eq. 4.2.

To validate the wetting and drying procedures an assessment of the distribution of the water content throughout the sample was performed in an attempt to achieve the most homogeneous distribution. This assessment involved the determination of the water content in the vertical direction as well as in the radial direction of samples (this procedure was also implemented in the compaction curve to assure the same homogeneity in the samples as-compacted).

As soon as the sample achieved the target water content/target mass from the application of the drying or wetting procedure, some samples were sliced into six layers (layer 1 is located at the top of the sample and 6 at the bottom; see Figure 4.4). Each layer was subdivided into three radial zones: outer ring, middle ring and core (Figure 4.5). And the water content was determined for each parcel of the layer.

Four water content values were measured from the outer ring and the middle ring; only two measurements of water content were taken from the core of the layer. A total of 10 water content values are therefore measured for each layer.

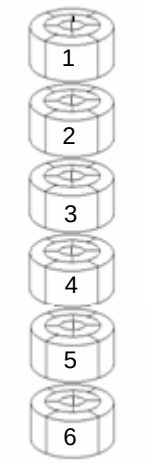

Figure 4.4 – Samples slices for vertical water content determination.

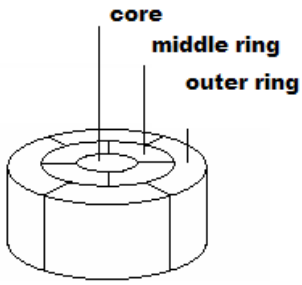

Figure 4.5 – Illustration of the zones for radial water content determination.

A typical result for a sample compacted at 20% water content is shown in Figure 4.6. The water content varied from 19% in layer 1 (top) to 20.9% for layer 6 (bottom). This shows that the water content was higher at the bottom than at the top of the sample. This is likely to be due to drying from the top (exposed) surface while compacting.

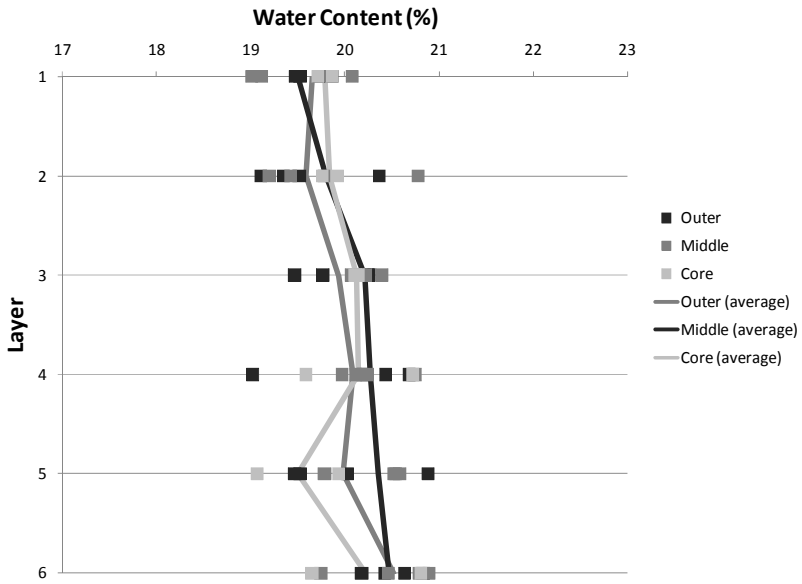

Figure 4.6 – water content distribution for a sample with 20% of water content.

4.4.1 Drying procedure

The drying procedure employed was air drying. Samples were left to dry to the atmosphere, while the sample mass was continuously measured. This was carried out inside a temperature controlled laboratory to ensure constant conditions (temperature) while drying. As soon as the sample reached the target mass (and hence target water content) it was wrapped in cling film and left to equalise. By sealing the sample and allowing a period of equalisation, the water inside the sample should distribute in a more homogeneous form. Tests were performed on different samples for various equalisation periods: 3 to 10 days.

The water content determination tests, were performed both on sieved and unsieved material. The results of these tests are summarized in Table 4.4:

Table 4.4 – Drying procedures water content results.

Compaction type	Test no.	Initial water content	Final water content after drying	Equalisation period	Final water content after equalisation	Test total duration
BSL 200	U Dry 1	20 %	13.5 %	3 days	13.5 %	10 days
BSL 200	U Dry 2	20 %	14.1 %	5 days	14.1 %	13 days
BSL 200 S	S Dry 1	20 %	14.8 %	5 days	14.8 %	13 days
BSL 200 S	S Dry 2	20 %	15.7 %	10 days	15.7 %	17 days

As explained previously in this section, the samples were left to dry to atmosphere, having initial water content around 20% and expecting to achieve a target water content value of 15%. The results presented on Table 4.4 show that the samples dried more than was needed due to poor control of the weight during the tests. However, the purpose of these tests was to find the best period of equalisation for the samples to obtain a homogeneous water content value throughout its layers (see Figure 4.4 as reference for the distribution of the layers). The lack of measurements in a radial distribution is due to the fact that it was found that the samples that were tested were too dry (brittle) to implement the core cutting, which would have destroyed the layer.

The differences in water content between U Dry 1 and U Dry 2 were due to poor control of the final weight in these two samples. They were both targeted at 15% but were dried to 13.5% and 14.1% respectively. Similarly, S Dry 1 and S Dry 2 were dried to different water contents of 14.8% and 15.7% respectively.

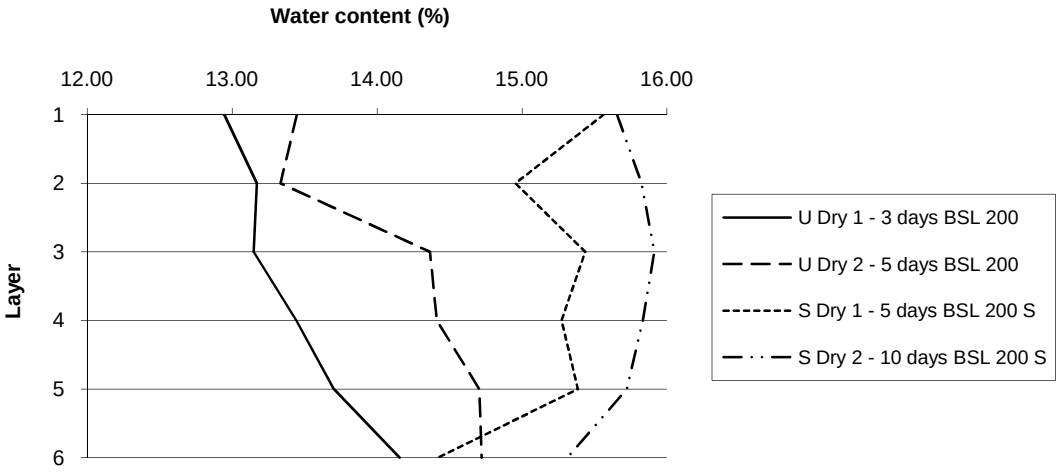

Figure 4.7 – Drying procedure: variation of water content in depth.

By observing the vertical variation of water content in Figure 4.7, the more homogeneous water content distribution encountered was for the sample S Dry 2 with an equalisation period of 10 days.

4.4.2 Wetting procedure

The procedure to increase the water content within the sample is a more laborious system when compared to the drying procedure. A system was developed that could wet the samples homogeneously and uniformly by using mini-foggers.

Mini-foggers are used to create mist on top of small pounds as a gardening bedazzlement product. The creation of finer particles of water suspended in the air is derived from the cavitation of water through ultrasounds without causing temperature changes, this is ideal for wetting soil

samples. By surrounding a sample in a mist the absorption of water will be homogeneous increasing its water content in a continuum.

A humidifying chamber was built to accommodate the mini-foggers; the scheme is shown in Figure 4.8.

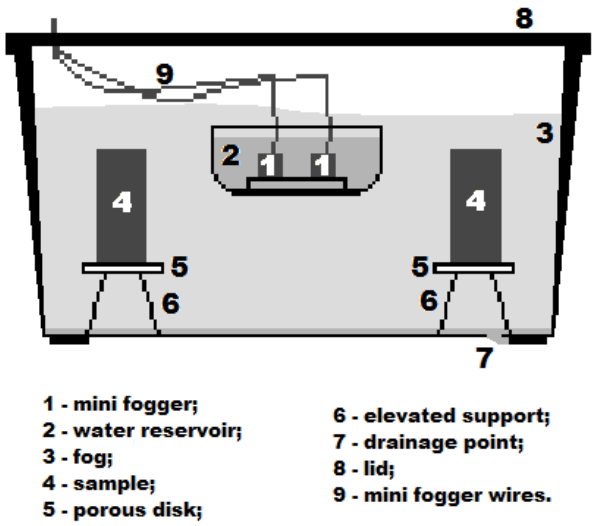

Figure 4.8 – Scheme of the humidification chamber.

The chamber was a plastic box and the mini-foggers were positioned inside a water reservoir positioned at a higher level than the samples. The fog descends around the reservoir and by constantly flowing mist from the reservoir it fills the chamber, see Figure 4.9. The samples were placed on a porous disc which served as a pedestal to avoid absorption of accumulated water from the bottom of the chamber. The weight of samples was checked regularly to achieve the desired water content.

By not causing a significant increase of heat inside the chamber and by creating a homogeneous distribution of water around the sample this system was adopted as the wetting procedure. The only disadvantage on using mini-foggers is that it is time consuming for wetting to

take place, requiring between two to four weeks to achieve the desired water content for the sample (the higher the desired water content the longer the wetting time).

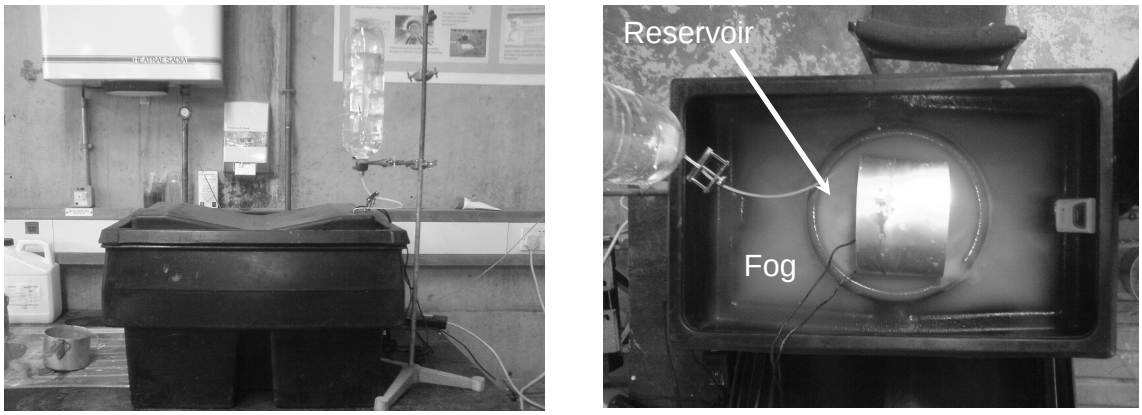

Figure 4.9 – Humidification chamber.

Even with this procedure the distribution of water within the sample could still be uneven, with more present at the outskirts of the sample than in the core. Therefore, after wetting, the samples were wrapped in cling film and left to equalise. To validate this procedure, and to chose the best equalisation period, samples were compacted with a initial water content value close to 15% and were humidified/wetted until the desired water content was reached – in this case 20%. Tests were performed on sieved and unsieved material. The obtained results are summarized in Table 4.5.

Table 4.5 – Wetting procedure water content results.

Compaction type	Test no.	Initial water content	Calculated water content after humidification	Equalisation period	Final average water content after equalisation
BSL 200	U Wet 1	15 %	20 %	1 week	20.4 %
BSL 200	U Wet 2	15 %	20 %	2 weeks	19.8 %
BSL 200	U Wet 3	15 %	22 %	2 weeks	19.1 %
BSL 200 S	S Wet 1	15 %	20 %	2 weeks	19.1 %
BSL 200 S	S Wet 2	15 %	20 %	3 weeks	20.1 %

For the unsieved material (U) two types of tests were carried out:

- Direct humidification, where the sample was humidified to a final water content of 20% (U Wet 1 to 2);

- Overshooting, where the sample was humidified to a higher water content than was required for the test and then allowed to dry back to the intended value of 20% (U Wet 3 to 4).

For sieved material (S) only one type of test was carried out where the sample was humidified to a final water content of 20% (S Wet 1 and 2);

Figure 4.10 shows the results for one week of equalisation, where it can be seen that the scatter in the water content for test U Wet 1 is as large as 6% for the radial variation and 10% in the vertical variation of the water content.

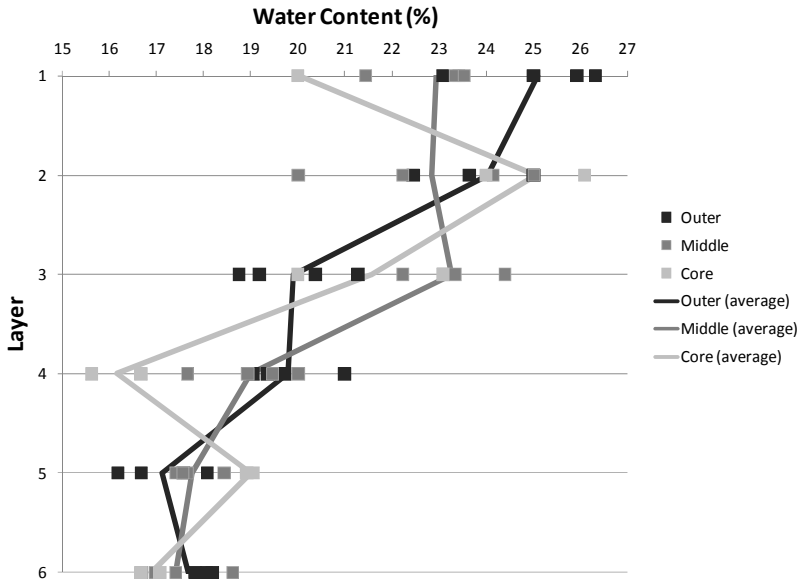

Figure 4.10 – Water content (vertical and radial) scattering after one week of equalisation for test U Wet 1(for layer position see Figure 4.4).

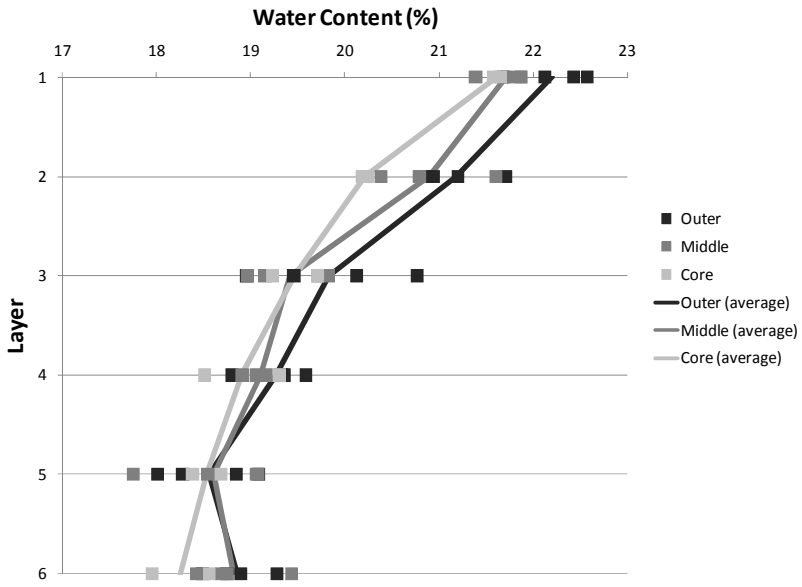

Figure 4.11 – Water content (vertical and radial) scattering after two weeks of equalisation for test U Wet 2(for layer position see Figure 4.4).

By increasing the equalisation time to two weeks the water content tends to be more homogeneous reducing the vertical - 4.5% - and radial – close to 2% - scattering of values (see Figure 4.11). From both Figures 4.10 and 4.11 it can be clearly observed the influence of the time allowed for the samples to equalise, reducing close to 4% for both vertical and radial distribution of water content.

The use of sieved material, test S Wet 1, reduced the scattering even more, decreasing to 3% in the vertical variation of water content and less than 2% in the radial variation on the water content (see Figure 4.12).

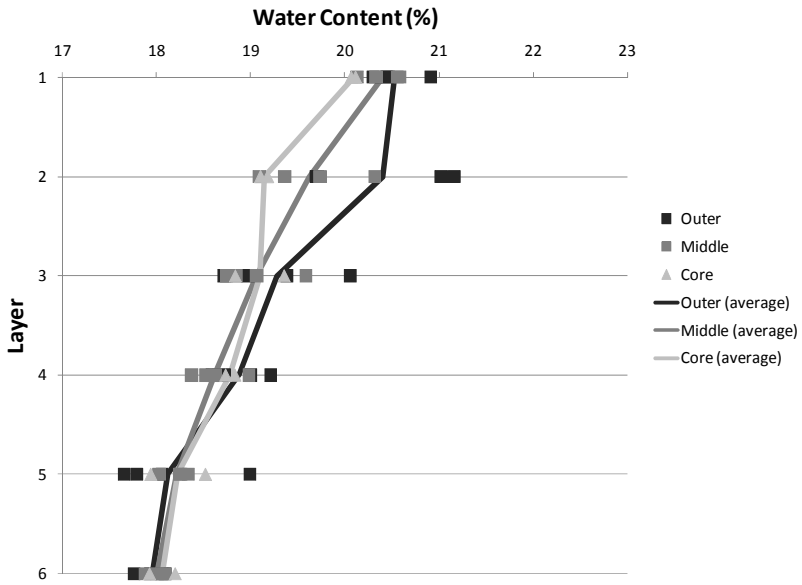

Figure 4.12 – Water content (vertical and radial) scattering for two weeks of equalisation for sieved material, test S Wet 1.

Besides the improvement obtained by increasing the equalisation time an attempt to further improve the distribution was performed by overshooting the target water content followed by drying with the intention of reducing the difference between core and outer ring. In all previous tests the core tended to be more dried. But also, to achieve a better vertical distribution where in all previous cases the tendency was to have a wetter top and drier bottom. Figure 4.13 present such test, U Wet 3, in which it was used the same equalisation time of 2 weeks.

Overshooting the water content appears to give better results than only leaving the material to equalise directly for two weeks. Although the scattering in water content, in both directions, is lower (see Figure 4.13) when overshooting takes place (suggesting a more homogeneous sample in water content throughout the sample), sample characteristics change, most importantly the fabric. By allowing the sample to absorb more water, the clay particles, in particularly, tend to increase in size which leads to a certain arrangement of the particles inside the sample, also altering the size of the voids. While drying the sample, afterwards, the opposite takes

place evolving in a new rearrangement. Considering the activity of the clay particles of the sample used in this work classified as normal, some uncertainties are present making it impossible to assure that using these samples would provide appropriate results.

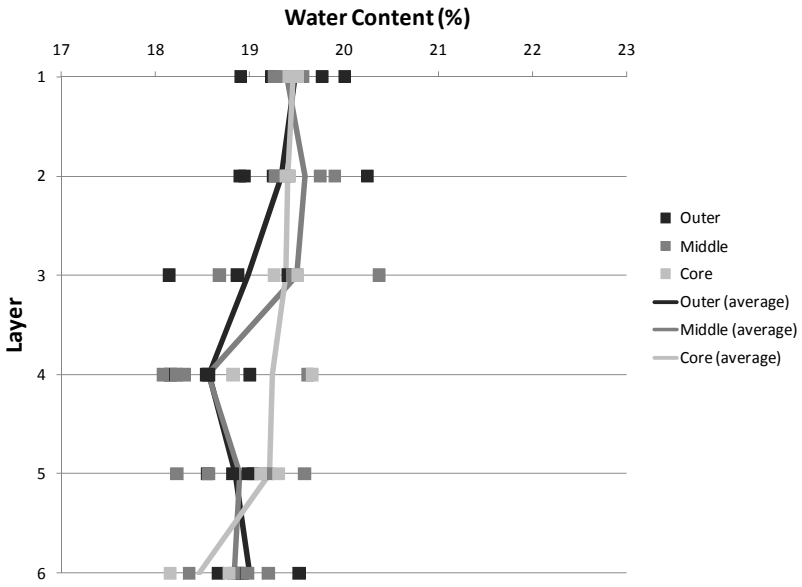

Figure 4.13 – Water content (vertical and radial) scattering for two weeks of equalisation with overshooting the water content value, test U Wet 3.

Since the overshooting of the target water content was considered to be inappropriate to produce reliable results the only option to improve the quality of the samples regarding the distribution of the water content was to increase the equalisation period, hence test S Wet 2. When allowing a period of equalisation of 3 weeks the water content distribution (Figure 4.14) presented a much lower scatter. In comparison with Figure 4.6 and 4.13 the distribution is very similar presenting a variation of at most 2% vertically and 1% horizontally. The sample still presented a drier bottom than the top; however, it was considered that extending the equalisation period would present some problems with the following testing. Notice that the total time from preparation and compaction until the point where the sample would be placed in a triaxial cell for testing would take already 1.5 months.

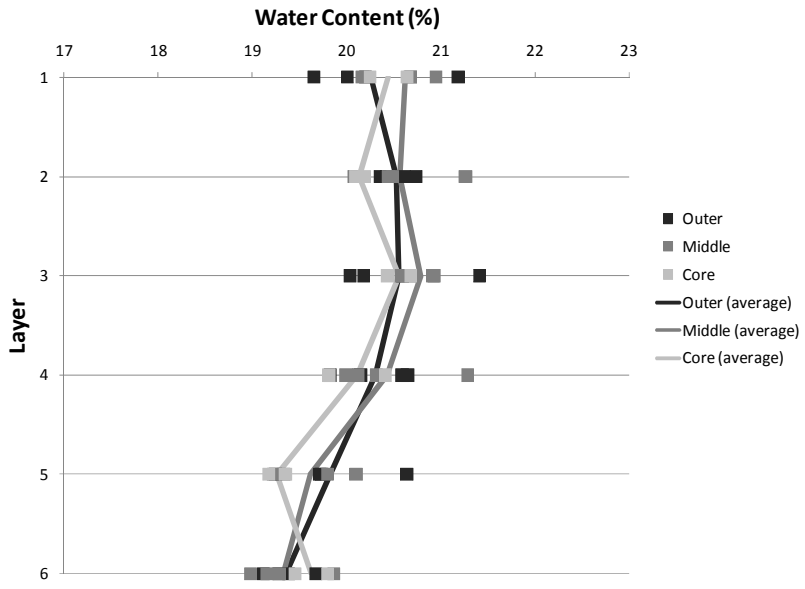

Figure 4.14 – Water content (vertical and radial) scattering for three weeks of equalisation for the sieved material, test S Wet 2.

From the homogeneity of the water content through the sample achieved the equalisation period selected was 3 weeks.

In all tests there is a noticeable decrease in water content with depth. This observed result could be due to the sample preparation methodology followed. During compaction, the sample was compacted in layers, as explained in section 4.2 in this Chapter. By doing so, the level of compaction can increase with depth, as a result of the additional energy transfer during the compaction of the subsequent layers. Therefore, the bottom layer may achieve a slightly greater level of compaction than the top layer. This could result in slightly different fabrics with depth, in which the bottom layer (being more compacted) would have less void space in comparison with the top layers. This difference between the layers could condition the retention behaviour resulting in the observed differences in water content with depth during wetting.

4.5 **Conclusions**

A successful sample preparation procedure was achieved that allowed replication of samples with same dry density for the same water content. However, to achieve it the maximum particle size of the soil was reduced by sieving through a 2.8 mm grid. The sieved material was classified as a sandy clay material.

Good agreement was observed between the densities obtained in the laboratory (using BS light (Proctor) compaction applied to 200mm high and 100mm diameter specimens) with the values obtained from field measurements.

Drying and wetting processes were developed from as compacted conditions and was assessed. Water content distribution after these processes was shown to be reasonably similar throughout the full size sample tested, but largely dependent on the equalisation time period.

5 Soil Water Retention Curve determination for the BIONICS fill material

5.1 Introduction

In unsaturated soils, a key factor in the study of the pore water pressure generated in the soil is the Soil Water Retention Curve (SWRC). The SWRC can be determined by an array of different techniques as presented in the literature review (Chapter 2). SWRCs were obtained in terms of total and matric suction for specimens of the BIONICS soil (using the modified grading used for other laboratory tests).

It is known that SWRC presents hysteric behaviour, meaning the SWRC obtained will be different depending on the path chosen to obtain the curve (drying or wetting). To obtain the primary drying branch of the SWRC, the initial conditions must be a fully saturated sample; otherwise, for samples starting from an unsaturated condition, the curve obtained will be on what is called a scanning curve (representing a state between the primary drying curve and primary wetting curve).

The initial part of this chapter presents experimental work on samples that were initially saturated. These tests were carried out by other authors, namely Sérgio Lourenço, a former PhD student and Teiko Noguchi, a former MEng student, both of Durham University. Sections 5.2-5.4 are based on the work of Noguchi (2009) who worked with the author on the

determination of the SWRC following a drying path using different techniques. Further results by Lourenço (2008) are also referred to in these sections. Section 5.5 reports results obtained by the author on samples from different initial compaction water contents. Tests were performed to determine both drying and wetting curves from different initial compaction conditions.

5.2 Measurement techniques of soil suction

5.2.1 Transistor Psychrometer

A 12-probe transistor psychrometer was used to obtain the SWRC for total suction. The device was the heavily-insulated laboratory model manufactured by Soil Mechanics Instrumentation (SMI) (Figure 5.1). The SMI psychrometer in Durham University's Civil Engineering Laboratory was positioned inside a temperature controlled room, since the equipment is very sensitive to temperature changes. As stated in the manual of the SMI psychrometer the temperature differences should be no more than 1ºC during the test duration. Even though the device was positioned inside the temperature controlled room and had internal insulation, an insulation chamber was also used to assure even better temperature control. The insulation chamber was custom built in the School of Engineering Mechanical Workshop. The custom built chamber was constructed to fit the dimensions of the

12-probe SMI psychrometer with insulation provided by a layer of polystyrene 15 cm thick all around the equipment enhanced by the wooden box (1cm thick), see Figure 5.1. An insulated lid to cover the box was also provided, with the same thickness of insulation.

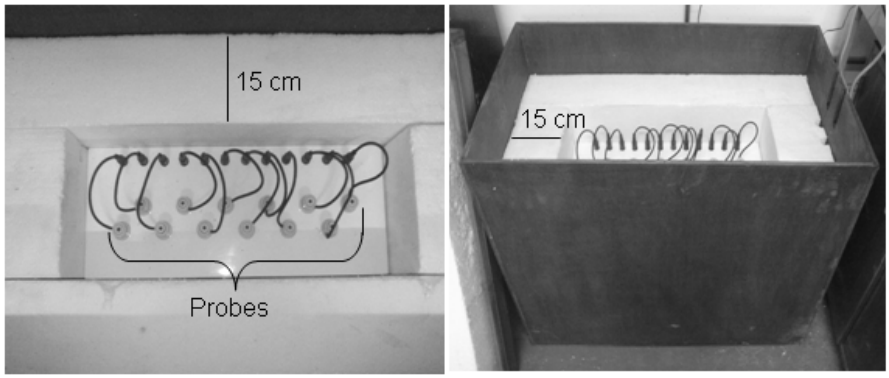

Figure 5.1 - Photos of the 12-probe transistor psychrometer heavily-insulated with polystyrene.

5.2.1.1 Calibration

The transistor psychrometer was calibrated before any soil suction measurements were taken following the procedure stated in the SMI Manual for the 12-probe Transistor Psychrometer (SMI, 2004). The psychrometer was stabilized overnight using filter papers saturated with distilled water, in order to produce a relative humidity of 100% inside the probes (which corresponds to total suction of 0kPa). A trimming potentiometer was used in the probe head to zero the probe outputs. The calibration of the probes was done using filter papers saturated with standard salt solutions; these were prepared with appropriate

concentrations to give equivalent relative humidity, ranging from 10 kPa to 10000 kPa. After calibrating the probes, they were cleaned with distilled water to avoid any contamination to the probe tips; also, for the same reasons, the water drop of the wet transistor was replaced. To ensure the calibration had been carried out correctly, the calibration tests were repeated three times and any unreliable results were ignored. Figure 5.2 presents an example of a set of calibration tests conducted for probe 1.

The calibration curve of log (kPa) versus log (mV) was produced for each probe using the output values. Figure 5.3 presents the calibration data obtained for probe1: not much difference was observed in the output voltage between total suctions of 10kPa and 100kPa. A similar trend was observed for the remaining probes, indicating that using the transistor psychrometer to obtain accurate measurements of total suction below about 100kPa would be difficult. Therefore, the calibration line was produced using data obtained from 100kPa to 10000kPa suction solutions (Figure 5.4) and the transistor psychrometer was used to determine the total suction above 100kPa. From the twelve probes of the SMI Psychrometer, only ten of them were found to been working properly (probe 8 and 11 were not functioning).

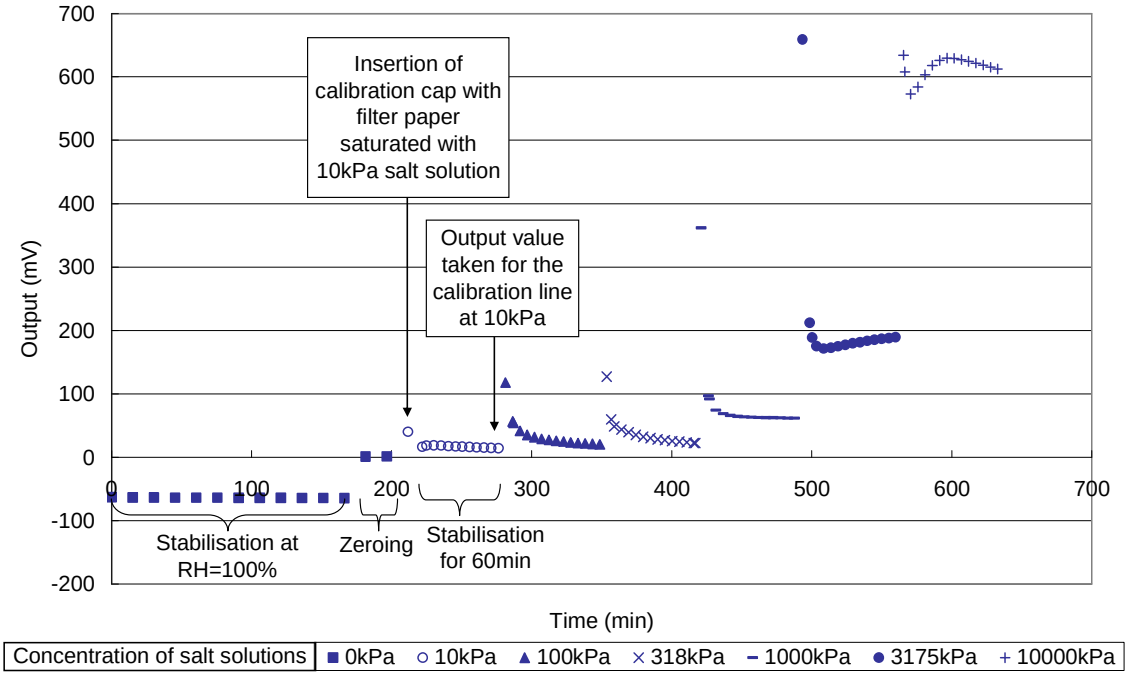

Figure 5.2 – Sequence of calibration tests showing the results for probe 1 (after Noguchi, 2009).

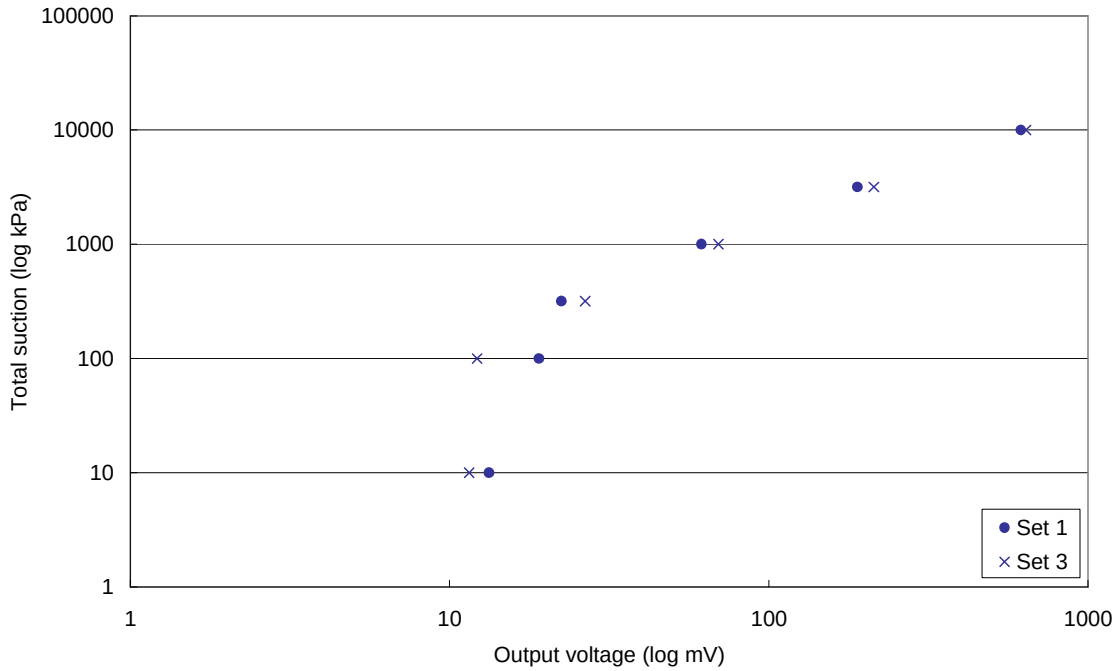

Figure 5.3 – Calibration data obtained for the probe 1 (after Noguchi, 2009).

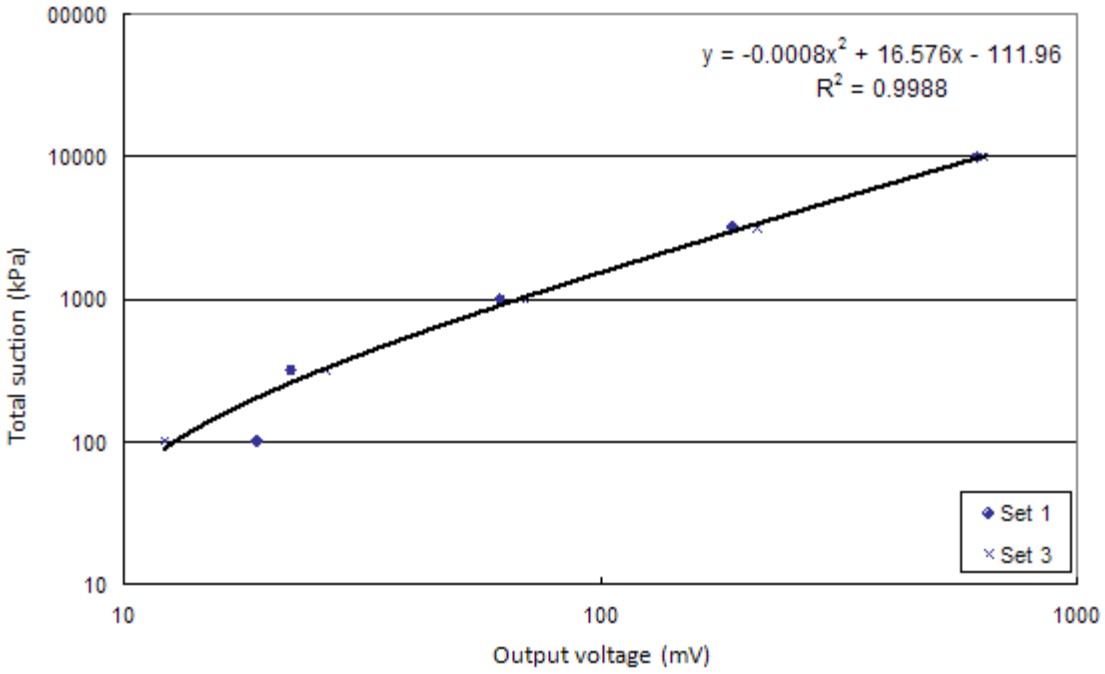

Figure 5.4 – Calibration curve determined for the probe 1 (after Noguchi, 2009).

5.2.1.2 Measurement of Soil Suction

Disc samples were taken from BIONICS soil samples. The samples were prepared as in Chapter 4, by compacting at gravimetric water content of 25%, and sliced to a thickness of 16mm and a diameter of 100mm. The samples were left to air dry to obtain five different gravimetric water contents (25%, 20%, 15%, 10% and 5%). From each disc sample, sub-samples were cut using standard 35mm long, 15mm diameter sampling tubes. For soft samples (the ones with higher water contents) a more cautious approach was used, where, the sampling tube was placed on top of the disc sample and pushed carefully into it so to produce a sub-sample inside the sampling tube. The end plug was then carefully pushed into the end of the

psychromer sampling cup.

After stabilizing and zeroing the psychrometer, the sampling cups were placed on the end of the probes, sealed with electric tape, and quickly replaced into the insulated container. The psychrometer was allowed to equalize for one hour while the data logger was set to take output readings every 5 minutes. After one hour of equalization, calibration curves for the soil samples were used to determine the total suction of the soil. Soil samples were then removed for water content measurement and the next set of sample was placed on the probes. Two sets of measurements were undertaken for each water content value. The detailed procedures of the soil suction measurement are described in SMI (2004).

5.2.2 Filter Paper

The filter paper method used originates from the technique by Bulut et al (2001). The BIONICS soil sample prepared as described in chapter 4 at a gravimetric water content of 25% was sliced to form sub-samples of 25mm thickness and these were air dried to the atmosphere until they reached the desired gravimetric water contents of 25%, 20%, 15%, 10%, and 5%. The sub-samples were then trimmed to smaller discs of 55mm diameter and 20mm thickness (diameter to match the Whatman 42 filter paper dimensions). Each set of soil suction measurements followed the arrangement shown in Figure 5.5: two of the small discs from sub-

samples at the same water content were placed on top of each other and a sandwich of 3 Whatman 42 filter papers was placed in between, with the middle filter paper of this sandwich (in-contact filter paper) being used to measure matric suction.

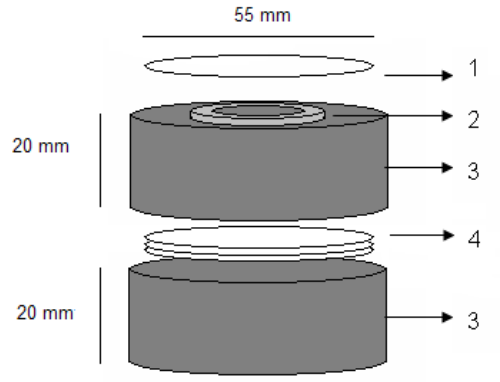

1. Non-contact filter paper for total suction measurement
2. PCV ring to avoid contact between non-contact filter paper and sample
3. Soil sample
4. In-contact filter paper for matric suction measurement (one filter paper in between two protective filter papers)

Figure 5.5 – Arrangement of filter papers and samples for the filter paper technique.

Electrical tape was used to tape together this set of disc samples with filter papers in between. Another Whatman 42 paper filter (non-contact) was used to measure total suction. In order to ensure that this non-contact filter paper was kept completely separate from the soil sample, a 10mm high PVC ring was used between the soil sample and the paper filter. This set was then placed in a glass jar, which was quickly closed, and its lid was also taped with electrical tape. Four layers of cling film were used to wrap the jar and, finally, the glass jar was coated in paraffin wax so to prevent exchanges of air. Three of these sets were prepared for each water content value.

The jar was allowed to equalize in a water bath at 25ºC for a period of 14 days,; after this period, the paraffin wax and the cling film layers were removed and the filter papers and soil samples were weighted as quickly as possible to an accuracy of 0.0001g. Afterwards, the filter papers and soil samples were oven-dried, which allowed a calculation of their water content and the determination of the corresponding suction (using an appropriate calibration equation).

5.2.3 Pressure Plate

The pressure plate apparatus used in this study was a 1500kPa range Soil Moisture Corp. pressure chamber in the configuration of Figure 2.6. Modifications to the original set up were carried out to allow independent multi sample testing (up to 4) by the substitution of the original porous ceramic disc with 4 independent ceramic discs with an air entry value similar to the original disc (1500 kPa), each of them connected to a different volume gauge (replacing the burette). As in Figure 2.6, the air supply was provided by nitrogen bottles instead of the laboratory air-compressor, allowing the possibility of imposing higher air pressures within the chamber. Before testing, the ceramic discs were saturated. This procedure is crucial for this testing technique, since for reliable measurements all air bubbles must be removed from ceramic discs. The saturation procedure adopted was as follows: the ceramic discs were placed inside the pressure plate apparatus submerged in deaired water (the deaired water level was

2cm above the discs). After tightly fastening the lid of the pressure plate, air pressure was increased slightly in steps to push water through the discs. This procedure lasted until no air bubbles were observed emerging from the discs. This procedure was performed prior to any testing carried out in the pressure plate apparatus.

The BIONICS sample prepared as outlined in Chapter 4 was sliced to a thickness of 20 mm and trimmed to a diameter of 75 mm. The sample was then placed on the saturated porous ceramic plate in a 1500kPa range Soil Moisture Corp. pressure chamber, ensuring an intimate contact between the sample and the plate. The chamber was filled with water to a shallow depth (below the ceramic plate) in order to humidify the air inside the chamber, to avoid excess drying of the sample. The chamber was tightly fastened; air pressure was applied inside the chamber and water pressure was applied underneath the plate to impose the desired value of matric suction on the sample (the difference between air and water pressure). Pressure was applied to the water reservoir underneath the plate through a volume gauge to measure the volume of water flowing in or out of the specimen as the suction was changed. Applying pressure to the water reservoir had the advantage of preventing dissolved air from coming out of the solution after passing through the ceramic plate; since a high air pressure is applied in the chamber, water passing through the ceramic plate has a high amount of dissolved air which, if no pressure is applied underneath the ceramic plate, might come out of

the solution and cause interruption of the water flow. In this case, applying pressure on the water reservoir prevents a misleading reading of the water volume change in the gauge. The volume change measured by the gauge is a function of both the volume changes due to air diffusion and water flow throughout the ceramic plate. In some cases, the air diffusion rate of the porous ceramic plate is negligible, but sometimes it can be significant enough to influence the resulting SWRC (Vaquero, 2007); although theoretical predictions of the volume of diffused air have been attempted, the many factors affecting the diffusion rates make them unreliable (Fredlund and Rahardjo, 1993). Identifying the air diffusion rate through the ceramic plate is then advisable (especially when the volume gauge measurement is the only process available to determine water volume change of a soil sample) in order to correct the measurements of volume change in the gauge.

A PC equipped with the TRIAX data acquisition software (Toll, 1999) was used for monitoring the volume change in the gauge and the pressures applied, logging the data every 30 minutes (during the experimental period). When the volume change read by the gauge was less than 0.35cc/day, the sample was considered to have reached equalization (Vaquero, 2007). After equalization, the sample was taken out of the pressure chamber and measured: weight was measured to the nearest 0.01g and dimensions were measured with an accuracy of 0.01mm using vernier callipers.

After the measurements were taken, the soil sample was placed back on the plate and the process was repeated for increasing pressures. The highest suction imposed was 1100 kPa, corresponding to an air pressure application of 1310 kPa and an applied water pressure of 210 kPa. When the experiment was finished, the soil sample was oven-dried to determine dry mass, and the water content of the sample at different suction stages was back calculated.

5.2.4 DU-WF High capacity suction probe

5.2.4.1 Continuous Drying

The soil sample prepared was sliced and trimmed to a 20 mm thick sub-sample of 75mm of diameter. The continuous drying apparatus was set up as shown in Figure 5.6.

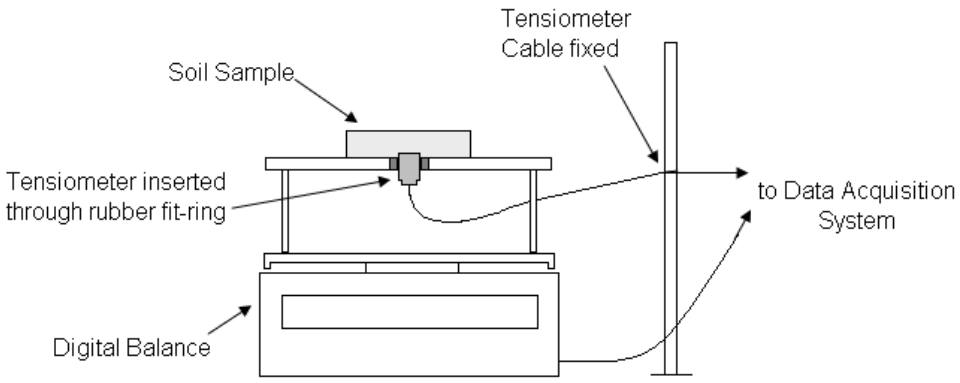

Figure 5.6 – Experimental setup for the continuous drying test (after Noguchi, 2009).

A high capacity suction probe was inserted through a support plate, from below, through a rubber O-ring. The soil sub-sample was placed on the support plate, and an intimate

contact between the sample and the high capacity suction probe was ensured, with the suction probe being gently pushed into the sample to an approximate depth of 2mm. This whole setup was placed upon a digital weighting scale and connected to a PC with TRIAX software; in order to minimize the influence of the suction probe cable on the weighing, its cable was fixed on a support (Lourenço, 2008). TRIAX software was set to take output readings every 10 minutes. The sample was left to dry to the atmosphere – during this time, the high capacity suction probe continuously read the matric suction and the digital weighting scale measured the change in the total mass (which represented the water loss from the sample). The mass measurement was later used to back calculate the soil water content throughout the test.

5.2.4.2 Stage Drying

The soil sub-sample was prepared in the same way as the ones for continuous drying. However, in stage drying, after each stage of drying the suction measurement was taken after the sub-sample was sealed inside a confined chamber to ensure the suction had equalised throughout the specimen. The sub-sample was air dried to the desired water content and equalized, for a period of 24 hours, inside the confined container used for the measurement (with 20mm by 100mm of diameter). A high capacity suction probe was inserted through the rubber O-ring at the bottom of the container so that the sample rested on it by its own weight.

In order to overcome situations when the sample was dried and hardened (and, therefore, an intimate contact was difficult to attain), a thin film of water was applied on the face of the high capacity suction probe before inserting it. The suction probe read the suction until equalization was observed. The sample was then taken out of the confined container and allowed to dry again, so the procedure was repeated for successive different water contents. The test was carried out in a temperature control room.

5.3 SWRCs obtained by the different methodologies

5.3.1 Transistor Psychrometer

The total suction SWRC determined by Noguchi (2009) using the transistor psychrometer technique is shown in Figure 5.7. For each probe, the corresponding calibration curve was used to determine the total suction from the output voltage measured. Suction values below 100kPa were discarded (since the psychrometer showed no reliability in measurements of suction below that value) and the calibration curves were developed for suctions between 100kPa and 10000kPa. Even so, a considerable scatter of results is still observable. Up to 500kPa suction, the scattering of the SWRC corresponds to values from 15% to 25% of gravimetric water content.

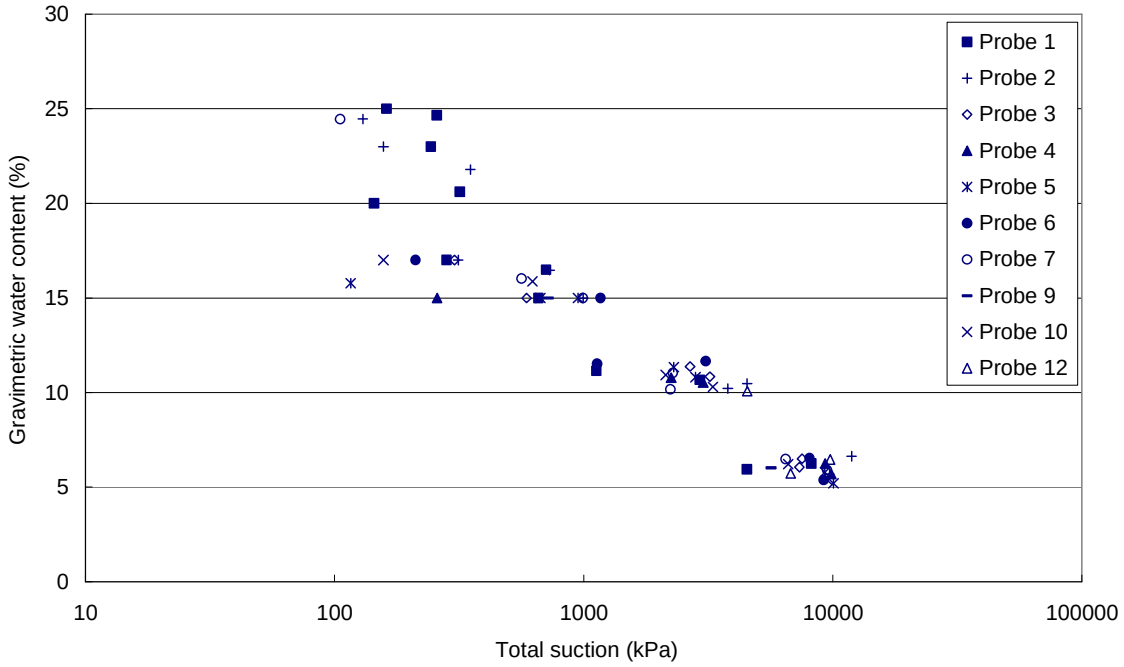

Figure 5.7 – Total suction WRC determined using the psychrometer (after Noguchi, 2009).

5.3.2 Filter Paper

The relationship between the water contents of the filter paper and the corresponding soil sample at the end of the 14-day equalization period is shown in Figure 5.8. For the in-contact filter paper, the moisture flow is via liquid transfer whereas for the non-contact filter paper the moisture flow is via vapour transfer (Noguchi, 2009). The water content of the in-contact filter paper (which is measuring the matric suction) is, therefore, much higher than the water content of the non-contact filter paper (which is measuring the total suction). However, below a gravimetric content of 11%, there is no significant difference between the water contents of in-contact and non-contact filter papers. This suggests that, below this value, the

samples are so dry that there is no continuous water path between the soil samples and the in-contact filter paper (so most of the moisture flow occurs via vapour transfer rather than liquid transfer). Leong et al (2002) also state that beyond 1000 kPa suction the filter paper measures only total suction, regardless of whether the filter paper is in-contact or non-contact.

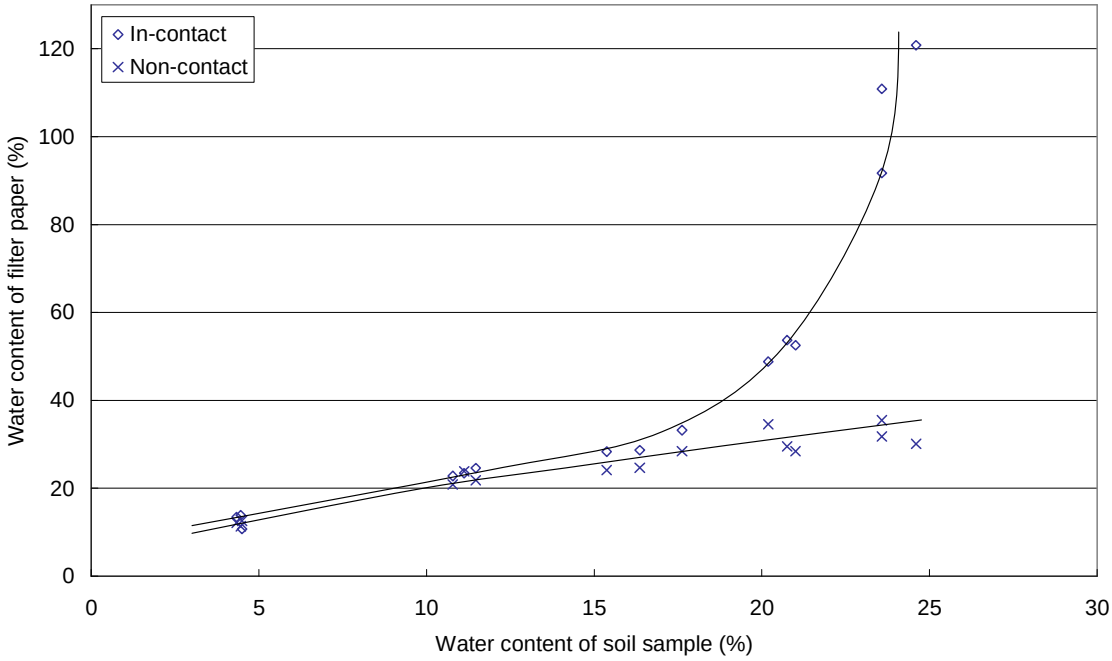

Figure 5.8 – Water contents of filter papers and corresponding soil samples at the end of equalisation period (after Noguchi, 2009).

The SWRCs were determined using three different calibration equations for the Whatman 42 filter paper suggested by different authors, all of which are presented below.

- van Genuchten (1980) :

$$\Psi = 0.051 \times \left[\left(\frac{248}{w_f} \right)^{9.615} - 1 \right]^{0.473}$$ (5.1 – for matric suction)

$$\Psi = 56180 \times \left[\left(\frac{37}{w_f} \right)^{0.44} - 1 \right]^{2.361}$$ (5.2 – for total suction)

- Hamblin (1981):

$$\log \Psi = 8.022 - 3.683 \log w_f$$ (5.3)

- Leong et al (2002):

$$\log \Psi = 2.909 - 0.0229\, w_f \qquad w_f \geq 47$$ (5.4.a)

$$\log \Psi = 4.945 - 0.0673\, w_f \qquad w_f < 47$$ (5.4.b)

In all of these equations, Ψ represents the soil suction (kPa), $\log \Psi$ is the logarithm of the soil suction (base 10) and w_f is the filter paper water content in percentage.

Some authors state that the calibration equations for both total and matric suction should be given by different equations. However, other studies suggest that if, during total suction measurement, the filter paper is allowed to equalize fully, then the matric suction calibration equation is valid for total suction determinations, which means there is no need for separate equations for total and matric suction determinations (Marinho, 2004, Stenke et al 2006). Therefore the matric suction calibration equations (Equation 5.4.a and 5.4.b) were

applied to both total and matric suction determinations in this study. The total and matric suction SWRCs determined using the calibration equations mentioned above are shown in Figure 5.9 and 5.10 respectively. The comparison between the total and matric suction SWRCs can be seen in Figure 5.11 (taking Hamblin equation as an example). Figure 5.11 shows that below a gravimetric water content of 11% (beyond about 1000kPa suction) the total and matric suction SWRCs come together (as also observed in Figure 5.8).

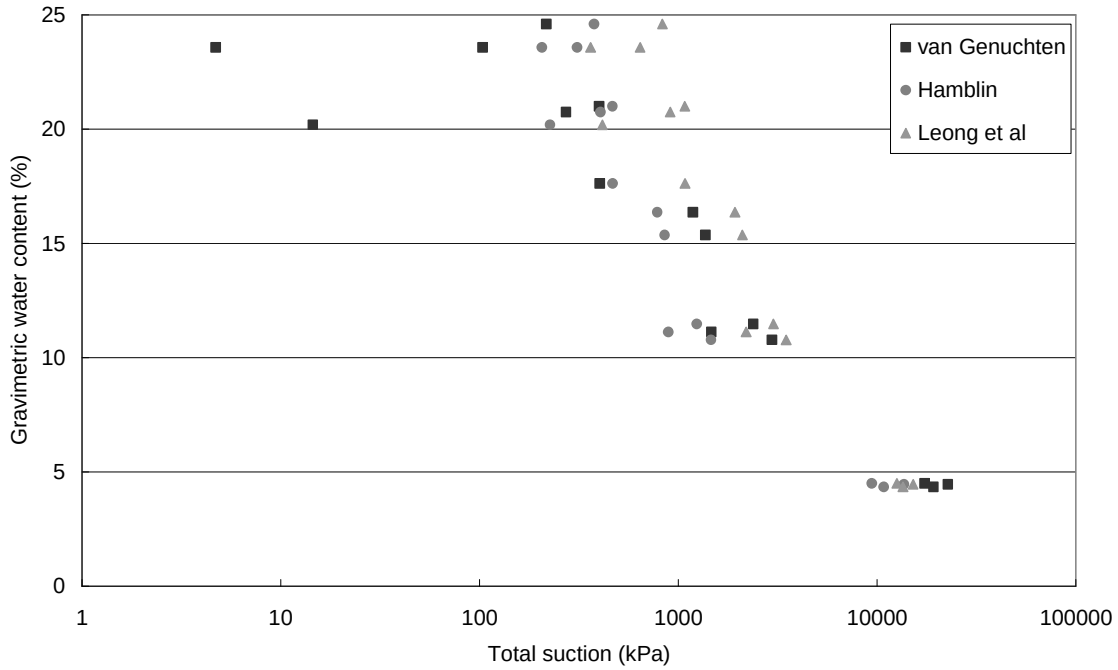

Figure 5.9 – Total suction SWRCs determined using the filter paper (after Noguchi, 2009).

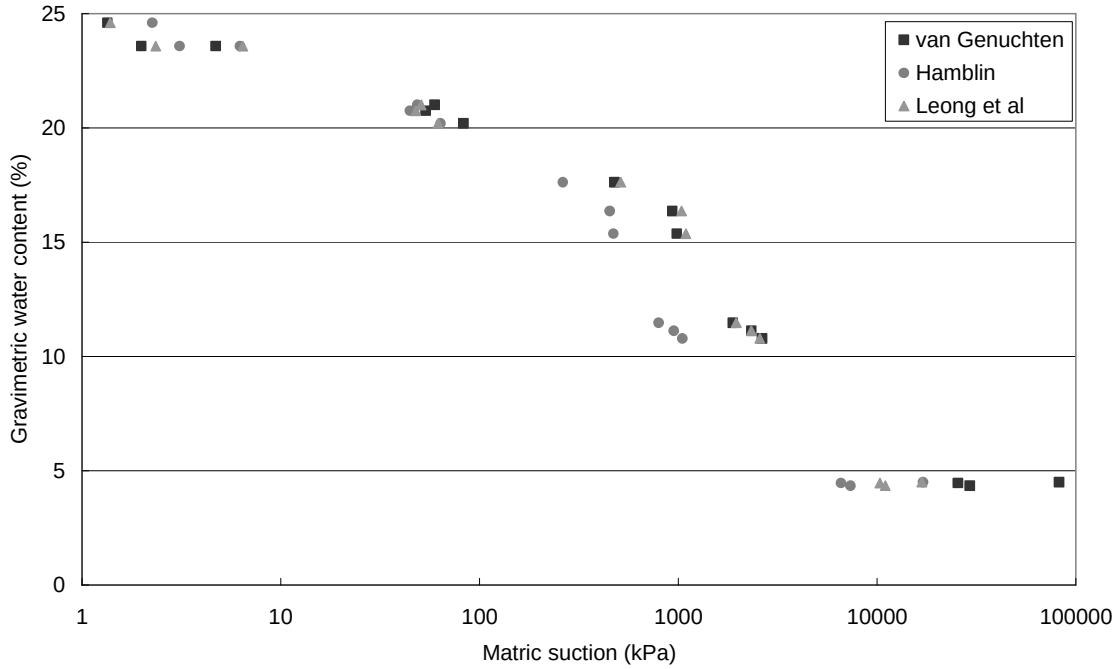

Figure 5.10 – Matric suction SWRCs determined using the filter paper (after Noguchi, 2009)

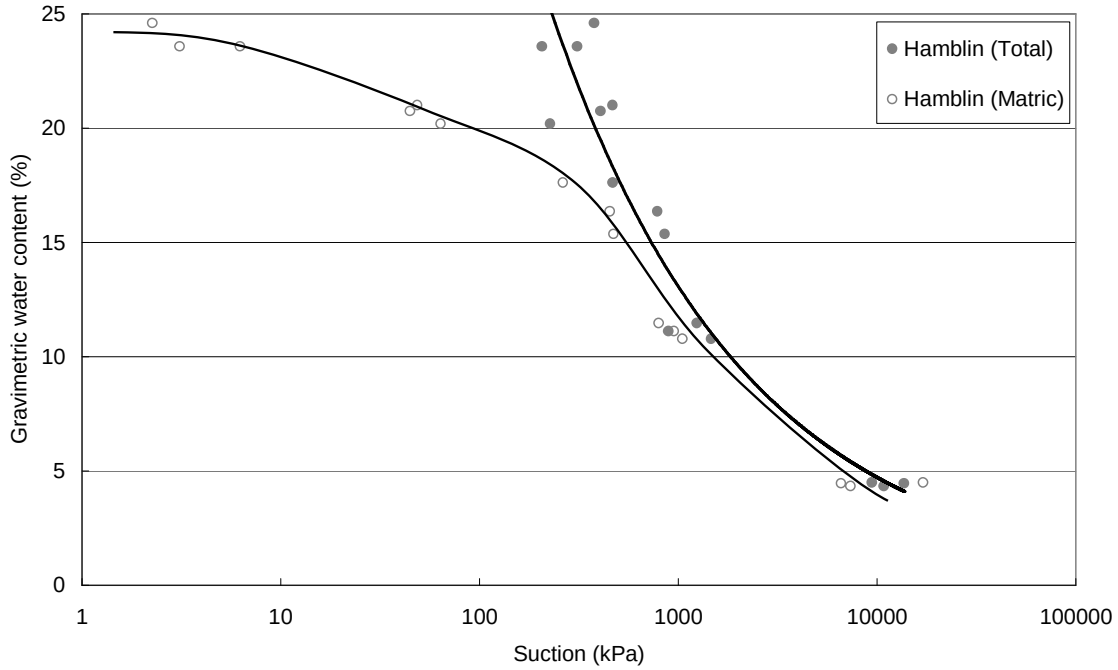

Figure 5.11 – Comparison between the total and matric suction SWRCs determined using the filter paper (after, Noguchi 2009).

In Figure 5.11 different values for total and matric suction can be observed which suggests that the component of osmotic suction was present in the soil, suggesting the pore water contained salts. However, as stated previously, the reason for the apparent presence of a osmotic suction value may be due solely to the equalisation time during each test not being sufficient. As stated by Marinho (2004) if the filter papers are allowed to fully equalise both curves should come together which may have not been the case in these tests.

5.3.3 Pressure Plate

The SWRCs determined by Noguchi (2009) using the pressure plate technique are shown in Figure 5.12. This figure also includes the results from Lourenço (2008), which can be directly compared with the ones obtained by Noguchi, since the pressure plate apparatus, the soil specification and the soil sample preparation procedure were the same for both experiments. Measurements for Samples 1 and 2 were taken only up to 300kPa suction since the ceramic plates on which the samples were placed were 500kPa plates and blow-through occurred before achieving an imposed suction of 400kPa. Similarly, Sample 3 was measured only up to 600kPa suction, since an inappropriate procedure in the experiment lead to cracking of the ceramic plate under an imposed suction of 700kPa.

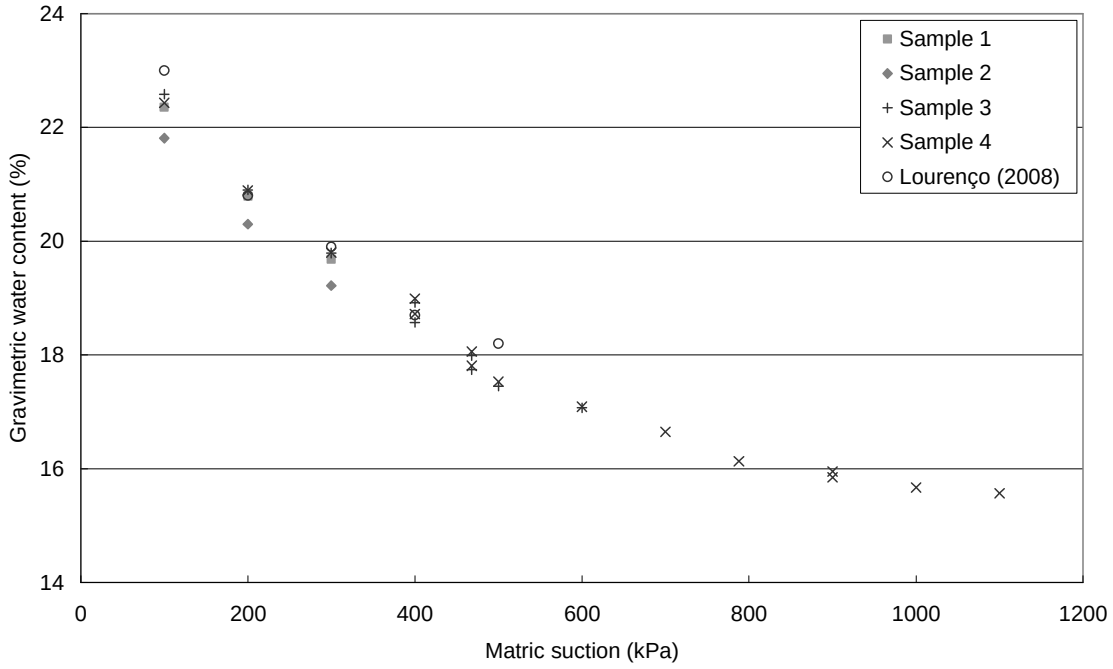

Figure 5.12 – Matric suction SWRCs determined using the pressure plate (after Lourenço, 2008, and Noguchi, 2009).

According to the obtained results, the pressure plate technique can be repeated with a small scatter of less than 0.5% of water content. For suction stages of 400kPa, 468kPa, and 900kPa, equilibrium was checked by successive weighing of the soil samples, rather than relying only on volumetric measurements. The first weighing was taken when the gauge read lower volume changes than 0.35cc/day. Samples were placed back in the pressure chamber and same suction was again imposed on them. The second weighing was done 48 hours after that. It was observed that the difference in the soil sample water content after 48hours was less than 0.35%, which is a relatively small value. It is, therefore, reasonable to assume that soil samples have reached equilibrium when the volume gauge is reading changes of less than

0.35cc/day.

5.3.4 High capacity suction probe

The SWRCs determined from two continuous drying tests and stage drying test are shown in Figure 5.13.

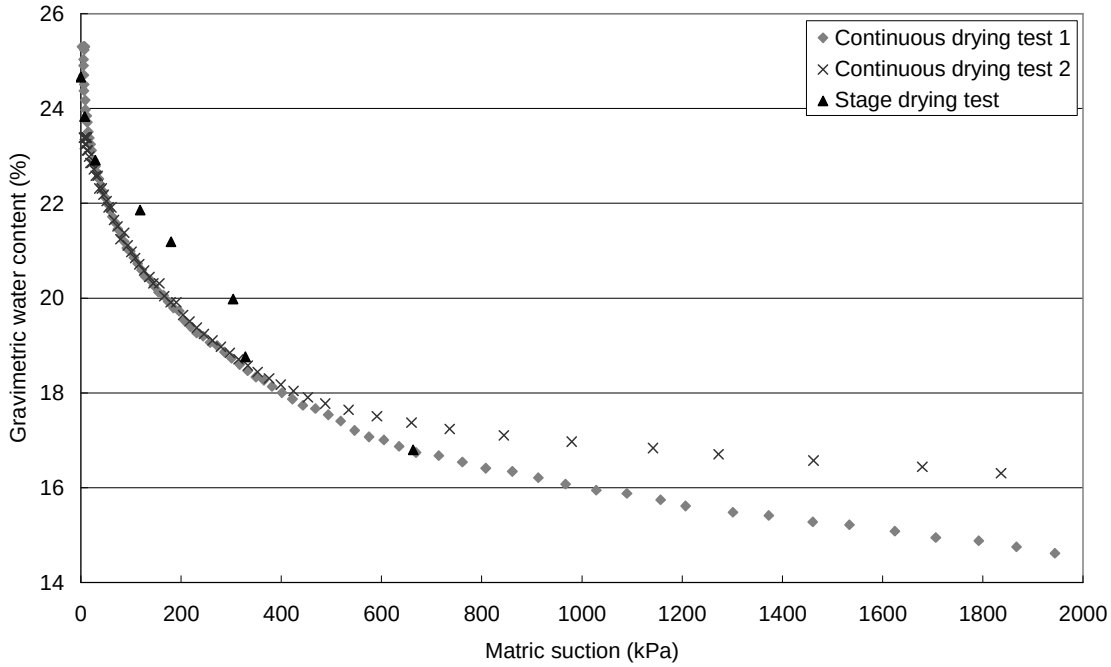

Figure 5.13 – Matric suction SWRCs determined using the high capacity suction probe (after Noguchi, 2009).

The two continuous drying tests followed a very similar curve up to about 400kPa suction. With the exception of the measurements taken between gravimetric contents of 20% and 22%, a similar curve was observed for the stage drying test. There are two main

explanations for these results: a) non-equalization of water content inside the soil sample or b) non-intimate contact between the high capacity suction probe and the soil sample.

a) Soil samples dry from the margin, where the high capacity suction probe is placed. Therefore the high capacity suction probe measures a higher suction at the beginning and, after equalization, suction would normally reduce. However, if equalization of water content is not achieved inside the soil sample when the measurement is taken, the suction value obtained would be higher than the actual value.

b) Stage drying test includes a lot of operator intervention, which can be a source of error. At every drying stage, the high capacity suction probe is placed on the sample ensuring an intimate contact, but this contact becomes more difficult as the sample gets drier. Pushing the high capacity suction probe into the sample deforms the surface of the sample (Figure 5.14) and this deformation can also be one of the reasons why intimate contact achievement is more difficult for successive suction measurements.

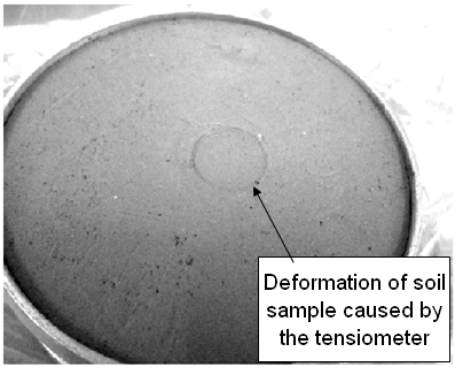

Figure 5.14 – Deformation of soil sample caused by the high capacity suction probe, (After Lourenço, 2008).

The SWRC determined from the continuous drying test 1 was compared with the tests carried out by Lourenço (2008) in Figure 5.15. As for the pressure plate technique results, a direct comparison between this work and the results by Lourenço (2008) was possible due to same soil specifications and same soil sample preparation procedures on both experiments. The continuous drying test 1 was in good agreement with the tests carried out by Lourenço (2008), which is a good indicator of the repeatability of the high capacity suction probe technique. These results also account and support the reproducibility of the SWRCs determined using the high capacity suction probe technique.

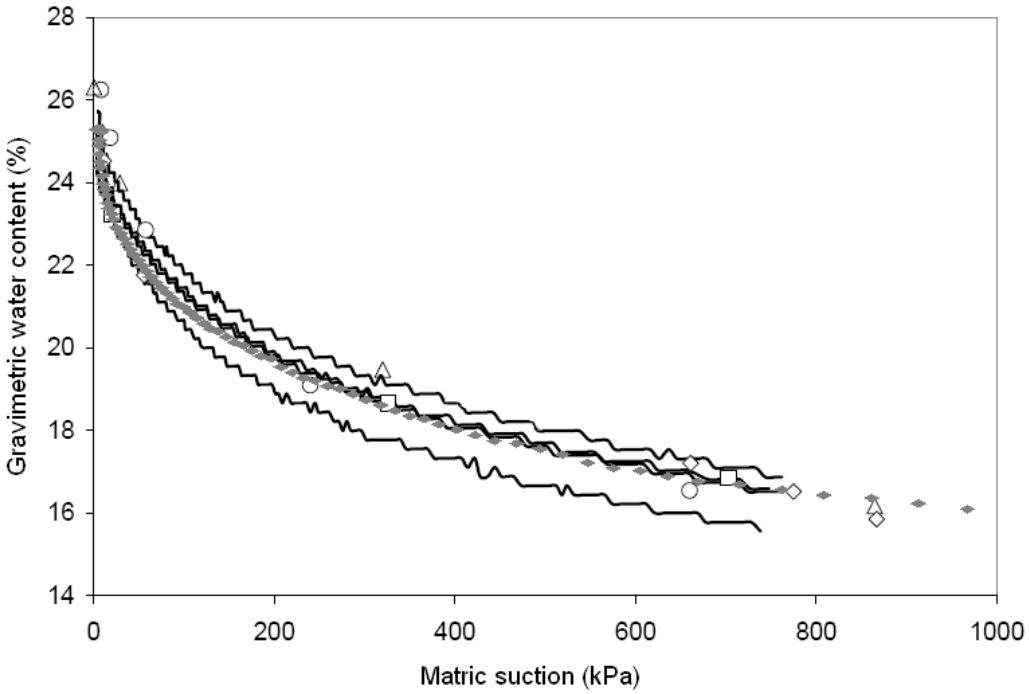

Figure 5.15 – Comparison between the continuous drying test 1 (grey symbols) and all drying tests obtained by Lourenço (2008) (lines correspond to four continuous drying tests and white symbols for four stage drying tests) (after Noguchi, 2009).

5.4 Soil water retention curves for the BIONICS soil

5.4.1 Total Suction SWRCs

The SWRCs determined using the total suction measurement techniques (i.e. the transistor psychrometer and the non-contact filter paper) are shown in Figure 5.16 (results determined using the transistor psychrometer are shown as an envelope). Comparing the SWRCs present in Figure 5.16, the one obtained from the psychrometer seems to fall at lower values than the ones obtained using the non-contact filter paper technique. Although both

techniques present significant scattering in the obtained results, it seems that the SWRC resulting from filter paper calibration equations suggested by van Genuchten and Hamblin shows better agreement with those resulting from the psychrometer than Leong et al.

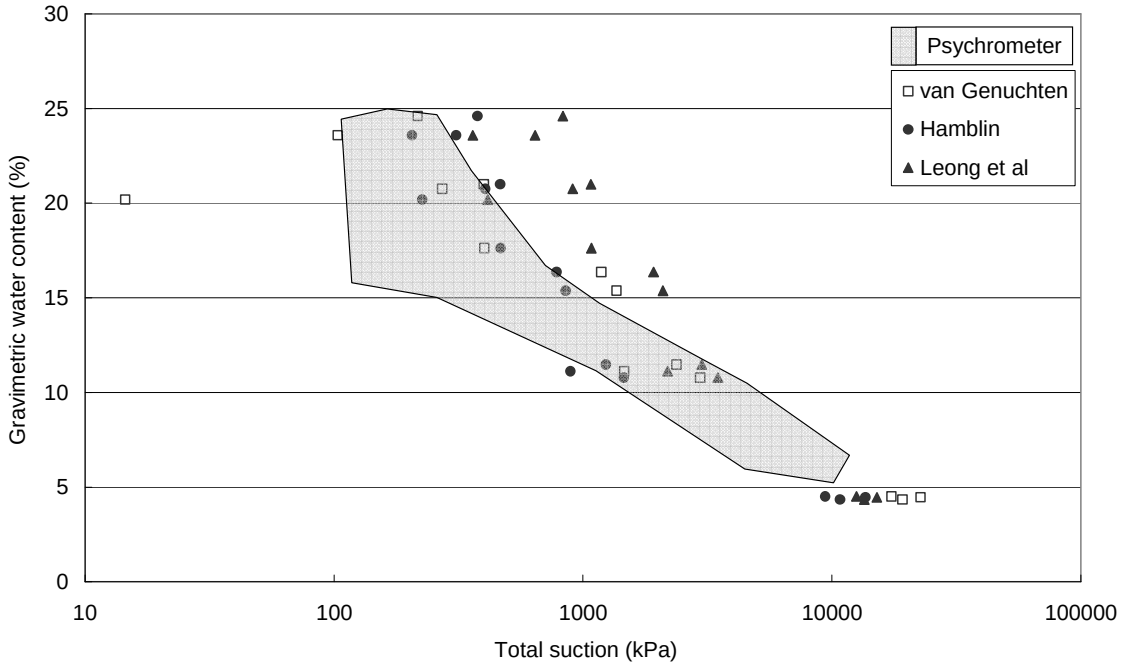

Figure 5.16 – Comparison of total suction SWRCs between the transistor psychrometer and the non-contact filter paper (After Noguchi, 2009).

5.4.2 Matric Suction SWRCs

Figure 5.17 shows the comparison of the SWRCs determined using different matric suction measurement techniques: pressure plate results are shown as an envelope, high capacity suction probe continuous drying test 1 is smoothed out and shown as a solid line and filter paper technique results are represented as triangle, circle and square symbols.

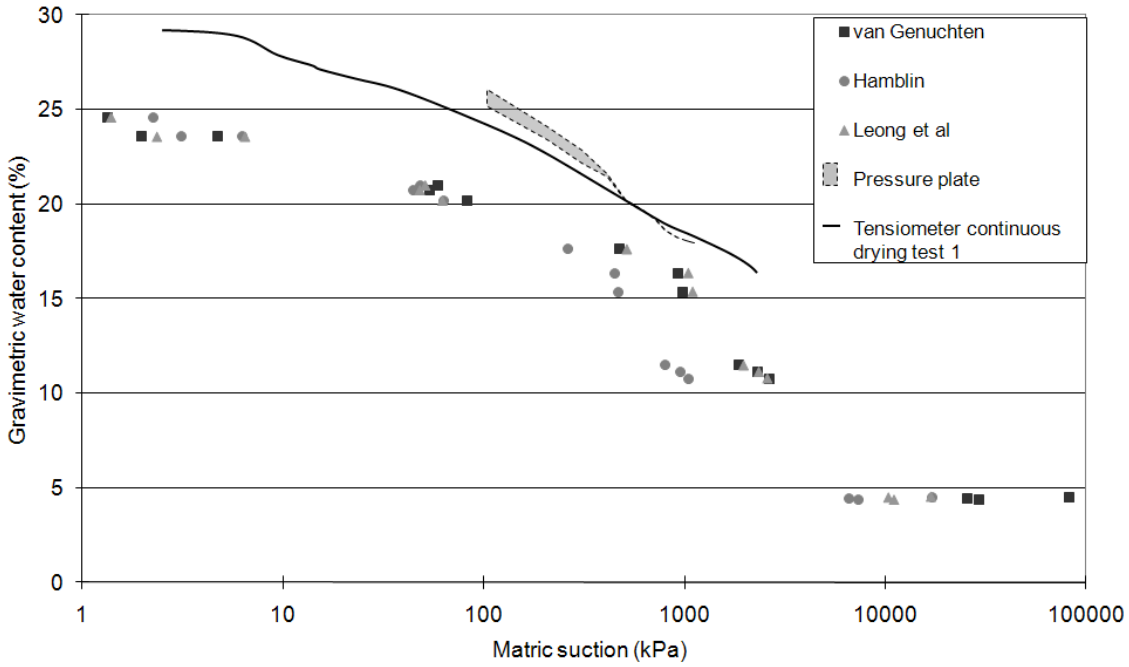

Figure 5.17 – Comparison between all matric suction SWRCs (After Noguchi, 2009).

All of the results for the filter paper technique are positioned below the ones for the pressure plate and the high capacity suction probe techniques. Furthermore, the SWRC determined using the pressure plate is positioned above both the in-contact filter paper and the high capacity suction probe.

Initially, it was considered that the higher water content determined for the pressure plate could result from water absorption by the soil samples while the pressure inside the pressure chamber was released. Following that perspective, the possible volume flow of water during this moment when pressure was released was calculated. Considering that the coefficient of permeability of the BIONICS soil at 15% gravimetric water content was 3.08x10^{-}

^{11}m/s, the area of the sample (in contact with the ceramic plate) was 4.49x10^{-3}m^2 and that to release the pressure and take the sample away from the ceramic plate could take up to 30 minutes, the possible volume of water that the soil sample could absorb was 2.48x10^{-10}m^3, (or 2.49x10^{-4}g). Around 1.56g of water are necessary to increase the water content in the sample by 1%; it is then possible to state that, considering the low value calculated, absorption has no significant effect on the water content of the sample.

It was then concluded that the absorption of water was not the main reason behind the high water content of the soil samples. Other reasons might explain this higher water content determined for the pressure plate.

The way water is expelled from the soil samples can have a significant effect on its water content. If a soil sample is drying to the atmosphere, water in its pores can cavitate due to soil suction, allowing movement of water towards the surface of the soil sample which can then evaporate. However, when the soil sample is placed inside the pressure chamber, since it is subjected to a water pressure of 200 kPa, cavitation is prevented. Although the soil sample, at the end of the suction stage, was exposed to atmospheric pressure again, possible cavitation occurring in the pores will, at this point, be a slower process. Since water pressure is imposed on the soil sample again, it is likely that the pores would become saturated with water again.

So, at the same suction value, the soil sample from the pressure plate can present higher water content than the sample being dried to the atmosphere.

Another possible reason for this is the way that the soil sample and the ceramic plate are placed in contact. An intimate contact between the soil sample and the ceramic plate enables a water path between the two. If this contact is not intimate, there might not be a sufficient contact surface to assure that water path, which could result in an insufficient water flow from the soil sample through the plate. A sample under these conditions could therefore, by the end of the experiment, present higher water content.

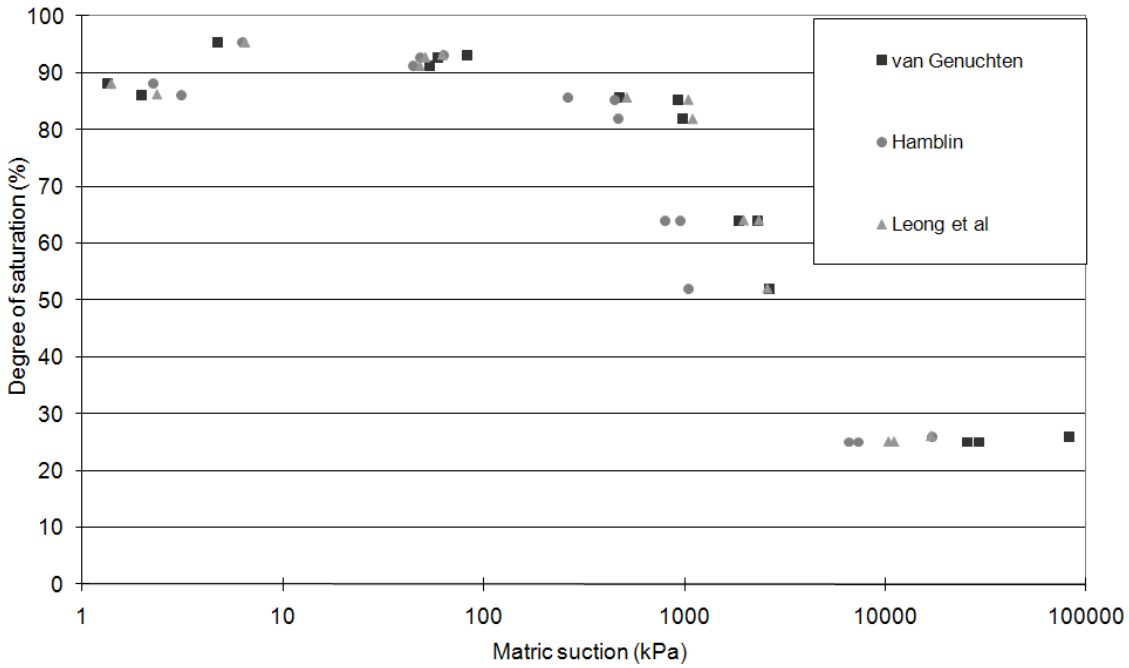

Figure 5.18 – Comparison between all matric suction SWRCs against degree of Saturation (obtained from Noguchi data, 2009).

Nonetheless from Figure 5.17 the SWRC for the BIONICS fill material presents a characteristic bimodal curve and presenting a very clear residual water content of 4%. The AEV, air entry value, could be determined from Figure 5.18, where matric suction was plotted against the degree of saturation resulting in a value around 200 kPa.

5.4.3 Comparison between Total and Matric Suction SWRCs

Figure 5.19 presents all but the non-contact filter paper determined SWRCs.

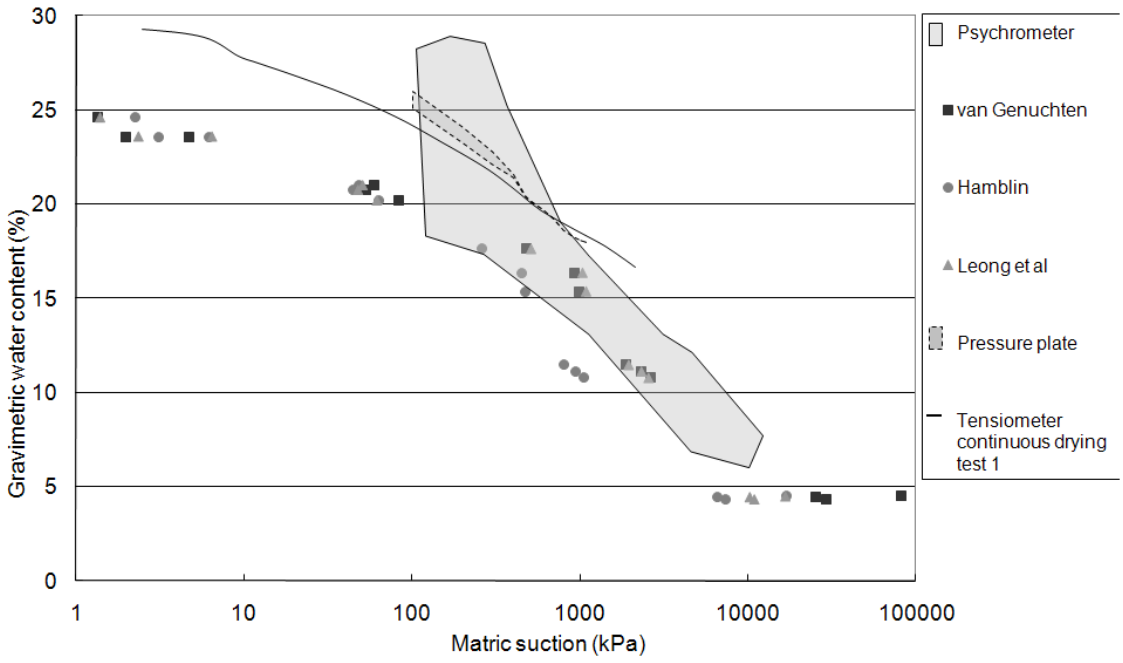

Figure 5.19 – Comparison between the transistor psychrometer and all matric suction SWRCs (After Noguchi, 2009).

Results from the transistor psychrometer show a huge scatter and it is possible to

observe overlapping with the matric suction SWRCs.

For gravimetric water contents below 16%, and suctions over 1000 kPa, the high capacity suction probe shows the highest suction measurements. An explanation for this might be, similarly to what happens and has been discussed above for the in-contact paper filter technique, the discontinuity on water paths between the sample and the high capacity suction probe when the soil sample is very dry. Continuous water paths between the soil sample and the high capacity suction probe water reservoir are more difficult. Also, since BIONICS soil has a shrinking behaviour (Lourenço 2008), the drying of the soil can also create a gap between the sample and the surface of the high capacity suction probe, where the suction probe loses the connection with the soil surface. These factors together would result in an over withdrawal of water from the high capacity suction probe reservoir, causing higher suction measurements, measuring suction of the air instead of the soil.

In all the obtained measurements a factor has to be added, related with the preparation method. The use of a dynamic process to compact samples can also affect the pore distribution and size throughout the samples. This can explain part of the observed scattering in techniques that rely on various samples, (variation between samples due to the preparation method), such as the filter paper and transistor psychrometer.

The shrinking behaviour of the BIONICS fill material studied by Lourenço (2008) was performed on a set of tests prepared at an initial water content of 25% that were dried to determine the shrinkage limit. By measuring the volume changes with a mercury porometer the shrinkage limit was found to be approximately 14% of water content.

Studies to understand the behaviour of suction – water retention and volumetric behaviour of the BIONICS fill material were carried out by Lourenço (2008). Using high capacity suction probes drying/wetting cycles were imposed on samples prepared at 25% Hysteric behaviour was observed. Furthermore, while measuring volumetric changes on those samples Lourenço concluded that the behaviour of suction – water retention and volumetric behaviour of the BIONICS fill material was essentially controlled by the shrinkage/swelling behaviour.

5.5 SWRCs for specimens compacted at lower water contents

The previous sections report on the study of SWRC for the BIONICS fill material determined on initially saturated specimens carried out by Noguchi and Lourenco. In this section, a series of tests was performed on specimens prepared at different initial water contents. These tests were carried out by the author. Tests were also performed on

specimens that had been wetted or dried prior to testing. This study was performed with the only technique that could measure high values of suction (>2MPa), the filter paper technique. Samples were prepared, according to the preparation method used for the SWRC, at different water contents (10%, 13%, 15%, 20% and 22%). Further specimens were also wetted or dried to the remaining water contents, i.e. for 15% samples were wetted to 20% and 22%, while other samples were dried to 10% and 13%.

The curves obtained for all water contents are presented for both total and matric suction using Van Genuchten calibration curves in Figures 5.20 to 5.24. The Van Genuchten curves seemed to give realistic comparisons with the psychrometer, pressure plate and suction probe for both total and matric suction in the earlier tests reported. In Figure 5.21 for matric suction the curves following drying paths show an apparent trend of being lower than the primary drying curve from 25% obtained by Noguchi (2009), where they all gather together at 10-11% of water content, around 1500-2000 kPa, suggesting the behaviour of scanning curves. For total suction, as shown in Figure 5.20, the trend is maintained, although less evident due to the large scatter in these readings.

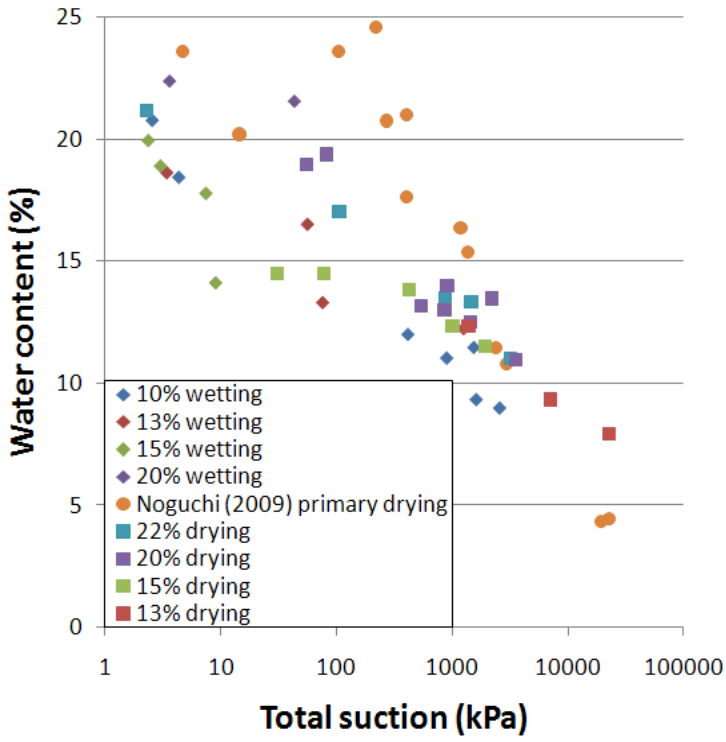

Figure 5.20 – SWRCs for all water contents for total suctions.

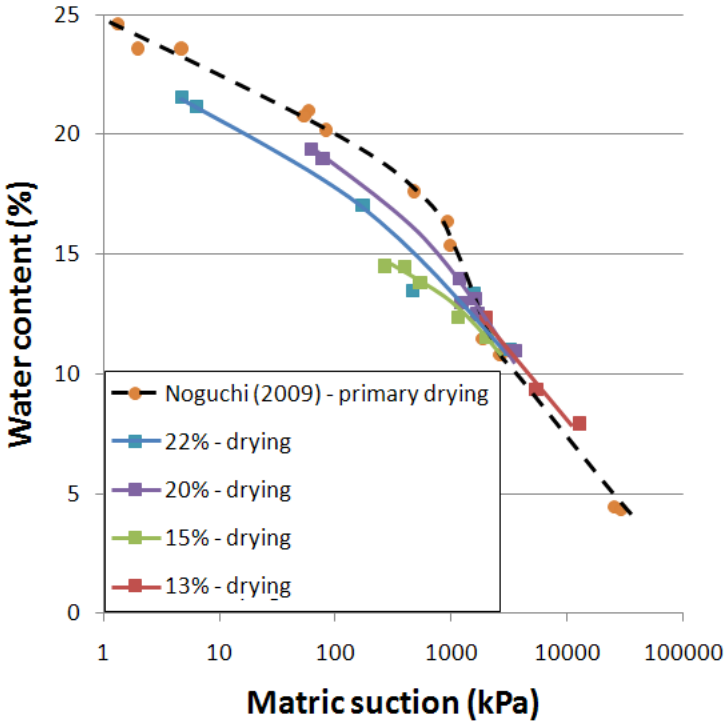

Figure 5.21 – SWRCs following a drying path for all water contents for matric suction.

Figure 5.22 shows the matric suction SWRC following drying path with the degree of saturation. Due to changes in methodology, volumetric measurements were only obtained in the later tests for water contents 20% and 22% of water content. Comparing them with the primary drying curve obtained by Noguchi (2009) the two curves 20% and 22% fall under, therefore showing the behaviour of a scanning curve, although eventually reaching the primary curve.

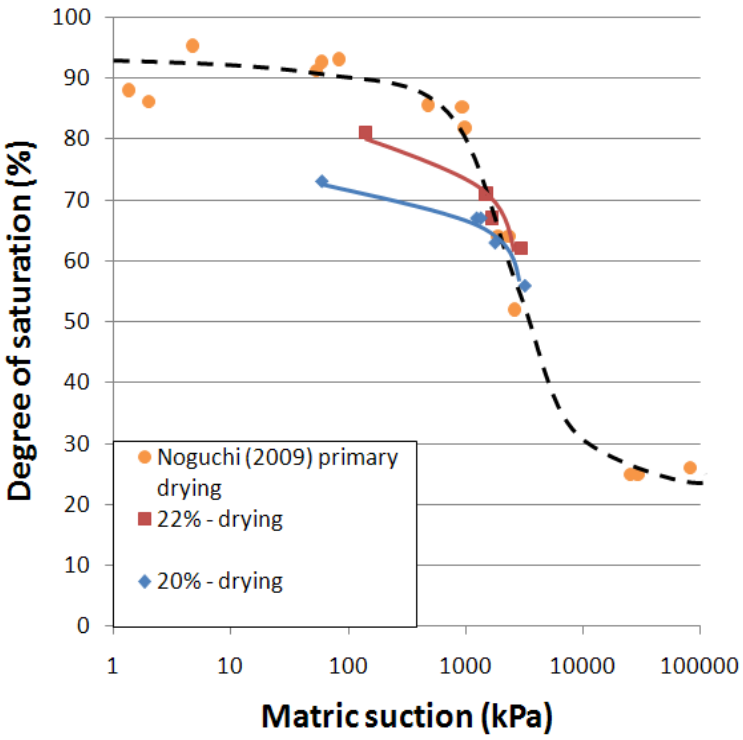

Figure 5.22 – SWRCs following a drying path for all water contents for matric suction-degree of saturation.

The behaviour of the SWRCs obtained following a wetting path shown untypical behaviour. As it is observed from Figure 5.23 the SWRC that followed a wetting path moved towards to the primary drying curve, where it should have moved towards the primary wetting curve. Although the primary wetting curve was not determined the impression of behaviour of the SWRC that followed a wetting path seems different from what would be expected. The SWRCs that followed a wetting path seem to cross the primary drying curve in an ascending form, where the SWRC obtained from 10% of water content was to first to cross at 300 kPa of suction followed by the SWRC for the water content of 13%, 15% and so on.

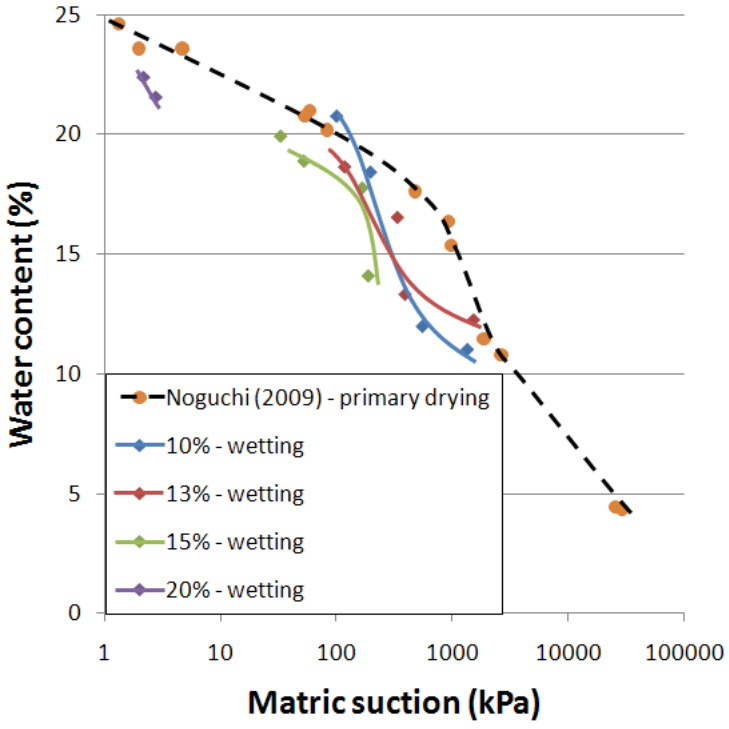

Figure 5.23 – SWRCs following a wetting path for all water contents for matric suction.

Similar results were observed in the matric suction – degree of saturation relationship for the SWRCs show in Figure 5.24. The lack of tests where volumetric measurements were obtained was not sufficient to fully understand the behaviour of the SWRCs that followed a wetting path. A general trend of the SWRCs was observed in Figure 5.24 where the SWRCs were overlapping each other showing different water retention behaviour.

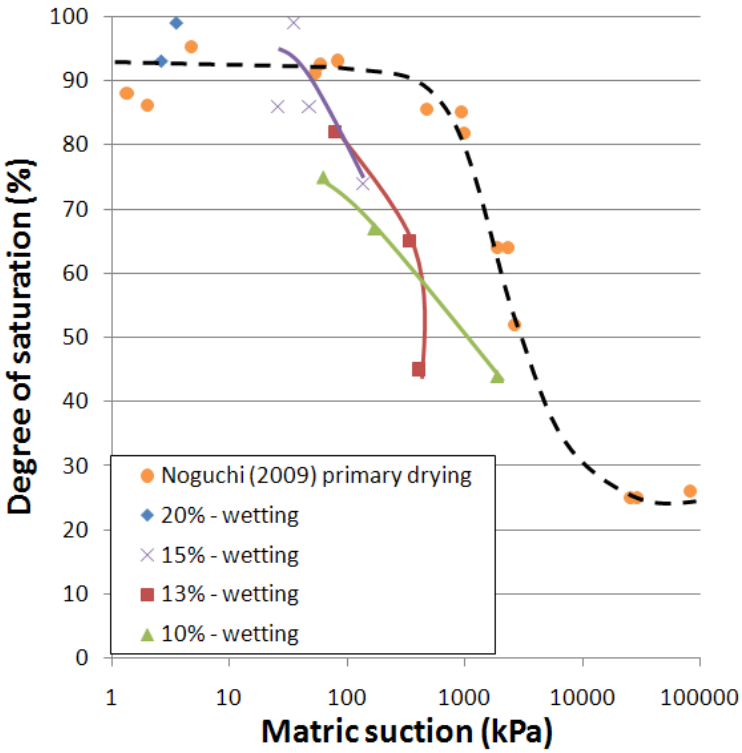

Figure 5.24 – SWRCs following a wetting path for all water contents for matric suction-degree of saturation.

5.6 **Conclusions**

This chapter presents the soil water retention curves (SWRCs) of the BIONICS fill material. The techniques involved in the determination of the SWRC were: high capacity suction probe, transistor psychrometer, filter paper and pressure plate. In the pressure plate suction is imposed by elevated air pressure (axis translation), whereas suctions are measured after natural drying in the other techniques.

Two types of SWRC were obtained, both following a drying path: one referenced to total suction, obtained from the measurements of the transistor psychrometer and non-contact filter paper and a second set of curves referenced to matric suction using measurements obtained from the high capacity suction probe, in contact filter paper and pressure plate. Scatter was present in both SWRCs, a factor that can be attributed to the inaccuracies associated to the particular testing techniques used as well as variations in samples that are inevitable when carrying out measurements on compacted samples.

On the matric suction SWRC, very good agreement was observed between measurements carried out by two different researchers (Noguchi and Lourenço) for both high

capacity suction probe and pressure plate, showing the test methods provide reasonable repeatability.

In terms of the curves obtained the SWRCs showed the expected shape, the bimodal curvature. The matric suction SWRC presented an air entry value close to 200-300 kPa for the BIONICS fill material and a residual gravimetric water content of 4%.

One important study performed as part of the characterisation of BIONICS material, was that scanning curves were obtained from different starting water contents using the filter paper technique. From this study it was clear the differences between the scanning curves and the primary drying SWRC. For both total and matric suction SWRCs, the drying scanning curves tended to merge around 11% (equivalent to a suction of 3000kPa).

The SWRCs that followed wetting paths showed atypical behaviour tending to intercept the primary drying curve at high water contents / low values of suction. Although the primary wetting curve was not determined in this study it generated the idea that the path followed by the SWRCs was different than the expected. In the matric suction – degree of saturation

relationship the tendency showed overlapping of the SWRCs with each other by still showing the atypical behaviour of intercepting the primary drying curve.

6 Mechanical behaviour of the BIONICS material

6.1 **Introduction**

To determine the mechanical behaviour of the BIONICS material a triaxial testing program was developed, where samples were tested at constant water content in unsaturated conditions. Considering the low permeability of the soil being studied, see Chapter 3, whatever the trigger would be to cause failure of an earth structure built with such material, it would be expected to occur while maintaining a constant water content. The pore water pressure was continuously monitoring using a high capacity suction probe during testing. Each test involved a stage of constant water content compression (CWC), where the sample was subjected to an increase in confining pressure (net stress) after which the pore water pressure was allowed to equalise. The specimen could change in volume during this stage due to expellation of air, but no flow of water should occur. After the constant water content compression, each sample was subjected to a shearing stage, where the sample was loaded axially until failure, while maintaining constant confining pressure. The triaxial testing program also included a series of saturated consolidated drained triaxial tests, to provide a reference for the testing program on unsaturated samples.

The triaxial testing program was performed on samples compacted at specific water contents being: 15% (the optimum water content, W_{opt}), 20% and 22%. Testing was restricted to this range of water content due to limitations of the suction range of the high capacity suction probe (2 MPa). In order to achieve an insight into the behaviour of samples subject to wetting and drying (due to climate influences), a further series of samples was prepared at these water contents that were wetted and dried after compaction. The wetting and drying was carried out outside the triaxial cells, as described in Chapter 4 and placed inside double cell triaxial cells and subjected to CWC and subsequent shearing.

This Chapter starts by presenting the saturated test series including equipment, test procedures and results, followed by the unsaturated constant water test series in the same order.

6.2 Saturated triaxial tests

To create a reference for the constant water triaxial testing for unsaturated samples, conventional consolidated triaxial tests were performed on fully saturated samples. Samples were prepared according to the sample preparation methodology (section 4.2) and were saturated inside the triaxial apparatus prior to consolidation and shearing.

In this case, due to equipment availability, the samples tested were 38mm diameter by 76mm and were tested in conventional triaxial cells using the configuration in Figure 6.1. The conventional triaxial cells were suited for the testing since the tests were performed in saturated conditions and the volume was being measured directly based on water flow out of the sample. The test consisted of three stages: saturation, consolidation and shearing.

Saturation was imposed by maintaining an elevated back pressure applied to the top and bottom of the sample (300 kPa) in order to dissolve any air in the sample. By maintaining the cell pressure at 5 kPa above the back pressure, the effective stress was maintained close to zero, at 5 kPa or less. To monitor the saturation progression, the B value was measured. The B value is the ratio of pore water pressure in response to an increase of cell pressure ($\Delta u/\Delta \sigma_c$) in which, for fully saturated samples the B value should be equal to 1. In triaxial testing it is common practice to saturate the sample until a B-value of 0.95 is achieved (BS 1377: 1990), which for soft clays resembles 99.9% in the degree of saturation (Black and Lee, 1973). To monitor the evolution of the B value the cell pressure was increased by 100 kPa and measurements (pore water pressure) were taken on the pressure transducers connected to the top cap and base pedestal, while maintaining undrained conditions by closing all drainage valves. When a satisfactory B-value was achieved (>=0.95) the test entered its second phase.

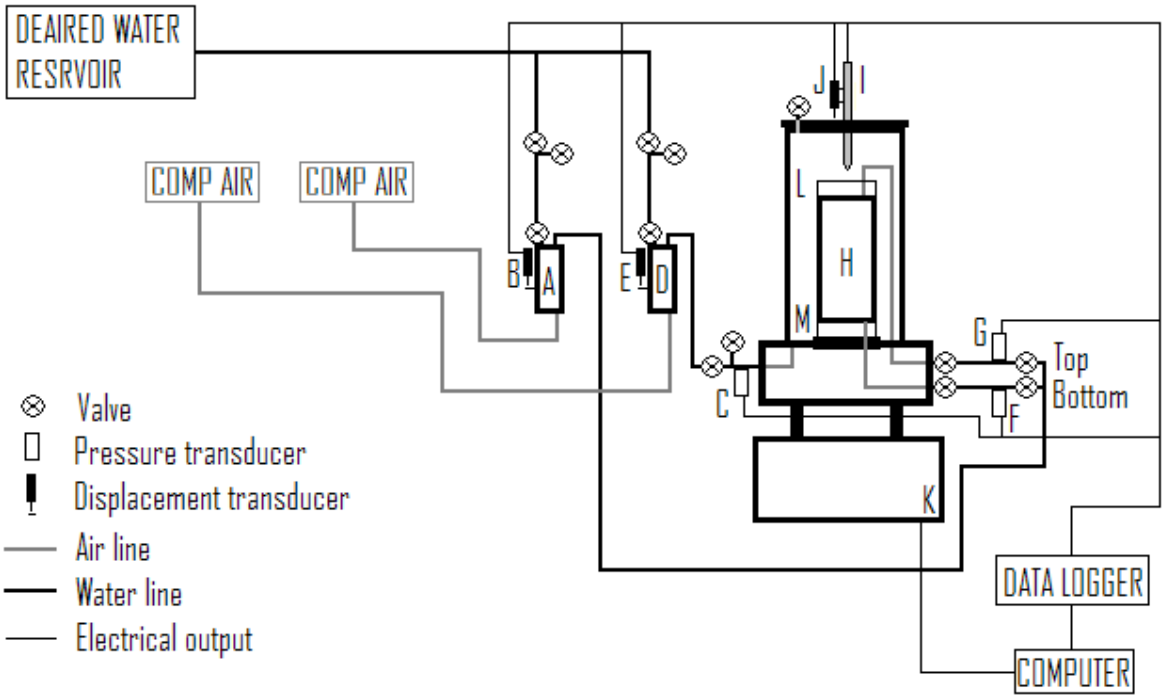

Letter

A	Volume gauge – sample
B	Volume change transducer – sample
C	Pressure transducer – cell pressure
D	Volume gauge – cell
E	Volume change transducer – cell
F	Pressure transducer – back pressure bottom
G	Pressure transducer – back pressure top
H	Sample
I	Load cell
J	Axial displacement transducer
K	Loading frame
L	Top cap with porous disc
M	Bottom cap with porous disc

Figure 6.1 – Triaxial testing apparatus for saturated samples.

The sample was then be subjected to consolidation, where the confining pressure was raised to a desired value to impose a known effective stress, but always maintaining back pressure at 300 kPa. Consolidation was continued until no further significant volume change

was recorded in the volume gauge, considered to be a constant change rate of volume close to 0.009 cm^3/hr.

After consolidation was complete, drained shearing was started at a rate of 0.005 mm/min..

The accuracy for each type of measuring equipment used during the saturated tests is presented in Table 6.1. The accuracy was determined differently for the different types of equipment used: during experimental procedures or prior to the experimental work in order to observe fluctuations in the recorded value. Accuracy values that were obtained between experiments where performed to the: volume gauge filled with water, displacement transducer and positioned at mid travel and load cell at rest. The accuracy for the pressure transducers was obtained while the cell was at a constant confinement pressure.

Table 6.1 – Accuracy of the measuring equipment used in saturated triaxial testing.

Measuring equipment	Unit	Accuracy
Volume gauge	cm^3	±0.002
Displacement transducer	Mm	±0.005
Pressure transducer	kPa	±0.2
5 KN load cell	N	±0.5

6.2.1 Triaxial testing program

The tests performed for the saturated triaxial testing program can be seen in Tables 6.2. The saturated tests (S) were identified in the form Sxx(yy) by the as-compacted water content (xx), and confining pressure applied during the triaxial testing (yy). Table 6.2 also presents the initial conditions of the samples (water content, dimensions, density, etc) and the test conditions including the total duration of each test.

Table 6.2 – Triaxial testing program for the saturated test series, showing testing conditions.

Test no.	As-compacted								Test conditions	
	Water content	Dimensions			Density		Void ratio	Degree of Saturation	Confining pressure	Duration*
		height	Area	Volume	Bulk	Dry				
		h	A	V	ρ	ρ_d	e	Sr		
	%	cm	cm^2	cm^3	Mg/m^3	Mg/m^3	-	%	kPa	Days
S15(50)	14.63	7.69	11.44	88.0	2.164	1.888	0.43	92	50	30
S15(150)	14.75	7.63	11.39	86.9	2.176	1.896	0.43	94	150	10
S15(300)	14.75	7.60	11.52	87.6	2.142	1.867	0.45	89	300	3
S20(50)	19.70	7.51	11.51	86.5	2.029	1.695	0.59	90	50	6
S20(150)	19.70	7.59	11.55	87.7	2.032	1.697	0.59	90	150	6
S20(300)	19.70	7.56	11.58	87.5	2.020	1.687	0.60	88	300	4
S22(50)	21.78	7.39	11.28	83.3	2.052	1.685	0.60	97	50	7
S22(150)	21.78	7.41	11.40	84.4	2.032	1.669	0.62	95	150	4
S22(300)	21.78	7.41	11.31	83.9	2.041	1.676	0.61	96	300	8

*- duration of the triaxial test (saturation, consolidation and shearing), not considering sample preparation time.

6.2.2 Saturated tests results

The saturated tests were performed using the setup presented in Figure 6.1. The samples used were of smaller size compared with the samples for the triaxial testing program for unsaturated samples due to limitations on the equipment available. However, sample preparation remained the same in all prepared samples; in the case of the saturated tests, the specimens used were cored from a compacted sample, where the source sample was prepared in the same way as those used for the unsaturated constant water content tests. From each compacted sample it was possible to core three specimens for the saturated test series. This meant that the tests were performed on specimens taken from a single compacted sample, thus the initial water contents obtained for each group of subsamples in Table 6.2 had the same value, apart from S15(50) which originated from a different batch.

The samples when placed inside the cell were subjected to saturation, where the degree of saturation was raised to 100%. Table 6.3, presents the conditions for the end of the saturation and consolidation stages of each specimen tested. As expected samples when wetted increased in volume after saturation, and with consolidation this volume decreased, as shown in Figure 6.2. The changes in sample volume were determined by measuring the changes of fluid volume inside the triaxial cell. This procedure is not ideal, since the perspex cell itself can change in volume. However, it provides an approximation of the changes in volume of the sample.

Table 6.3 – Conditions at start and end of the consolidation stage for the saturated testing series.

Test No.	Initial Water content %	Consolidation	Volume V cm^3	Dry density ρ_d Mg/m^3	void ratio e	Degree of Saturation Sr %
S15(50)	14.63	**Initial**	91.1	1.744	0.55	100
		Final	89.2	1.782	0.52	
S15(150)	14.75	**Initial**	92.7	1.788	0.51	100
		Final	89.9	1.844	0.47	
S15(300)	14.75	**Initial**	91.1	1.789	0.51	100
		Final	85.9	1.897	0.42	
S20(50)	19.70	**Initial**	87.0	1.686	0.60	100
		Final	85.1	1.724	0.57	
S20(150)	19.70	**Initial**	88.7	1.678	0.61	100
		Final	84.3	1.758	0.54	
S20(300)	19.70	**Initial**	89.2	1.656	0.63	100
		Final	83.8	1.763	0.53	
S22(50)	21.78	**Initial**	84.1	1.670	0.62	100
		Final	82.5	1.702	0.59	
S22(150)	21.78	**Initial**	86.3	1.633	0.66	100
		Final	81.7	1.724	0.57	
S22(300)	21.78	**Initial**	85.0	1.654	0.63	100
		Final	81.0	1.735	0.56	

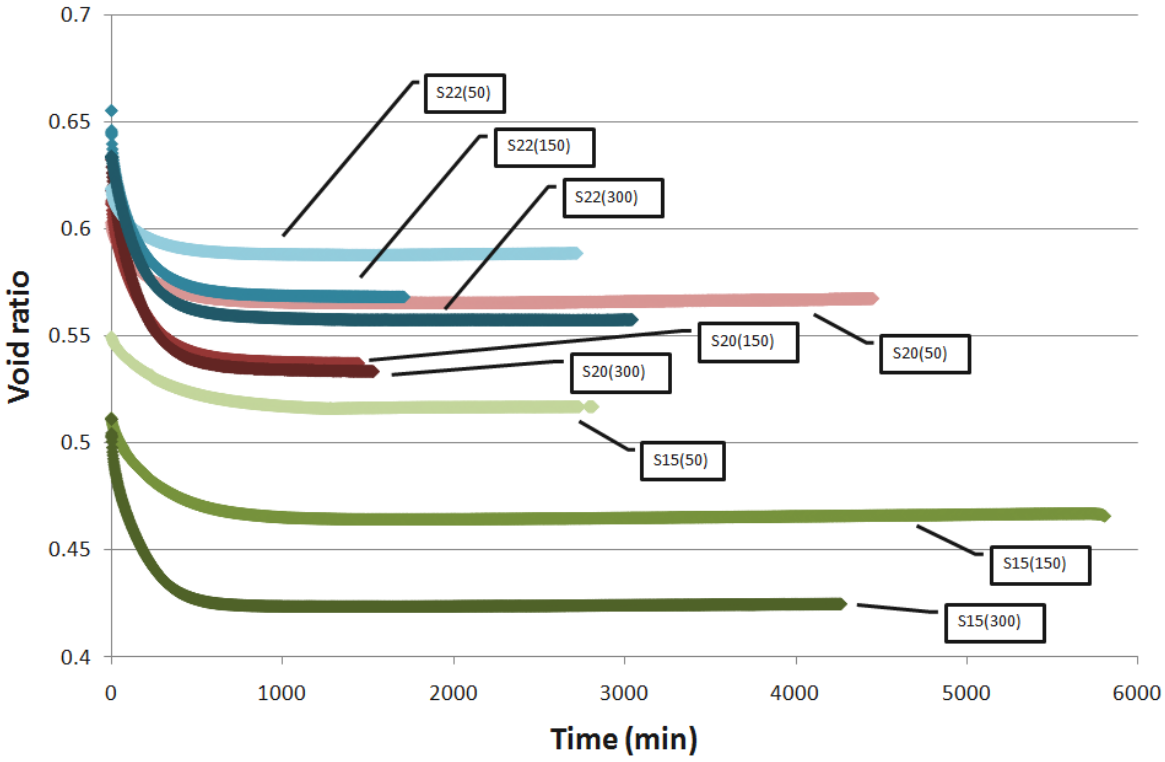

Figure 6.2 – Consolidation stage for each respective sample.

After consolidation the final stage of shearing was started. The shearing stage was performed under drained conditions, meaning water could flow in or out of the sample without significant increase in pore water pressure, the maximum variation observed was found to be smaller than 3 kPa. The final conditions of each sample tested are presented in Table 6.4.

Figure 6.3 shows the variation in the deviatoric stress with axial strain for all saturated tests at the different confining pressures used during each test. It can be seen that samples prepared at 15% of water content failed between 3% of axial strain at 50 kPa of confinement up to 8% at 300 kPa of confinement. The samples prepared at higher water contents tended to fail at higher values of axial strain between 10% at 50 kPa of confinement up to 17% at 300% of confinement.

Table 6.4 – Saturated test series: sample characteristics at the end of each saturated test.

Test No.	Initial Water Content	Final Water Content	Sample weight	Dry density ρ_d	void ratio e
	%	%	g	Mg/m^3	
S15(50)	14.63	21.85	193.7	1.701	0.59
S15(150)	14.75	18.77	196.6	1.744	0.55
S15(300)	14.75	17.82	192.1	1.826	0.48
S20(50)	19.70	21.78	176.1	1.711	0.58
S20(150)	19.70	19.44	176.6	1.790	0.51
S20(300)	19.70	18.50	175.4	1.839	0.47
S22(50)	21.78	22.25	170.1	1.689	0.60
S22(150)	21.78	21.47	166.8	1.767	0.53
S22(300)	21.78	21.73	165.9	1.778	0.52

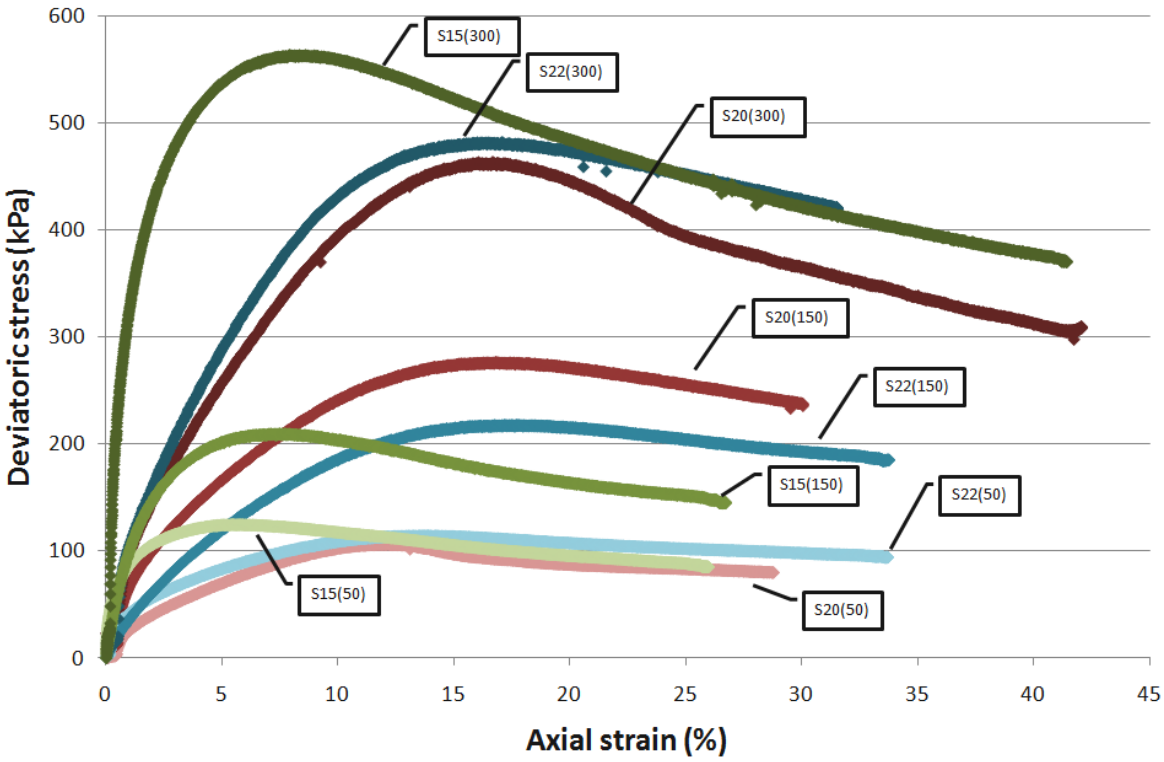

Figure 6.3 - Deviatoric stress-strain relationships for the saturated test series.

Figure 6.4 presents the relation between axial and volumetric strains developed through the shearing stage of each sample (Compressive strains are shown as positive). It is observable that most of the samples are still changing in volume at the end of each saturated test, specially the samples that were prepared at 15% of water content. Figures 6.5 to 6.7 show the stress paths for each test.

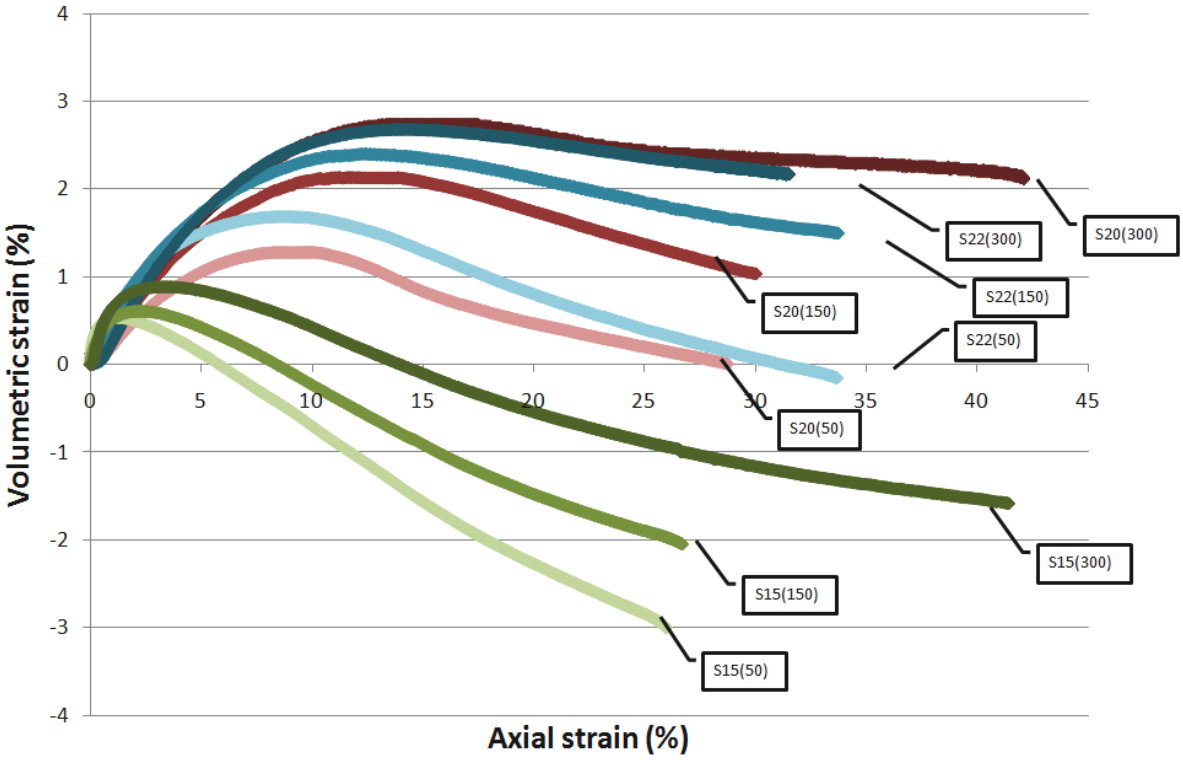

Figure 6.4 - Volumetric-axial strain relationships for saturated samples.

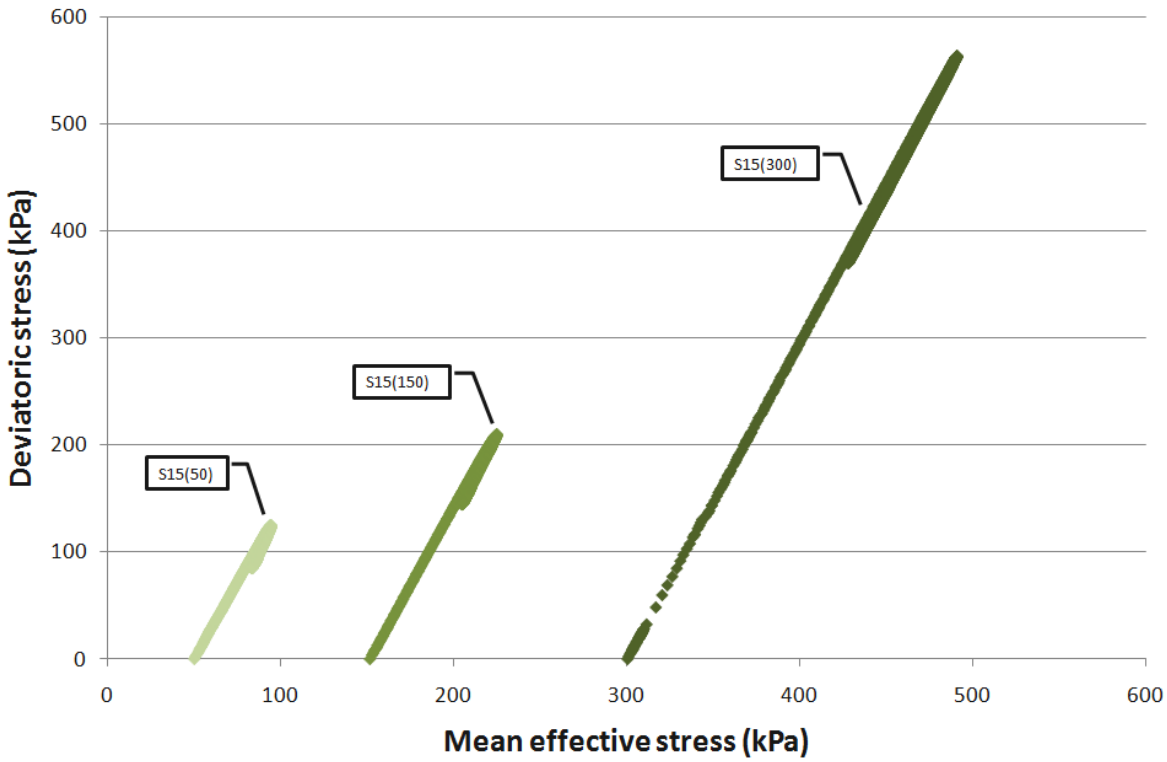

Figure 6.5 – Stress paths for the saturated samples with as-compacted water content of 15%.

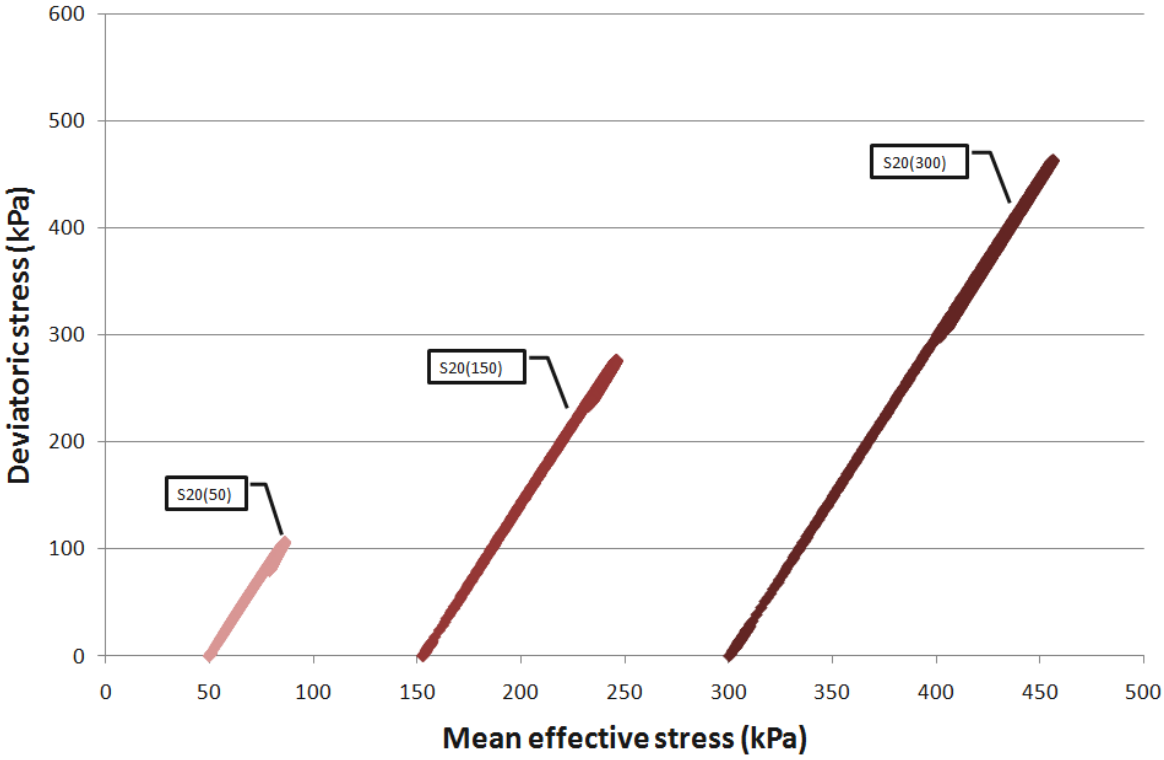

Figure 6.6 – Stress paths for the saturated samples with as-compacted water content of 20%.

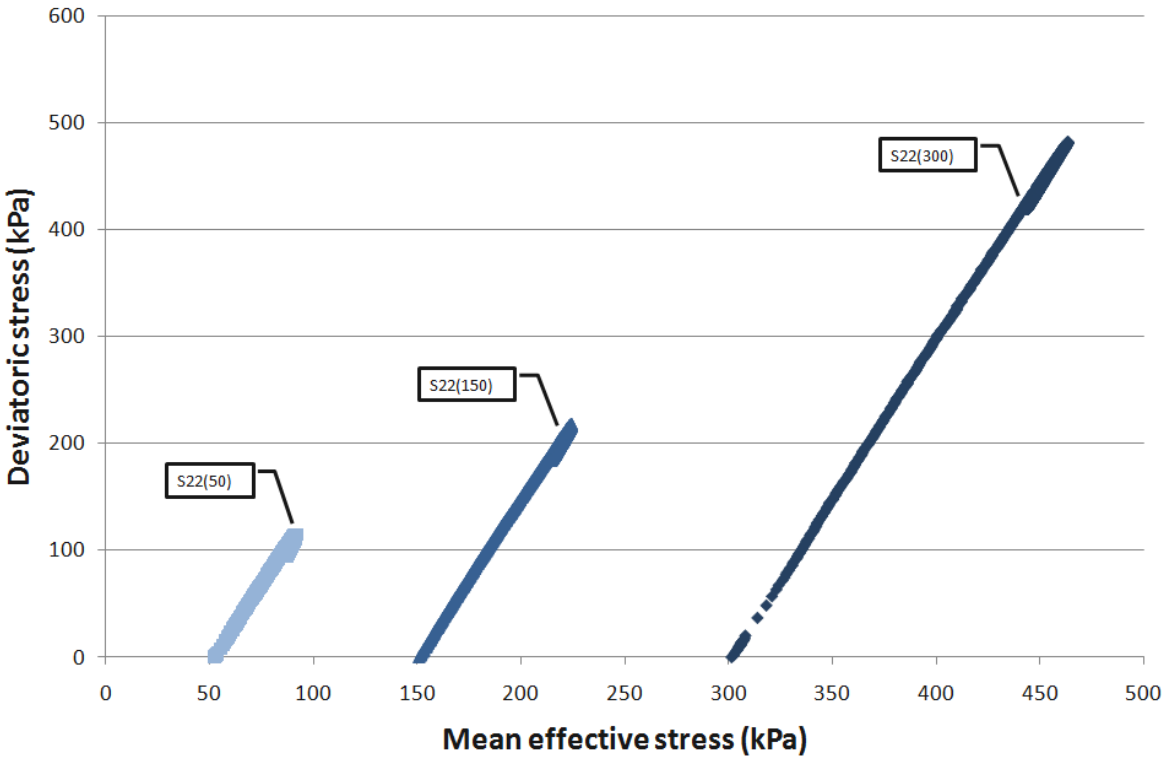

Figure 6.7 – Stress paths for the saturated samples with as-compacted water content of 22%.

6.2.3 Critical state limit analysis for the saturated tests

The end points of the tests at which a state of plastic behaviour characterized by continuous deformation without any further increase in stress was observed are presented in Table 6.5. These are assumed to be close to Critical State conditions, although with reservations, as it has been shown volumetric deformations were still occurring at the ends of the tests, as can be seen in Figure 6.4.

As the table shows, the critical state points were achieved at high values of axial strain (ε_a), reaching values from 25% up to 40%. Of course, at such large axial strains there can be concerns about non-uniformity of deformations and constraints due to boundary conditions. Nevertheless, it does seem that strains in excess of 25% are needed before the deviator stress and volumetric strains start to level off at constant values suggesting the critical state is being achieved.

Table 6.5 – Critical state points of each saturated test.

Test No.	$w_{(ac)}$ %	w_i %	p' kPa	q kPa	ε_a (%)	e	v 1+e	S_r (%)
S15(50)	14.63	21.85	81.0	79.4	26.38	0.59	1.59	100
S15(150)	14.75	18.77	210.0	160.4	25.46	0.55	1.55	100
S15(300)	14.75	17.82	438.0	400.8	38.63	0.48	1.48	100
S20(50)	19.7	21.78	79.7	83.2	28.06	0.58	1.58	100
S20(150)	19.7	19.44	240.5	255.5	28.74	0.51	1.51	100
S20(300)	19.7	18.5	417.5	344.7	40.56	0.47	1.47	100
S22(50)	21.78	22.25	88.0	97.2	33.19	0.60	1.60	100
S22(150)	21.78	21.47	236.7	251.6	33.22	0.53	1.53	100
S22(300)	21.78	21.73	454.7	451.4	30.28	0.52	1.52	100

The final specific volume values are plotted against mean effective stress, p’ in Figure 6.8. The slope of the critical state lines in the v – p’ plane (λ) was found to be 0.051 for samples saturated from 22%, 0.062 for the samples saturated from 15% and 0.066 for samples saturated from 22% with intercepts (Γ) of 1.820 for samples saturated from 22%, 1.866 for samples saturated from 15% and 1.870 for samples saturated from 20%. While in Figure 6.9 the slope of the CSL in the plane q – p’, M, was found to be 0.90 for samples saturated from 15% and 20% and 1.01 for samples saturated from 22%.

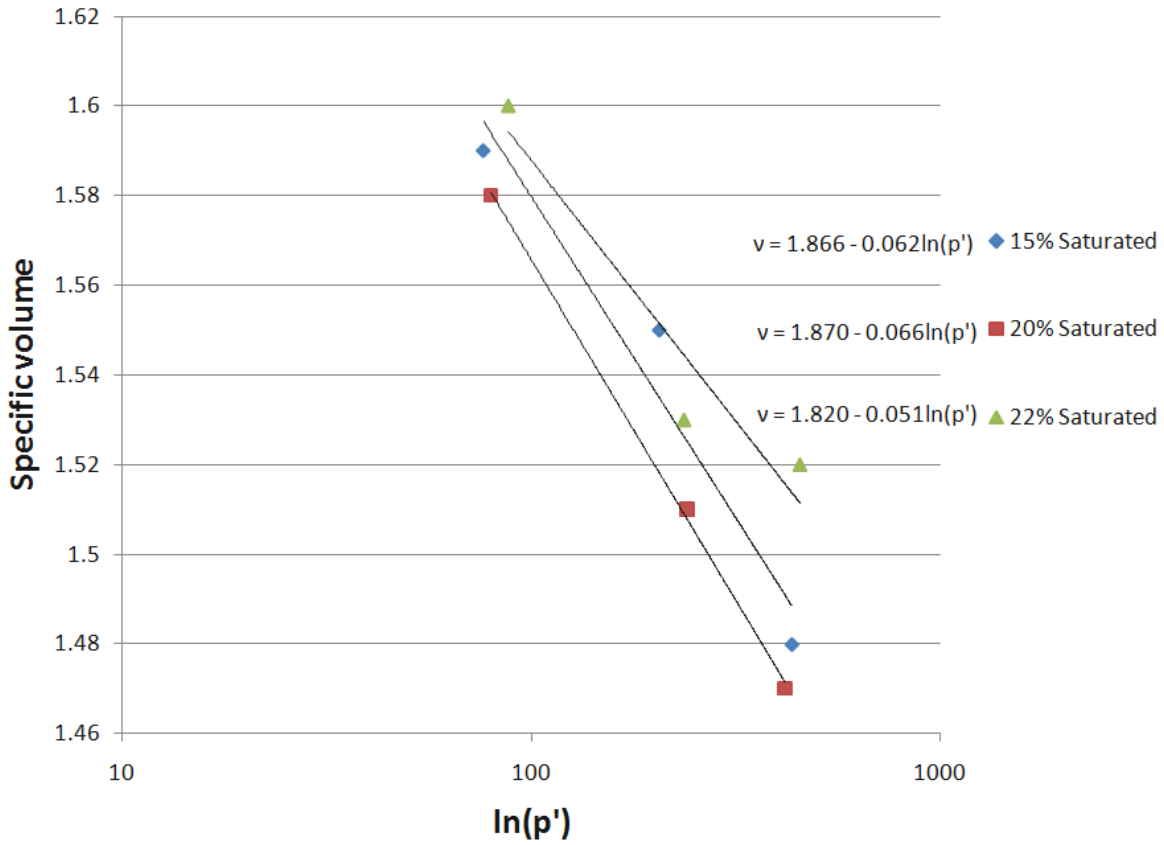

Figure 6.8 – Critical state line of the saturated test series in v-ln(p') plane.

From equation 2.15 the critical state friction angle for the saturated tests was found to be 23° for samples saturated from 15% and 22% and to be 25° for samples saturated from 22%.

Similar results were obtained for the samples that were saturated from 15% and 20%, suggesting a similar critical state limit, while for samples saturated from 22%, the critical state limit differed significantly.

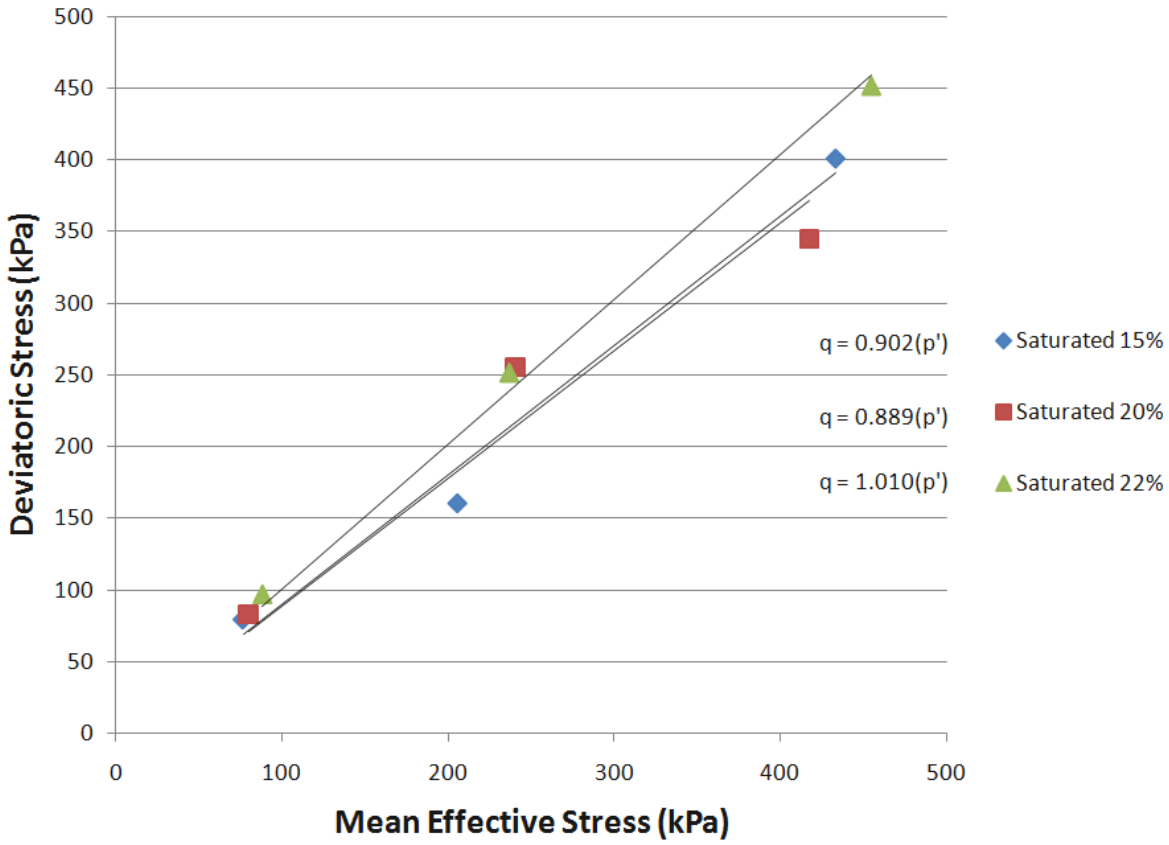

Figure 6.9 - Critical state line of the saturated test series on q-p' plane.

During the triaxial tests, the samples did not fully reach a critical state. The observed trends in Figure 6.3 suggest that the critical state would be reached at lower values of deviatoric stress, which would result in the slope of the critical state in the q-p' plane (M) being similar for all water contents. For the saturated tests M was found to be 0.93.

The observed trends in Figure 6.4 suggest that samples would continue to dilate, increasing in specific volume. On the critical state in the ν-p' plane, this would suggest higher intercepts of the critical state line on the ν axis (Γ) for each water content. However, due to the scatter and overlap present in Figure 6.8, it was impossible to infer if the intercepts would differ between the different water contents. Therefore, the interpretation of critical state for the ν-p' plane was based on Figure 6.8. The intercept of the critical state line in ν axis (Γ) and slope of the critical state lines in the ν – p' plane (λ) was considered to be unique for all water contents, Γ =1.868, while, λ=0.062.

6.3 **Constant water content triaxial testing**

To describe the mechanical behaviour of the BIONICS soil, constant water content tests **(**Fredlund and Rahardjo, 1993**)** were carried out. The constant water content triaxial testing consisted of two stages:

- The specimen was subjected to constant water content compression under isotropic conditions at a fixed confining pressure σ_3 until the volume stabilised and the pore water pressure equilibrated.

- The specimen was sheared, under constant water content conditions by increasing the deviatoric stress (σ_1- σ_3); in each test the shearing stage was continued to reach 20% strain, to attempt to observe ultimate conditions. Pore-water pressure changes during shear were measured.

6.3.1 Wykeham Farrance double cell triaxial cell

6.3.1.1 The double cell principle for testing unsaturated samples

The samples prepared with the BIONICS material were unsaturated. The presence of air in an unsaturated soil poses a problem due to its compressibility when attempting to monitor the volume change of a sample while testing (consolidation/compression or shearing). The traditional method for sample volume change used in triaxial testing of saturated soils, of measuring the pore fluid that leaves or enters the sample, is no longer sufficient as water volume and sample volume are not linked in an unsaturated soil. To monitor volume change of unsaturated samples the simplest arrangement is to monitor the volume of the fluid (i.e. water) that leaves or enters the cell (Bishop and Donald, 1961). Using a single wall cell, i.e. the traditional triaxial system, built in Perspex the indirect method to monitor the volume of fluid is not very reliable due to elastic behaviour from the Perspex part of the cell when varying

pressure and also creep, which occurs under constant stress. These changes are due to water absorption, thermal expansion and cell volume changing with cell pressure (Wheeler, 1988); although small, these still impose significant variations on the results obtained in terms of volume measured.

To overcome these difficulties, a double cell was preferred, such as the Wykeham Farrance (WF) double cell triaxial cell (Figure 6.10a)). The cell volume resulting from changes in cell pressure is greatly reduced by having two cells as the inner cell is subject to equal pressures on both sides of the cell wall. The WF design is similar to the Wheeler modified triaxial cell (Wheeler, 1988). However, the WF double cell system differs from the Wheeler cell by having an interior cell wall made of glass instead of Perspex; with the intention to eliminate the water absorption by the wall of the inner cell. One second important feature of the WF double cell triaxial cell is being double celled, meaning that also the top cap of the inner cell is subjected to equal pressures inside and out. With this configuration and by applying an equal cell pressure inside and outside the inner cell the expansion of the cell is eliminated, hence, no volume change is caused by cell pressure. The dimensions of the double cell triaxial cell are presented in Table 6.6 and the cell components are shown in Figure 6.10b) and c).

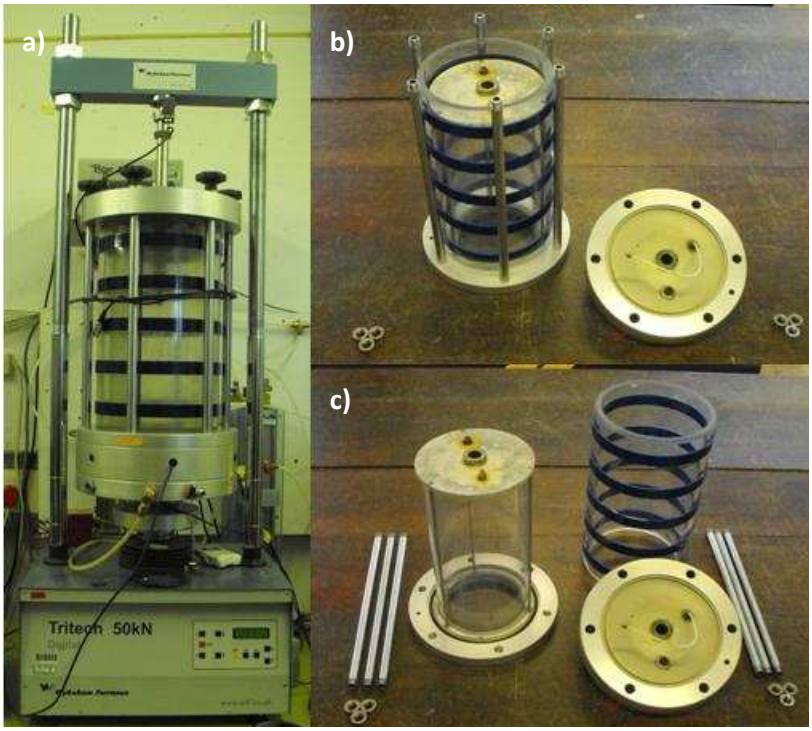

Figure 6.10 – Wykeham Farrance double cell triaxial system **a)** fully assembled, **b)** without outer cell top cap and **c)** view of the inner cell.

Table 6.6 – Dimensions of the double cell triaxial cell, after Lourenço (2008).

Dimensions of the DCTC		
Height	41.6	cm
Inner cell inner diameter	19	cm
Inner cell outer diameter	20	cm
Outer cell inner diameter	22.35	cm
Volume of water in the inner cell	11794.8	cm^3
Volume of water in the outer cell	3251.66	cm^3

Calibrations were preformed on the WF double cell triaxial for creep under a constant pressure. The inner and outer cells were filled with de-aired water and afterwards a constant pressure of 600kPa was applied in both cells. The pressure was maintained for an extended period (weeks) to observe and quantify possible creep of the inner cell. Later, pressure cycles were performed to verify the volume changes due to pressure changes. A full view of the test can be observed in Figure 6.11.

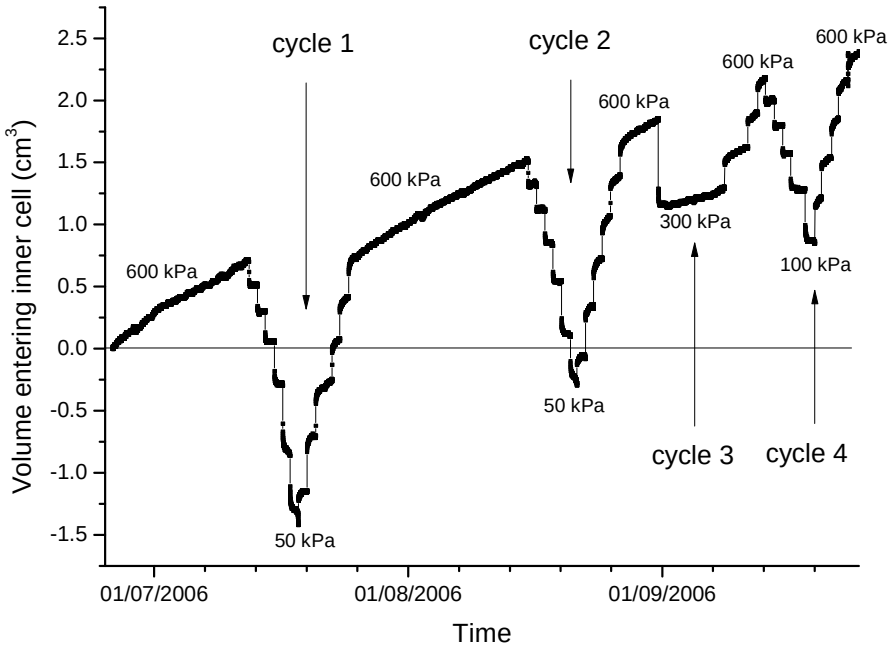

Figure 6.11 – Volume changing of the inner cell as a response to pressure.

It was observed that at a constant pressure of 600 kPa there was a small flow of water entering the inner cell ranging between 0.0016 to 0.0027 cm^3/hour.

Pressure cycles were performed by changing the pressure initially starting from 600 kPa, then decreasing in increments of 100 kPa to 100 kPa with a further reduction of 50 kPa and then increasing back to 600 kPa. These cycles had the intention of observing the reaction of the cell to pressure changes but also to attempt to estimate the flow rates for other pressures.

Figures 6.12 to 6.14 show the obtained flow rates when increasing pressures for cycles 1, 2 and 4. It can be observed that a fixed flow rate was not achieved for the reason that the cell did not reach an equilibrium state; however, the flow rates generated were extremely low reaching a maximum for a pressure of 400 kPa (0.0042 cm^3/hour during cycle 2).

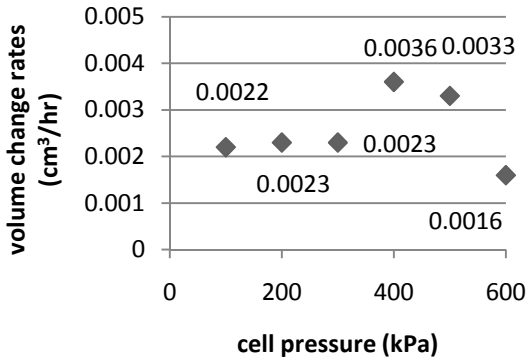

Figure 6.12 – Rates of volume change for 1st cycle (increasing pressure).

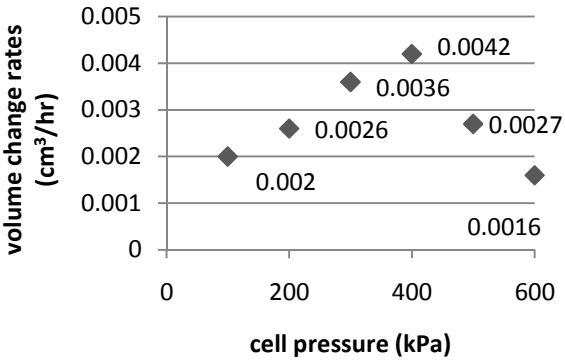

Figure 6.13– Volume changing rates for 2nd cycle.

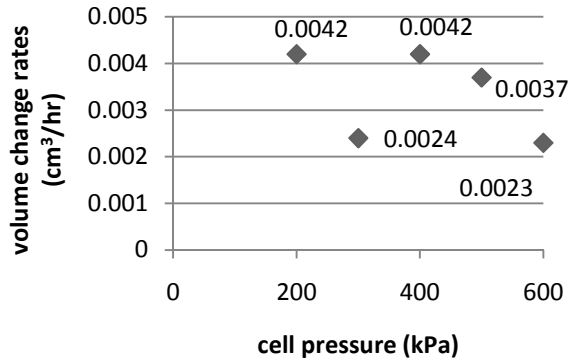

Figure 6.14 – Rates of volume change for 4th cycle.

Cycle 3 was preformed differently; the pressure was reduced from 600 to 300 kPa and the cell was left to equalise, the observed flow rate entering the cell was as small as 0.0008 cm^3/hour. Afterwards, the pressure was increased in regular steps of 100 kPa reaching 600 kPa. The obtained rates can be observed in Figure 6.15.

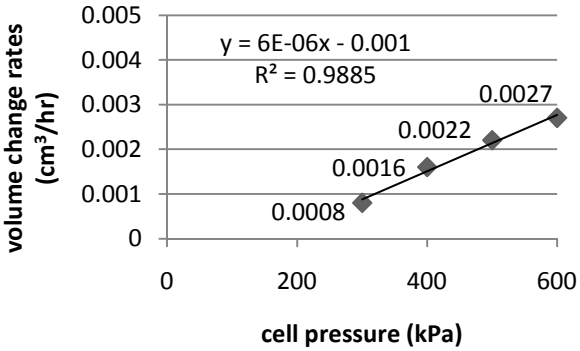

Figure 6.15 – Volume changing rates for 3rd cycle.

In conclusion, the creep effect on the double cell triaxial cells was found to be minimal, as low as 0.0008 cm^3/hour reaching a maximum of 0.0042 cm^3/hour. During testing this creep effect would have: during 3 months of testing at constant pressure (such as the constant water content compression stage) a maximum increase of the measurement by 9 cm^3 and, during 24 hours (such as a shearing stage) a maximum increase by 0.1 cm^3. When compared with the volume of sample at study, 1571 cm^3, this represents an error of 0.6% for the period of 3 months and as low as 0.006% for 24 hours.

The calibration also included the effect of volume changing due to the penetration of the loading shaft into the inner cell. The piston was pushed inside the inner cell increasing its volume inside the inner cell. The load cell was lowered by 8mm inside the inner cell at a rate of 0.05 mm/min and maintaining a constant pressure of 1500 kPa, as presented graphically in Figure 6.16. This meant that, considering the diameter of the shaft of the load cell as 25 mm, where each millimetre of travel from part of the piston represents an increase 0.49 cm^3, a displacement of 3.93 cm^3 of water exiting the inner cell should have been observed. In fact, the measured volume was slightly higher, 4.24 cm^3, resulting in a difference of 0.31 cm^3.

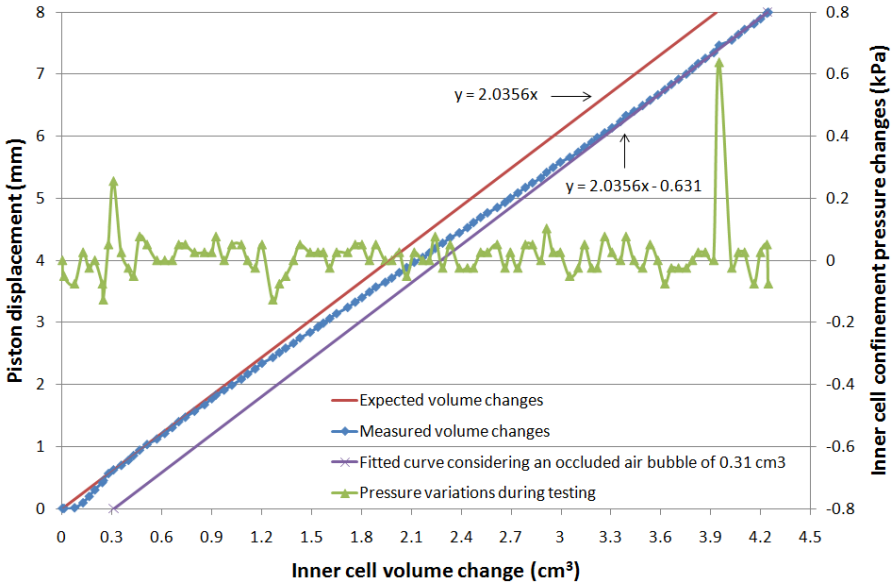

Figure 6.16 – Volume change originated by the displacement of the piston of the load cell entering the inner cell.

The volume was measured using a volume gauge using a bellofram skirt, where, for a good operation of this system it necessary to ensure that no air bubbles are trapped inside. To eliminate air bubbles the common practice is to flush de-aired water a number of times through the system while allowing full travel of the bellofram skirt, eliminating air bubbles trapped inside both the volume gauge and in the wrinkles of the bellofram when compressed. However, being enclosed in a metallic frame, it is impossible to completely assure the lack of air bubbles inside.

It is possible that the differences between measured and expected values in Figure 6.16 could be related with the performance of the volume gauge itself. When pressure is building up, with water flow entering the cell, the volume gauge will respond accordingly. However, when the flow of water is exiting the cell, i.e. by the loading piston entering the cell at a constant pressure, the volume gauge lags in response. In summary, the change in direction of the water flow could possibly result in the differences between the predicted and measured values.

A close examination of pressure changes in Figure 6.16 can give the necessary explanation for the difference between measured and expected volumes. Close to the start it was observed a sudden increase in pressure (0.3 kPa) coinciding with the sudden increase in volume change, this could be attributed to the start of the stretching of the bellofram skirt; after this first peak both measured and expected volumes coincide until the moment where a negative pressure peak occurred where, both curves start to diverge significantly. This negative peak, of less than 0.2 kPa, could coincide with an air bubble occluded inside a wrinkle that emerged while the bellofram was being stretched. In fact, the fitted curve considering an air bubble of 0.31 cm^3, see Figure 6.16, precisely shows this. After the dissolution of the air bubble into water, assumed to be completely dissolved at 5.66 mm of piston displacement, the measured value started to coincide with the new fitted curve.

The information presented clearly shows that the WF double cell triaxial cell is adequate for the triaxial testing of unsaturated samples where, volume changes can be accurately measured indirectly from the changes of cell volume changes during i.e. shearing. However, it is important to acknowledge the fact that even with the precaution of flushing the volume gauge in the full travel of the bellofram skirt, it was impossible to remove all the air bubbles from the volume gauge. In a real test, where the volume changes would be greater, the influence of such air bubble would not greatly affect the measured value and could be almost, if not completely, neglected bearing in mind that the possible occluded air inside the volume gauge remains small.

6.3.1.2 Other observations about the WF double cell

One important deficiency encountered while testing with the WF double wall cell was the design of the top caps in both the inner and outer cells. It was found that a substantial volume of air was always trapped in the top of both cells when filling the cell.

Considering that volumetric measurement is made indirectly, having air bubbles trapped will affect greatly the obtained results. However, if the cell is pressurised the air bubbles are compressed and eventually dissolve in the water. The effect of the air bubbles was

observed during calibration. In Figure 6.11 the volume was still changing inside the cell at a constant pressure of 600 kPa even after a month period. This could mean that the air bubbles were still being compressed into solution even after such a long equalisation period. Nevertheless, providing the pressure remains constant through the test the effects of initial air bubbles on the volumetric measurement can be neglected.

If air bubbles do remain, if the pressure changes it will affect the volumetric measurement as air is compressible, which could explain the erratic behaviour observed in Figures 6.12-6.15 during the pressure cycles.

The solution was to pressurise the cell while maintain the sample net stress close to zero so no deformation (consolidation) of the sample should occur. This was achieved by creating a new stage in the constant water content test, named the equilibrium stage. In the equilibrium stage, apart from increasing the pressure in both cells to the desired confining pressure, a positive air pressure with the same value was imposed within the sample, thus maintaining the net stress equal to zero. This stage was maintained until stable readings were achieved on the volume gauge, meaning that all air in the inner cell had been

compressed/dissolved. After this stage the constant water content compression stage could be started.

Initially it was intended to use only one hydraulic pump to pressurise the whole system (inner and outer cell). However, some increase in pressure in the outer cell was observed when the load cell was entering the inner cell. In this configuration the pressure was controlled only by the pressure transducer measuring the pressure in the inner cell. This increase in pressure in the outer cell, while maintaining the pressure constant in the inner cell endangered the glass wall of the inner cell. To avoid failure of the glass wall, both cells were separated by a valve and a second pump was installed, with each pump controlled independently by separate pressure transducers as shown in Figure 6.1. The cause of the pressure rise in the outer cell was not fully identified, but it was thought to be due to sticking of the volume gauge allowing a differential pressure to build up between the pressure at the base of the gauge (feeding the outer cell) and the top (feeding the inner cell).

6.3.2 Constant water content tests

To perform the constant water content (CWT) tests on unsaturated samples the equipment configuration presented in Figure 6.17 was utilized.

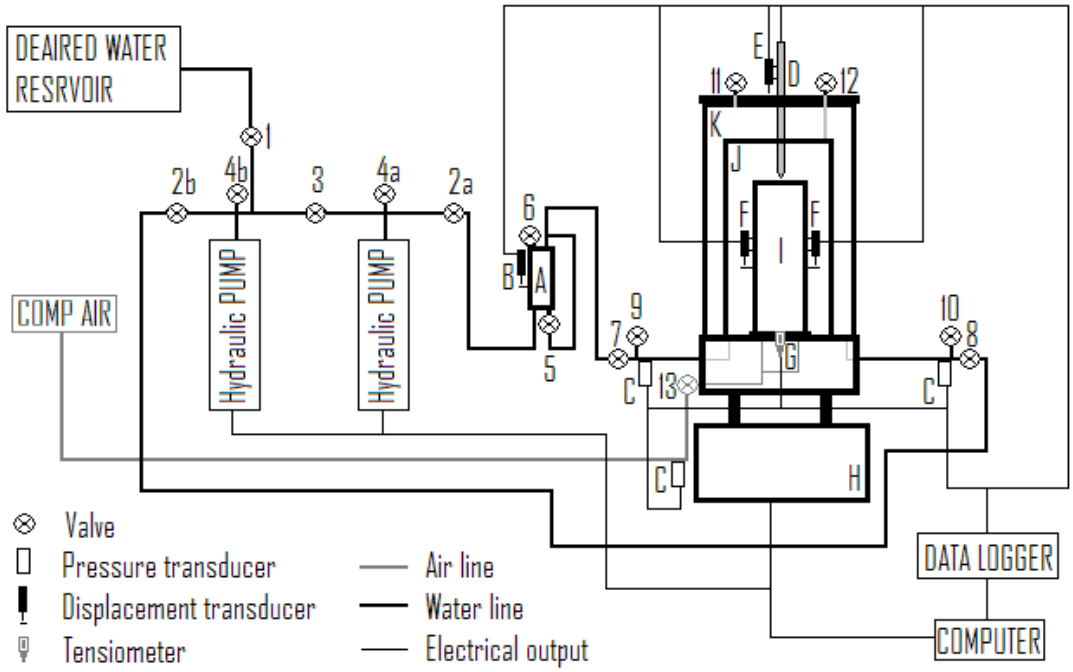

Letter	
A	Volume gauge
B	Volume change transducer
C	Pressure transducer
D	Load cell
E	Axial displacement transducer
F	Mini LVDT
G	Suction probe
H	Loading frame
I	Sample
J	Inner cell
K	Outer cell

Valves	
1	Main deaired water supply
2a	Water supply/pressure line – inner cell
2b	Water supply/pressure line – outer cell
3	Separator valve
4a	Bleed valve – hydraulic pump
4b	Bleed valve – hydraulic pump
5	Overlap – volume gauge
6	Bleed valve – volume gauge
7	Main valve - inner cell
8	Main valve - outer cell
9	Drain valve - inner cell
10	Drain valve - outer cell
11	Bleed valve – outer cell
12	Bleed valve – inner cell
13	Air supply – sample

Figure 6.17 – Constant water content triaxial testing apparatus.

Referring to Figure 6.17, the components used in the testing were as follows:

- The confining pressure (σ_3) was imposed in the inner cell by a stepper motor driven hydraulic pump built by Wykeham Farrance. It was measured using a 2000 kPa pressure transducer C in the water pressure line; to maintain a constant pressure in the outer cell a similar configuration was adopted, resulting in both cells being completely independent from each other.

- A Wykenham Farrance loading frame H was used to provide a constant rate of displacement 0.025mm/min, with displacement measured by the vertical displacement transducer E. Measurements of axial stress (σ_1) were taken inside the cell by a 10 kN capacity load cell D;

- The volumetric behaviour of the sample (ε_v) was measured at the volume gauge A, built in Durham University's School of Engineering workshop. This is a rolling bellofram device of the type developed at Imperial College (Maswoswe, 1985). By measuring the flow of water of the inner cell and maintaining the principle that water is incompressible, the volume changes observed on the volume gauge A were due to volumetric changes in the sample. To achieve a reliable measurement

in such a manner, the presence of air bubbles had to be completely eliminated in order to consider the water as incompressible, something that will be discussed further in this chapter.

- Vertical deflections (ε_a) were determined from the axial displacement transducer, with 75 mm range, mounted externally and also using sample-mounted mini linear variable differential transformers F (mini LVDTs), with a nominal range of 5mm but actually capable of operating over a 10 mm range.

- Pore water pressure (u_w) was measured by a WF-DU high capacity suction probe (also referred to in the literature as a high capacity tensiomenter) G placed at in bottom platen in direct contact with the sample.

- The bottom platen had a flat surface with 2 air lines (see Figure 6.18); the intention of these tests was to perform constant water content triaxial tests while measuring the evolution of suction using a suction probe. By measuring the pore water pressure directly using a high capacity suction probe without the

implementation of axis translation there was no need to install an high air entry value stone in the platen.

- The air lines were used to impose air pressure within the sample while the cell was equilibrating during the equilibrium staged mentioned in Section 6.3.1.2. The value of air pressure applied was dependent on the confining pressure, being 5 kPa lower than the confining pressure, to avoid the inflation of the rubber membrane surrounding the sample.

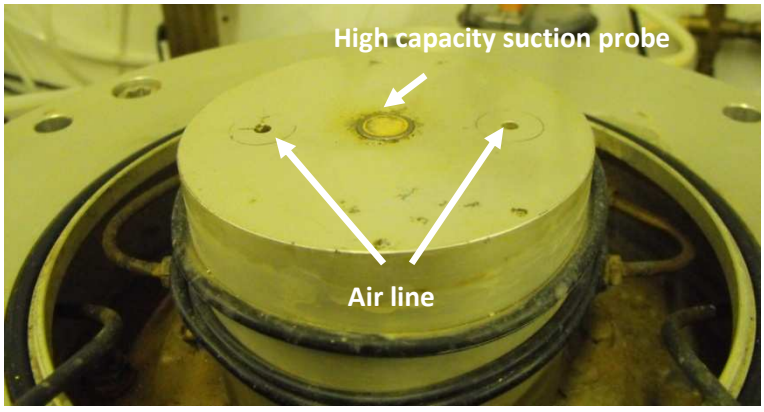

Figure 6.18 – Close view of the pedestal on the triaxial frame, with 2 nozzles and high capacity suction probe.

The whole system was connected to a personal computer with Windows XP as operating system. In the case of this testing program 2 types of computers were used: 1 Pentium™ 4 and 2 Pentium™ D (core duo), with RAM equal or above 1 Gb. Older computers

with a lower RAM value had communication speed difficulties when working with the two hydraulic pumps. The software Triax, a dedicated computer control system for triaxial testing (Toll, 1999), was used to control inner and outer cell pressures, loading rate of the loading frame and to record data from all the measurement equipment into a file compatible with Microsoft Excel™ spreadsheet software.

The accuracy for each type of measuring equipment used during testing is presented in Table 6.7. In similarity with the accuracies determined for the equipment used in the saturated tests, the accuracy was determined differently for the different types of equipment used: during experimental procedures or prior to the experimental work in order to observe fluctuations in the recorded value. Accuracy values that were obtained between experiments where performed to the: volume gauge filled with water, displacement transducer and mini LVDTs positioned at mid travel, high suction probe placed under free water (suction equal to 0) and load cell at rest. The accuracy for the pressure transducers was obtained while the cell was at a constant confinement pressure.

Table 6.7 – Accuracy of the measuring equipment used in saturated triaxial testing.

Measuring equipment	Unit	Accuracy
Volume gauge	cm^3	±0.002
Displacement transducer	mm	±0.005
Mini LVDT	mm	±0.002
Pressure transducer	kPa	±0.2
High capacity suction probe	kPa	±0.5
10 KN load cell	N	±2

The constant water tests were performed on compacted samples according to the preparation methodology presented in Chapter 4 and were carried out using the Double Cell Triaxial Cells (DCTCs) described in Section 6.3.1. Table 6.8 presents the triaxial testing program. In similarity with the saturated testing series each test was indentified in the forms Cxx(yy) by the as-compacted water content (xx) and confining pressure (yy) for samples tested as-compacted, Dxx(yy) for samples dried from as-compacted conditions and Wxx(yy) for samples wetted from as-compacted conditions.

Table 6.8 - Triaxial testing program for the constant water content test series.

Test no.	As-compacted Water content (%)	AC/W/D*	Test conditions Water content (%)	Test conditions Confining pressure (kPa)	Duration** Days
C15(50) 1	14.77	AC	14.77	50	10
C15(50) 2	14.75	AC	14.75	50	52
C15(150)	15.17	AC	15.17	150	15
C15(300)	14.62	AC	14.62	300	20
W15-19(150)	15.21	Wetted	18.45	150	125
W15-19(300)	15.44	Wetted	19.37	300	46
W15-20(50)	14.61	Wetted	19.70	50	45
W15-20(150)	15.09	Wetted	19.75	150	86
W15-22(50)	14.67	Wetted	21.24	50	79
W13-17(300)	13.24	Wetted	17.09	300	105
C20(50)	19.41	AC	19.41	50	14
C20(150)	19.77	AC	19.77	150	31
C20(300) 1	19.37	AC	19.37	300	18
C20(300) 2	20.17	AC	20.17	300	88
D20-15(50)	19.72	Dried	15.08	50	17
D20-15(150)	19.15	Dried	15.56	150	17
D20-15(300)	18.75	Dried	15.19	300	14
W20-21(150)	19.24	Wetted	20.68	150	70
W20-22(50)	19.40	Wetted	21.53	50	66
W20-22(300)	19.89	Wetted	21.29	300	24
C22(50)	21.82	AC	21.82	50	65
C22(150)	21.16	AC	21.16	150	46
C22(300)	22.01	AC	22.01	300	61
D22-20(50)	21.96	Dried	19.44	50	12
D22-20(150) 1	21.92	Dried	19.78	150	18
D22-20(150) 2	22.09	Dried	20.08	150	16
D22-19(150)	21.37	Dried	19.04	150	34
D22-16(50)	21.45	Dried	16.84	50	22
D22-16(300)	21.00	Dried	15.80	300	35
D22-14(150)	21.74	Dried	13.97	150	33

* - process involved in the change of the water content for testing: as-compacted (AC), wetted (W) or dried (D).

** - duration of the time spent of each sample during testing, without sample preparation time.

The samples used for the CWT tests were 100 mm diameter by 200 mm high, larger than the sample size on the saturated tests were 38 mm diameter by 74 mm high. This had an influence of the duration of the test, where samples could remain inside the DCTC for periods of more than 4 months (W15-19(150)). The main factor in determining this duration was the water content of the samples tested, as mentioned, different samples were tested as-compacted, wetted or dried from an as-compacted condition. The tests which the duration

took the longest time were the tests in which samples were wetted from 15% of as-compacted water content.

6.3.3 Constant water content tests results

6.3.3.1 Initial conditions

Tables 6.9, 6.10 and 6.11 presents the initial conditions of the samples at the start of each constant water content test. These initial conditions refer to the point when the samples were placed inside the triaxial cell, where $w_{(ac)}$ and w_i represent water content obtained after compaction and initial water content at the start of the test. Also presented are the initial suction, sample dimensions, etc. Table 6.9 refers to the tests performed on samples that were prepared at the 15% as-compacted condition, with a total of 10 CWT tests: 4 samples were tested as-compacted, 4 samples were wetted to 20% and the remaining 1 sample was wetted to 22%. Included in this table is a sample that was wetted from 13% to 17%, in fact the later sample (test W13-17) was intended to be a sample wetted from 15% to 22%, however a confusion with the initial measurement of water content resulted in different conditions. Table 6.10 refers to the tests performed on samples that were prepared at the 20% as-compacted condition, with a total of 10 CWT tests: 4 samples were tested as-compacted, 3 samples were

dried to 15% and the remaining 3 samples were wetted to 22%. Table 6.11 refers to the tests performed on samples that were prepared at the 22% as-compacted condition, with a total of 10 CWT tests: 3 samples were tested as-compacted, 3 samples were dried to 15% and the remaining 4 samples dried to 22%.

Table 6.9 – Initial conditions at the start of the constant water tests for samples compacted at 15%.

Test No.	Water content		Weight	Dimensions			Dry density	Void ratio	Degree of Saturation	Initial Suction
	Wc_{ac}	Wc_i		Length	Area	Volume	ρ_d	e	S_r	s_i
	%	%	g	cm	cm^2	cm^3	Mg/m^3		%	kPa
C15(50) 1	14.77	14.77	3521	20.32	81.71	1660	1.839	0.47	87.91	227
C15(50) 2	14.75	14.75	3550	20.28	83.16	1687	1.831	0.48	83.77	420
C15(150)	15.17	15.17	3520	20.31	82.89	1684	1.815	0.49	83.80	255
C15(300)	14.62	14.62	3549	20.30	82.84	1682	1.837	0.47	83.87	420
W15-19(150)	15.21	18.45	3729	20.82	87.03	1812	1.715	0.58	93.83	7
W15-19(300)	15.44	19.37	3631	20.77	86.06	1788	1.693	0.60	90.56	17
W15-20(50)	14.61	19.70	3720	20.78	86.09	1789	1.732	0.56	96.51	35
W15-20(150)	15.09	19.75	3717	20.86	87.55	1827	1.667	0.62	95.84	3
W15-22(50)	14.67	22.00	3684	20.90	87.11	1821	1.659	0.63	94.43	0.3
W13-17(300)	13.24	17.09	3719	20.86	87.20	1819	1.676	0.61	96.99	2

Table 6.10 – Initial conditions at the start of the constant water tests for samples compacted at 20%.

Test No.	Water content		Weight	Dimensions			Dry density	Void ratio	Degree of Saturation	Initial Suction
	Wc_{ac}	Wc_i		Length	Area	Volume	ρ_d	e	S_r	s_i
	%	%	g	cm	cm^2	cm^3	Mg/m^3		%	kPa
C20(50)	19.41	19.41	3495	20.33	82.35	1674	1.748	0.55	96.08	19
C20(150)	19.77	19.77	3431	20.31	80.12	1657	1.728	0.56	94.77	15
C20(300) 1	19.64	19.64	3459	20.52	81.71	1676	1.725	0.57	93.55	11
C20(300) 2	20.17	20.17	3445	20.55	81.71	1678	1.709	0.58	93.69	18
D20-15(50)	19.72	15.08	3318	19.74	79.93	1578	1.828	0.48	85.11	600
D20-15(150)	19.15	15.56	3352	19.81	81.71	1618	1.792	0.51	82.76	264
D20-15(300)	18.75	15.19	3326	19.91	79.82	1590	1.816	0.49	84.05	350
W20-21(150)	19.24	20.68	3522	20.29	85.16	1728	1.677	0.61	95.12	4
W20-22(50)	19.40	21.53	3527	20.35	84.05	1710	1.709	0.58	96.08	4
W20-22(300)	19.89	21.29	3482	20.26	84.86	1719	1.670	0.62	92.99	5

Table 6.11 – Initial conditions at the start of the constant water tests for samples compacted at 22%.

Test No.	Water content		Weight	Dimensions			Dry density	Void ratio	Degree of Saturation	Initial Suction
	Wc_{ac}	Wc_i		Length	Area	Volume	ρ_d	e	S_r	s_i
	%	%	g	cm	cm^2	cm^3	Mg/m^3		%	kPa
C22(50)	21.82	21.82	3376	20.52	83.32	1710	1.621	0.67	88.34	5
C22(150)	22.16	22.16	3358	20.51	83.32	1709	1.609	0.68	88.03	7
C22(300)	22.01	22.01	3357	20.52	82.60	1695	1.624	0.66	89.50	7
D22-20(50)	21.96	19.98	3234	20.17	79.64	1606	1.678	0.61	88.41	95
D22-20(150) 1	21.92	19.78	3261	20.09	80.66	1620	1.680	0.61	87.80	2.5
D22-20(150) 2	22.09	20.08	3376	20.57	82.86	1704	1.649	0.64	84.94	107
D22-19(150)	21.37	19.04	3334	20.44	82.97	1696	1.651	0.64	80.84	91
D22-16(50)	21.45	16.84	3198	19.17	80.09	1536	1.782	0.52	88.13	
D22-16(300)	21.00	15.80	3186	19.52	77.86	1520	1.811	0.49	86.65	131
D22-14 (150)	21.74	13.97	3173	19.51	77.99	1521	1.830	0.48	79.18	243

It can be seen in all tables that the samples tested at the same water content (w_i) had similar values for most variables in terms of weight, dimensions, dry densities, void ratio and degree of saturation, although, showing some differences in the suction values.

It was clear from the tables 6.9, 6.10 and 6.11 that the dimensions increased with the increase of water content when wetted or dried from an as-compacted condition. As expected, dry density and suction was generally higher in samples tested at w_i close to 15%. Higher dry density would be expected as this coincides with optimum water content, and suctions would be expected to be highest as it is the driest water content.

In all tables (Tables 6.9-6.11) it can be observed that the volume of sample was different depending on the water content tested. Samples that were wetted from an as compacted condition increased in volume while sample that were dried decreased in volume. For example, from Table 6.10, in C20(150) the initial volume was 1674 cc (sample tested as compacted), while in D20-15(150) (sample tested dried to 15%) the volume after drying was 1618 cc and in W20-21(150) (sample tested wetted to 22%) the volume after wetting was 1728 cc.

The suction values measured at the start of the tests proved to be well inside the measurements obtained with the in-contact filter paper technique in section 5.5 in the previous chapter, as is shown in Figures 6.19 – 6.21. Some scatter was observed for the CWT tests at the lower levels of suction (<100 kPa) at wc_i higher than 20%, especially for samples where the wc_{ac} was 15% and 22%.

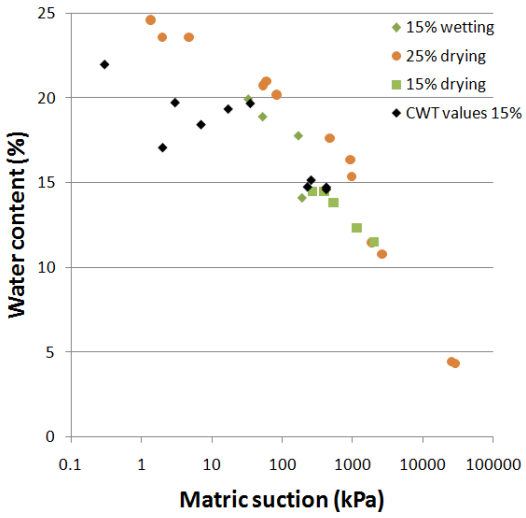

Figure 6.19 - Matric suction of in-contact filter paper and high capacity suction probe for 15%.

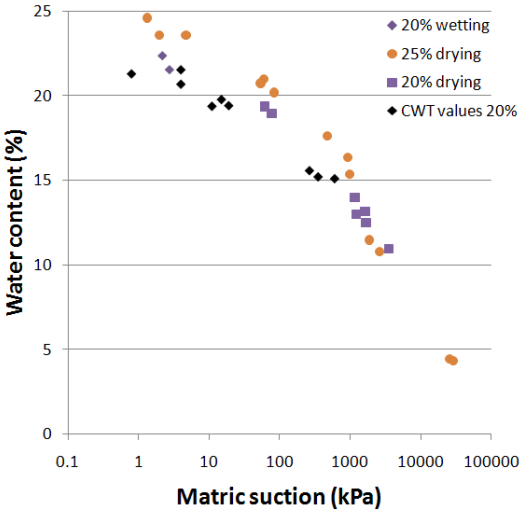

Figure 6.20 – Matric suction of in-contact filter paper and high capacity suction probe for 20%.

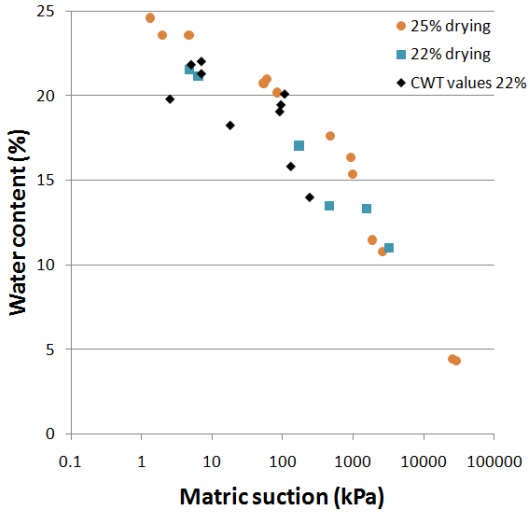

Figure 6.21 – Matric suction of in-contact filter paper and high capacity suction probe for 22%.

6.3.3.2 Constant water compression

After the initial equilibrium stage, when volume change stabilized it was considered that the double cell triaxial cell had achieved equilibrium and all air bubbles had been dissolved. When this was achieved the constant water compression stage started. Table 6.12, 6.13 and 6.14 shows the conditions of each sample at the time of the start and end of the constant water compression stage. In this stage each sample was subjected to isotropic stress. During this stage, the void space of each sample reduced, increasing the saturation level. Albeit, on the CWT tests that were performed on dried samples (D20-15(50), D20-15(150) and D20-15(300) in Table 6.13 and D22-20(50), D22-19(150), D22-20(150) 1, D22-20(150) 2, D22-16(50), D22-16(300) and D22-14(150) in Table 6.14) and on samples tested at 15% of water

content at as-compacted conditions (C15(50) 1, C15(50) 2, C15(150) and C15(300) in Table 6.12) volumetric changes were almost negligible.

The general tendency in all tests during the constant water compression stage was for the pore water pressure to decrease, apart from test D20-15(150). During the compression stage with the size reduction of the samples it would be expected that the pore water pressure would increase, as a reduction in sample size implies voids getting smaller which relates to increase in the degree of saturation under constant water conditions. However, in the case of these CWT tests, before the compression stage there was the equilibrium stage where, air pressure was applied to the samples. It seems the dissipation of air pressure was not as immediate as expected, instead a gradual dissipation over time explains the observed abnormality. Therefore, although the initial values of pore water pressure at the start of the compression stage were influenced by the previous equilibrium stage at the end of the compression stage the air pressure had totally dissipated, specially helped by the long duration of this stage.

In all tables (6.12 to 6.14), samples tested with Wc_i close to 15% remained with negative pore water pressure values (suction) during the compression stage. Tested samples

with Wc_i close to 20% reached only small negative values of pore water pressure at the end of the compression stage, at lower values of confinement (50 and 150kPa). Samples that were wetted from as-compacted conditions, whatever the as-compacted water content, always maintained positive values of pore water pressure during the constant water compression stage.

Table 6.12 – Sample conditions at the start and end of the constant water compression for samples compacted at Wc(ac) close to 15%.

	Test No.		Volume	Dry density	Void ratio	Degree of saturation	Pore water pressure	Confining pressure
			cm^3	Mg/m^3		%	kPa	kPa
Wc_i close to 15%	C15(50) 1	Initial	1660	1.840	0.47	87.94	-210.8	50
		Final	1653	1.848	0.46	89.20	-241.5	
	C15(50) 2	Initial	1687	1.834	0.47	84.12	-74.3	50
		Final	1679	1.843	0.47	85.42	-185.8	
	C15(150)	Initial	1683	1.816	0.49	83.96	-173.2	150
		Final	1681	1.818	0.49	84.22	-236.2	
	C15(300)	Initial	1676	1.847	0.46	85.35	-148.8	300
		Final	1664	1.860	0.45	87.28	-176.7	
Wc_i close to 20%	W15-19(300)	Initial	1788	1.702	0.59	88.97	283.2	300
		Final	1735	1.753	0.54	96.62	153.7	
	W15-19(150)	Initial	1812	1.737	0.56	89.71	136.3	150
		Final	1774	1.775	0.52	95.40	39.7	
	W15-20(50)	Initial	1789	1.737	0.56	95.73	4.5	50
		Final	1777	1.749	0.55	97.65	2.1	
	W15-20(150)	Initial	1827	1.699	0.59	90.37	99.4	150
		Final	1796	1.729	0.56	94.70	43.8	
Wc_i close to 22%	W15-22(50)	Initial	1821	1.669	0.62	92.64	24.9	50
		Final	1792	1.695	0.59	96.57	9.4	
	W13-17(300)	Initial	1819	1.746	0.55	84.27	294.7	300
		Final	1757	1.808	0.49	93.33	73.3	

Table 6.13 – Sample conditions at the start and end of the constant water compression for samples compacted at Wc(ac) close to 20%.

	Test No.		Volume	Dry density	Void ratio	Degree of saturation	Pore water pressure	Confining pressure
			cm^3	Mg/m^3		%	kPa	kPa
Wc_i close to 20%	C20(50)	Initial	1674	1.753	0.54	91.75	17.5	50
		Final	1664	1.763	0.53	93.35	-10.1	
	C20(150)	Initial	1627	1.753	0.54	95.28	77.2	150
		Final	1600	1.782	0.52	99.95	-1.1	
	C20(300) 1	Initial	1676	1.717	0.57	91.24	218.2	300
		Final	1667	1.727	0.56	92.70	206.5	
	C20(300) 2	Initial	1677	1.722	0.57	86.55	154.5	300
		Final	1638	1.763	0.53	92.36	97.6	
Wc_i close to 15%	D20-15(50)	Initial	1578	1.827	0.48	84.97	-695.1	50
		Final	1574	1.831	0.48	85.57	-681.9	
	D20-15(150)	Initial	1618	1.792	0.51	82.76	-245.2	150
		Final	1616	1.794	0.51	83.05	-261.1	
	D20-15(300)	Initial	1590	1.815	0.49	83.94	-22.5	300
		Final	1586	1.820	0.49	84.61	-353.2	
Wc_i close to 22%	W20-21(150)	Initial	1710	1.686	0.60	92.66	49.4	150
		Final	1664	1.733	0.56	99.91	26.9	
	W20-22(50)	Initial	1728	1.670	0.62	94.04	18.0	50
		Final	1708	1.689	0.60	97.0	12.5	
	W20-22(300)	Initial	1719	1.670	0.62	92.99	287.7	300
		Final	1710	1.679	0.61	94.32	274.1	

Table 6.14 – Sample conditions at the start and end of the constant water compression for samples compacted at Wc(ac) close to 22%.

	Test No.		Volume	Dry density	Void ratio	Degree of saturation	Pore water pressure	Confining pressure
			cm^3	Mg/m^3		%	kPa	kPa
Wc_i close to 22%	C22(50)	Initial	1710	1.615	0.67	87.52	23.9	50
		Final	1688	1.635	0.65	90.32	9.5	
	C22(150)	Initial	1709	1.608	0.71	81.30	117.6	150
		Final	1735	1.583	0.68	84.44	77.3	
	C22(300)	Initial	1695	1.620	0.67	82.30	224.3	300
		Final	1658	1.655	0.63	86.95	147.5	
Wc_i close to 20%	D22-20(50)	Initial	1606	1.738	0.56	94.59	-75.8	50
		Final	1603	1.742	0.55	95.17	-50.7	
	D22-20(150) 1	Initial	1620	1.672	0.62	86.69	33.2	150
		Final	1606	1.686	0.60	88.70	-0.2	
	D22-20(150) 2	Initial	1704	1.646	0.64	84.58	11.9	150
		Final	1690	1.661	0.63	86.47	-4.1	
	D22-19(150)	Initial	1647	1.686	0.60	85.31	-	150
		Final	1631	1.702	0.59	87.55	0.8	
Wc_i close to 15%	D22-16(50)	Initial	1536	1.798	0.50	90.44	-	50
		Final	1529	1.806	0.50	91.61	-299.1	
	D22-16(300)	Initial	1520	1.818	0.49	87.70	-	300
		Final	1521	1.816	0.49	87.43	-131.3	
	D22-14(300)	Initial	1521	1.829	0.48	79.04	-40.0	150
		Final	1515	1.837	0.47	80.09	-179.1	

6.3.3.3 Shearing

The start of the shearing stage, in this study, coincides with the end of the constant water compression stage, thus the conditions at which the samples entered the shearing stage correspond to the final values on Tables 6.12, 6.13 and 6.14.

The measurements during the shearing stage are presented in Figures 6.22 to 6.39. To help in the visualization of the behaviour, for the different variables presented, constant water tests that were performed at the same Wc(ac) were represented in the same colour scheme. Each set of tests presents the same colour graduation through the various plots. Refer to Tables 6.12, 6.13 and 6.14 to link the respective CWT with the initial shearing stage values.

Figures 6.22, 6.28 and 6.34 shows typical stress-strain relationships for the constant water content tests. The shearing stage in each test started with a rapid increase of deviatoric stress over a small range of the axial strain which was followed by a continued increase in deviatoric stress in a wider range of axial strain. After these two phases of increase of deviatoric stress two different end conditions were observed: the first was observed in the tested samples that had Wc_i close to 15% (C15(50) 1, C15(50) 2, C15(150), and C15(300) in Figure 6.22; D20-15(50), D20-15(150) and D20-15(300) in Figure 6.28 and D22-16(50), D22-16(300) and D22-14(150) in Figure 6.34) where a strength peak was followed by an abrupt decline on the deviatoric stress over a short range of axial strain followed by a continued reduction in deviatoric stress over a wide range of axial strain; for the remaining tests after the maximum deviatoric stress was achieved, the deviatoric stress was maintained at almost a constant level.

Pore water pressure behaviour during the shearing stage changed, and in general the tendency was similar in all tests. Pore water pressure increased with the initial contraction as the load was initially applied and, when samples started to dilate, it coincided with the decrease in pore water pressure, see Figures 6.23 and 6.24, for tests performed on samples with Wc_i close to 15%; Figures 6.29 and 6.30, for tests performed on samples with Wc_i close to 20%; Figures 6.35 and 6.36, for tests performed on samples with Wc_i close to 22%.

The stress path achieved in each test is presented in Figure 6.25 (for samples prepared from samples with Wc(ac) close to 15%), Figure 6.31 (for samples prepared from samples with Wc(ac) close to 20%) and Figure 6.37 (for samples prepared from samples with Wc(ac) close to 22%) where, $p\text{-}u_w$ represents mean net stress minus pore water pressure. In the case of saturated tests it would be mean effective stress, however, as the specimens were not saturated, $p\text{-}u_w$ cannot be taken as effective stress. As expected, samples that were tested at Wc_i close to 15%, coinciding to the higher values of suction in this testing program (lowest values of pore water pressure) experienced the highest changes in deviatoric stress. Opposing to the CWT tests, where samples with Wc_i close to 22% experienced the lowest changes of deviatoric and $p\text{-}u_w$.

Changes in void ratio experienced during shearing by each test are presented in Figures 6.27, 6.33 and 6.39.

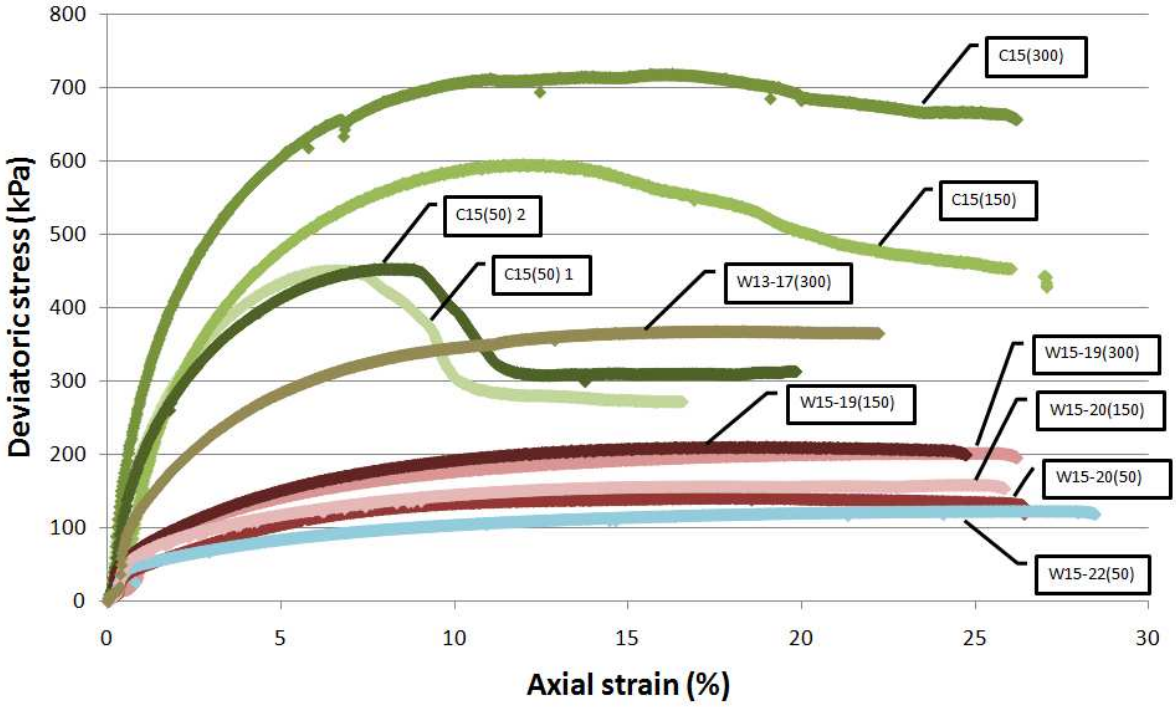

Figure 6.22 – Deviatoric stress- strain relationships for samples with Wc(ac) of 15%.

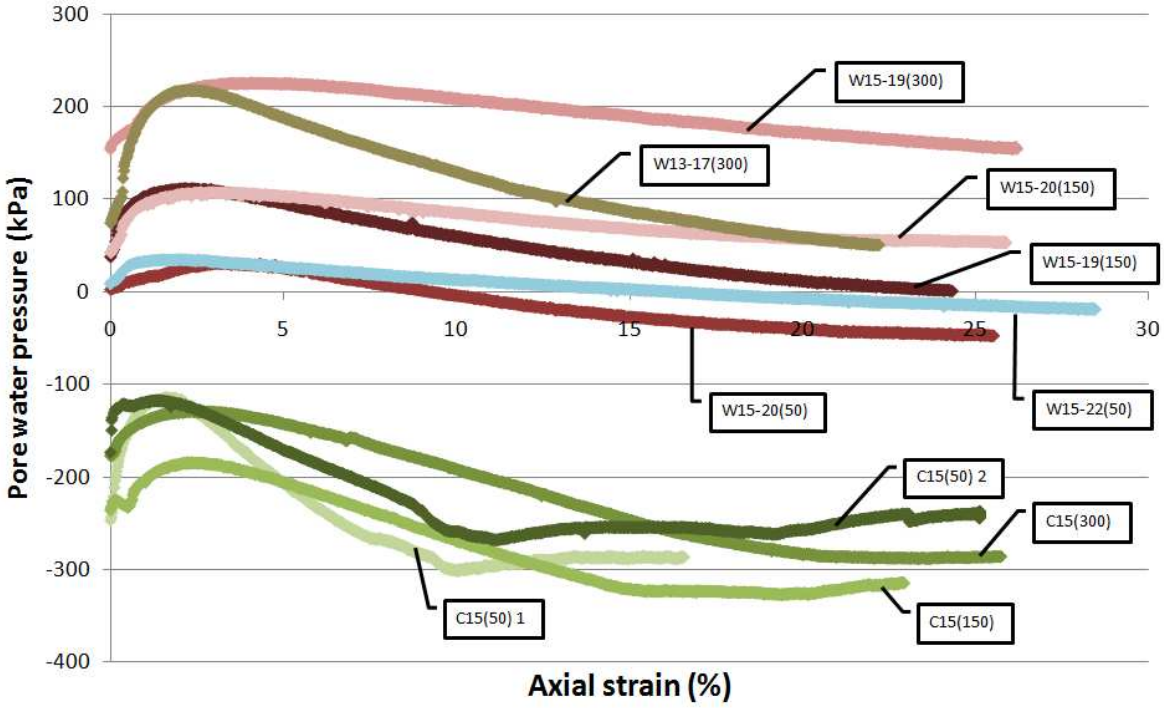

Figure 6.23 – Variation of pore water pressure with axial strain for samples with Wc(ac) of 15%.

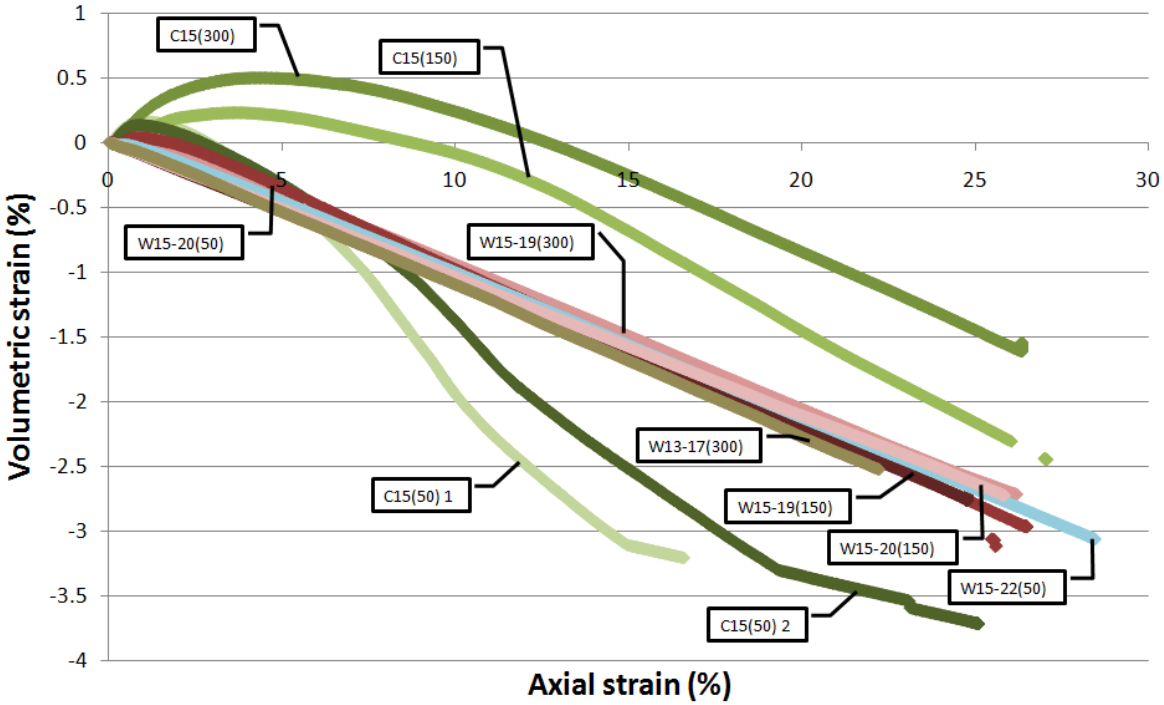

Figure 6.24 – Volumetric-axial strain relationships for samples with Wc(ac) of 15%.

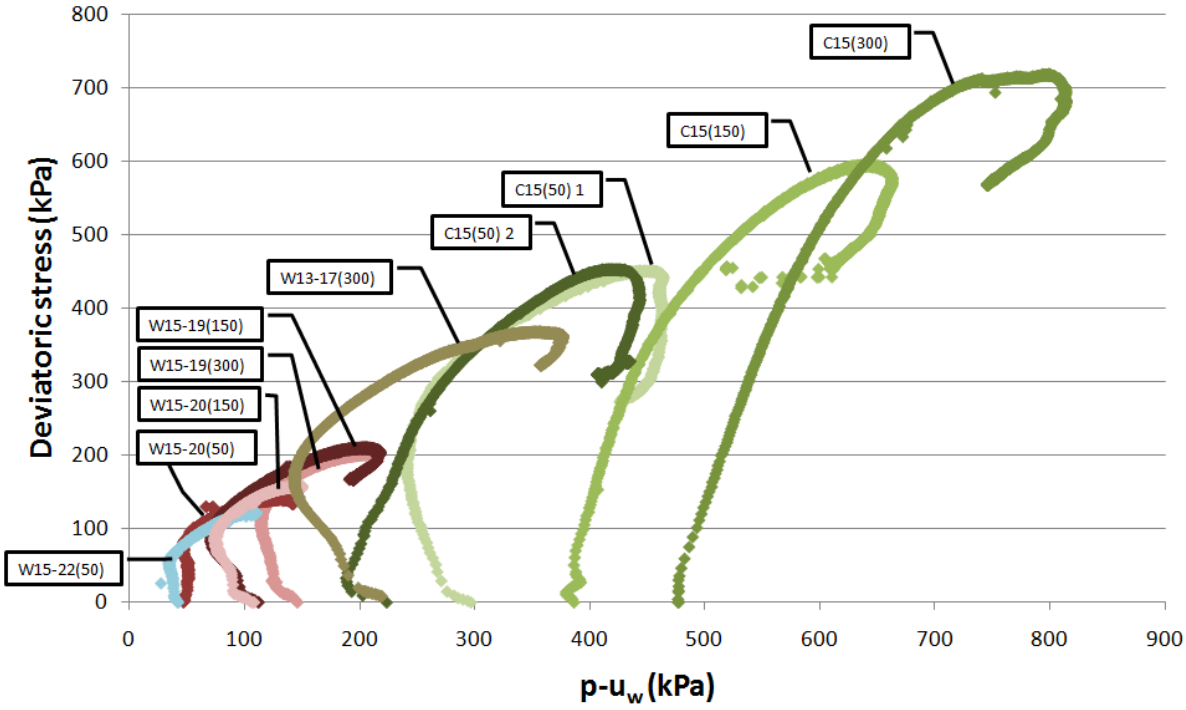

Figure 6.25 – Constant water content stress paths in the (p-u_w)-q plane for samples with Wc(ac) close to 15%.

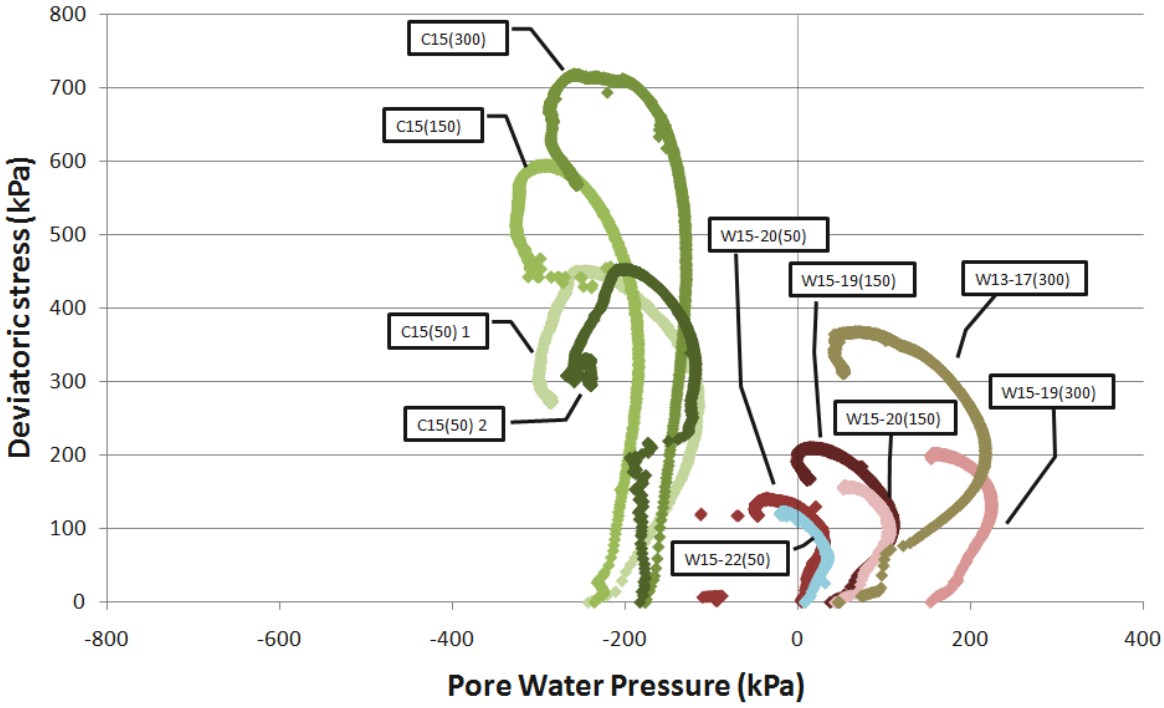

Figure 6.26 – Deviatoric stress- pore water pressure relationships for samples with Wc(ac) of 15%.

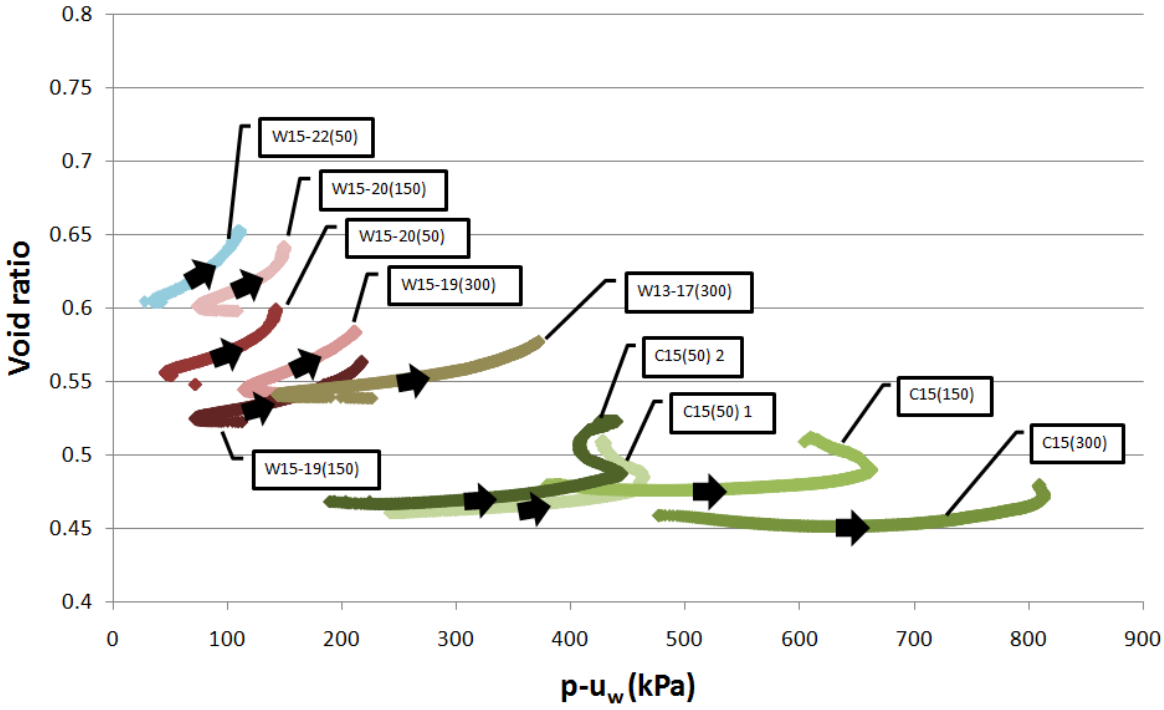

Figure 6.27 – Void ratio - (p-u_w) relationships for samples with Wc(ac) of 15%.

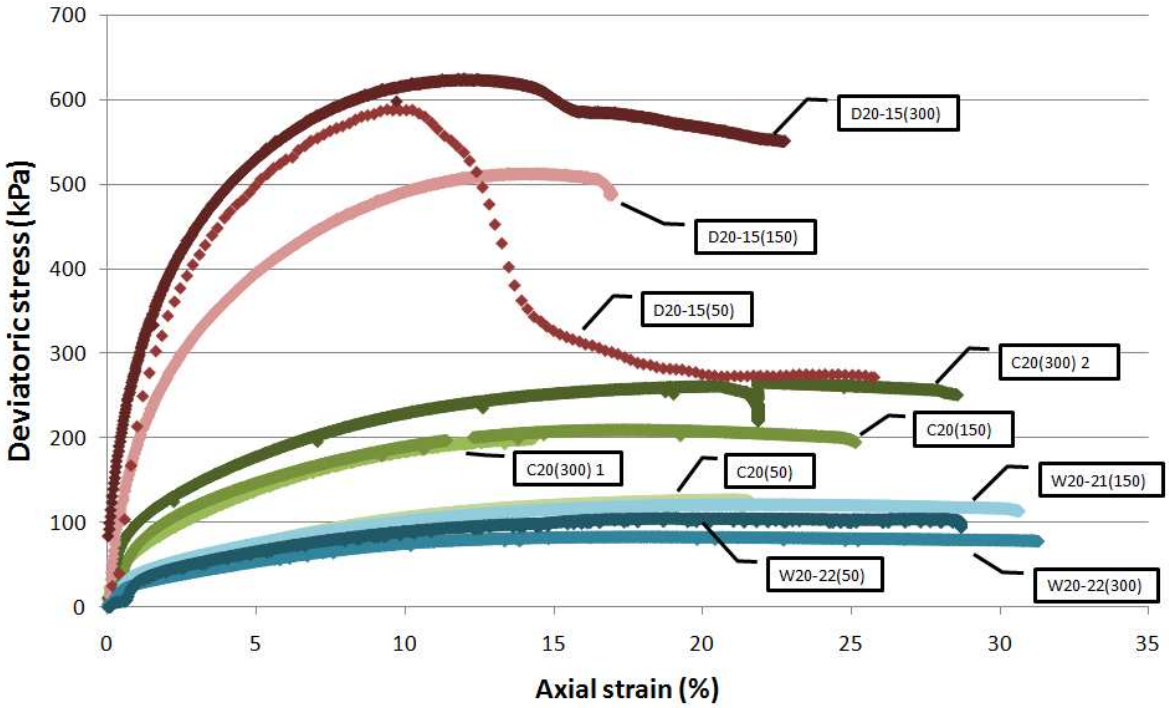

Figure 6.28 – Deviatoric stress- strain relationships for samples with Wc(ac) of 20%.

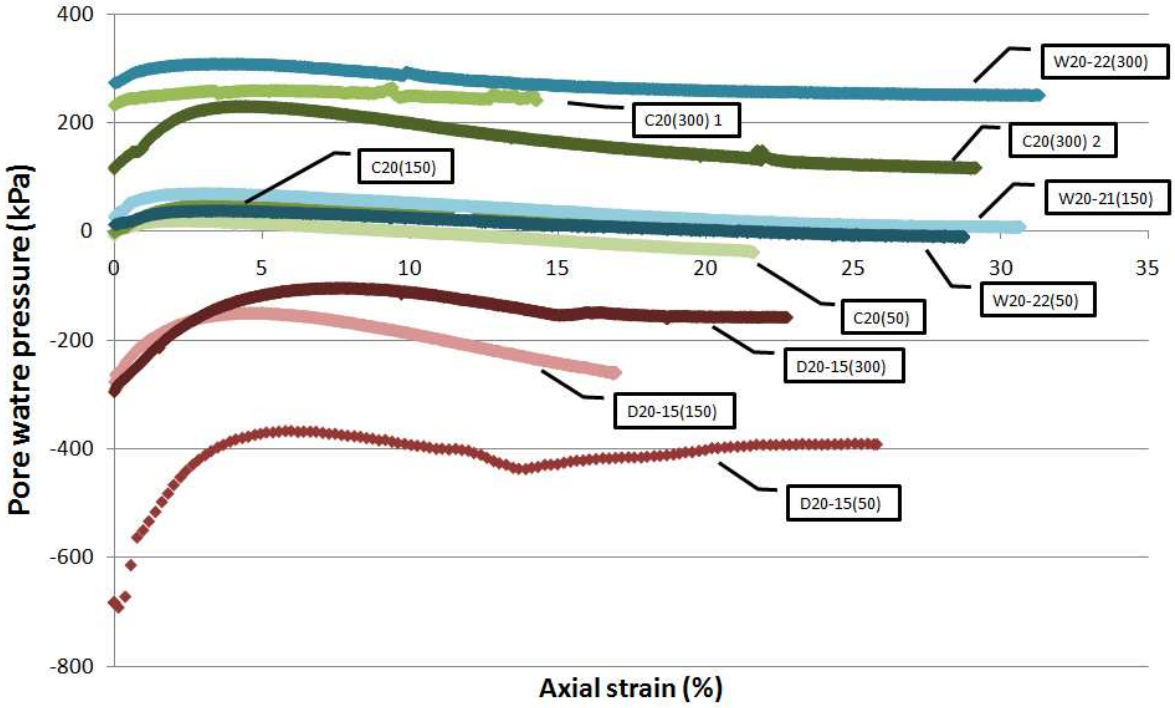

Figure 6.29 – Variation of pore water pressure with axial strain for samples with Wc(ac) of 20%.

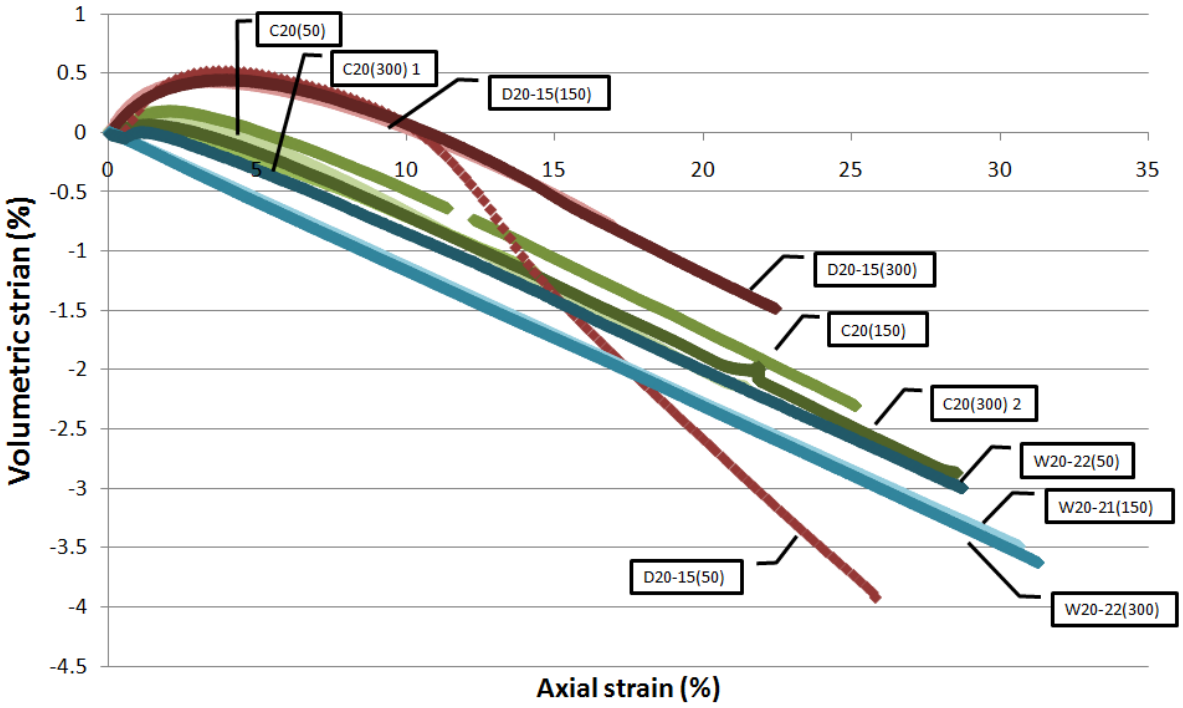

Figure 6.30 – Volumetric-axial strain relationships for samples with Wc(ac) of 20%.

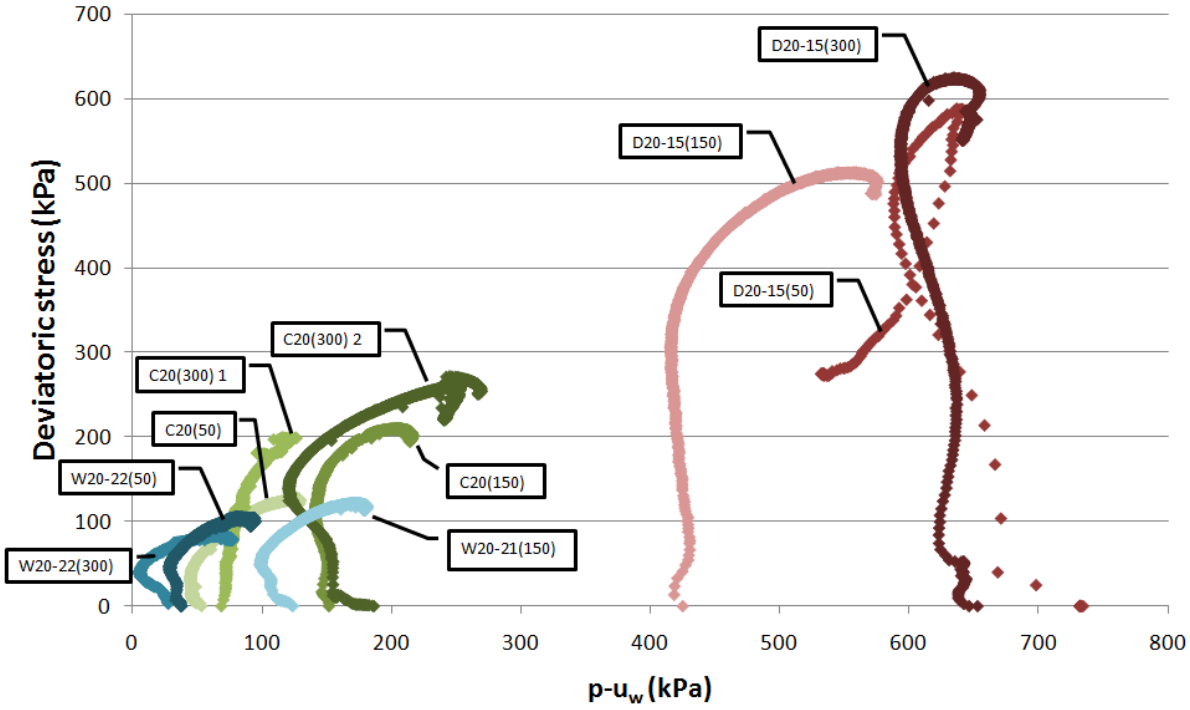

Figure 6.31 – Constant water content stress paths in the (p-u_w)-q plane for samples with Wc(ac) close to 20%.

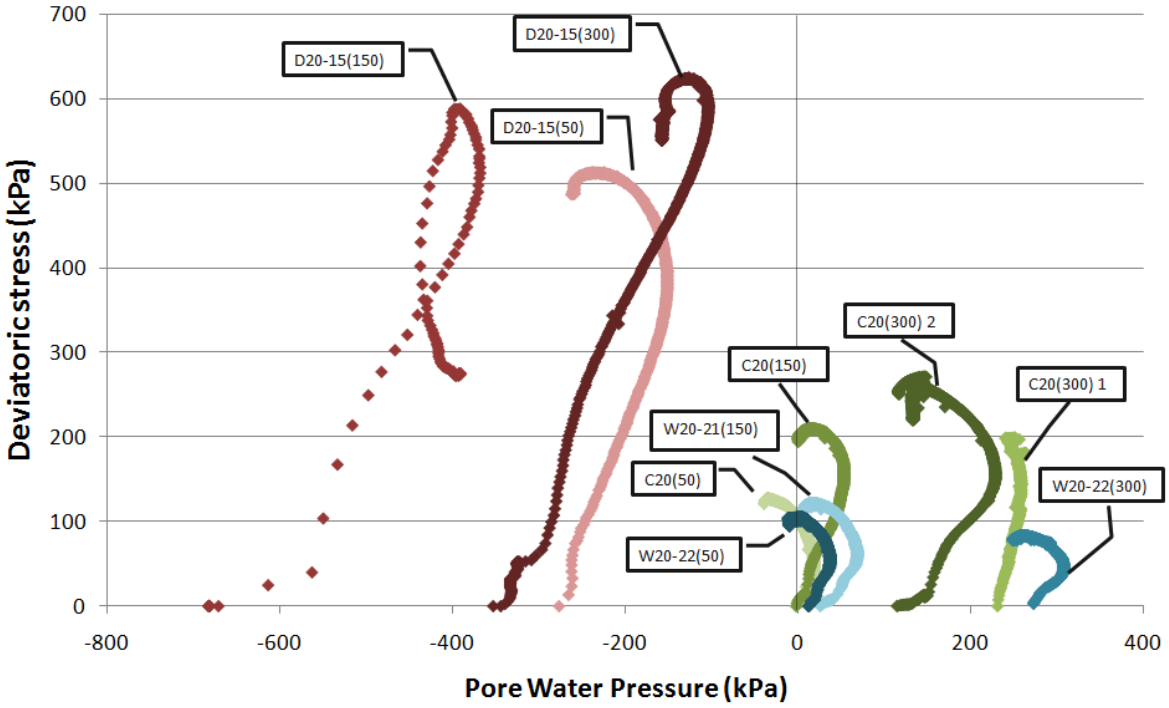

Figure 6.32 – Deviatoric stress- pore water pressure relationships for samples with Wc(ac) of 20%.

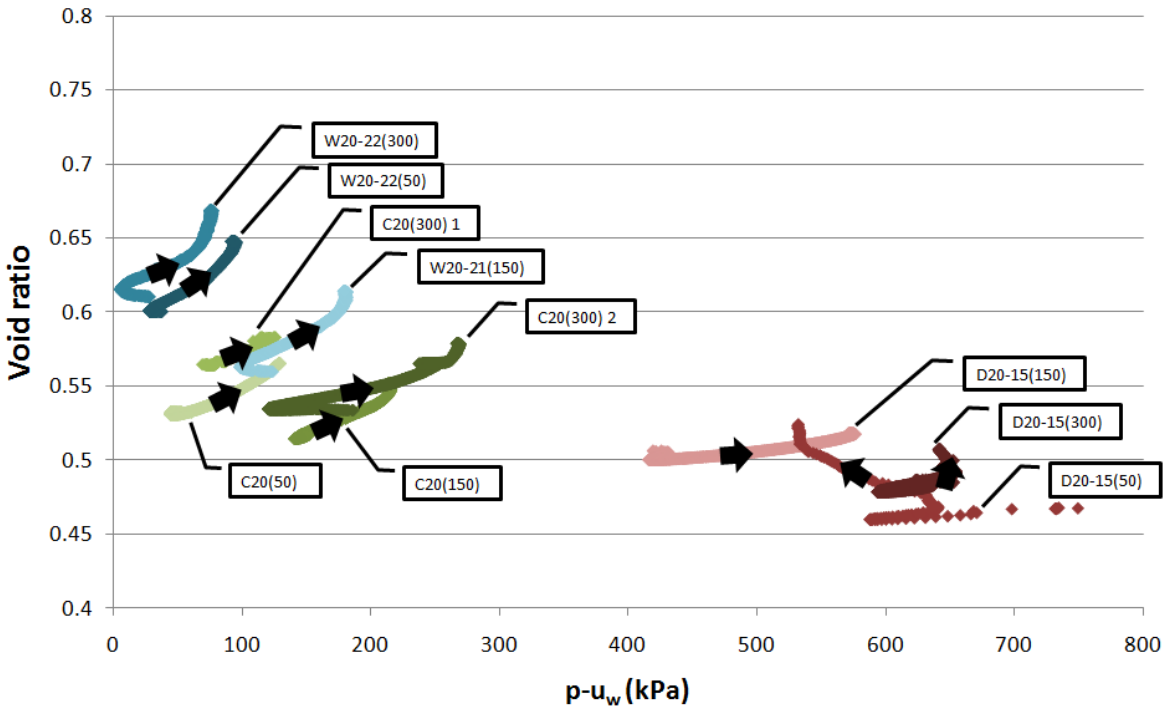

Figure 6.33 – Void ratio - (p-u_w) relationships for samples with Wc(ac) of 20%.

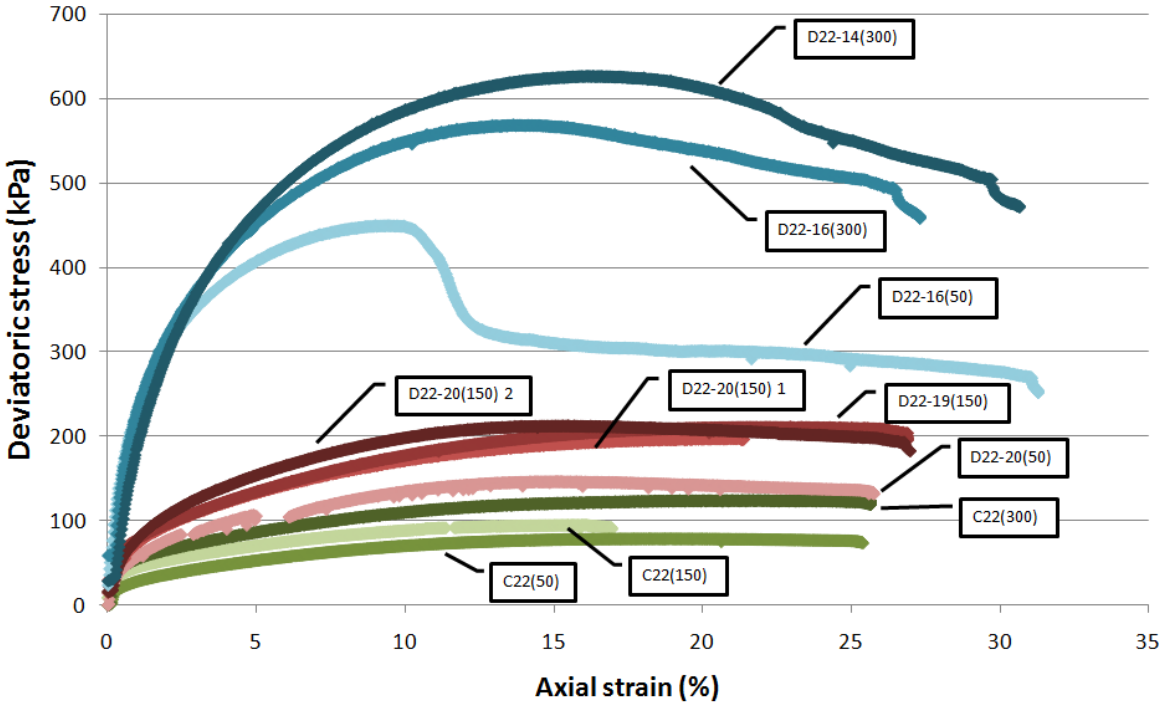

Figure 6.34 – Deviatoric stress- strain relationships for samples with Wc(ac) of 22%.

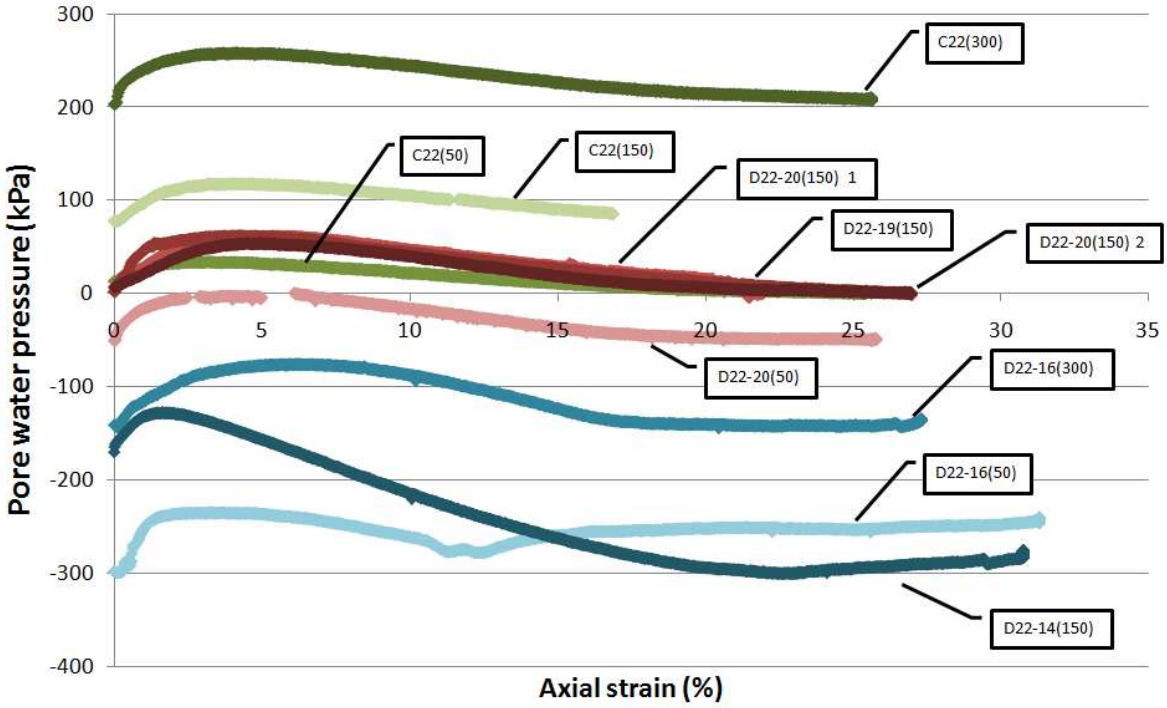

Figure 6.35 – Variation of pore water pressure with axial strain for samples with Wc(ac) of 22%.

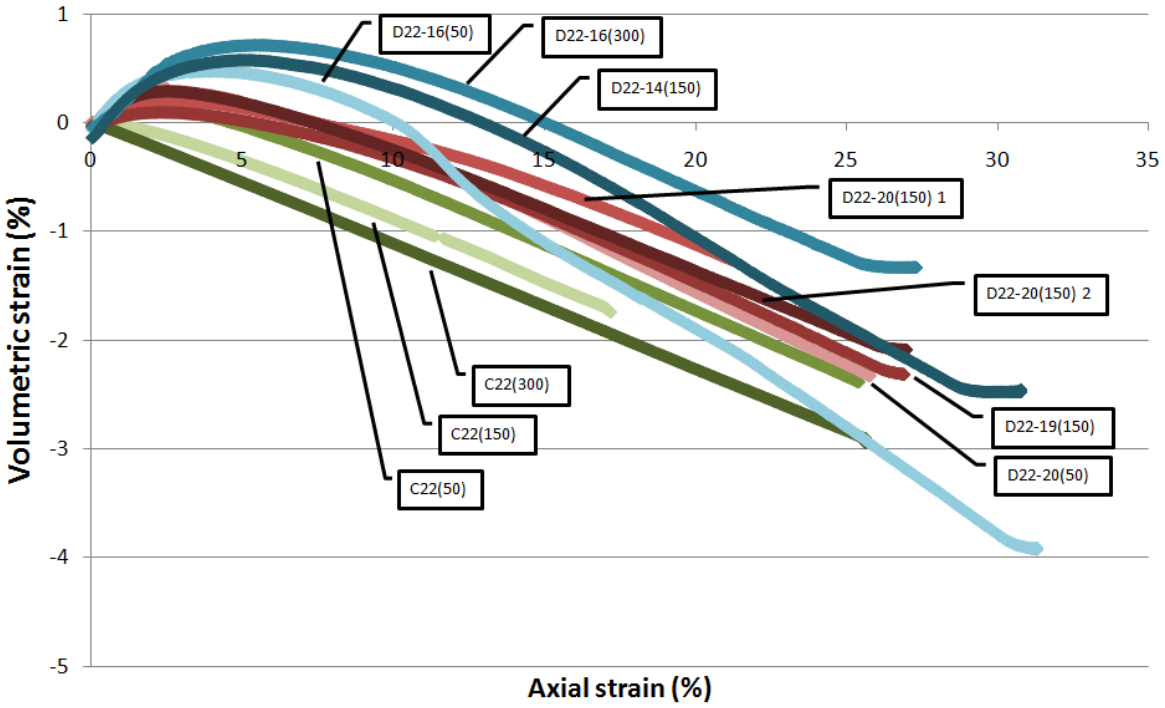

Figure 6.36 – Volumetric-axial strain relationships for samples with Wc(ac) of 22%.

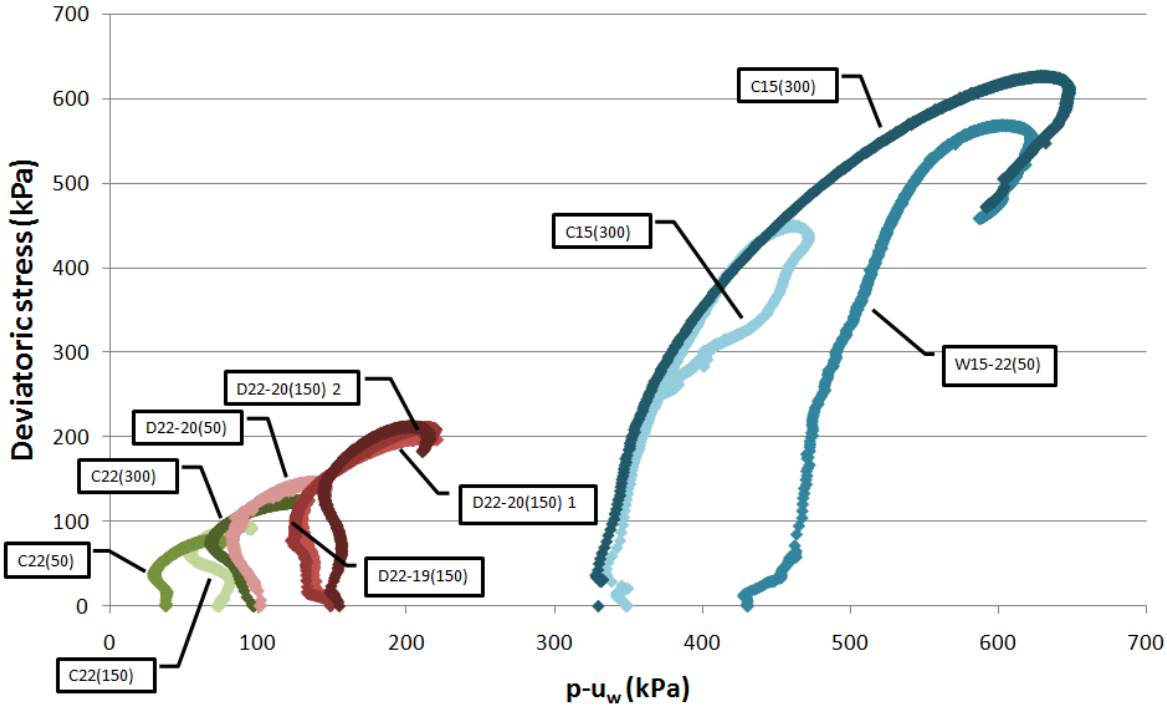

Figure 6.37 – Constant water content stress paths in the (p-u_w)-q plane for samples with Wc(ac) close to 22%.

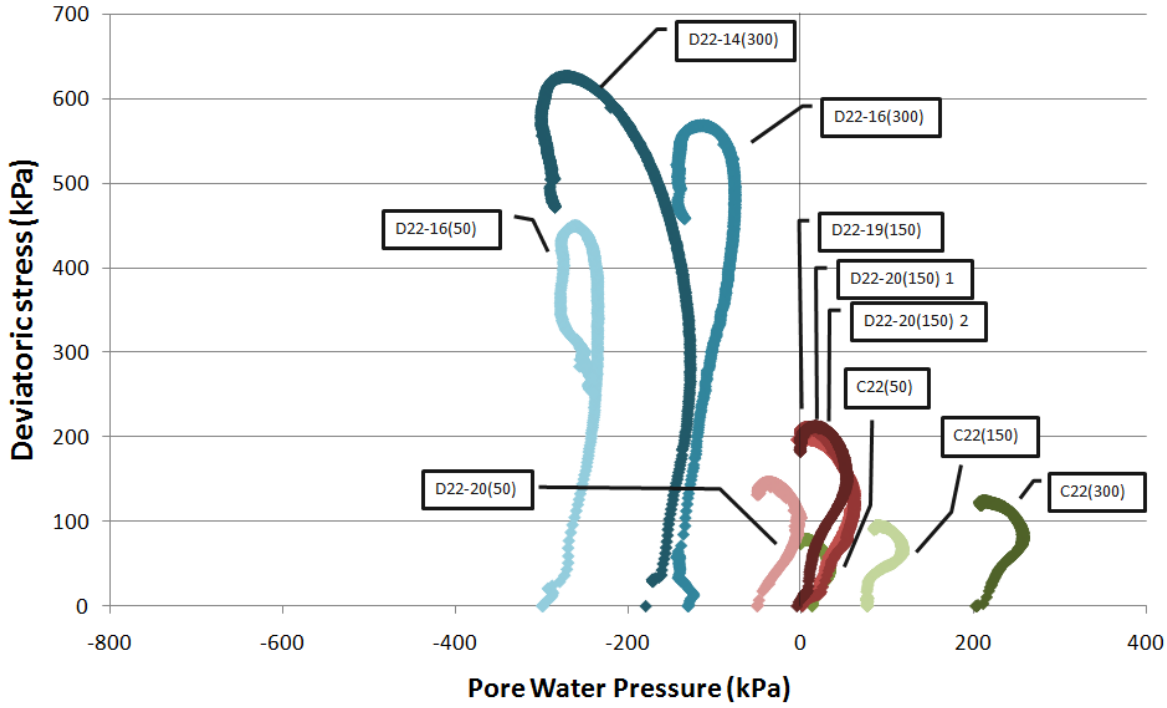

Figure 6.38 – Deviatoric stress- pore water pressure relationships for samples with Wc(ac) of 22%.

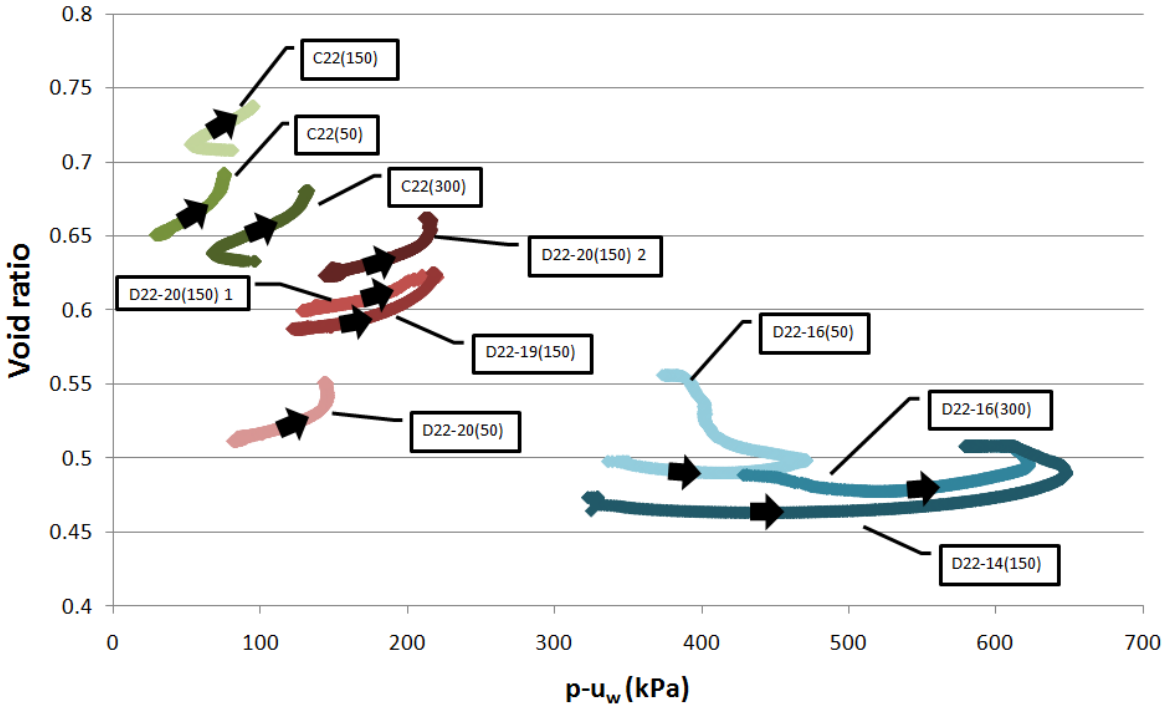

Figure 6.39 – Void ratio - (p-u_w) relationships for samples with Wc(ac) of 22%.

6.3.3.3.1 Maximum deviatoric stress results

Table 6.15, 6.16 and 6.17 presents the conditions at which each test achieved maximum deviatoric stress, for samples tested at Wc(ac) close to 15%, 20% and 22% respectively. It was noticed that conditions were different for different tests at this stage, as has been mentioned. The tests that were performed at values in which Wc_i was close to 15% the maximum value of deviatoric stress was achieved at negative values of pore water pressure. This was also true in tests where Wc_i was close to 20% when the confining pressure

was 50 kPa, although in this case the pore water pressures had small negative values. The remaining tests reached this level at positive values of pore water pressure.

Table 6.15 – Conditions of each sample at maximum deviatoric stress for samples with Wc(ac) close to 15%.

	Test No.	Dry density	Void ratio	Degree of saturation	Mean net stress	Deviatoric stress	Pore water pressure	$p\text{-}u_w$
		Mg/m^3		%	kPa	kPa	kPa	kPa
Wc_i close to 15%	C15(50) 1	1.835	0.47	87.19	200.4	450.8	-242.8	443.2
	C15(50) 2	1.826	0.48	83.03	204.1	461.4	-210.2	414.4
	C15(150)	1.827	0.48	85.53	355.4	616.0	-292.3	647.7
	C15(300)	1.836	0.47	83.65	523.9	671.7	-287.8	811.7
Wc_i close to 20%	W15-19(150)	1.739	0.55	90.05	220.2	210.7	17.3	202.9
	W15-19(300)	1.710	0.58	90.17	367.3	201.9	160.2	207.1
	W15-20(50)	1.712	0.58	92.01	97.31	141.6	-35.4	132.7
	W15-20(150)	1.686	0.60	88.53	202.9	158.4	55.1	147.8
Wc_i close to 22%	W15-22(50)	1.646	0.64	89.39	91.3	123.3	-17.9	109.2
	W13-17(300)	1.773	0.52	88.06	423.2	368.9	71.2	352.0

Table 6.16 – Conditions of each sample at maximum deviatoric stress for samples with Wc(ac) close to 20%.

	Test No.	Dry density	Void ratio	Degree of saturation	Mean net stress	Deviatoric stress	Pore water pressure	$p\text{-}u_w$
		Mg/m^3		%	kPa	kPa	kPa	kPa
Wc_i close to 20%	C20(50)	1.728	0.56	88.12	93.0	128.2	-34.9	127.9
	C20(150)	1.756	0.54	95.87	220.3	209.5	13.6	206.7
	C20(300) 1	1.708	0.58	89.82	366.5	199.5	251.1	115.4
	C20(300) 2	1.727	0.57	87.18	391.1	271.9	146.2	244.8
Wc_i close to 15%	D20-15(50)	1.834	0.47	85.97	246.0	588.0	-387.1	633.1
	D20-15(150)	1.788	0.51	82.23	321.1	512.6	-224.2	545.4
	D20-15(300)	1.818	0.49	84.35	508.4	624.6	-126.6	635.0
Wc_i close to 22%	W20-21(150)	1.692	0.60	93.47	190.7	121.1	18.6	172.1
	W20-22(50)	1.658	0.63	92.34	85.4	105.6	3.5	81.9
	W20-22(300)	1.646	0.64	89.62	327.9	83.4	263.5	64.4

Table 6.17 – Conditions of each sample at maximum deviatoric stress for samples with Wc(ac) close to 22%.

	Test No.	Dry density	Void ratio	Degree of saturation	Mean net stress	Deviatoric stress	Pore water pressure	p-u_w
		Mg/m^3		%	kPa	kPa	kPa	kPa
Wc_i close to 22%	**C22(50)**	1.61	0.68	86.80	76.4	78.7	5.4	71.0
	C22(150)	1.56	0.74	78.24	182.0	95.2	87.8	94.1
	C22(300)	1.62	0.67	81.80	341.5	124.2	213.3	128.2
Wc_i close to 20%	**D22-20(50)**	1.726	0.57	92.87	98.9	146.4	-37.3	136.2
	D22-20(150) 1	1.667	0.62	85.97	216.2	198.3	-0.3	216.5
	D22-20(150) 2	1.647	0.64	84.60	221.2	212.6	16.7	204.6
	D22-19(150)	1.671	0.62	83.39	221.2	211.7	5.6	215.6
Wc_i close to 15%	**D22-16(50)**	1.808	0.49	91.99	200.1	449.8	-258.9	458.9
	D22-16(300)	1.820	0.49	87.95	489.8	568.7	-112.4	602.2
	D22-14(150)	1.829	0.48	79.05	358.8	626.3	-270.6	629.4

The axial strain at which each test achieved the maximum deviatoric stress are presented in Tables 6.18, 6.19, 6.20 and 6.21. This time the data is gathered by Wc_i and confining pressure. For samples tested at Wc_i close to 15% it was observed that the maximum deviatoric stress was reached at lower axial strain values when compared with Tables 6.19 and 6.20: for confining pressures of 50 kPa the axial strain was between 6-9% in Table 6.18 while in Table 6.19 axial strain values reached values from 17-21% and in Table 6.20 18-27%. The same analogy was also observed for the remaining confining pressures.

Table 6.18 – Strain conditions at maximum deviatoric stress for samples with Wc_i close to 15%.

Confining pressure	Test No.	Water content		Strain			Deviatoric Stress	Pore water pressure
		Wc(ac)	Wc_i	Axial	Volumetric	Shearing		
kPa		%	%	ε_a(%)	ε_v(%)	ε_s(%)	kPa	kPa
50	C15(50) 1	14.77	14.77	6.409	-0.730	6.768	450.8	-242.8
	C15(50) 2	14.75	14.75	9.014	-0.914	9.552	461.4	-210.2
	D20-15(50)	19.72	15.08	9.393	0.153	9.579	588.0	-387.1
	D22-16(50)	21.45	16.84	9.615	0.136	9.818	449.8	-258.9
150	C15(150)	15.17	15.17	10.818	0.702	10.892	616.0	-292.3
	D20-15(150)	19.15	15.56	13.469	-0.335	14.101	512.6	-224.2
	D22-14(150)	21.74	13.97	17.787	-0.420	18.871	626.3	-270.6
300	C15(300)	14.62	14.62	22.572	-1.148	24.578	671.7	-287.8
	D20-15(300)	18.75	15.19	11.966	-0.143	13.945	624.6	-126.6
	D22-16(300)	21.00	15.80	14.911	0.191	15.477	568.7	-112.4

Table 6.19 – Strain conditions at maximum deviatoric stress for samples with Wc_i close to 20%.

Confining pressure	Test No.	Water content		Strain			Deviatoric Stress	Pore water pressure
		Wc(ac)	Wc_i	Axial	Volumetric	Shearing		
kPa		%	%	ε_a(%)	ε_v(%)	ε_s(%)	kPa	kPa
50	W15-20(50)	14.61	19.70	17.974	-1.954	19.641	141.6	-35.4
	C20(50)	19.41	19.41	21.026	-2.062	23.138	128.2	-34.9
	D22-20(50)	21.96	19.98	15.067	-0.879	16.034	146.4	-37.3
150	W15-19(150)	15.21	18.45	18.424	-2.041	20.177	210.7	17.3
	W15-20(150)	15.09	19.75	23.953	-2.511	26.705	158.4	55.1
	C20(150)	19.77	19.77	18.161	-1.448	19.666	209.5	13.6
	D22-20(150) 1	21.92	19.78	21.383	-1.193	23.224	198.3	-0.3
	D22-20(150) 2	22.09	20.08	16.274	-0.853	17.351	212.6	16.7
	D22-19(150)	21.37	19.04	23.425	-1.851	25.836	211.7	5.6
300	W15-19(300)	15.44	19.37	24.130	-2.515	26.914	201.9	160.2
	C20(300) 1	19.64	19.64	14.168	-1.159	15.153	199.5	251.1
	C20(300) 2	20.17	20.17	21.912	-2.067	24.160	271.9	146.2

Table 6.20 – Strain conditions at maximum deviatoric stress for samples with Wc_i close to 22%.

Confining pressure	Test No.	Water content		Strain			Deviatoric Stress	Pore water pressure
		Wc(ac)	Wc_i	Axial	Volumetric	Shearing		
kPa		%	%	ε_a(%)	ε_v(%)	ε_s(%)	kPa	kPa
50	**W15-22(50)**	14.67	21.24	27.873	-2.994	31.580	123.3	-17.9
	W20-22(50)	19.40	20.68	19.108	-1.893	20.894	105.6	3.5
	C22(50)	21.82	21.82	18.927	-1.603	20.584	78.7	5.4
150	**W20-21(150)**	19.24	21.53	21.682	-2.470	24.044	121.1	18.6
	C22(150)	22.16	22.16	16.317	-1.624	17.677	95.2	87.8
300	**W20-22(300)**	19.89	21.29	17.239	-1.987	18.832	83.4	263.5
	C22(300)	22.01	22.01	21.548	-2.442	23.879	124.2	213.3

Table 6.21 - Strain conditions at maximum deviatoric stress for the sample with Wc_i close to 17%.

Confining pressure	Test No.	Water content		Strain			Deviatoric Stress	Pore water pressure
		Wc(ac)	Wc_i	Axial	Volumetric	Shearing		
kPa		%	%	ε_a(%)	ε_v(%)	ε_s(%)	kPa	kPa
300	**W13-17(300)**	13.24	17.09	17.545	-1.980	19.172	368.9	71.2

6.3.3.3.2 Constant water content tests observations

The peaks in stress-strain behaviour observed during shearing, see Figures 6.22, 6.28 and 6.34, on samples tested at a Wc_i close to 15%, were shown by samples with starting values of pore water pressure that were negative, from: samples tested as-compacted at 15% of water content (tests C15(50) 1, C15(50) 2, C15(150) and C15(300) in Figure 6.22); and samples compacted at water contents of 20% and 22% and dried to 15% (tests D20-15(50), D20-15(150) and D20-15(300) in Fig 6.28 and tests D22-16(50), D22-16(300) and D22-14(150) in Fig.

6.34). The drying resulted in massive pore water pressure reduction reaching negative pore water pressure sufficient enough to be maintained during shearing.

Strength peaks were not evident in the remaining tests i.e. in tests where the Wc_i was 20% or 22%, in which pore water pressure was mainly positive from the start. During the shearing stage, as is observable in Figures 6.23, 6.29 and 6.35, even samples that had small negative values of pore water pressure after the compression stage increased to positive values during shearing, apart from the test dried from 22% to 20% at 50 kPa of confinement, D22-20(50).

The patterns of deviatoric stress with axial strain in Figures 6.22, 6.28 and 6.34 can be explained by the modes of failure. The samples tested at a Wc_i close to 15%, as Figure 6.40 illustrates, failed by the formation of a shear surface, resulting in the strength peaks and brittleness that can be seen in the stress strain relationships. Other samples that failed by bulging symmetrically under considerable deformations in a plastic and ductile manner and reached higher values of axial strain without the formation of shear planes, see Figure 6.41.

In terms of the critical state limit, the type of failure, under unsaturated conditions, implies different approaches. For the CWT tests in which samples bulged, samples failed in a plastic and ductile manner. The systematic deformations mean that the variables based on principal stresses and strains were appropriate in describing the mechanical behaviour, as stresses and deformations can be assumed to be reasonably uniform throughout the specimen. For the CWT tests in which samples developed shear surfaces, there would be concerns that the deformations become highly non-uniform, and the overall stresses and strains no-longer represent the specimen as a whole. In this case, the assessment of the critical state point was based on an analysis of each test, mainly on Figures 6.27, 6.33 and 6.39 for the constant water content tests C15(50) 1, C(50) 2, C15(150), C15(300), D20-15(50), D20-15(150), D20-15(300), D22-16(50), D22-16(300) and D22-14(150) to determine the point whenever the void ratio changed dramatically. It was assumed that behaviour after this point could no longer represent the critical state.

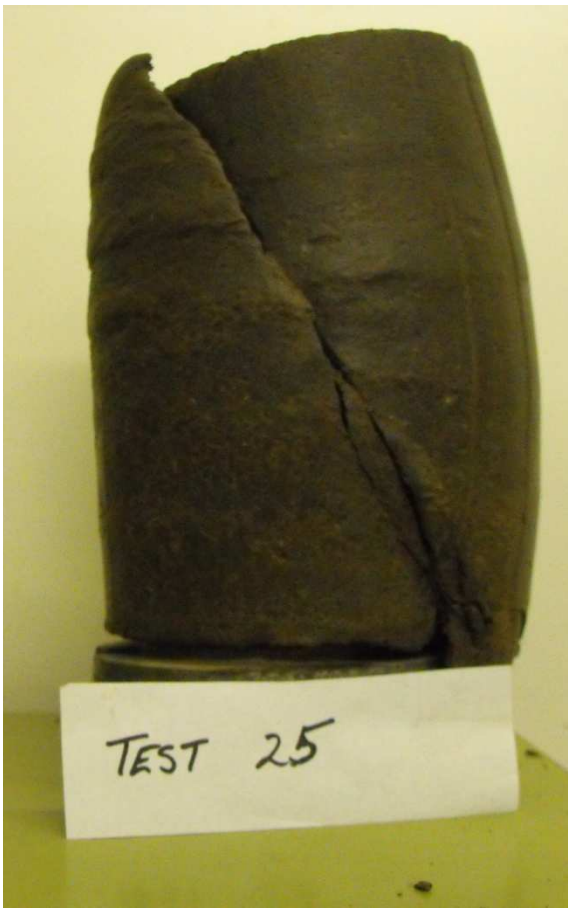

Figure 6.40 – Typical shape of failure on samples tested for with Wc_i close to 15%.

Figure 6.41 – Typical shape of failure on samples tested with Wc_i close to 20% and 22%.

6.3.4 Critical state limit

The conditions of the samples at critical state are shown in Table 6.22, 6.23 and 6.24. For samples that failed by bulging, the end of test data has been taken to represent critical state. However, as mentioned, some samples failed with shear surfaces. In these cases, the stress-strain and volumetric strain data was examined for each test result individually. If sharp changes in deviator stress or volume strain were noted, then the point immediately before such changes were taken as critical state points.

In Table 6.22 and 6.23 some tests were not used for the determination of the critical state line, the tests that were not used were: C20(50), C20(150), C20(300) and D20-15(50) (samples prepared from Wc(ac) close to 20%) and D22-20(50) (samples prepared from Wc(ac) close to 22%). C20(150) was not used for the determination of the critical state due to unreliability of the values measured by the load cell used. While C20(50), C20(300) 1, D20-15(50) and D22-20(50) presented some discrepancies in relation with the general tendency observed in terms of volumetric measurements.

Table 6.22 – Critical state parameters for samples with Wc(ac) close to 15%.

Test No.	Wc(ac) %	Wc_i %	p kPa	u_w kPa	$p-u_w$ kPa	q kPa	e	v 1+e	Sr (%)
C15(50) 1	14.77	14.77	169.3	-291.7	461.0	357.5	0.49	1.49	81.76
C15(50)2	14.75	14.75	190.7	-252.8	443.5	421.7	0.49	1.49	81.89
C15(150)	15.17	15.17	324.0	-326.7	650.7	521.7	0.50	1.50	82.19
C15(300)	14.62	14.62	521.3	-286.1	807.4	663.7	0.48	1.48	82.12
W15-19(150)	15.21	18.45	217.4	0.3	217.1	202.0	0.56	1.56	88.37
W15-19(300)	15.44	19.37	365.5	156.1	209.4	196.6	0.58	1.58	89.69
W15-20(50)	14.61	19.70	90.3	-48.0	138.3	120.8	0.60	1.60	89.39
W15-20(150)	15.09	19.75	201.5	52.8	148.7	154.7	0.64	1.64	83.24
W15-22(50)	14.67	22.00	89.5	-19.5	109.0	118.7	0.65	1.65	91.03
W13-17(300)	13.24	17.09	398.8	45.2	353.6	296.8	0.55	1.55	83.32

Table 6.23 – Critical state parameters for samples with Wc(ac) close to 20%.

Test No.	Wc(ac) %	Wc_i %	p kPa	u_w kPa	p-u_w kPa	q kPa	e	v 1+e	Sr (%)
C20(300)2	20.17	20.17	384.1	117.3	266.7	251.8	0.58	1.58	94.25
D20-15(150)	19.15	15.56	312.5	-259.3	571.8	487.3	0.51	1.51	82.73
D20-15(300)	18.75	15.19	487.4	-157.1	644.6	562.3	0.49	1.49	83.19
W20-22(50)	19.4	21.53	85.3	-9.6	94.9	91.2	0.66	1.66	88.44
W20-22(300)	19.89	21.29	328.8	250.3	78.5	76.0	0.68	1.68	84.25
W20-21(150)	19.24	20.68	188.4	8.5	179.9	115.1	0.61	1.61	91.13

Table 6.24 – Critical state parameters for samples with Wc(ac) close to 22%.

Test No.	Wc(ac) %	Wc_i %	p kPa	u_w kPa	p-u_w kPa	q kPa	e	v 1+e	Sr (%)
C22(50)	21.82	21.82	74.8	-0.1	74.9	74.5	0.68	1.68	86.44
C22(150)	22.16	22.16	180.9	86.8	94.1	92.7	0.71	1.71	81.34
C22(300)	22.01	22.01	340.9	208.6	132.3	123.0	0.68	1.68	87.39
D22-20(150) 1	21.92	19.78	216.0	-0.7	216.7	197.8	0.60	1.60	88.68
D22-20(150) 2	22.09	20.08	215.9	-0.2	216.1	198.1	0.66	1.66	82.19
D22-19(150)	21.37	19.04	218.7	-0.1	218.8	205.7	0.62	1.62	82.42
D22-16(50)	21.45	16.84	179.8	-276.3	456.1	389.2	0.50	1.50	90.77
D22-16(300)	21.00	15.8	466.7	-142.4	609.1	499.8	0.51	1.51	84.13
D22-14(150)	21.74	13.97	325.0	-290.8	615.9	525.0	0.51	1.51	74.32

Figure 6.42 presents the critical state point achieved by each constant water content test, identified by water content at compaction. A linear regression through the critical state points gave the slope of the critical state lines on the v – p-u_w space (λ) as being 0.088 for samples tested that had Wc(ac) close to 22%, 0.087 for samples tested that had Wc(ac) close to 20% and 0.102 for samples tested that had Wc(ac) close to 15%. The critical state line for

saturated samples is also shown in the figure for reference. In Figure 6.42, samples that were tested with a Wc(ac) closer to 22% presented higher values in the v – (p-u_w) plane, explained by the initial 22% water content that represents a lower degree of saturation when compared with samples wetted from the 15% and 20%.

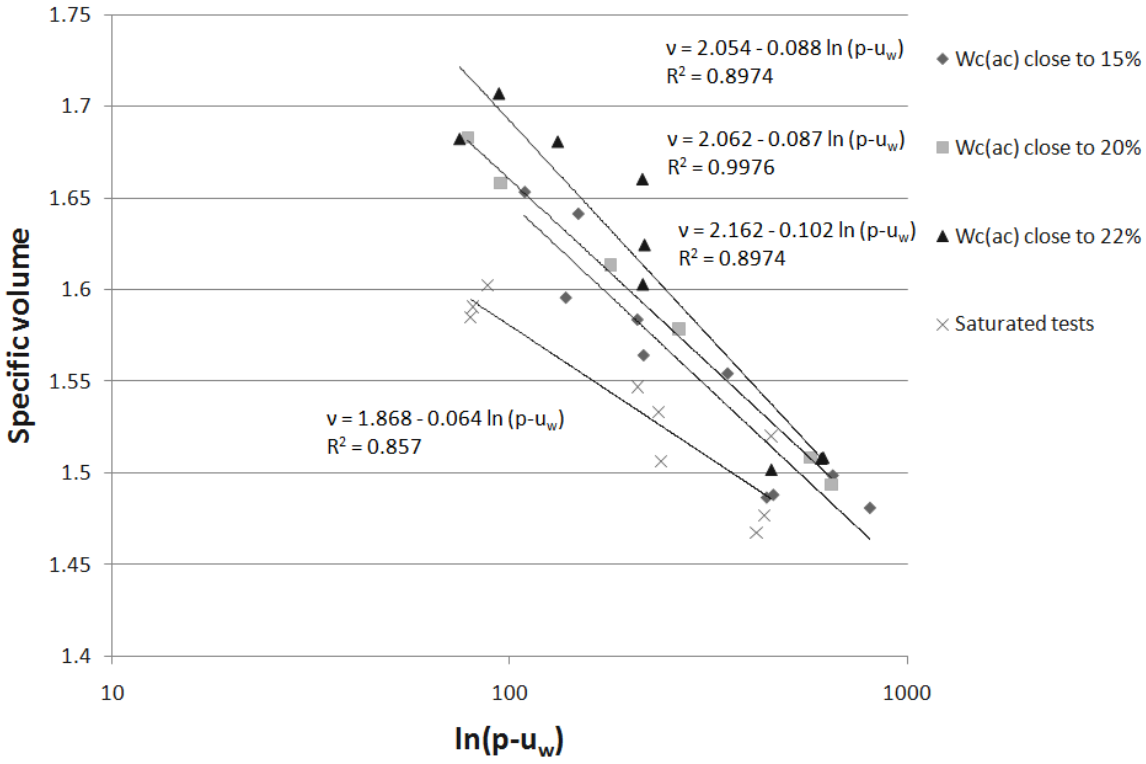

Figure 6.42 – Critical state line of the constant water tests by Wc(ac) including the saturated test series on v-(p-u_w) plane.

Figure 6.43 presents the critical state points over the stress plane (q – (p - u_w) plane). In the same analogy, a regression analysis was carried out on the critical state points for each

group of tests at similar compaction water content. The resulting M values were: 0.838, 0.863 and 0.854 for samples that Wc(ac) were 15%, 20% and 22%, respectively. Apart from the critical state lines of the constant water content tests, the resulting CSL of the saturated tests is also shown.

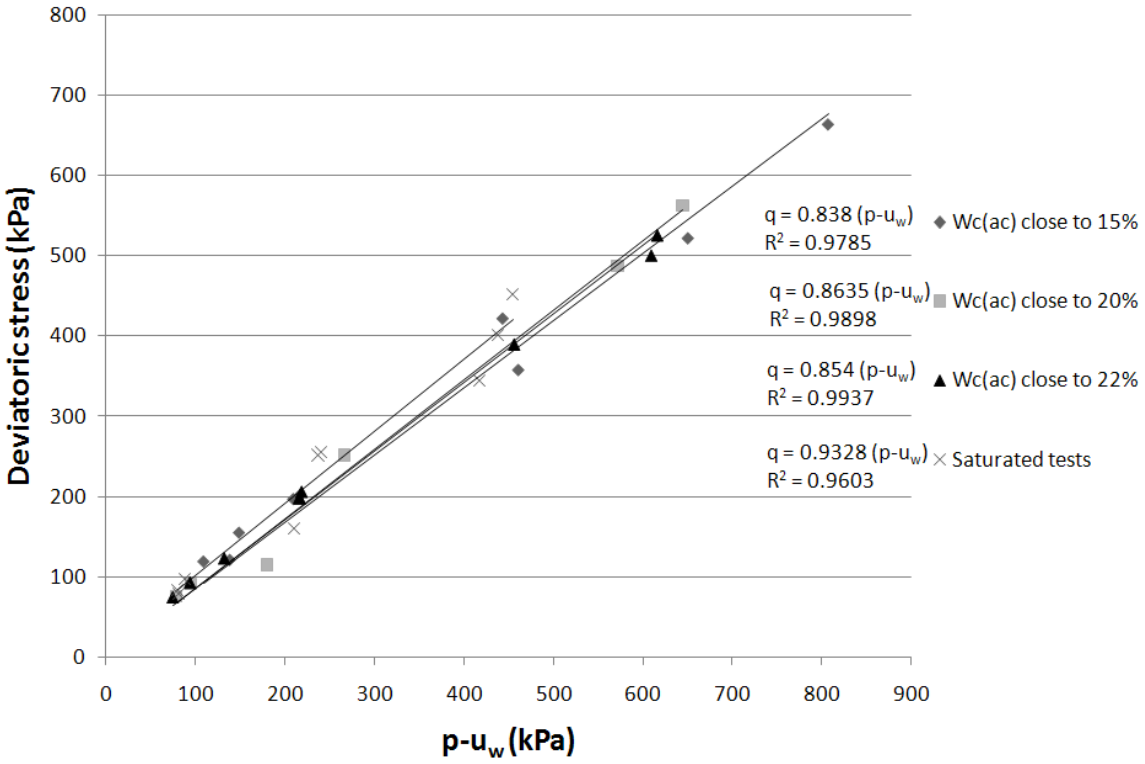

Figure 6.43 – Critical state line of the constant water tests by Wc(ac) including the saturated test series on q-(p-u_w) plane.

Table 6.25 presents a resume of the critical state line parameters determined from the constant water content and saturated tests. In the stress plane (q vs. P-u_w) similar M values

were obtained for the constant water tests, giving similar critical state friction angles (ϕ'_{cv}) of 22^o.

Table 6.25 – Critical state line parameters of saturated and constant water content tests including the resulting friction angle.

	ν – (p-u_w) plane		**q – (p-u_w) plane**	
	Γ	**λ**	**M**	**ϕ'_c**
Saturated tests	1.868	0.062	0.93	24^o
CWT test with Wc(ac) close to 22%	2.162	0.102	0.85	22^o
CWT test with Wc(ac) close to 20%	2.062	0.087	0.86	22^o
CWT test with Wc(ac) close to 15%	2.054	0.088	0.84	22^o

The slope of critical state line on the (ν-p-u_w) plane (λ) for the constant water content tests seem to be similar in values, however the intercept of the critical state line in ν axis (Γ) increasing with the increase of the Wc(ac) tested.

Comparing with the parameters determined in the saturated tests to the CWT tests on the stress plane, a certain similarity was observed: M differed by 0.09 resulting in the saturated tests to have a ϕ' 2^o higher.

However, in the plane ν – (p-u_w) some differences were observed between the saturated tests and CWT tests. The presence of suction in some of the samples tested in CWT series resulted in increased Γ and λ in comparison with the saturated tests.

A different approach for the analysis of the critical state is to use the average skeleton stress assumption (like the Bishop stress) which incorporates the degree of saturation as shown in Equation 2.20, however during testing pore air pressure (u_a) was maintained at zero which results in Equation 6.1. Table 6.26 presents the obtained values using Bishop stress.

$$p^* = p - Sr.u_w \tag{6.1}$$

Table 6.26 - Critical state parameters for the CWT tests using the Bishop stress (p*).

Test No.	Wc(ac) %	Wc_i %	p kPa	u_w kPa	Sr (%)	p* kPa	q kPa	e	v 1+e
C15(50) 1	14.77	14.77	169.3	-291.7	81.76	407.8	357.5	0.49	1.49
C15(50)2	14.75	14.75	190.7	-252.8	81.89	397.7	421.7	0.49	1.49
C15(150)	15.17	15.17	324	-326.7	82.19	592.5	521.7	0.5	1.5
C15(300)	14.62	14.62	521.3	-286.1	82.12	756.2	663.7	0.48	1.48
W15-19(150)	15.21	18.45	217.4	0.3	88.37	217.1	202	0.56	1.56
W15-19(300)	15.44	19.37	365.5	156.1	89.69	225.5	196.6	0.58	1.58
W15-20(50)	14.61	19.7	90.3	-48	89.39	133.2	120.8	0.6	1.6
W15-20(150)	15.09	19.75	201.5	52.8	83.24	157.5	154.7	0.64	1.64
W15-22(50)	14.67	22	89.5	-19.5	91.03	107.3	118.7	0.65	1.65
W13-17(300)	13.24	17.09	398.8	45.2	83.32	361.1	296.8	0.55	1.55
C20(300)2	20.17	20.17	384.1	117.3	94.25	273.5	251.8	0.58	1.58
D20-15(150)	19.15	15.56	312.5	-259.3	82.73	527.0	487.3	0.51	1.51
D20-15(300)	18.75	15.19	487.4	-157.1	83.19	618.1	562.3	0.49	1.49
W20-22(50)	19.4	21.53	85.3	-9.6	88.44	93.8	91.2	0.66	1.66
W20-22(300)	19.89	21.29	328.8	250.3	84.25	117.9	76	0.68	1.68
W20-21(150)	19.24	20.68	188.4	8.5	91.13	180.7	115.1	0.61	1.61
C22(50)	21.82	21.82	74.8	-0.1	86.44	74.9	74.5	0.68	1.68
C22(150)	22.16	22.16	180.9	86.8	81.34	110.3	92.7	0.71	1.71
C22(300)	22.01	22.01	340.9	208.6	87.39	158.6	123	0.68	1.68
D22-20(150) 1	21.92	19.78	216	-0.7	88.68	216.6	197.8	0.6	1.6
D22-20(150) 2	22.09	20.08	215.9	-0.2	82.19	216.1	198.1	0.66	1.66
D22-19(150)	21.37	19.04	218.7	-0.1	82.42	218.8	205.7	0.62	1.62
D22-16(50)	21.45	16.84	179.8	-276.3	90.77	430.6	389.2	0.5	1.5
D22-16(300)	21	15.8	466.7	-142.4	84.13	586.5	499.8	0.51	1.51
D22-14(150)	21.74	13.97	325	-290.8	74.32	541.1	525	0.51	1.51

From the critical state points obtained in Table 6.26 the critical state lines in the q-p* plane were generated, Figure 6.44, and the v – p* plane, Figure 6.45. As it is shown in Figure 6.44, by incorporating the degree of saturation, all the critical state points (saturated and unsaturated) fit on a single regression line. The slope of the critical state line in the stress plane (q vs. p* plane) was found to be M=0.91, resulting in a critical state friction angle (ϕ'_{cv}) of 23^o.

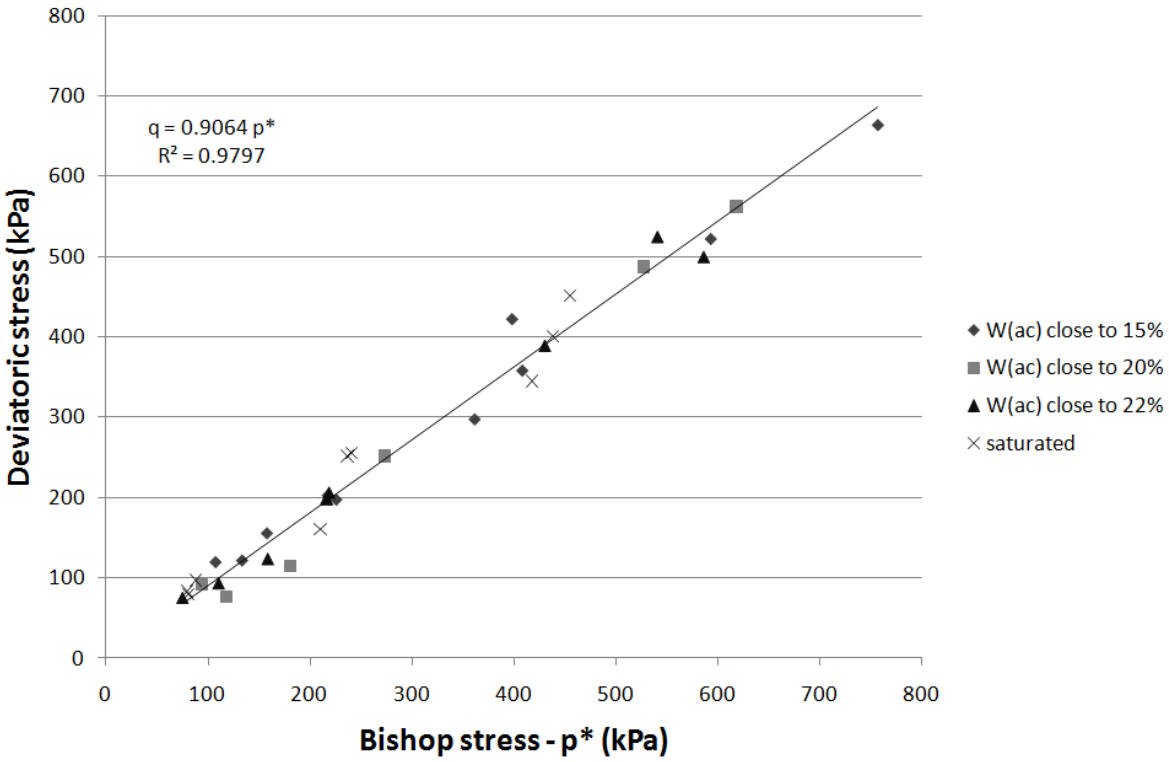

Figure 6.44 - Critical state line of the constant water tests by Wc(ac) including the saturated test series on p*-q plane.

In the v – p* plane (Figure 6.45), however, different regressions for the critical state points for different Wc(ac) were obtained, as in v – p-u_w plane in Figure 6.42. This time, for the CWT tests λ increased with as-compacted water content (Wc(ac)) ranging 0.109 for samples with Wc(ac) close to 22%, 0.098 for samples with Wc(ac) close to 20% and 0.091 for samples with Wc(ac) close to 15%.

Table 6.27 summarises the obtained critical state parameters using the Bishop stress. Although a better fitting of the critical state points was achieved in the stress plane, on the volumetric plane different parameters were obtained for different water contents as-compacted as in similarity with the analysis performed without the incorporation of the degree of saturation.

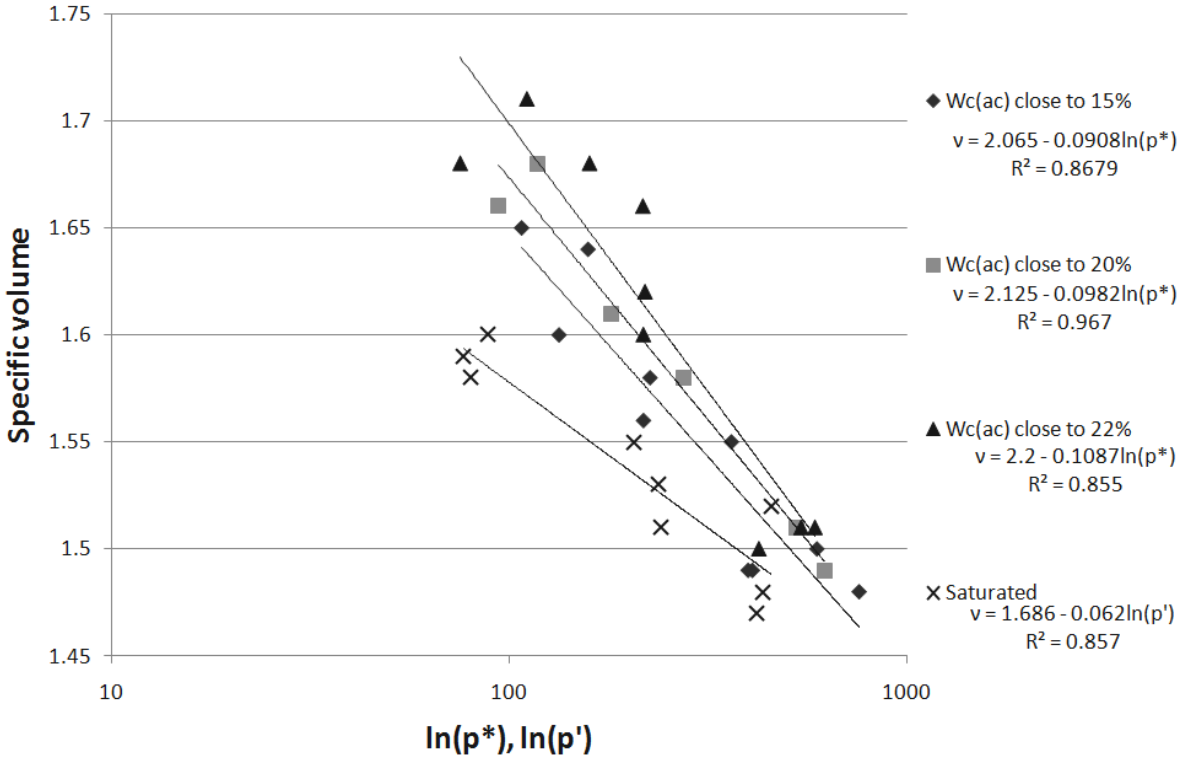

Figure 6.45 - Critical state line of the constant water tests by Wc(ac) including the saturated test series on v-p* plane.

Table 6.27 - Critical state line parameters of saturated and constant water content tests including the resulting friction angle using Bishop stress.

	ν – p* plane **ν – p' plane**		**q – p* plane** **q – p' plane**	
	Γ	**λ**	**M**	∅′
Saturated tests	1.868	0.062	0.91	23^0
CWT test with Wc(ac) close to 22%	2.2	0.109		
CWT test with Wc(ac) close to 20%	2.125	0.098		
CWT test with Wc(ac) close to 15%	2.065	0.091		

Nevertheless, from the analysis performed using a critical state approach, it could be determined that the mechanical behaviour of the BIONICS fill material is governed by the initial water content, the as-compacted condition of the samples showed to have more influence on the mechanical behaviour of the material than the processes of wetting and drying. The similarity in the critical state parameters M in stress plane and λ obtained for the volumetric plane clearly shows this, although major differences were observed in the intercept of the critical state line in the ν axis (Γ) in the volumetric plane.

An alternative framework for analysing the material behaviour that was considered was Toll's framework for unsaturated soil behaviour (Toll, 1990). However, since the data presented generally has high degrees of saturation (>80%) it was felt that approaches based on

p-u_w and p* were sufficient. Toll's approach suggests that the stress ratios (M^a and M^b) approach similar values to the saturated stress ratio at degrees of saturation above 80%.

6.4 **Conclusions**

This chapter presented an attempt to describe the mechanical behaviour of the fill material of the BIONICS embankment. A testing program involving a series of constant water content triaxial tests backed by a small series of saturated tests was carried out.

While the saturated tests were performed in conventional triaxial cells, the constant water content tests were performed in a double cell triaxial cell. The two cell arrangement where the outer cell surrounds the inner cell, enables a more accurate measurement of the volume change of samples when the sample voids are not saturated. Two features makes the DCTC a suitable piece of equipment to carry out triaxial tests on unsaturated samples: the wall of the inner cell being made in glass eliminates the water absorption problem identified in cell walls built in Perspex, hence improving the accuracy of the cell volume changes; and the possibility of placement of a high capacity suction probe in the pedestal inside the inner cell enabling pore water pressure measurements directly in the sample without the necessity of

using pore air pressures to simulate matric suction. Since the pressure is maintained equal in both cells (inner and outer), the pressure surrounding the wall of the inner cell will be the same, eliminating the majority of deformations of the wall reducing the error in the measurement of the volume changes inside the cell.

Constant water tests were carried out on samples at pre-determined water contents (15%, 20% and 22%). From these starting water contents samples were tested under dried, wetted or as-compacted conditions. Testing was carried out at different confining pressures (50, 150 and 300kPa).

Sets of critical state parameters were determined from the triaxial tests for each starting water content, where similarities in v-($p-u_w$) plane and the q – ($p-u_w$) were obtained. The slope of critical state line on the v-($p-u_w$) plane (λ) and slope of critical state line on the q-($p-u_w$) plane (M) did not differ much from the different water contents tested, 0.088, 0.087 and 0.102 for λ and 0.84, 0.86 and 0.85 for M, respective to Wc(ac) close to 15%, 20% and 22%. Only the intercept of the critical state line in v axis (Γ) differed, increasing with an increase in water content (at compaction), 2.054 (Wc(ac) close to 15%) to 2.062 (Wc(ac) close to 20%) to 2.162 (Wc(ac) close to 22%).

With an approach using Bishop stress (p*) a better fitting was achieved in the stress plane where it was possible to bring together all the critical state points in the same critical state line, where M was found to be 0.91. However, in the v – p* plane, different critical state lines were obtained for different as-compacted water contents, as in the v – p-u_w plane, increasing the difference between as-compacted conditions when compared.

The comparison of the critical state parameters of the constant water content test and the saturated test suggested that samples that were tested at the higher values of suction (samples tested at water contents close to 15%) increased the failure and critical strength of the material, the samples tested in these conditions had lower degree of saturation with a lower void ratio resulting in stiffer samples.

The mechanical behaviour of the BIONICS fill material was found to be governed by the initial conditions, the as-compacted conditions. Whatever the process involved in the testing, wetting or drying, did not seem to influence the behaviour when the differences in initial pore water pressure were taken into account.

7 Design and installation of a continuous monitoring system for pore water pressure at the BIONICS embankment.

7.1 Introduction

Pore water pressure can have a negative impact on slope stability; an increase in pore water pressure results in a decrease of effective stress (or suction in an unsaturated soil) leading to loss of strength. Few measuring systems exist in the market that can provide measurements of the "full range" of pore water pressure, meaning, negative (suction) and positive measurements. The majority of the existing systems that do provide measurements in the "full range" are limited either by climate conditions (i.e. GeoObservations high capacity probe, since it is recommended for use only with dry weather) or by the maximum range of measurements (i.e. jet fill tensiometers, flushable piezometers that are limited by cavitation to -100 kPa) or even by the capability of providing continuous monitoring. This chapter presents a system developed at Durham University School of Engineering using a variation of the Durham University - Wykeham Farrance – (DU-WF) high capacity suction probe for field use that is capable of continuous long-term monitoring, whatever the weather conditions, in the "full range" of pore water pressure. The positioning of the suction probes allows measurement of pore water pressure in the same vertical line at the measuring point enabling the creation of suction profiles. Two systems to systematically monitor pore water pressure in time and with depth were installed at the BIONICS embankment referred to previously in Chapter 3.

7.2 Pre conditions for the design

The measuring system that would be installed at the BIONICS embankment had to obey to various conditions: to provide continuous monitoring in time and with depth, to be easily installed in two boreholes at the embankment taking account of the final dimensions allowed for the monitoring system, to be easy to use and to satisfy safety conditions at the site.

The choice of the type of probe to be used, the DU-WF high capacity suction probe, influenced greatly the final design of the monitoring system: cavitation is always a concern in these types of probes and therefore there was a necessity for allowing these probes to be easily removed and inserted; the DU-WF high capacity suction probe needed to be adapted for field conditions; a 5 Volts supply was necessary to power the probes and a datalogger was required to log the measurements continuously in field conditions.

7.3 The monitoring system

The monitoring system design can be described as follow:

- Borehole Probe Locator to allow installation of the probes in one borehole and allow the probes to be removed or replaced;
- Five DU-WF high capacity suction probes adapted to field conditions were used in each Borehole probe locator;
- A data logger and a computer to retrieve the data from the probes.
- Saturation vessels for the probes to allow transportation from the laboratory to the embankment and to allow saturation through pressurisation. The design of these vessels also allows field calibration of the probes, if necessary.

The first concern was the location of the logger, which was installed at the top of the embankment sealed in a cemented metal box to minimize the length of cable necessary to reach the high capacities suction probes and also to reduce the amount of cables running over the embankment. The logger could not be powered by a 240V AC power supply because of safety concerns of operating in wet, outdoors conditions and having high voltage cables trailing across the embankment, therefore the power had to be reduced to 24V DC (minimum required by the logger). This was provided by a power converter placed in the site hut near the embankment, where the computer was also located. The connection between the logger and power converter and the communication link to the computer (necessary to store the measurements obtained from the probes) was made by a single multi-core cable stretching for

70 metres. In case of power surges a USP system was added to the system as a backup battery that could sustain the computer and logger for a maximum period of 30 minutes.

To process the information obtained from the probes the software Triax was used, as for laboratory procedures. For each probe, the software converts the electrical signal from the probes into pore water pressure by means of a specific calibration.

7.3.1 Borehole Probe Locator

The Borehole Probe Locator (BPL) is the central part of the monitoring system. The BPL is a hollow PVC pipe with outer diameter of 90mm (due to installation constraints of a maximum borehole radius size of 100mm) with a wall thickness of 10mm and length of 3 metres, see Figure 7.1. Both ends were sealed to prevent infiltration; the bottom end had a PVC cap backed by layers of silicone sealer while the top seal was created with layers of foam and silicone.

Figure 7.1 – Borehole Probe Locator.

Inside the BPL casing were 5 flexible reinforced plastic hoses with 19mm internal diameter. These flexible hoses were used to guide the probes to their measuring position. The measuring points of the BPL (hereafter called Suction Stations), are the exit points where the probes are in contact with the fill material of the embankment. In the three metre height of the BPL the suction stations are positioned at 0.5, 1, 1.5, 2, 2.5 and 3 metres, as presented in Figure 7.2. Limitations regarding the diameter of the BPL forced the number of probes to be limited to 5. It also limited the exit angle at the suction station to 45º, as shown in Figure 7.3a and 7.4, except the suction station located at the base at 3 metres, which is vertical, Figure 7.3b.

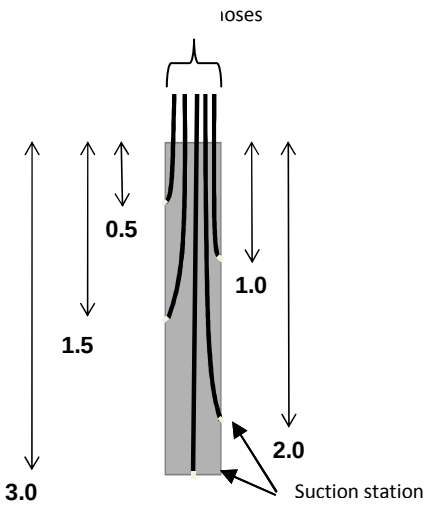

Figure 7.2 – Schematic of the BPL.

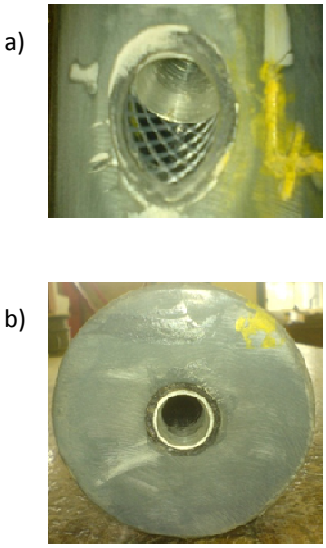

Figure 7.3 – a) Lateral and **b)** bottom suction stations.

To locate the probe in each suction station an aluminium fitting was fitted to reduce the diameter from 19mm (ID of the flexible hose) to 14mm (diameter of the probe) see Figure 7.4. The inner diameter of the fitting providing a tight fit with the diameter of the probe was to prevent movement of soil particles into the guide tube. The part of the aluminium fitting protruding past the edge of the suctions station was cut off, see Figure 7.4 (except at the suction station at 3 metres). This was to prevent the BPL from jamming when installing in an open borehole.

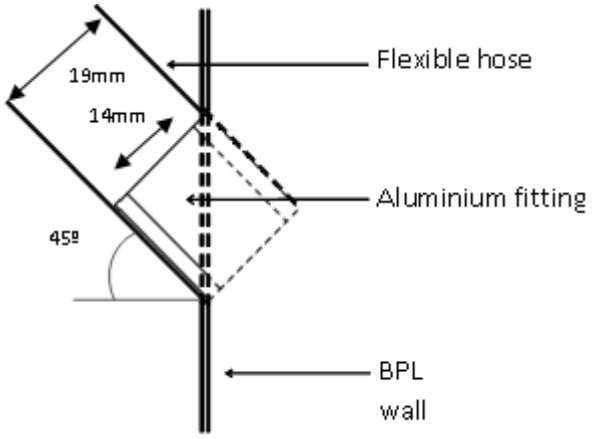

Figure 7.4 – Schematic of Lateral suction station showing the interaction of aluminium fitting and flexible hose; showing the cut face in dashed line.

This design was needed because of the possibility of cavitation of the DU-WF high capacity suction probes, preventing the probe from providing reliable measurements. With this configuration of guide tubes, the probes can be easily inserted and removed when necessary.

7.3.2 DU-WF high capacity suction probe for field use

The probe to be used at the BIONICS embankment was chosen to be the DU-WF high capacity suction probe, which is a variation from the laboratory probe used in the constant water content triaxial testing and characterisation of the soil water retention curve presented in

earlier chapters. The field version of the suction probe had the same characteristics as the laboratory version having the same high air entry value porous disc of 1.5MPa, a small water reservoir and a 2MPa ceramic pressure transducer (Lourenço, 2006), with the arrangement shown in Figure 7.5. For good operation of the probes they have to be fully saturated.

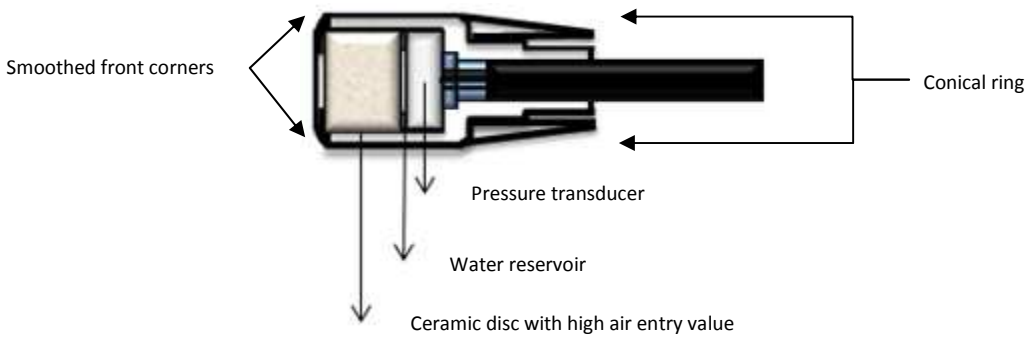

Figure 7.5 – DU-WF high capacity suction probe for field use.

Measurements taken during construction of the embankment justified the usage of such high capacity probes to monitor suction during the life span of the embankment. As shown in Figure 7.6 a) and b) values of suction greater than 100 kPa were observed at different layers in most panels; a suction value that exceeds the range of most of the existing equipment found in practice, e.g. the flushable piezometer of GeObservations. The measurements obtained during construction in Figure 7.6 for both panels show that in the well compacted panels higher values of suction were measured than in the poorly compacted panels. . This

could be due to greater compaction inducing additional suctions due to the tendency of the BIONICS sandy clay to dilate under loading, as seen in Chapter 6. Compaction –induced shearing would cause a reduction in pore water pressure i.e. an increase in suction.

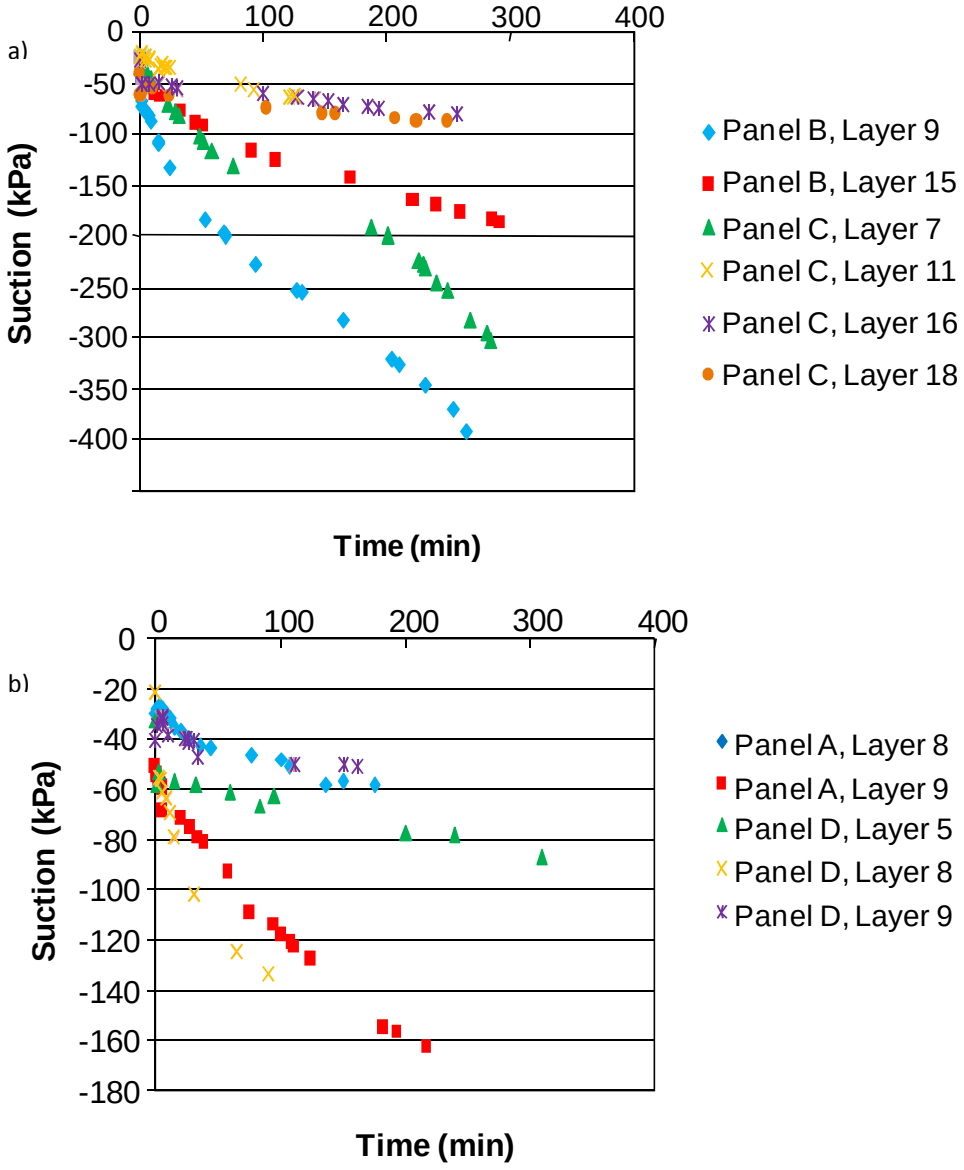

Figure 7.6 – a) Soil suctions recorded in samples taken from the "poorly" compacted sections of the embankment (Panels A and D), and **b)** Soil suctions recorded in samples taken from the "well" compacted sections of the embankment (Panels C and D). (After Hughes, 2007).

To allow installation of the probes in the field, the shape of these probes had to be modified. The electrical cables of the probes were extended to 11 metres. To stiffen the cable a nylon tube with a length of 10 metres and 8mm of diameter was fitted over the connecting cable, enabling the probes to be pushed and pulled in and out of position. This also protected the electrical cable to avoid damage.

To ease the progression of the probes during insertion and removal when passing through the guide tube and aluminium fittings at the suction stations, the front corners of the suction probes were smoothed and a conical ring was fitted at the back end, see Figure 7.5, to prevent the probe snagging.

To achieve good contact between the probes and fill material of the embankment a paste of sieved material from the embankment fill was added to the front end of each suction probe (roughly 1 mm thickness) as shown in Figure 7.7. The paste was fully saturated, which resulted in pore water pressures close to 0kPa. By doing so it enabled full contact between the probe preventing any misreading during monitoring and also avoiding cavitation by drying out while positioning the probes in place. Using a paste of the same material as the embankment meant that it would have the same properties as the fill (such as air entry value) and would not

affect the long-term readings of suction. However, it was necessary to allow for an equilibration period between the probe, paste and fill material after installation.

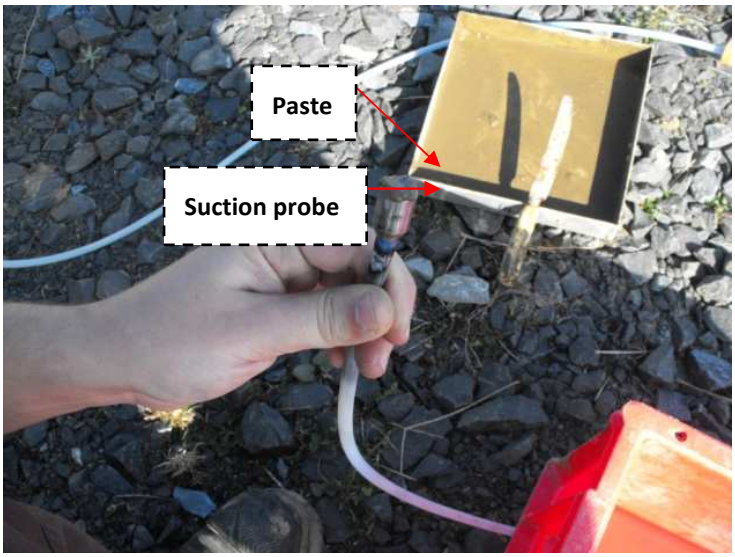

Figure 7.7 – Application of the soil paste on a suction probe.

7.3.2.1 Saturation

Prior to any usage of the DU-WF high capacity suction probes it was necessary to saturate each probe. The initial saturation of the probe is very important for the correct operation of these high capacity suction probes. The saturation process for the field version of the DU-WF high capacity suction was similar to the saturation process adopted for the conventional version of the DU-WF suction probes used in the laboratory. The suction probes

were saturated inside a saturation manifold (Figure 7.8). The suction probes were fixed inside the manifold, which was initially subjected to a vacuum and subsequently filled with de-aired water while maintaining the vacuum. The water was then pressurized to around 1500 kPa. The suction probes were left exposed to such pressure for a period of two weeks. This full saturation process, including the initial application of vacuum followed by an extended pressurization period of two weeks, was only needed for the first saturation or in the event that the probe had cavitated and had been left unsaturated for a long period. However, for re-saturation shortly after cavitation had occurred, a pressurization interval of 24 hours was usually enough. During usage, however, given that visits to the site were scheduled every 2 weeks, a longer pressurization of 2 weeks was often adopted for re-saturation following cavitation.

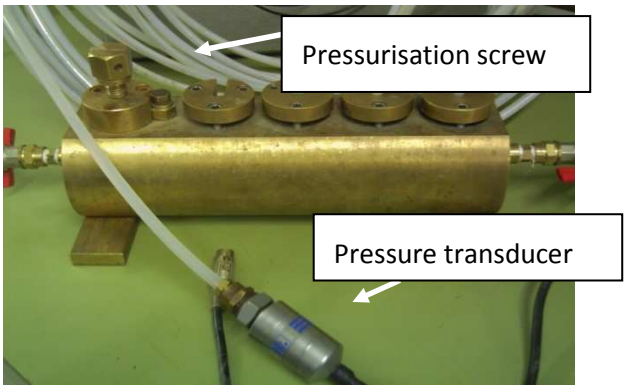

Figure 7.8 – Saturation manifold (Donoghue, 2006).

The saturation of the probes was performed in the Laboratory, due to difficulties of installing such a system in the field but also because it was easier to monitor and control the process in the laboratory.

7.3.2.2 Calibration

Lourenço et al (2009) showed that calibrations of the DU-WF high capacity suction probe can be conducted in the positive pressure range and extrapolated to the negative pressure range. Two calibrations procedures were selected: a laboratory based calibration procedure, which would correspond to the initial calibration of the probes; and a field based calibration procedure, allowing the possibility of calibration of the probes in field conditions if necessary. The laboratory based calibration procedure was conducted only once, before installation of the system in the field, and could potentially be affected by changes in connection arrangements and slight differences in the power supply voltage between the laboratory and the field set-up. The field based procedure allowed the calibration to be performed using the exact set-up as was used in the field.

Lourenço et al suggested the following procedure as the most satisfactory for calibrating the probes. The probes were submersed in water in a triaxial cell and the pressure was gradually increased in steps to a maximum of 600 kPa. The obtained calibration in the positive pressure range would afterwards be extrapolated to the negative pressure range. However, such a set-up (triaxial cell) could not be used in the field, so a saturation manifold was used (Figure 7.8). The saturation manifold pressurises the chamber by the means of a pressurisation screw, which can be regulated by the readings obtained by a pressure transducer. The pressure transducer was powered by a battery (5V) that could be used in the field and this was calibrated using a dead-weight calibrator in the laboratory. Therefore, this provided a reliable reference pressure reading for field calibration. Again, the measurements are extrapolated from the positive pressure range to the negative pressure range.

The disadvantage of this technique was that Lourenço et al found that the calibration was affected by the manner in which the probes were fixed in the saturation manifold. It was also difficult to maintain a constant pressure using the pressurisation screw for values greater than 400 kPa. However, the lack of availability of a pressurising system in the field made it the only available contender for the purpose of conducting calibrations in field conditions.

7.3.3 Installation concerns

Before installation of the system at the BIONICS embankment a number of issues had to be addressed regarding the installation of the BPLs in the borehole.

The first concern was the issue of contact between the BPL and the embankment material. Consideration was given to using a grout mixture to fill and seal any gap between the BPL (90mm diameter) and the drilled borehole (100 mm diameter) or whether the natural closure of the borehole once the BPL was placed in position would be sufficient to ensure a seal.

7.3.3.1 Grout test

Studies regarding the performance of the high capacity suction probes were performed on a grout mixture that had been used for similar equipment such as the GeoObservation flushable piezometers present at the embankment. The grout mixture was composed by 44% of cement, 3% of bentonite and 53% of water. The test consisted of preparing two layers inside a container: one layer of fill material and another layer of grout

and to subjecting both ends to drying stages while measuring suction with a high capacity probe. The size of the layer of the grout mixture was prepared to replicate the expected maximum length of 20 mm between probes and fill material, see Figure 7.9. For comparison purposes the same high capacity probe was used for measuring suction in both layers (top and bottom). Except, when deliberately inducing drying, both ends were sealed to avoid dehydration when measurements were being taken. Figure 7.10 shows the procedure during the test.

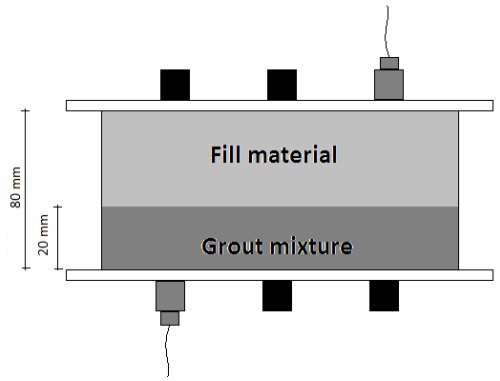

Figure 7.9 – Grout test scheme.

Figure 7.10 – Grout test set up.

Initially there was a good agreement in the readings for both grout and fill material achieving similar results where the difference was no greater than 20 kPa, see Figure 7.11 and 7.12. However, when a greater drying stage was achieved a very significant difference of almost 300 kPa was observed (Figure 7.13). Therefore, while a suction equilibrium between the fill and the grout was being achieved at suctions up to 300 kPa, above this value readings

on the grout side showed much larger readings than that observed in the fill. From this it was concluded that the grout was not an option since readings obtained during construction showed suction values near 400 kPa. Therefore, the contact from part of the BPL with the fill material of the embankment relied entirely on the natural closure of the borehole. The natural closure of boreholes has been observed at the embankment by Hughes (2005) where boreholes previously drilled in the embankment had closed up quite quickly.

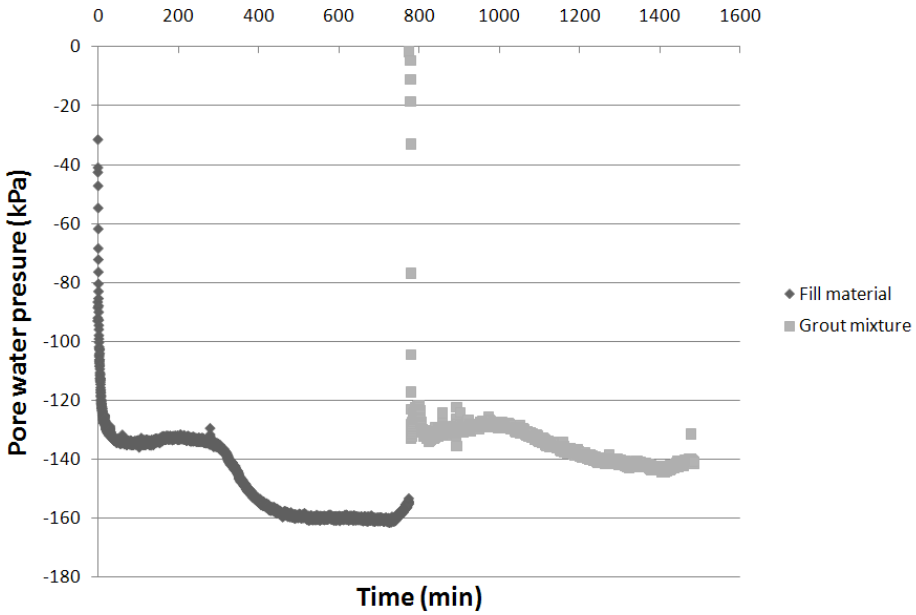

Figure 7.11 – Pore water pressure measurements on fill material and grout mixture after the first drying stage.

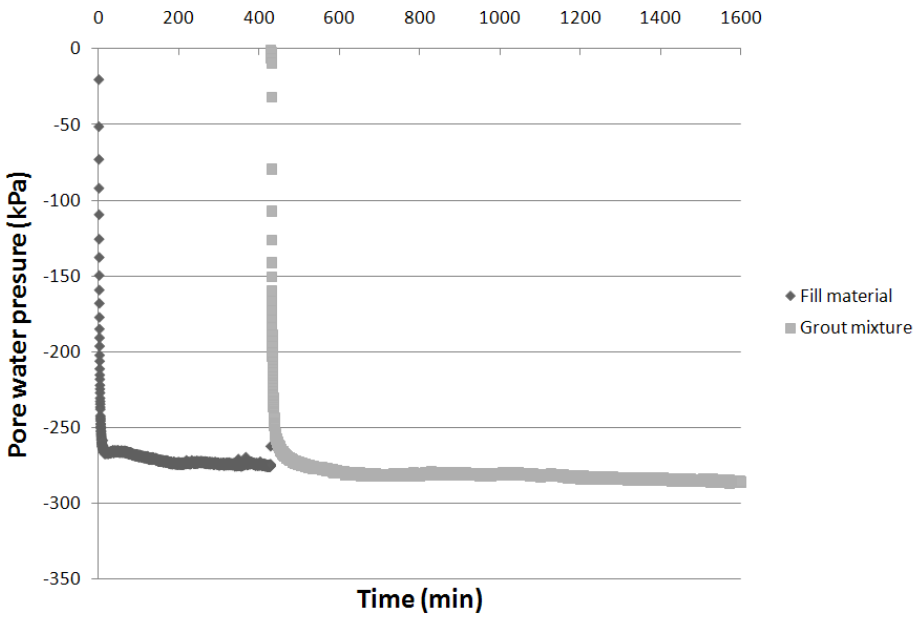

Figure 7.12 – Pore water pressure measurements on fill material and grout mixture after the second drying stage.

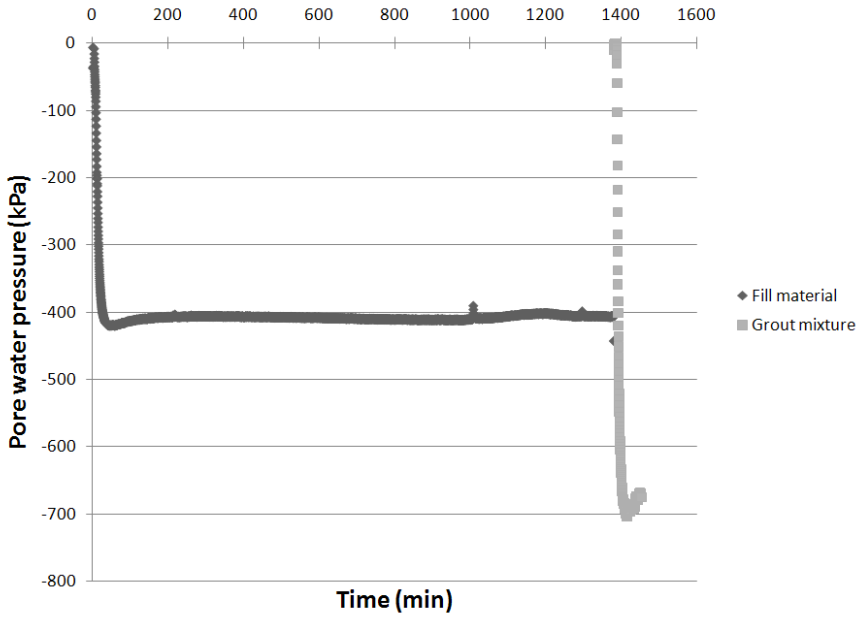

Figure 7.13 – Pore water pressure measurements on fill material and grout mixture after the final drying stage.

7.3.3.2 Suction station plug

During installation, the probes were not present in the BPL to prevent any damage to the probes. To prevent soil entering the guide tubes and potentially blocking them, plugs were placed in the suction stations. These plugs were designed to have the same dimensions as the probes and to occupy similar space at the different suction stations.

The suction station plugs remained in place for the 2 months period until the gap between the wall of the BPL and the fill material closed, prior to the installation of the suction probes. The ability to retrieve the plugs gave reassurance that the guide tubes and suction stations were clear and the probe would be able to travel to and be correctly positioned at the desired suction station.

The plugs were also used to replace the probes whenever there was any malfunction of a probe, such as poor saturation, cavitation, etc.

7.4 Installation of the monitoring system at the BIONICS embankment

As explained in Chapter 3 the BIONICS embankment was built using two different construction methods, panels A and C were “poorly compacted” (built to resemble old Victorian embankments) and panels B and D were “well compacted” (resembling modern construction methods), see Figure 7.14. To allow a comparison of the behaviour of each construction method it was decided to drill two boreholes in panels A and B to accommodate two BPL i.e. one in a poorly compacted panel and one in a well compacted panel.

In late February 2007 two boreholes of 3.5 metres deep (3 metres in the fill material plus 0.5 metres through the overlying coarse layer) were cut, roughly 2 metres from the impermeable membrane at the limit of the crest of the embankment close to the south slope as presented in Figure 7.14. The boreholes was carried out using a Premier Tracker Compact 110 Series percussive driven sampling rig, Figure 7.15, involving recovery of the samples in 1 metre sections, Figure 7.16. Later, the recovered samples were tested to obtain some information on the state of the fill material such as water content and void ratio. The BPLs were inserted into position, Figure 7.17, while fitted with suction station plugs. The top of each BPL was enclosed within a bin which was placed through the overlying coarse layer (see Figures 7.18a and b) to prevent any further infiltration of water and to allow better clearance for the top of the flexible hoses. At the same time, preparations were made to install the

logger enclosure at the top of the embankment. A heavy, sturdy metal casing was cemented to the top of the embankment mid-way between the two BPLs, Figure 7.19.

Uncertainties about how long it would take before the closure of the boreholes led to a waiting period of 2 months. After this two months, in April 2007, the first batch of 5 DU-WF high capacity suction probes for field use, logger, computer and accessories (cables, power converter, etc) were installed. Initially just 5 probes were installed at the shallower suction stations, 3 probes in panel B (well compacted panel) and the other 2 in panel A (poorly compacted). The remaining probes were installed as soon as they were ready for field use.

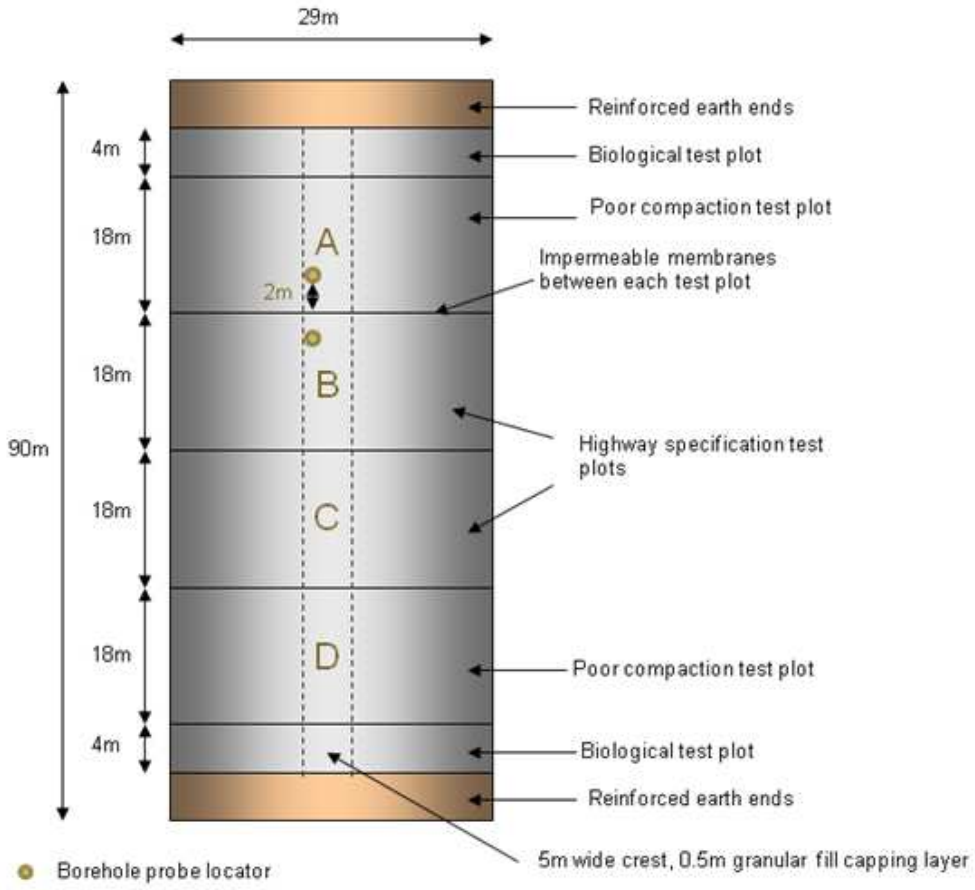

Figure 7.14 – Bionics embankment plan view with marked location of the BPLs.

Figure 7.15 – Cutting of the borehole.

Figure 7.16 – Recovering the core of the borehole.

Figure 7.17 – Insertion of the BPL in the borehole

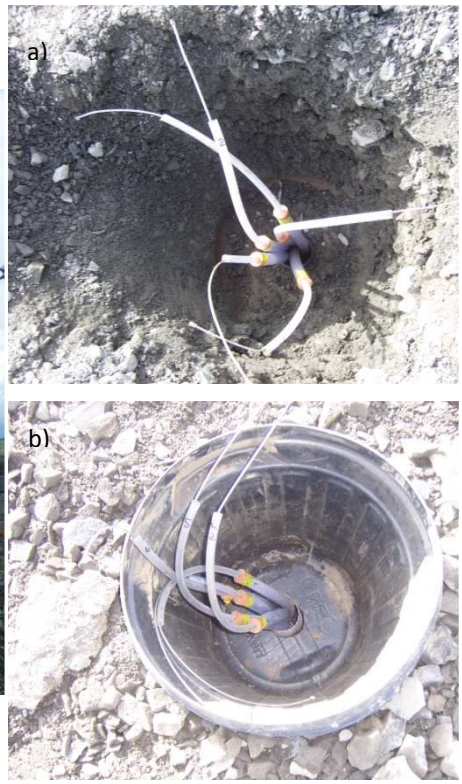

Figure 7.18 –Top of the BPL **a)** without and **b)** with the bin protection.

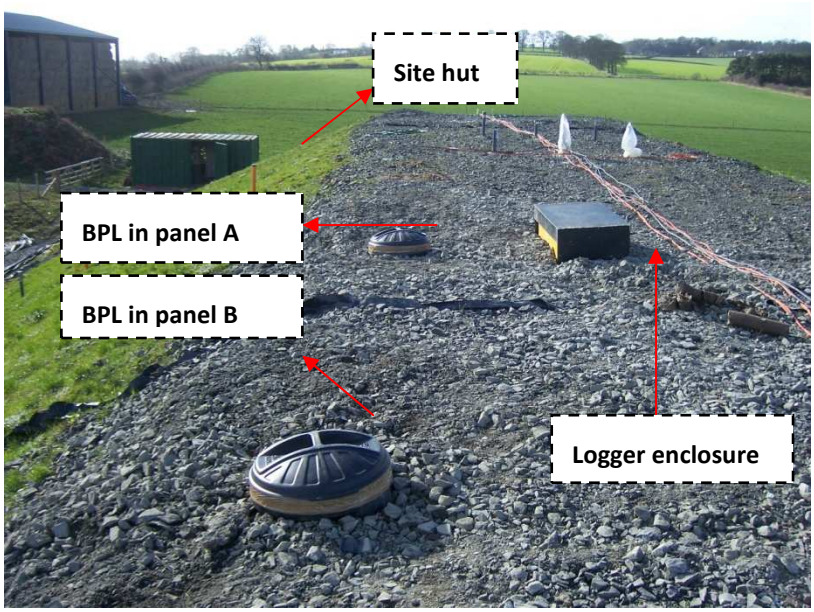

Figure 7.19 – Final arrangement of the equipment on the crest of the embankment.

7.5 *Continuous monitoring*

Initially, the monitoring system was intended to perform continuously without intervention, meaning the probes would be left at the respective suction station only to be removed due to poor saturation, cavitation, re-calibration or other malfunction.

However, checks on the zero readings of the probes after some time (September 2007) showed that a noticeable creep developed. This could be seen when removing the probes and plunging them in free water. They should read zero pressure under these conditions, but it was found that the zero value could shift by up to 5 kPa. This was consistent with observations by Lourenco (2008), who noted a suction induced shift. Clearly such shifts are more of a concern at low suctions as a change in reading of the order of 5 kPa would be a significant error. In fact, initial results showed that low suctions were observed, as will be described in Chapter 8. For this reason visits were made to the field each fortnight to retrieve the probes from their respective suction station, clean them of any paste left on the front face and plunge them in free water. A reset of the calibration of each probe was then imposed to set them back to a zero reading; afterwards the probes were refitted with a new layer of paste and were placed back into their respective position. This process will be called the reset stage in later discussions.

It was assumed that any drift in the zero value would be related to time. To correct for this drift, the obtained results, between visits, were then recalculated using a linear relationship and by doing so would eliminate the drift effect of extended time usage of the probes.

7.6 Conclusion

In this chapter the evolutionary process from design to installation and *modus operandi* of the monitoring system for pore water pressure at the BIONICS embankment was presented.

Measurement of pore water pressure during construction of the embankment suggested that suctions in the fill material would exceed the 100 kPa suction limit of conventional tensiometers. This lead to the usage of DU-WF high capacity suction probes that have a wide range of measurement on both negative and positive pressure range. To allow their usage in field conditions the design of the probes had to be modified to work with the Borehole Probe Locators.

The development of the Borehole Probe Locators with their suction stations allowed the correct positioning of the probes in contact with the fill material of the embankment. They provide the opportunity to measure suction profiles with depth within a single borehole. The installation of two of these systems in different panels (built under different conditions) enhances the possibility of obtaining a comparison of the evolution of pore water pressure with time and in depth in the long term.

8 Field monitoring

8.1 Introduction

The following chapter will present the measurements of pore water pressure obtained for the BIONICS embankment and will discuss the response of the fill material of the BIONICS embankment to climate events by considering the annual patterns of changes of pore water pressure. Details of the instrumentation system used for monitoring were previously described in Chapter 7.

8.2 Initial conditions of the fill material pre monitoring

During the installation of the Borehole Probe Locators (BPLs) in 2007, two years after the construction of the embankment, the cores recovered from the boreholes were preserved in order to perform a set of tests to describe the initial conditions of the material (water content, void ratio and degree of saturation). Each core was divided in different sections of 1 metre that comprises the full length of the borehole: 0-1m, 1-2m and 2-3m.

After the retrieval of the core from each borehole, it was wrapped in cling film and placed in sealed plastic bags. Table 8.1 shows the water contents obtained for both cores with depth. The amount of tests performed was dependent on the quality of recovery of the core of each section, but a minimum of 4 water contents were possible to be obtained. The water content tests shown that the top section on both cores were the wettest section ranging from 20.9% in the well compacted panel and 23.7% on the poorly compacted panel.

Table 8.1 – Water content values in the full depth of the borehole cores for both well and poorly compacted panels.

	Water content (%)	
Depth	**Well compacted**	**Poorly compacted**
	18.59	24.85
	21.33	23.27
	21.81	24.76
0-1 m	21.10	23.52
	21.54	22.06
	20.59	
	21.23	
Average	**20.88**	**23.69**
	18.12	19.93
	21.16	22.26
1-2 m	19.38	21.83
	19.83	17.42
	21.54	20.84
		21.20
Average	**20.01**	**20.58**
	20.90	21.33
	19.19	21.79
2-3 m	19.75	21.24
	19.08	21.00
		20.89
Average	**19.73**	**21.25**

In the core of the well compacted panel borehole, on average, the water content decreased gradually with depth showing a decrease of 1% from the top to the final section. In the poorly compacted panel the water content in depth changes significantly, more than 3% to the middle section, and more than 2% to the final section. These variations on the poorly compacted panel are the expected result for a more permeable and a result of a less controlled construction.

To evaluate the void ratio and degree of saturation of the core of the boreholes in each section smaller samples were cut using a sampler of 20mm by 55mm (diameter) to be able to determine the volume of the subsamples with vernier callipers. Table 8.2 presents the final results

showing differences in both parameters between both cores of the different panels. As expected the void ratio on the poorly compacted panel was slightly higher when compared with the results for the well compacted panel, 0.66-0.70 and 0.59-0.64 respectively. Dry density was also calculated from the void ratio in Table 8.2.

Table 8.2 – Water content, Void ratios (e) and resulting degrees of saturation (S_r), dry densities (γ_d) in the full depth of the borehole cores for both well and poorly compacted panels.

	Well compacted panel B borehole samples				**Poorly compacted panel A borehole samples**			
Depth	**e**	**S_r (%)**	**Wc (%)**	**γ_d Mg/m^3**	**e**	**S_r (%)**	**Wc (%)**	**γ_d Mg/m^3**
0-1 m	0.65	73.72	17.7	1.64	0.65	99.19	23.7	1.64
	0.66	89.62	21.9	1.63	0.68	98.90	25.0	1.61
	0.62	87.17	20.0	1.67				
	0.63	89.64	20.8	1.66				
Average	**0.64**	**85.04**	**20.1**	**1.65**	**0.66**	**99.04**	**24.3**	**1.62**
1-2 m	0.63	94.29	22.1	1.65	0.71	92.80	24.2	1.59
	0.62	82.19	19.0	1.66	0.69	94.71	24.0	1.60
Average	**0.63**	**88.24**	**20.5**	**1.66**	**0.70**	**93.76**	**24.1**	**1.59**
2-3 m	0.57	90.92	20.3	1.72	0.68	81.18	19.1	1.61
	0.61	87.34	20.6	1.68	0.68	82.30	17.0	1.61
Average	**0.59**	**89.13**	**20.4**	**1.70**	**0.68**	**81.74**	**18.0**	**1.61**

In terms of degree of saturation the poorly compacted panel was almost saturated (99%) in the top metre reducing with depth down to 82% at 3 metres. In the well compacted panel an inversion was observed with the degree of saturation increasing from 85% up to 89%. Still it is reasonable to conclude that the degree of saturation in the well compacted panel remained almost constant when compared with the variation of almost 20% in the poorly compacted panel, a result of the different construction methods employed on the different panels.

The description of the initial characteristics also involved the study of the hydraulic properties of each core of the boreholes. Soil water retention curves (SWRC) were obtained using involving high capacity suction probe, by stage drying, as presented in chapter 5. Two samples from the section 0-1m from each borehole were used to determine the SWRCs and are presented in Figure 8.1.

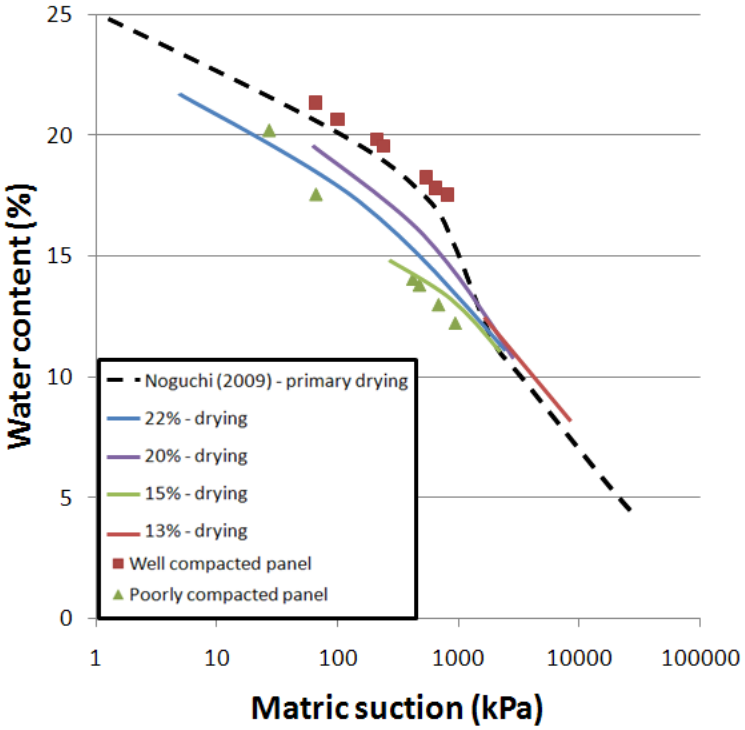

Figure 8.1 – SWRCs obtained from samples of the first metre of the cores of the boreholes of the well and poorly compacted panels compared with results from SWRCs (drying path) obtained in Chapter 5.

From Figure 8.1 there are noticeable differences in the hydrological characteristics of both boreholes. The curvature of the SWRC for both samples differs. In the well compacted panel higher values of suction were achieved at higher water contents while on the poorly compacted panel changes in the water content related to smaller variations in suction up to 14% of water content.

The obtained SWRCs should be only considered qualitatively since the test was performed under no confining pressure, a factor that differs from the actual reality in the field.

Also in Figure 8.1 are presented the SWRCs that followed drying paths determined in Chapter 5. Before comparing results it is necessary to note that the borehole samples tested were recovered two years after the construction of the embankment, therefore different water retention behaviour was expected. Comparing the results of all SWRCs presented in Figure 8.1 it was observed that the SWRC obtained from the core of the poorly compacted panel was comparable with the SWRC dried from 15% on the high range of the measured suction while at low ranges of suction the values move towards SWRC dried from 20%. While the SWRC for samples retrieved from the core of the well compacted panel fell at slightly higher values when compared with the primary drying curve obtained by Noguchi.

8.3 **Weather data**

Weather data during the pore water pressure monitoring at the BIONICS embankment was recorded primarily by a nearby weather station complemented by two mini weather stations located in the slopes of the embankment itself, as presented in Chapter 3. Figure 8.2 shows the monthly natural precipitation and average minimum and maximum temperatures during the monitoring period.

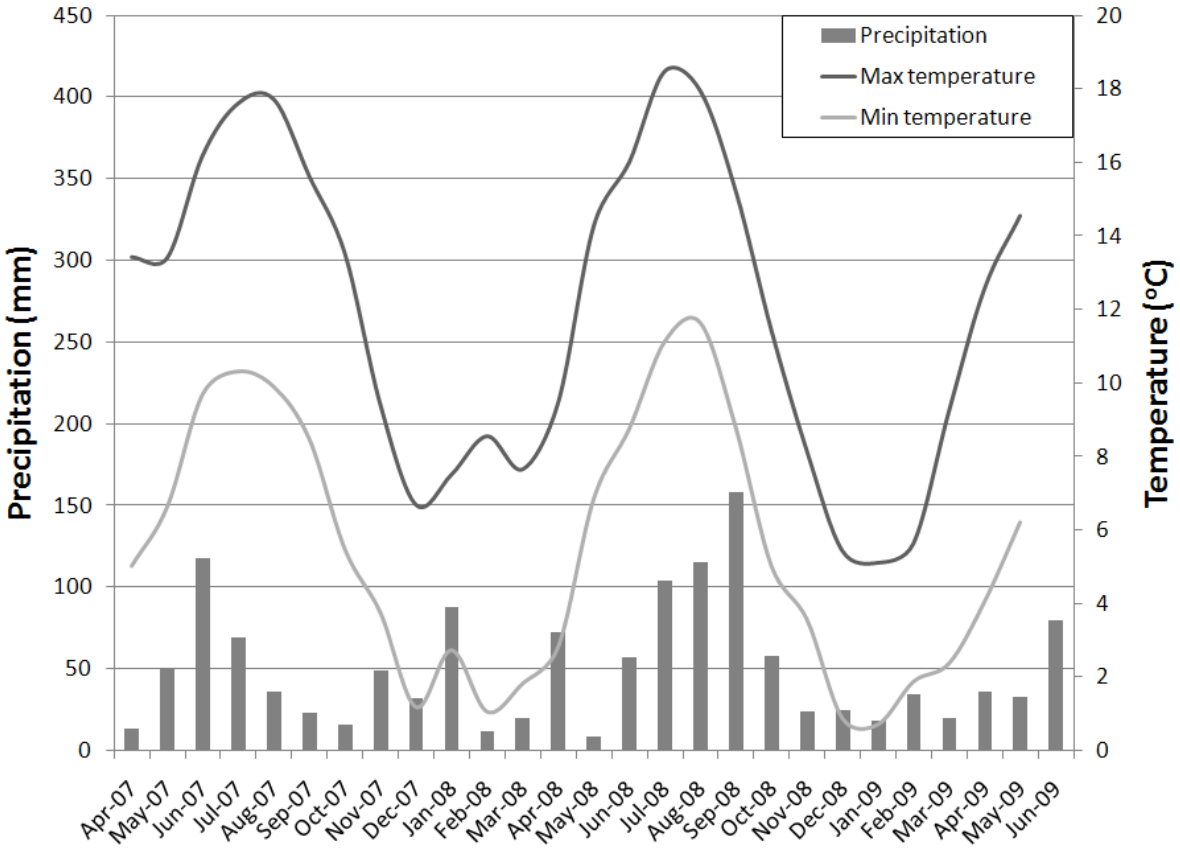

Figure 8.2 – Natural precipitation and temperature (minimum and maximum) monthly averages recorded at the BIONICS site during the pore water pressure monitoring.

In Figure 8.2 it can be seen that the months with more precipitation were the summer months, although this might not have been expected. This is due to sparse intense showers events during these periods occurring in the region. Annual precipitation generally maintained constant through the years of monitoring (600 mm).

The highest monthly precipitation occurred in September 2008 with more than 158mm while May 2008 was the month with least precipitation of only 8.4mm. Although, the precipitation was higher during the summer months, these coincide with periods when the temperature was also higher which results in more evaporation. These two factors, rainfall events and evaporation

combined with the hydraulic characteristics of the material are major factors that will control the pore water pressure behaviour at the site.

With the climate control system, the sprinkler system was used to apply more water to the embankment during pre determined periods. The total precipitation at the site, combining natural rainfall and that induced by the climate control system) is presented in Figure 8.3.

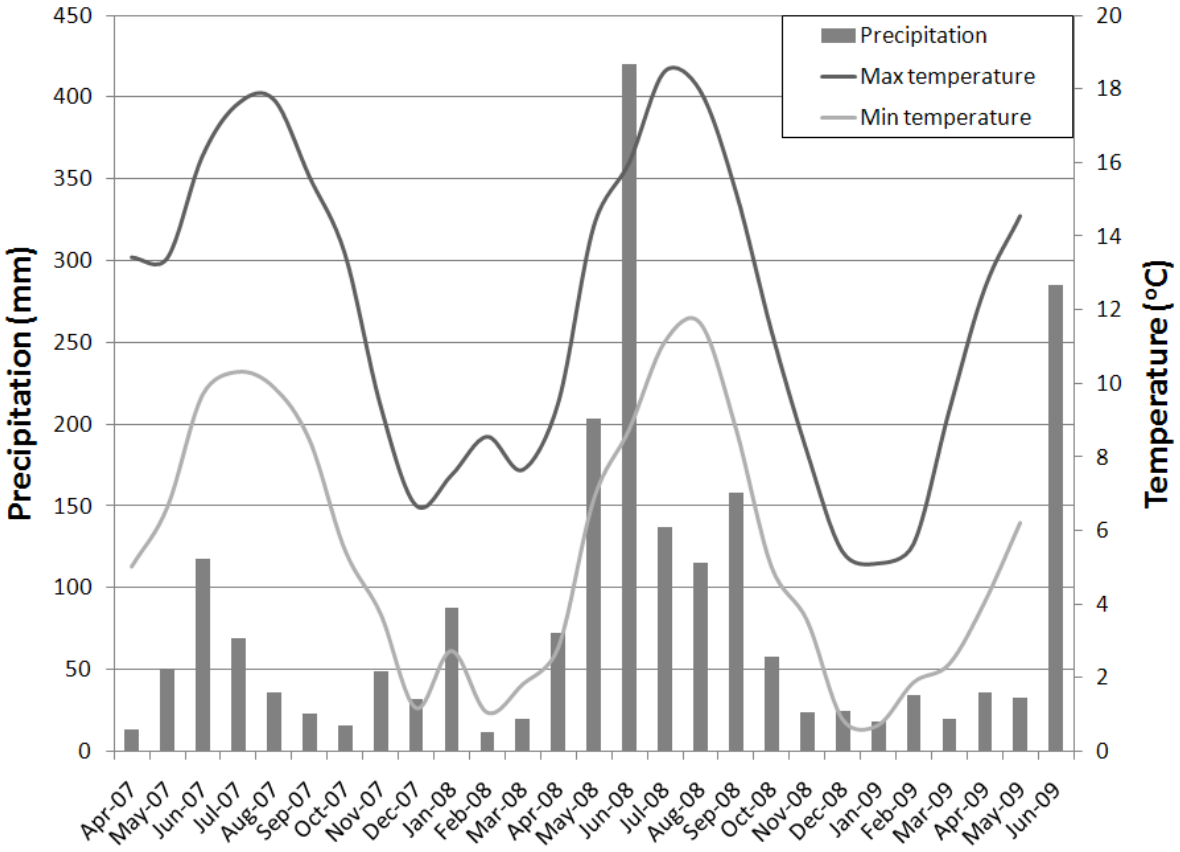

Figure 8.3 – Total precipitation (natural + induced by the climate control system) and temperature (minimum and maximum) recorded at the BIONICS site during the pore water pressure monitoring.

Various types of rainfall patterns were used for the precipitation applied by the climate control system, based on climate change predictions (Stephenson, 2008). An initial test for

commissioning the climate control system was carried out during 19-21 of May 2008 and added 27.5mm over a period of 3 days (above total ambient conditions of 0.2mm). This was followed by an inundation test, where the precipitation rate was increased, resulting on 363mm in 19 days from 26 May until 13 June 2008 (above total ambient conditions of 18.8mm). The final test performed was simulating a storm event during the period of 30 June until 2 July where 66mm were added (above the total ambient conditions of 3mm). A similar test to the storm event simulation started in June 2009 (Nattrass, 2009).

8.4 Monitoring of pore water pressure

The DU-WF high capacity suction probes were installed in the BPLs starting from 4th of April 2007. An initial batch of 5 high capacity suction probes was installed and Table 8.3 presents the dates of subsequent installation of all high capacity suction probes. The depths of the probes are related to the depth referenced to the top of the fill material in Figure 3.2 (Chapter 3), excluding the coarse layer, 0.5 metres thick, that was placed above.

Table 8.3 – Installation dates and depths of the high capacity suction probes in the well and poorly compacted BPLs.

Borehole Probe Locator	Suction station	Depth (m)	Installation date
Well Compacted Panel	SS1	0.5	4th April 2007
	SS2	1.0	4th April 2007
	SS3	1.5	4th April 2007
	SS4	2.0	17th May 2007
	SS5	3.0	17th May 2007
Poorly Compacted Panel	SS1	0.5	4th April 2007
	SS2	1.0	4th April 2007
	SS3	1.5	4th May 2007
	SS4	2.0	4th May 2007
	SS5	3.0	20th September 2007

As explained in the Chapter 7, it was found that the zero values of the suction probes were drifting with time. From the 20th of September 2007 the reset stage was added to the *Modus Operandi* in use, whereby the probe zeros were checked and set back to zero, and this practice has continued until today.

8.4.1 Monitoring pre-"reset stage"

The monitoring carried from April until September in 2007, named pre-"reset" stage monitoring, was the period where the high capacity suction probes were tested in a non-controlled environment (i.e. outside the laboratory) for the first time. Various uncertainties with the equipment had to be analysed: the ability of the probes to measure for an extended time, the quality of the measurement, the quality of the protection on the probe (electrical cable protection) and to test the insertion and removal of the probes from the respective suction station.

The pre-"reset" stage period was disregarded from the monitoring data set for further analysis, but some of the data is presented here to demonstrate the lessons learnt. Due to the similarity of behaviour from the probes between the two BPLs only one set of data discussed in this chapter (from the well compacted panel). The measured values of pore water pressure for the well compacted panel during this period are presented in Figure 8.4. One factor that affected the monitoring was power cuts on the main power line that resulted in gaps in the collected data. Power cuts occurred 4 times during the initial period of monitoring (2-13 June, 6-13 July, 25-26 July and 17-23 August). If a power cut happened between visits (usually every 2 weeks) the computer logging system would be shut off and would only be restarted on the following visit, losing all the data in between. At this time, there was no wireless connection to the site that could have allowed checking

of satisfactory operation between site visits. The problem of power cuts was only resolved close to the end of September when a backup battery powered system was installed.

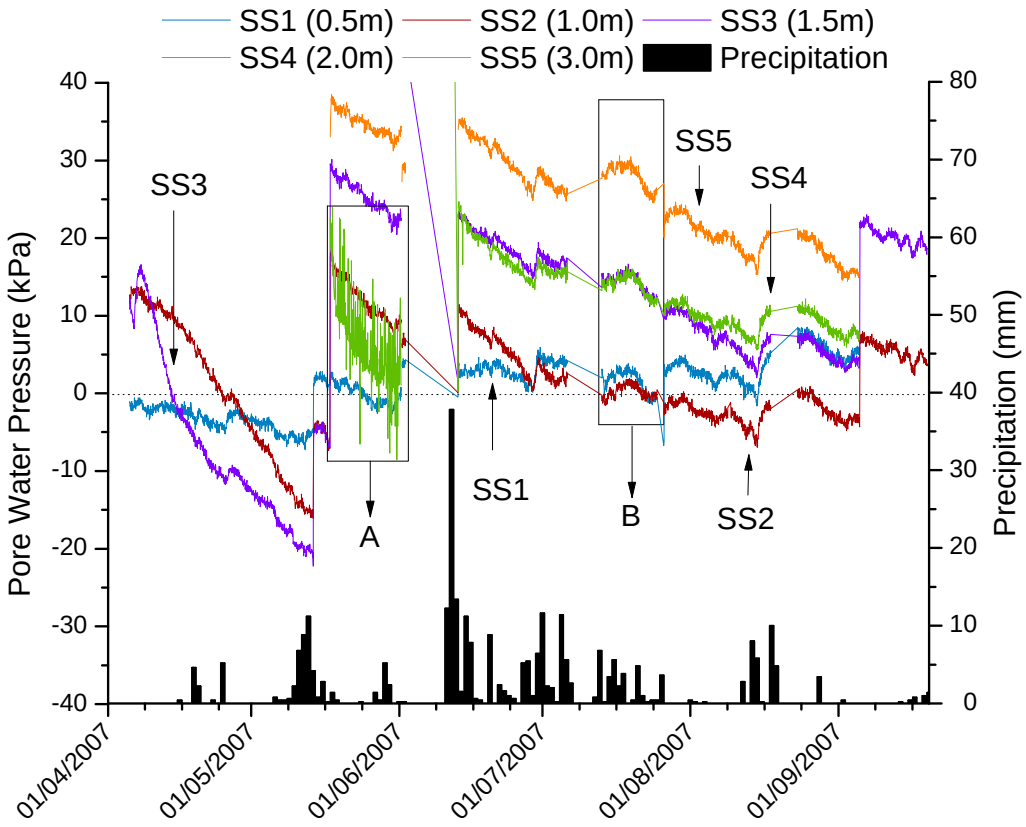

Figure 8.4 – Pore-water pressure records for the well compacted panel and rainfall during the pre-reset stage monitoring. SS (X.Xm) indicates suction station at X.X metres depth.

From Figure 8.4 the initial period between 4th of April and 15th of May was considered an equalisation period, probably representing the final period of closure of the soil around the boreholes. Therefore, the large variations in the recorded values were expected. Beyond the 15th of May until 5th of September all 5 probes were left measuring, although the suction probe installed in suction station 4 (SS4) had to be removed for saturation, as will be explained later and only started continuous measuring with valid results from 13th of June. During this period, reaction from some of

the probes was evident when rainfall events occurred, showing large increases in pore water pressure values at all depths. However noticeable also was the fact that there was a downward trend in the measurements with time. In the long term the probes showed a tendency to measure lower values of pore water pressure than expected. This was evident even during the longer wetter periods, June and July, where it was expected that the recorded values would either maintain or increase in pore water pressure values. The observation of this downward shift coincided with observations obtained in the laboratory that at the end of a test using this type of probe small shifts in the zero value occurred, especially during tests carried out at low levels of suction. A test to check the shift of the zero value of the calibration of the suction probes was carried out at the embankment on the 5th September 2007 where the probes were removed from the respective suction stations and were plunged into free water. The probes were reset so they read a zero value (reset stage) and were then placed back into each respective suction station. Problems with use of the software lead to losses of some of the recorded values but for two probes placed at SS2 and SS3 the differences between the final and post reset values were quite evident. The probe at SS2 shown an increase from a negative value of -4.3 kPa to 6.9 kPa, and similarly the probe at SS3 increased from 3.6 kPa to 20.7 kPa. These observations of the differences in the measured values lead to the implementation of a reset stage in every following visit.

During the pre-"reset" stage other observations were made on the reliability of the high capacity suction probes, such as the case of the probe installed at SS4. As shown in the highlighted area A in Figure 8.4, the probe shown symptoms of poor saturation showing scattering in the measurements. The probe was removed on 1st June from SS4 and was re-saturated during two weeks (period between visits) and was reinstalled after this period. From the 13th June, as is easily observable in Figure 8.4, the scatter in the measurement of the probe installed at SS4 reduced

dramatically, the scatter was comparable with the remaining probes. This demonstrates how important and crucial the saturation stage is in the usage of these probes.

To validate the quality of the probes regarding the obtained measurement, the probe from SS1 was switched with the probe from SS5 (without reset being performed), during the time period highlighted as the area B in Figure 8.4. The measurements obtained by the probe installed on SS5 were congruent with the other measurements obtained at the same location both before and after the probes were switched. The same was observed on SS1. The measurements taken during the time period highlighted in Figure 8.4 were in accordance with the other measurements recorded before and after that probe was installed, showing a maximum error between the switched probes of 5 kPa. This gives a degree of confidence in the measurements obtained.

The results obtained from the monitoring showed a considerable difference to the initial results obtained for pore water pressures measured during construction (compare Figure 8.4 with Figure 7.6 in Chapter 7 that shows the initial values). The initial values of pore water pressure during construction were as low as -400 kPa while the measured values of pore water during this initial monitoring were generally positive.

The small values of suction observed did throw into question the usage of the DU-WF high capacity suction probes with a range exceeding -2 MPa. Clearly, probes with such a large range were not required for this period of monitoring. It also raised the question of appropriate accuracy for the small suctions being measured. An error for the equipment of 0.5% would represent 10 kPa. While 10 kPa in 400 kPa would not be too significant, in values close to zero, the error has a much greater influence. As will be presented further in this chapter, in both well and poorly compacted panels the

recorded values of pore water pressure ranged from -10 kPa up to 30 kPa. That is not to say there might not be larger negative values in the future that might require the capacity of the DU-WF devices. In any case, while the actual values could be overestimated / underestimated due to errors in the measurement, the overall trend in pore water pressure should still be clearly defined.

8.4.2 Field monitoring

Following the decision to start periodic resets of the zero value of the calibration of each probe, the monitoring data considered in this study started in September 2007 and finished in June 2009. The probes are still recording at the field, but the work presented will only consider data up to June 2009. Continuous monitoring of pore water pressure was performed in both poorly compacted and well compacted panel to depths of 3m.

8.4.2.1 Factor affecting the probe usage with the new procedure

With the new *reset procedure* the probes needed to be removed from the respective suction station more regularly then initially expected. As was mentioned in Chapter 7, to protect the electrical cable of the probes a Ø8 mm nylon tube was used; this nylon tube was glued to the end of the probe itself with “Nomorenails” adhesive backed by silicon sealant due to its hydrophobic properties. In each reset stage the probes would be removed and inserted back into each respective suction station; this regular removal of the probes added some strain to the sealant and after some reset stages the sealant started to fail. This meant the probes could fail in the event of infiltration of water into the electrical connections.

This problem of infiltration of water to the electrical connections did occur resulting in mis-functioning of the probe. In this event the probe would be removed from the respective suction station, brought to the laboratory and left to dry inside an oven at a constant temperature of 60-75^0 C. The time needed for the probes to recover was not time dependant, in some cases more than 2 months were necessary. After recovery the probe would be taken back to the field and a new calibration would be performed using the field calibration suction vessel (see Figure 7.8 in Chapter 7) before installation in the respective suction station.

8.4.2.2 Monitoring on the well compacted panel

Figure 8.5 shows the record of pore water pressure in the well compacted panel B together with the observed rainfall for the period September 2007-June 2009. Inspection of Figure 8.5 indicates that the high capacity suction probes at all suction stations react to rainfall. When the rain is absent the probes tend to maintain the same value, although there is a general tendency for pore water pressure to decrease gradually with time (due to drying). At all suction stations in the well compacted panel the probes presented similar response to changes of climatic conditions showing analogous trends of variation with time.

The general tendency with depth was an increase of pore water pressure; in the shallower suction station (SS1) pore water pressures down to small negative values (-10 kPa) were recorded and the largest values up to greater than 30 kPa were observed at 3 metres (SS5). A discussion of the results for each suction station in the well compacted panel (Figure 8.5) is presented independently as follows.

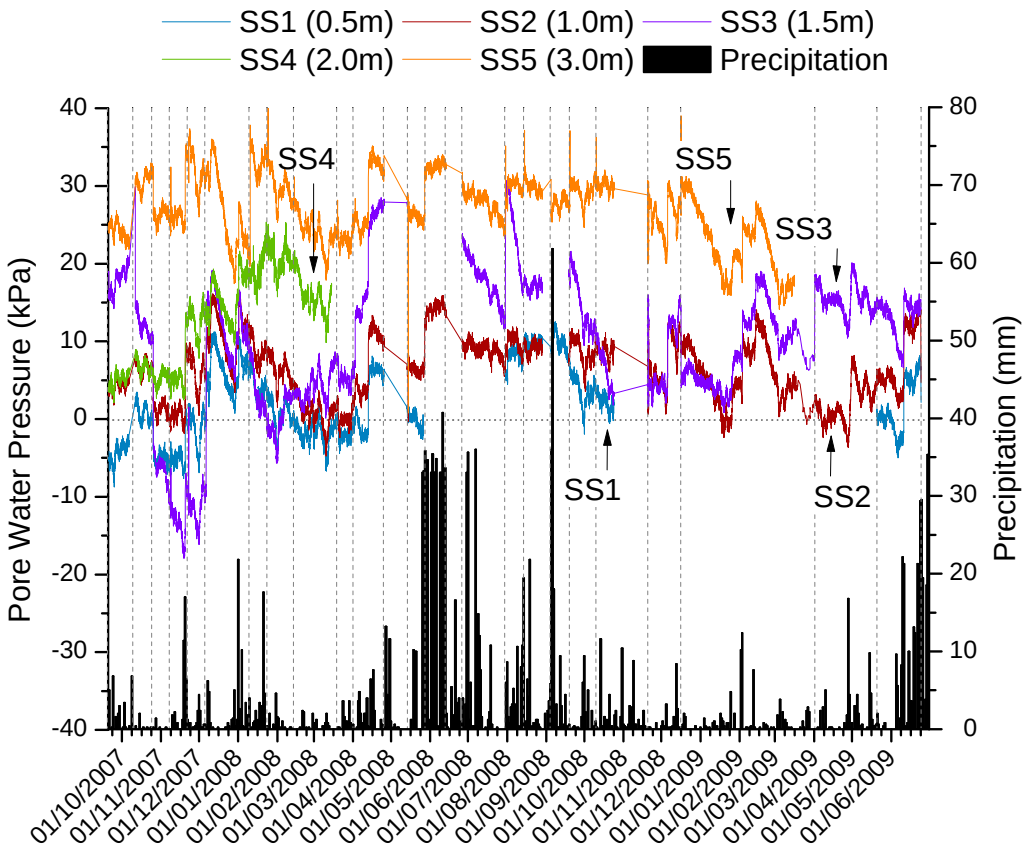

Figure 8.5 – Pore-water pressure records for the well compacted panel and rainfall. SS (X.X) indicates suction station at X.X metres depth and vertical dashed lines represent the reset stages.

SS1, the shallowest suction station at the depth of 0.5 metres on the fill material, presented as expected the lowest values of pore water pressure, in similarity with other observations from other researchers (i.e. work performed in Hong Kong (Gasmo, 1997) and Singapore (Tsaparas et al, 2003)). The recorded values at this location ranged between -10 kPa and 15 kPa.

In the almost two years of monitoring, in SS1 the probe recorded the lower values of pore water pressure during the colder months (autumn and winter seasons), a fact that is explained by the elevated precipitation during the summer months. Measurements close to -10 kPa of pore water pressure were recorded in the autumn months of 2007 followed by positive oscillations until January

2008 reaching up to 10 kPa. The tendency that followed was a gradual reduction of pore water pressure reaching values close to 0 kPa until May 2008. In June 2008 the probe stopped working due to infiltration of water in the electrical system and had to be taken back to the laboratory and was not placed back until August of the same year. This probe missed the first batch of water infiltration tests using the climate control system (June and July 2008), and when it was placed back in the respective suction station the pore water pressure value was as high as 10 kPa oscillating according to rainfall events but maintaining values close to the same value. When the precipitation reduced the pore water pressure started to drop and returning to values around 5 kPa between October and November 2008. In November 2008 the probe again suffered from problems related to water infiltration on the electrical system and was removed from monitoring until May 2009. At this time the probe was recording values close to zero and with time the pore water pressure reduced to a negative value of -10 kPa. In June 2009 the second batch of infiltration tests using the climate control system started and from the start the probe reacted positively to the infiltration tests. The pore water pressure has gradually increased after a first abrupt jump culminating with a final recorded value close to 10 kPa.

The probe located at SS2 (1.0 m) maintained continuous monitoring of pore water pressure throughout the whole period of monitoring, showing no problems of infiltration or cavitation. Like all the probes installed at the well compacted panel BPL the probe showed analogous behaviour to the probe located at SS1, meaning higher values of pore water pressure during the hotter months concomitant with the period of more precipitation and showing reductions during the months when lesser precipitation occurred. Due to its greater depth the pore water pressures recorded increased in range when compared with the values obtained in SS1, ranging between values close to 0 and 15 kPa. As in SS1, the probe located at SS2 started by recoding pore water pressure between 0 to 10 kPa during the autumn months of 2007, increasing to sporadic values of 15 kPa during the intense

rainfall periods of January of the following year. From these occurrences the pore water pressure gradually dropped reaching values close to 0 kPa at March 2008, increasing in value with the start of a wetter period in April and maintaining a constant value around 10 kPa until mid November 2008 apart from June (time of the infiltration tests) where the pore water pressure values were as high as 15 kPa, but reducing to lower values after the infiltration tests to 10 kPa. Between November and December reductions to values close to zero were again recorded increasing after to a value close to 5 kPa in April-May 2009, increasing again to 12 kPa when the second batch of infiltration tests started in June 2009.

At SS3 the behaviour of the probe installed was thought to be erratic in the initial stages, although it showed the same general behaviour as the remaining probes for most of the monitoring time. However, after some of the reset stages the probe shown discrepancies in readings, from a period of positive measurements to negative values after the reset stage. This probe was taken back to the laboratory for evaluation in mid May 2008. After the evaluation and re-saturation of the probe followed by re-calibration in the field the probe was again placed in the same position for monitoring at the end of July 2008. From this period the probe behaviour seemed more consistent by recording values consistent with the other probes. It started by showing reduction in values from a value of 22 kPa of pore water pressure to a value close 5 kPa. The probe installed at SS2 (mid November 2008) recorded similar values until the January 2009. Oscillations on the recorded values were observed in February, as in the other probes installed, reaching almost 20 kPa, followed by dissipation of the pore water pressure, only to increase to values close to 15 kPa at the start of the second infiltration test at the end of the monitoring period presented in this work.

At SS4 the same analogous behaviour can be observed. However, in this case the probe got stuck in the suction station. This meant the probe was never reset and therefore the recorded values can be only be analysed in a qualitative manner. When compared with the other probes installed at the different suction stations this probe showed the same oscillation related with rainfall events: increasing after the events followed by the dissipation on the recorded pore water pressure. This probe started to show symptoms related with saturation in the end of March 2008, as had been observed during the pre reset stage monitoring (not presented in Figure 8.4). A forced retrieval of the probe was attempted which culminated with the complete loss of probe (we were left with the cable in our hands). The head of the probe is still in the suction station and it is impossible to replace it.

In SS5, the probe located at the lowest depth (3.0 m), recorded the highest values of pore water pressure, as high as 35 kPa. Throughout the monitoring presented, this probe recorded oscillations between 20 and 35 kPa in a comparable manner to all other probes in the well compacted panel. During September 2007 until February 2009, it reached a minimum value of 15 kPa in the last days of February 2009. This probe suffered from water infiltrations related problems in mid March 2009 and was retrieved and taken back to the laboratory for evaluation. After the recovery this probe was placed in a different suction station, SS3 of the poorly compacted panel, due a major loss of high capacity suction probes in this BPL.

From the monitoring in all suction stations on the well compacted panel it was possible to elaborate pore water pressure profiles. To create the profiles the information obtained on the first day of recorded values for each month was used. For the well compacted panel this information was divided into years to produce Figures 8.6: a) 2007, b) 2008 and c) 2009. To try to obtain an

understandable picture of the evolution of the pore water pressure of each profile; refer to the colour scheme used in each figure (from brown in January to purple in December).

a)

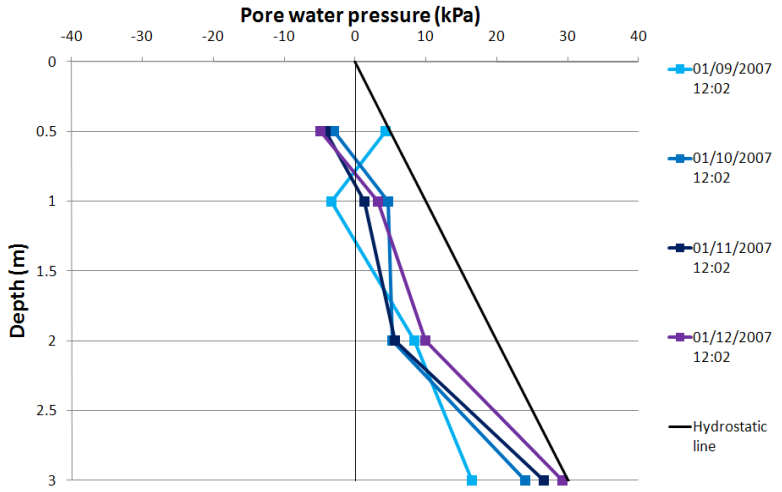

b)

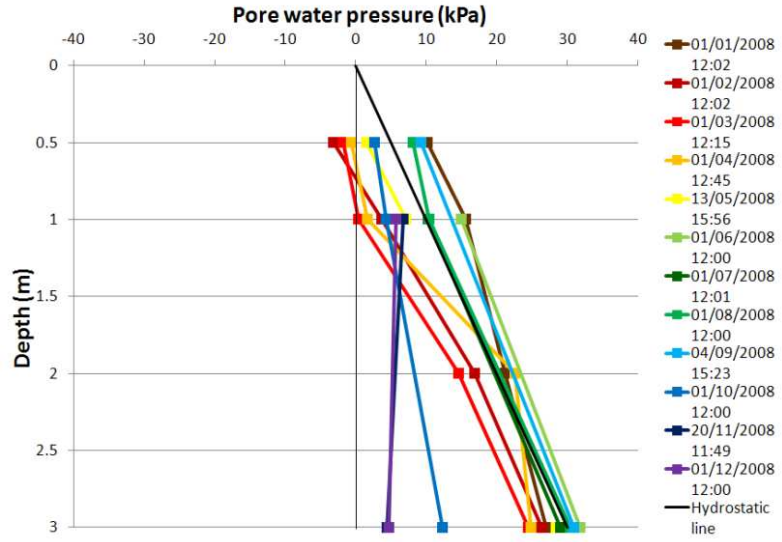

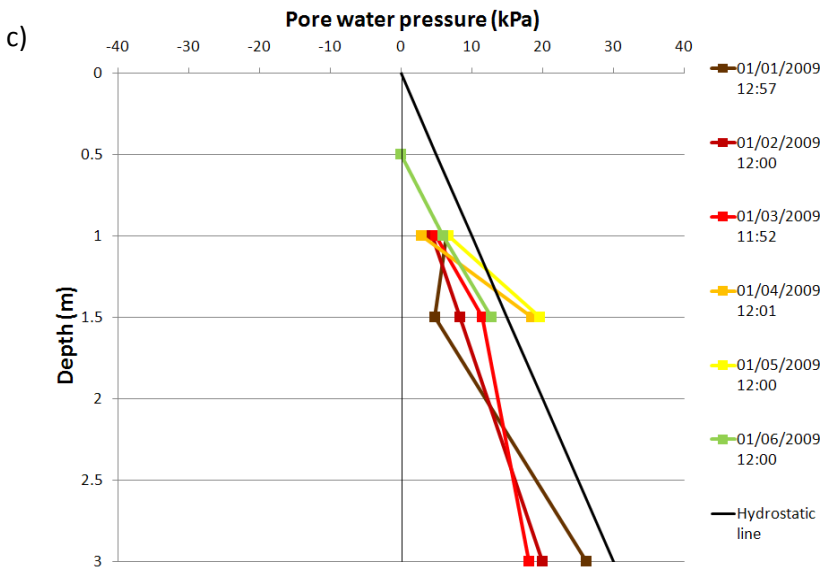

Figure 8.6 – Pore water pressure profiles along depth in the well compacted panel for first day of each month according to different years: **a)** 2007 **b)** 2008 **c)** 2009.

From the pore water pressure profiles for the well compacted panel a clearer view of the observations that have been presented so far can be obtained: the tendency of the pore water pressure to increase to higher values during the summer months while dissipating afterwards. In the final months of 2007 (Figure 8.6a), the pore water pressure reduced in the shallow depths with slight increases at greater depths, this excludes the results from SS3 (1.5 m deep) as explained in the paragraph related to this suction station. The final results for 2007 were a small negative value of -5 kPa at 0.5 metres increasing to values close the 30 kPa at 3.0 metres (SS5). In January 2008 (coincident with significant rainfall events) the values of pore water pressure increased to above the hydrostatic line for most of the full extent of the profile, decreasing in the following months due to a dryer period with smaller rainfall events. With the start of the summer the pore water pressure started to increase, reaching similar values of pore water pressure as were recorded in January of the same year, the wet summer of 2008 was the cause of such an increment. With the reduction of rainfall events the pore water pressure dropped again, only to increase again in April and May 2009.

One interesting observation that can be taken from the pore water pressure profiles was the extent of influence of the changes recorded at different depths. It was quite noticeable that at greater depths (3.0 m) changes in pore water pressure were still evident when compared with shallower depths (0.5 m).

During the summer months of 2008 (Figure 8.6b)) the recorded values of pore water pressure in all probes maintained higher levels above the hydrostatic line. This raised the possibility that the probes might have overestimated the real values. However, it has to be remembered that a 0.5 metre thick coarse layer of ballast exists above the clay fill. It is possible that water retention within this layer could explain the reason for such apparently abnormal pore water pressures. The raised pore water pressure values would be consistent with the coarse ballast layer being flooded, thereby shifting the hydrostatic profile by 5 kPa. The closeness observed of the pore water pressures in depth on the pore water pressure profiles with the hydrostatic line gives the idea that the material is close to saturation.

8.4.2.3 Monitoring on the poorly compacted panel

The monitoring data for the poorly compacted panel is only presented from the start of the use of the reset stage as for the well compacted panel. As presented in the Chapter 3 this panel was constructed differently from the well compacted panel. The expected behaviour for this panel would be of more noticeable differences in pore water pressure in comparison with the measurements obtained for the well compacted panel, due to higher permeability. The monitoring for the poorly compacted panel is presented in Figure 8.7. From Figure 8.7 it is observable that during monitoring

the probes reacted to the weather behaviour: increase of pore water pressure during extended rainfall periods followed by reductions during periods with less rainfall events.

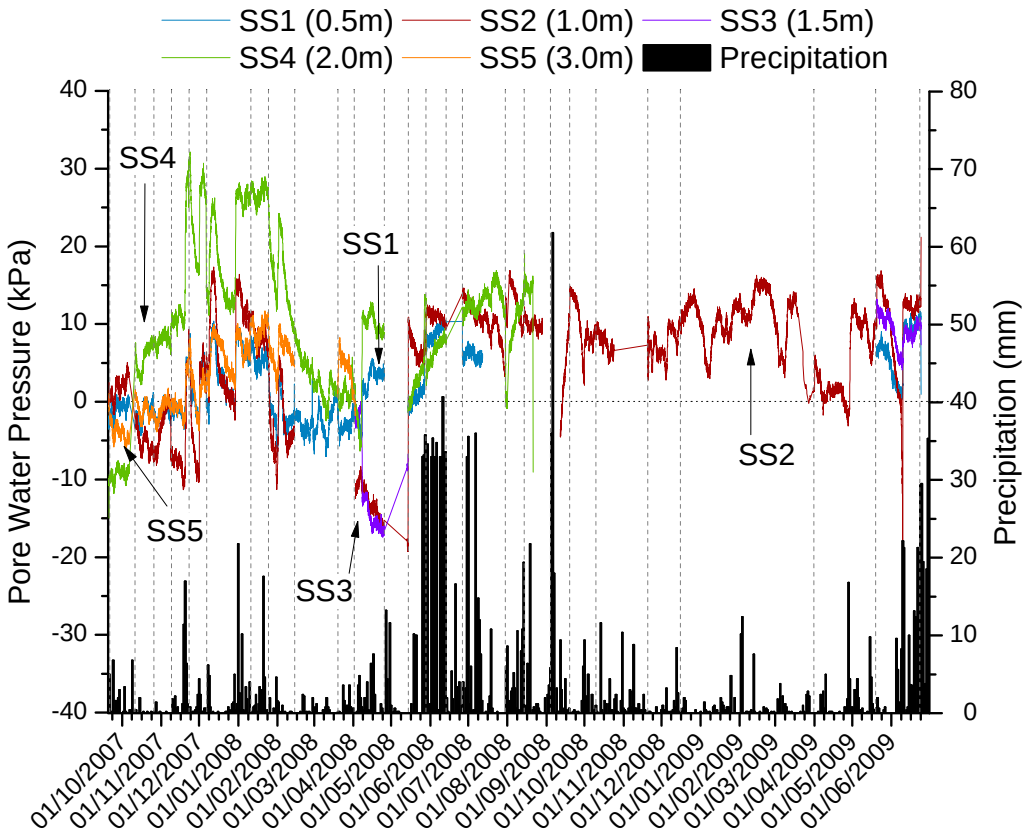

Figure 8.7 – Pore-water pressure records for the poorly compacted panel and rainfall. SS (X.X) indicates suction station at X.X metres depth and vertical dashed lines representing the reset stages.

From Figure 8.7 each probe was analysed and the results are discussed for each suction station in the following paragraphs.

In SS1 (0.5 m deep) at the start of the monitoring (September-October 2007) the probe recorded small variations between 0 and -3 kPa until the period of greater rainfall activity in January,

where the pore water pressure rose to values close to 10 kPa. After individual rainfall events an abrupt rise in pore water pressure was followed by a rapid reduction. At this depth, positive values of pore water pressure were maintained during periods of continued precipitation, in fact during January 2008 this probe recorded values between 10 kPa and 5 kPa. With a period of sparser rainfall events (February until April 2008) negative values were again recorded at SS1. Apart from some sporadic rainfall events where pore water pressure rose to positive values, it maintained values close to -5 kPa. With the start of another wetter period (during April) the pore water pressure rapidly rose again to positive values between 3 and 5 kPa. Although there was no recorded values during the first two weeks of May and considering the observed behaviour at this location so far, a possible negative value should have been reached explaining the fact that during the first batch of infiltration tests carried out at the embankment (June 2008) this probe started by recording small negative values followed by a gradual increase to 10 kPa. At the end of the infiltration tests, first week of July, the probe maintained a constant value of 5 kPa. After the infiltration tests the probe stopped working due to water infiltration into the electrical connections. The period when no values were recorded was quite extended, almost 10 months, due to a long recovery time for the probe and because there were no replacement probes. The probe was reinstalled mid May 2005 recording values close to 5 kPa, a fact possibly explained by the previous rainfall events. Showing similar behaviour as previously, a fast reduction to zero was recorded during the period where less precipitation was observed, only to rise again, to values close to 10 kPa, with the start of the second batch of infiltration tests in June 2009. In general at this location (SS1) the probe showed abrupt behaviour with rainfall events, increasing rapidly, followed by fast reduction of pore water pressure, which can be explained by the permeability of this panel.

The probe installed in SS2 (1.0 m) was the only probe in the poorly compacted panel that maintained continuous readings without suffering from any problems related with water infiltration

into the electrical system. The initial value (end of September and beginning of October 2007) was close to 5 kPa coincident with some precipitation. As in SS1, during a period where the precipitation decreased (October until mid November 2007) so did the value of pore water pressure, this time to negative values around -8 kPa. At this depth the reaction to a single rainfall event was still very quick; between November and December 2007 jumps in the readings from negative to positive values of pore water pressure, almost 20 kPa of difference, were recorded. More significant, however, was the time that it took the pore water pressure to drop back to negative values when no or small events of rainfall occurred, which was less than one week. From January until February 2008, after the rapid increase in the recorded value of pore water pressure caused by the intense rainfall event at the 1st of January the following rate of reduction of the pore water pressure decreased in comparison with previous events due to the smaller, but continuous, rainfall events always maintaining positive pore water pressure values. By the time that rainfall events ceased completely (late February) the rapid reduction occurred, as observed previously, culminating with negative values of pore water pressure close to -10 kPa. During March 2008, the probe was retrieved for inspection when it stopped recording. Although it was retrieved and taken back to the laboratory the problem was related with the respective channel in the logger and, as soon it was changed (the channel in the logger) the probe continued the monitoring. The probe returned to SS2 on the 1st of April. The pore water pressure values recorded straight after were abnormal when compared to previous observations during rainfall events; the pore water pressure values increased to a positive value. However, during this period, even with constant precipitation, the pore water pressure was constantly decreasing, recording the lowest recorded value at this depth of -17 kPa. From May 2008 until April 2009 almost daily precipitation was observed, a fact that explains the positive pore water pressure values recorded. Apart from oscillations related with periods of less precipitation, the pore water pressure kept between 5 up to 15 kPa. With the start of another drier period, the pore water pressure at SS2 started to drop, reaching values close to zero only to increase again with the single rainfall events of May 2009 followed again by rapid reduction. In June, at the end of the monitoring

period which coincided with the second batch of infiltration tests at the embankment, the pore water pressure increased to values close to 10 kPa and maintained the same values afterwards.

By the time of the post reset stage of monitoring there was no probe positioned at SS3. From all the probes, including the probes in the well compacted panel, the probe at SS3 was the first to stop recording due to water infiltration into the electrical system. The probe was recovered and only placed back in the respective position in April 2008. In mid May the probe stopped working again, but during this period (April/May) the recorded values were similar in value and behaviour with the probe at SS2. As presented in SS2, this result was considered abnormal; since the period coincides with daily rainfall events increases in pore water pressure values were expected, not a drop. Since there was no previous information at this depth no further conclusion on the obtained measurements can be made. Back in the laboratory it was impossible to recover the probe from the second failure due to water infiltration. The recorded values in mid May 2009 were performed with the probe that was transferred from SS5 in the well compacted panel. From this date, the pore water pressure behaviour was very similar with the remaining probes, showing increases in the pore water pressure value during rainfall events followed by reduction when limited rainfall events were observed. The pore water pressure values recorded were close to 10 kPa, with the lowest (during the reduction period) being 5 kPa.

In SS4, 2.0 metres deep, the rapid changes in the pore water pressure to higher values influenced by the weather conditions was still evident. Abrupt jumps of 20 kPa were recorded by the probe. Reduction of pore water pressure, when the conditions permitted, was also observed. From the beginning, the probe located at SS4 recorded small negative values of pore water pressure (-10 kPa) which, with time, was considered erroneous, since after the second reset the probe was

recording positive values of 5 kPa with no clear evidence of a significant rainfall event that could justify it. After the second reset stage, until the rainfall event in mid December 2007, the pore water pressure gradually increased from 5 kPa to 10 kPa. During this event the pore water pressure increased abruptly to 32 kPa, the highest value of pore water pressure recorded in all the monitoring carried out on the poorly compacted panel. Subsequence oscillations on the pore water pressure between singular rainfall events were observed (November-December 2007). In the second half of December, during a period of less precipitation, a clear reduction of the pore water pressure was observed, reducing to a value of 12 kPa. In the beginning of 2008 (January/February) an initial abrupt jump of the pore water pressure reaching 25-26 kPa was recorded, with subsequent daily precipitation, this value was maintained, only to change again during the drier period of February-March 2008. A longer period of reduction of pore water pressure, in comparison with shallower probes, was observed during February-March 2008, culminating in values of pore water pressure around zero. Within April, the precipitation intensified and remained constant resulting in an increase in the pore water pressure, this time to values not greater than 12 kPa. Previous to the infiltration test there was no evident precipitation and since no data was recorded, it is likely that the pore water pressure decreased to lower values (possibly negative), an assumption based on the observed behaviour of the pore water pressure at SS4. This can explain the fact that during the infiltration tests the first abrupt jump is missing. With the continuous infiltration of water into the embankment the pore water pressure at SS4 increased continuously, from 0 kPa in 14th May up to 15 kPa in 20th July. The probe stopped recording in mid August 2008 and it was impossible to recover it. With no replacement probes the monitoring at this depth stopped at 21st August 2008.

At SS5 (3.0 m deep) the pore water pressure behaviour with time was less reactive in comparison with the remaining probes. From the beginning of the monitoring until the first intense rainfall event in mid November the probe recorded values of pore water pressure between small

negative values down to -5 kPa and zero. With the rainfall events, this probe started to show the abrupt jumps that were recorded in all other suction stations. Differences in the behaviour of pore water pressure were observed, comparible with those observed at the same period at the remaining suction stations: the abrupt jumps were less significant with a maximum jump of 9 kPa and the general tendency during this period was that the pore water pressure seemed to increase gradually with time (possibly showing some water retention at this depth). The short time of monitoring for this probe (19th September 2007 until the 1st April 2008) showed small differences in behaviour of pore water pressure suggesting that at this depth the influence of the weather was less evident. For the gradual increase of pore water pressure with time at this depth, a continuous infiltration can be suggested, which can be related with the suggestion for the higher values of pore water pressure above hydrostatic values in the well compacted panel monitoring.

The recorded values of pore water pressure of the poorly compacted panel were used to generate pore water pressure profiles, as for the well compacted panel. Figure 8.8 presents the pore water pressure profiles obtained. From the profiles it is evident that pore water pressure changes are different with depth, in the case of 2007 as an example, pore water pressure at 0.5 m was close to hydrostatic values in September and December, while during October and November values reduced to close to zero; at 1.0 m the profile shows that pore water pressure in September was negative (-15 kPa) increased to positive in October, reducing to small negative values in November and increasing back to positive in December. This heterogeneous behaviour between probes can be observed in the remaining profiles.

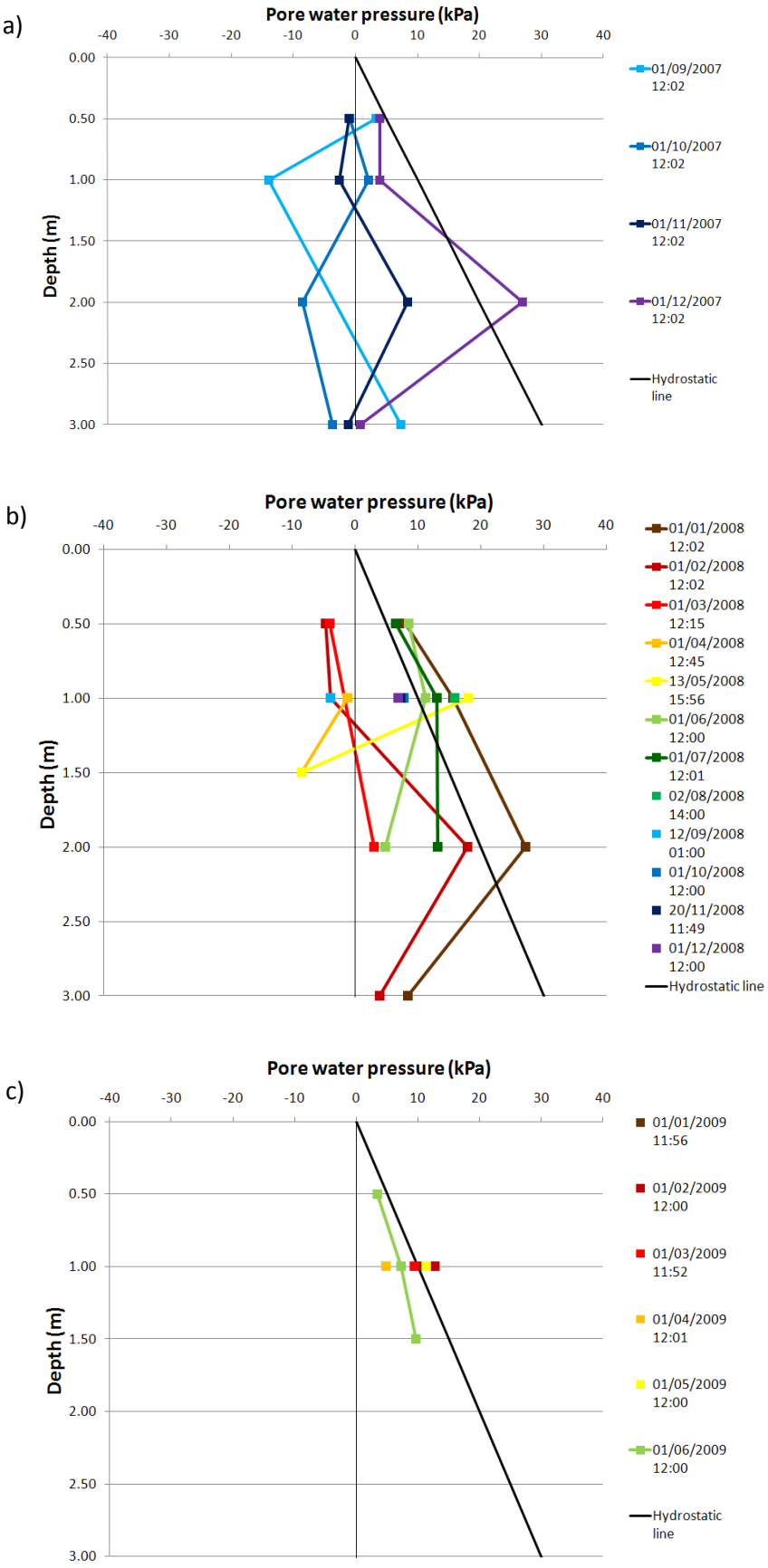

Figure 8.8 – Pore water pressure profiles along depth in the poorly compacted panel for first day of each month according to different years: **a)** 2007 **b)** 2008 **c)** 2009.

The heterogenic behaviour of the probes observed in the profiles for the poorly compacted panel can be related with single climatic events; as was mentioned in the description of the monitoring during rainfall events, abrupt jumps in the recorded pore water pressure were observed and normally reduced rapidly afterwards when the climatic conditions permitted. These rapid changes can be related with the permeability of the material that allowed a faster flow of water inside this panel, during both rainfall events (infiltration) and drier periods (evaporation). The record result of January is a clear evidence of this: the 1st of January coincides with a major rainfall event and the values of pore water pressure up to 2 metres deep were greatly affect by it, reaching values above the hydrostatic line, apart from SS5 at 3 metres where the pore water pressure changed significantly less.

8.4.3 Well compacted panel versus poorly compacted panel

The generated data of pore water pressure for both poorly compacted and well compacted panels showed similarities and differences between panels.

The similarities refer to the rapid response on the part of the high capacity suction probes installed related with the climatic events; positive response to rainfall events and gradual reduction, during periods with less precipitation activity, on the recorded pore water pressure.

Although the behaviour of the probes was similar to climatic events, the actual pore water pressure behaviour when compared between panels could not be more different. In the well compacted panel, the pore water pressure changed almost in sync at different depths, resulting in the pore water pressure gradually increasing with depth, closely following the hydrostatic line in the

pore water pressure profiles. In the poorly compacted panel the story was more varied, where the pore water pressure changes were independent of depth. Changes in pore water pressure on the poorly compacted panel were more dramatically related to singular rainfall events, with abrupt positive changes on the pore water pressure in all the monitored depths, being more evident down to 2 metres. The behaviour of pore water pressure in the poorly compacted panel did not show any consistency, and did not showing any clear relation between probes at different depths.

The data therefore shows clear differences between the panels which can be explained by the different compactive effort employed during construction. Being more permeable the pore water pressures in the poorly compacted panel were prone to bigger changes, thus abrupt jumps were observed during rainfall events, and the reduction in pore water pressure after a rainfall event was vastly faster when the conditions permitted.

In terms of the actual values of pore water pressure measured in both panels, the well compacted panel showed measurements of pore water pressure closely following the slope of the hydrostatic line. This suggests there was limited water flow inside the panel as the pressure head profile would not encourage this. However, the observed oscillations between negative to positive values in the poorly compacted panel could be related to permeability. However, in this case the value of the permeability was sufficient to allow a more varied water flow inside the panel.

8.5 **Conclusions**

The monitoring of pore water pressure at the BIONICS embankment had the intention to generate sufficient data to explain the behaviour of pore water pressure in time and with depth. Monitoring was performed for two different compaction conditions, a poorly compacted and a well compacted panel, promoted the comparison of pore water pressure between different conditions. The different values on water contents and void ratio (with differences also in degrees of saturation) obtained from the cores indicated the different environments for the monitoring. These differences would greatly influence the recorded values of pore water pressure at the different panels, even though both responded to the observed weather at the site (natural and induced).

The initial monitoring (pre-"reset stage" monitoring) lead to major findings and generated some concerns about the usage of high capacity suction probes in field conditions. However, it has been shown that the suction probes have the capacity for long-term measurement. Swapping the location of the probes showed reproducibility of measurements. The importance of saturation to ensure reliable measurements has been demonstrated. However, the probes were unable to maintain a constant zero value of the calibration, which lead to the implementation of reset stages every two weeks where the probes were reset back to zero values.

Due to the constant movement of the probes (in and out of the Borehole Probe Locator) needed to implement regular resetting, a new technical problem arose. This movement gradually destroyed the sealant used between the protective nylon tube and the electrical cable. With the loss of this defence, water could infiltrate the electrical system of the probes which jeopardised the monitoring. A recovery methodology was developed and in the majority of the recorded cases was successful.

The responses of the probes (in both panels) during the monitoring were consistent with the reaction to weather events. Under a single rainstorm or after continued precipitation, values of pore water pressure increased positively and reductions in pore water pressure were observed only when precipitation was less intense.

The monitoring of the well compacted panel showed that the pore water pressure behaviour had the tendency to increase with depth, always recording values either, slightly negative at shallower depths and positive at greater depths. This general increase with depth followed closely the hydrostatic line (shown in the profiles) leading to the assumption that the material was close to saturation.

A different behaviour was observed on the poorly compacted panel. Pore water pressure behaviour was more heterogeneous, showing no relation with depth as in the well compacted panel. The reactions of the probes to weather events were more dramatic with abrupt jumps, increasing up to 20 kPa, and a more rapid reduction of pore water pressure when conditions permitted. This behaviour of pore water pressure was more evident at depths less than 2 metres. Being more permeable than the well compacted panel, the water flow within the poorly compacted panel was more rapid resulting in the observed behaviour of pore water pressure.

9 From the laboratory to the field

9.1 Introduction

The experimental study of the BIONICS fill material has been carried out in both laboratory and field conditions. From the laboratory experimental chapters, Chapters 5 and 6, the hydraulic and mechanical properties of the fill material were determined on compacted samples. For the field work, an extended period of monitoring of pore water pressure has been presented in Chapter 8. This chapter intends to correlate these results in an attempt to take the results obtained in the laboratory to the field.

9.2 Initial construction conditions

9.2.1 Initial conditions at the embankment

To correlate the data from field and laboratory, in an attempt of describing the possible behaviour of BIONICS embankment fill material, it is important to acknowledge the initial conditions at construction. As has been described in Chapter 3, the BIONICS embankment, with glacial till as a fill material, was built to resemble embankments commonly found throughout the transportation network in the NE of England, divided in panels representing two different construction methods. During construction two of the panels were compacted according to Method 3 as set out in the Highways Agency Specification for Highway Works (Highways Agency, 1998) (the well compacted panels), and 2 other panels were constructed where compaction was not controlled in order to simulate compaction methods of Victorian times (the poorly compacted panels). Differences in the fill material properties from both compaction methods were presented in Table 3.3, in Chapter 3, where differences were found between the two. The well compacted panels presented generally

better characteristics. The measured permeability values showed that the well compacted panels were the less permeable, where laboratory permeability tests results ranged in values greater than 10^{-11} opposing to 10^{-10} obtained for the poorly compacted panel. Preliminary results obtained in the field for the top metre on each individual panel by Natrass (2009), using a Guelph permeameter, suggests that at field conditions the permeability was much higher increasing to average values close to 10^{-8} in the case of poorly compacted panels and 10^{-9} for the well compacted panels.

More importantly, regarding the laboratory work performed, were the initial conditions in terms of water content and dry densities. The initial water content and the dry densities varied during construction. However, it can be assumed that water content during construction was between 17% and 24%, and dry densities between 1.60 to 1.73 Mg/m^3 for the most of the determinations of both construction methods, as shown in Figure 3.10.

Table 9.1 – Water content and dry density of the BIONICS fill material at construction from the first three 3 metres.

		Well compacted panel B at-construction		**Poorly compacted panel A at-construction**	
	Depth m	**γ_d Mg/m^3**	**Wc (%)**	**γ_d Mg/m^3**	**Wc (%)**
Layer 1	0.3	1.68	19.7	1.71	19.5
Layer 2	0.6	1.61	23.2	1.63	18.3
Layer 3	0.9	1.61	20.4	1.67	19.9
Layer 4	1.2	1.70	18.8	1.63	22.2
Layer 5	1.8	1.68	20.7	1.65	21.0
Layer 6	2.1	1.64	21.4	1.65	20.5
Layer 6	2.4	1.72	18.2	-	-
Layer 7	2.7	1.71	18.4	-	-
Layer 8	3.0	1.68	20.4	1.61	20.1

Table 9.1 presents a more detailed information on the values of dry density and water content for the top 3 metres of panel A (poorly compacted) and panel B (well compacted) presented in

Figure 3.10 referent to the comparison of the compaction curves with field results obtained during construction in Chapter 3. It is also important to mention that the monitoring of pore water pressure carried out in the BIONICS embankment was performed down to the depth of 3 metres on these panels.

From Table 9.1 on average, for the first three metres, both panels present slightly different conditions, as previously mentioned. At depth, in panel B, the dry density tended to increase from an average value of 1.63 Mg/m^3 in the first metre to 1.67 Mg/m^3 in the second metre to a higher value of 1.70 Mg/m^3 in the third metre; in the same analogy, the correspondent water contents decrease from 21% at the top metres to 20% reducing further to 19% at 3 metres. In the poorly compacted Panel A, during construction dry densities were slightly smaller below one metre, around 1.65 Mg/m^3 and seemed to decrease with depth, although there is a lack of information between 2 and 3 metres deep.

9.2.2 Laboratory and field soil material comparison

The values of dry density and water content seemed to agree with the wet part of the curve of the compaction curve from the BS Light (2.5 kg) compaction test obtained in the laboratory, see Figure 3.10. The same analogy could not be obtained for the dry side of the compaction curve for the values obtained in the field at lower water contents, especially for the values obtained for the well compacted panel, where these values tended to be higher in comparison. The original fill material, however, was found to be too heterogeneous, being difficult to give reproducible densities in the laboratory. Thus the BIONICS soil was sieved using a 2.80 mm mesh to reduce the observed heterogeneity (Chapter 4). Larger samples (200mm by Ø100mm) were compacted under the sample preparation methodology developed in chapter 4 at different water contents (10%, 13%, 15%, 20%

and 22%) and these gave an close agreement with the measurements obtained from the field, in similarity with the light compaction curve, in Figure 4.3 the BSL – 200 S.

As described in chapter 7, core samples were retrieved from each borehole of panels A (poorly compacted panel) and B (well compacted panel) in 2007, two years after the construction. In Chapter 8 the results of water content and density were reported in Table 8.2. The comparison of Table 8.2 with 9.1 shows that after two years the material in the poorly compacted panel on average had a higher water content value and lower dry densities for the first 2 metres deep, on the first metre the average value of dry density changed from 1.67 Mg/m^3 (during construction) to 1.62Mg/m^3 while the average water content increased from 19% to 24 % and in the second metre changes in dry density were from 1.64 Mg/m^3 during construction to 1.59 Mg/m^3 and water content increased from 21% to 24%. At 3 metres there was a noticeable decrease of the water content 20% to 18% where no variation in the dry density was observed.

On the well compacted panel little seemed to change over the two years that separated the measurements apart from the first metre, where, the water content reduced by 1%, although this might not be statistically significant.

From the core samples, differences in the water retention properties of both panels were shown in Figure 8.1 (reproduced again in this chapter as Figure 9.1), which were determined by high capacity suction probes. Also shown in Figure 9.1 are the water retention curves following drying paths that were obtained in the laboratory using the sieved material. The results from the core samples are drying curves from the natural water contents: 22% in the case of the well compacted panel and 20% in the case of the poorly compacted panel presented again as Figure 9.1.

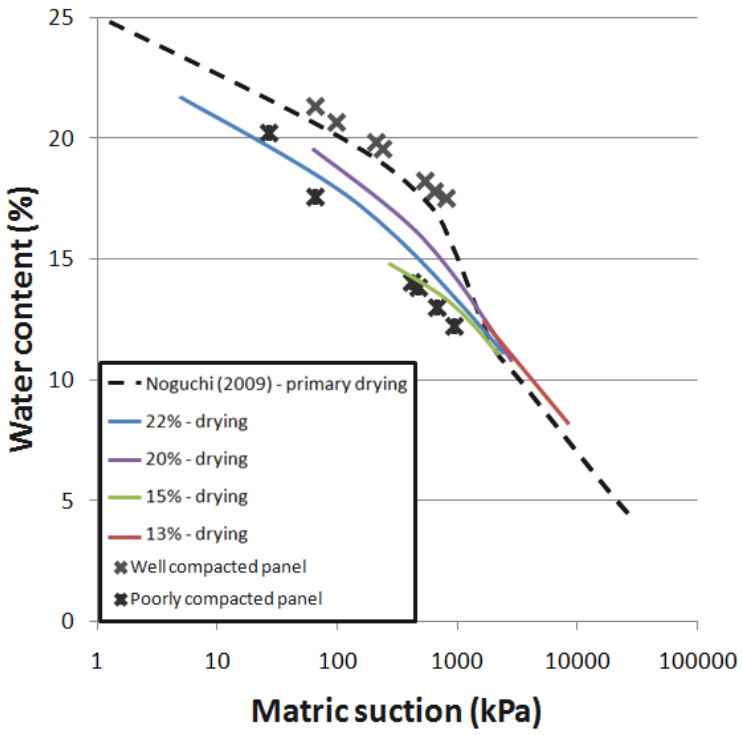

Figure 9.1 - SWRCs obtained from samples of the first metre of the cores from boreholes in the well and poorly compacted panels compared with results from SWRCs on laboratory compacted samples (drying path).

From Figure 9.1 it can be observed that the water retention curve obtained for the well compacted material fell at higher values than the SWRC (primary drying curve in the figure). The water retention curve obtained for the poorly compacted panel, however, showed some degree of agreement with the SWRCs that were dried from different water contents as observed in the figure. The behaviour of the two SWRCs obtained from core samples was dependent on the initial conditions. For the SWRC obtained for the well compacted panel the initial conditions were: water content of 21.3%, void ratio 0.64 meaning a degree of saturation close to 90% and recording a suction of 66 kPa by the high capacity suction probe; while for the SWRC obtained from core samples of the poorly compacted panel the initial conditions were: water content 20.2%, void ratio 0.66 hence a degree of saturation close to 83% and suction of 27 kPa. The difference between the

two SWRCs is evident from the start: higher degree of saturation corresponding to a higher suction for the well compacted SWRC against an initial lower degree of saturation with lower value of suction on the SWRC for the poorly compacted panel. Due to the manner in which the tests were carried out the volumetric changes of the sample due to drying was not determined, and because shrinking behaviour was observed during the tests it makes impossible to infer the air entry values based on changes in degree of saturation. However it is possible to recognize that it would be the first to desaturate due to the nature with higher void ratio, lower density and higher permeability of the poorly compacted panel and the initial value of degree of saturation.

The initial suctions for the cores taken from the embankment (values of 66kPa for the well-compacted panel and 27kPa for the poorly compacted panel, in Fig 9.1) are smaller than the observed values of suction during construction presented in Chapter 7 (Fig 7.6) ranging between values of 75 to 400 kpa for the well compacted panels and between 50 to 160 for the poorly compacted panels. These cores were taken from the embankment in the Spring of 2007 during the installation of the borehole probe locators. After two years of the embankment being subject to precipitation, it was shown that suctions had reduced significantly. Moreover, the obtained measurements were also obtained under no confinement at the laboratory which was different from the field conditions. Under confinement, as it was presented in Chapter 8, suction reduced even further to small values of suction at the shallower depths to positive values of pore water pressure at deeper depths on both well and poorly compacted panels.

9.3 Climate conditions and influence on the pore water pressure

Pore water pressure measurements in the field correlated with recorded precipitation in two of the panels of the embankment (well compacted panel B and poorly compacted panel A), were presented in chapter 8 and are again shown as Figures 9.2 for the well compacted panel and Figure 9.3 for the poorly compacted panel.

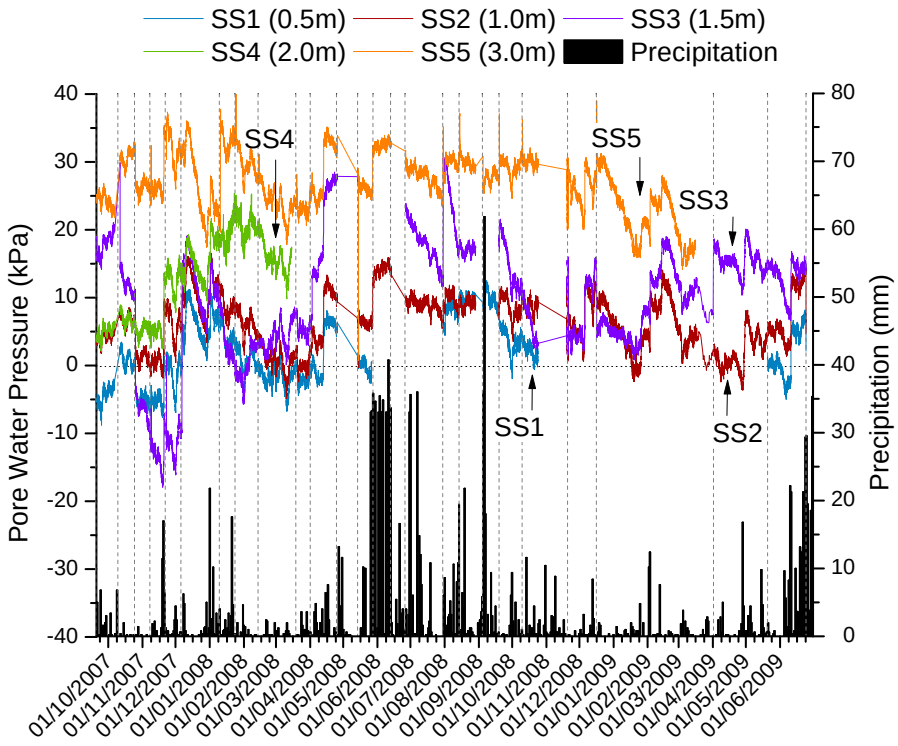

Figure 9.2 – Pore-water pressure records for the well compacted panel and rainfall. SS (X.X) indicates suction station at X.X metres depth and vertical dashed represent the reset stages.

In the well compacted panel, Figure 9.2, pore water pressure behaviour had the tendency to increase with depth; always recording either small negative values at shallower depths and positive values at the deeper depths. However, in the poorly compacted panel, reactions to weather events were more evident with abrupt positive jumps in the pore water pressure followed by a dissipation period when weather conditions permitted.

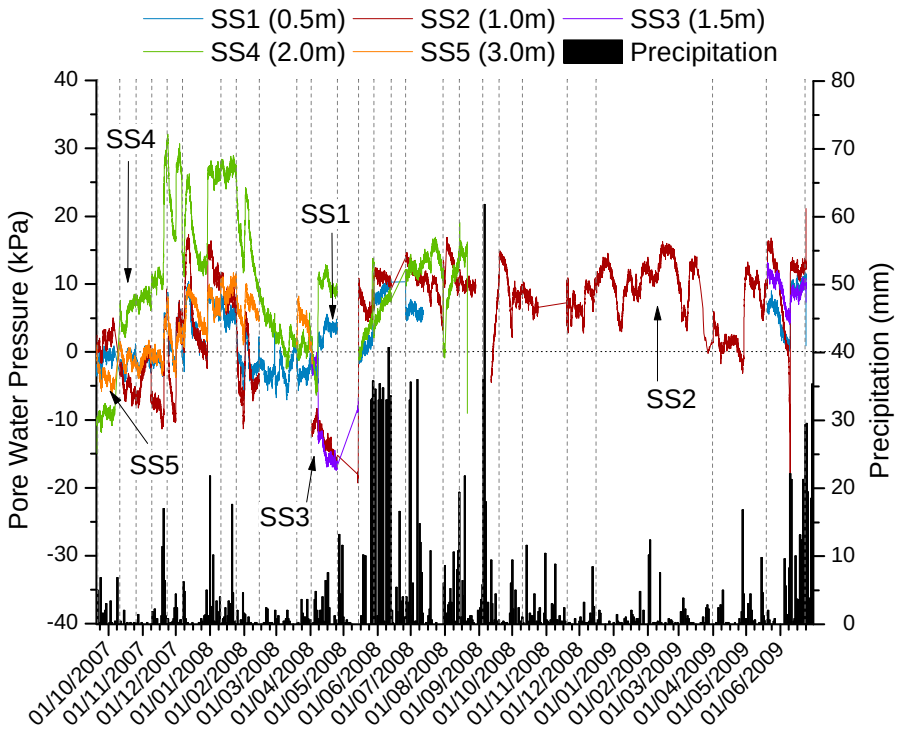

Figure 9.3 – Pore-water pressure records for the poorly compacted panel and rainfall. SS (X.X) indicates suction station at X.X metres depth and vertical dashed representing the reset stages.

The pore water pressure behaviours for the first three metres observed in both panels have shown that the fill material reacted differently to weather conditions. An important observation was the dramatic behaviour of pore water pressure in the poorly compacted panel when compared with the better engineered well compacted panel. In the particular case of the BIONICS embankment this behaviour can only be explained from the nature of the properties of the material at the given conditions. The permeability of the poorly compacted panel is higher when compared with the well compacted panel resulting in faster flow of water in different forms such as liquid water (infiltration) or vapour water (evaporation) resulting in the observed sharp reactions from the high capacity suction probes during different climate conditions.

Differences arise when comparing the initial values of pore water pressure obtained from the core samples from both panels with the observed changes in pore water pressure in depth and in time during monitoring. During monitoring, in both panels, the values of pore water pressure were only slightly negative (-5 to -10 kPa) or positive (reaching up to 30 kPa) never reaching the measured pore water pressures of -27 (poorly compacted) and -66 kPa (well compacted) measured during the trials for the determination of the SWRCs for the core samples. There are two possibilities to explain such inconsistency: the manner in which core samples were retrieved and transported and the ballast layer that serves as a boundary condition for the numerical modelling.

The core samples were retrieved from the embankment and taken to the laboratory, from retrieval until testing, changes in water content were only minimised and not totally eliminated, which, by drying, would increase the value of suction.

In order to make the numerical modelling of the embankment easier, a boundary condition was created in the form of a ballast layer of 0.5 m thickness at the top of the embankment which lies above both locations of the BPLs. This layer made it impossible to make observations of the surface of the fill material where the possibility of water being retained could exist. In the event of such a case, water that would be retained underneath the ballast layer would have a major impact on the natural behaviour of the internal flow of water since there would be no, or limited, runoff and the water would slowly infiltrate the embankment increasing the actual water content of the fill material making the changes in pore water pressure less evidently related to climate conditions. Being a coarse material the water flows through the ballast layer rapidly and could lie above the less permeable surface of the fill material. As it has 0.5 m thickness it could also act as a cover for this water resulting in the reduction of actual evaporation.

9.4 Future climate scenarios and pore water pressure

During the monitoring of 2007-2009 pore water pressure in both panels varied from small negative to positive. This suggests that the embankment is close to saturation. However, this might not be true for future climate scenarios.

Climate change predictions suggest that we will experience temperature changes and this will lead to changes in the weather patterns. For the UK it is expected that we will experience stronger winters with intense rain showers and dry summers with longer drying periods.

In terms of pore water pressure response within the BIONICS embankment, during extended dry periods pore water pressure are likely to change to negative values, possibly reaching lower values than those observed during the period presented (2007-2009). Moreover, there is also the possibility that negative pore water pressures may exist at greater depths. During winter months it is likely that pore water pressure will increase to positive values, up to hydrostatic levels, as it has been observed so far. Therefore, higher fluctuations of pore water pressure between seasons should be expected, which could lead to a decrease in serviceability of infrastructure embankments.

9.5 Mechanical behaviour of the well compacted panel B

From what has been presented through this chapter the well compacted panel seems to present more similarity with the samples prepared in the laboratory. The densities are more similar

to those reported in Chapter 8 and the SWRCs for the sample taken from the well compacted panel coincides with the drying path for laboratory prepared samples (although the SWRC for the poorly compacted panel did present more similarities with the determined SWRCs involving drying from lower water contents than the primary drying SWRC). Of course, some cautiousness has to be considered when comparing SWRCs since laboratory prepared samples were wetted or dried only once from as compacted conditions, whereas the weather records show reversals of wetting and drying in the field.

The better engineered well compacted panel, resembling modern highway embankments, has not responded so dramatically to the weather patterns observed at the BIONICS site, as is observed from Figure 9.2, despite the fact of pore water pressure still reached hydrostatic values. The observed smaller variations in pore water pressure in depth (variations were less than 15 kPa, compared with almost 20 kPa for the poorly compacted panel) and the fact that less dramatic events due to climate conditions were recorded indicates a more homogeneous structure. This of course is a direct cause of the methodology used for the construction of each panel. Albeit being built of the same material, the higher density achieved during construction on the well compacted panel resulted in a less permeable material which in turn affected the hydraulic behaviour of the material by reducing the water infiltration rate.

The mechanical behaviour described in Chapter 6 can only be representative of the stage of construction since weather cycles of precipitation/evaporation occurred subsequently in the field but no cyclic tests were performed in order to observe the behaviour during the later stages. The lack of equipment to measure strength parameter in the embankment also impedes better correlations of field and laboratory behaviour.

Therefore, at construction, since the values of dry density were close to 1.6-1.7 Mg/m^3 and water content ranged between 17% - 24% from the described mechanical behaviour in Chapter 6 the Critical State Line (CSL) for construction conditions were the values presented around the parameters of critical state of 20% and 22% Wc(ac) as shown in Table 9.2.

Table 9.2 – Critical state parameters representative of the initial conditions during construction.

	v – (p-u_w) plane		**q – (p-u_w) plane**	
	Γ	**λ**	**M**	$\emptyset'_c$
CWT test with Wc(ac) close to 22%	2.162	0.102	0.85	22^o
CWT test with Wc(ac) close to 20%	2.062	0.087	0.86	22^o

Since the mechanical testing is only representative of the initial conditions, only broad observations are possible. The pore water pressure changes were relatively small during the monitoring. Through the years of monitoring, values close to hydrostatic were observed which is representative of water contents higher than 22%. This would suggest the behaviour would be characterised by small changes in strength. Based on the results with 50 kPa of confinement achieved by samples tested at 22% of water content as compacted and dried to 20% and tests carried out on samples wetted from 20% to 22% of water content it can be foreseen that changes in shear strength would be much smaller than 50 kPa (as observed in the tests) as at the monitored depths the confining stress is expected to be much lower (perhaps 20-30kPa). Furthermore, during the monitoring period there was no evidence of any significant movement of the embankment, meaning that the changes of pore water pressure were not sufficient to influence the stability of the embankment. In all panels of the BIONICS embankment the measurements obtained from both inclinometers and extensometers fell within small changes, inside the accuracy of the measuring equipments (Hughes et al. 2009).

The same observations could be made for the poorly compacted panel, however due to a more dramatic behaviour of pore water pressure during monitoring and acknowledging the heterogeny of the fill material it is more difficult to infer that all the material would behave in a similar manner. Nevertheless, if such is not true and the material does behave in similar manner the behaviour in terms of changes in strength on the material would be expected to be higher than in the well compacted panel, using the recorded values of pore water pressure present in Figure 9.3 as a reference.

10 Conclusions and further work

10.1 Conclusions

Slopes in embankments and cuttings comprise a large part of a transportation network therefore it is important to understand the impact of climate changes on this part of the network infrastructure. The BIONICS embankment is a highly valuable potential tool to study the effect of climate change. Built with material that is present in various earth structures throughout the UK and resembling different structures (old and modern), with its disposition of panels, it can be related to other existing structures. The climate control system backed by a wide range of instrumentation can be used to generate a clear view of the behaviour of the embankment through different climate events. It also enables the testing of new field methodologies that can help future design of earth structures.

Throughout the study various conclusions have been drawn relative to each subject of study. In this final chapter a summary of these conclusions is presented.

10.1.1 BIONICS fill material at the laboratory

An important aspect of doing studies on soils is to have a sample preparation procedure that can be replicated. The original material from the BIONICS fill material was found to be to heterogenic. Therefore, the material was sieving to a maximum particle size dimension of 2.80 mm. Processes to wet and dry samples were developed in order to achieve uniform water contents, including a new mechanism to wet the samples using mini-foggers.

The soil water retention curve for the BIONICS fill material was investigated using an array of different techniques. SWRCs following drying paths were determined for total and matric suction by other researchers. The matric suction SWRC presented a typical bi-modal curvature with a residual gravimetric water content of 4%. The air entry value was determined to be around 220 – 300 kPa. The study of SWRC starting from lower water contents also added more information on the behaviour of the BIONICS fill material. SWRCs that followed drying paths seemed to behave as scanning curves joining the primary drying curve obtained by Noguchi (2009) at similar value of 11% of gravimetric water content, around 3000 kPa of suction. The SWRCs curves that followed wetting paths, however, show instead atypical behaviour, where they seemed to follow paths joining the primary drying curve.

The mechanical behaviour study involved constant water content triaxial tests on as-compacted, wetted and dried conditions from samples with initial water content of: 15%, 20% and 22% at different confining pressures. Under a critical state limit framework the material seemed to present similar behaviour, where it was found that the slope of the critical state line (CSL) in deviatoric stress space (*M*) was found to be similar for all water contents. The slope of the CSL in v-ln(p-u_w) space (λ) was found to be similar for all water contents, however the CSL shifted position due to variation in the intercept, Γ. Since specimens were at high degrees of saturation, calculations based on effective stress showed a reasonable interpretation of the data. However, by using the Bishop's average skeleton stress a better agreement was reached in the p*-q plane where all water contents tested fitted on a single line where M was found to be 0.91. However, in the v – ln (p*) plane, different critical state lines were obtained for different as-compacted water contents.

10.1.2 BIONICS fill material at the site

A new field measurement system to continuously measure pore water pressure at different depths using high capacity suction probes has been developed in this study. Two of these systems were installed at the BIONICS embankment (well and poorly compacted panels) and have continuously monitored pore water pressure changes since April 2007.

The observed behaviour of pore water pressure was different in both panels. In the well compacted panel pore water pressure behaviour had the tendency to increase with depth, always recording values that were slightly negative at shallower depths and positive at greater depths, showing profiles which were roughly parallel to the hydrostatic line suggesting that the material was close to saturation. In the poorly compacted panel the behaviour was found to be more variable showing abrupt reactions from the probes to weather events.

10.1.3 Correlation of the field and laboratory data

The samples prepared in the laboratory most closely represent the well compacted panel. The densities are more similar and the SWRCs for the sample taken from the well compacted panel coincides with the drying path for laboratory prepared samples (although the SWRC for the poorly compacted panel did present more similarities with the determined SWRCs involving drying from lower water contents than the primary drying SWRC).

The better engineered well compacted panel, resembling modern highway embankments did not responded so dramatically to the weather patterns observed at the BIONICS site, despite the fact of pore water pressure still reached hydrostatic values. The observed smaller variations in pore

water pressure in depth and the fact that less dramatic responses to climate conditions were recorded indicates a more homogeneous structure. The higher density achieved during construction on the well compacted panel resulted in a less permeable material which in turn affected the hydraulic behaviour of the material by reducing the water infiltration rate.

The pore water pressure changes were relatively small during the monitoring. Through the years of monitoring, values close to hydrostatic were observed which is representative of water contents higher than 22%. The laboratory measurements would suggest the behaviour would be characterised by small changes in strength. Based on samples tested at water contents of 20 or 22% it can be foreseen that changes in shear strength would be much smaller than 50 kPa.

10.2 **Present and Future work**

This thesis has focused on the determination of the hydro-mechanical behaviour of the fill material of the BIONICS embankment using state-of-the-art double cell triaxial cells in conjunction with high capacity suction probes. It also reports on the determination of SWRCs using different methodologies (filter paper, psychrometer, pressure plate and high capacity suction probes). Furthermore, a novel system was developed for measuring pore water pressure in field conditions using the DU-WF high capacity suction probe. When combined, this information provides the necessary experimental data to facilitate coupled numerical modelling of the hydrological and mechanical behaviour of the BIONICS embankment.

The BIONICS study will continue for many years as further climate experiments and seasonal variations in monitoring are required to build up a full database of embankment performance data.

Once a full set of data is available it will be possible to refine the numerical models and therefore, to develop a greater understanding of the potential impacts of climate change on infrastructure slopes. The work carried out as part of this thesis has been an essential first step in the process to achieving this goal.

10.3 Further work

To correlate the data from the field with laboratory data it would be necessary to carry out a series of triaxial tests where the water content was cycled using a wetting/drying system. When compared with the constant water content tests, these tests would take a longer time thus the starting point for a new researcher would be to carry the tests on an as-compacted gravimetric water content of 20%-22% resembling the average initial conditions of the well compacted panel.

For the poorly compacted panel a sample preparation methodology should be determined. A more irregular compaction methodology should be considered, enabling a different distribution of voids and creation of larger voids in the sample. This would mean a total new series of tests for the hydro-mechanical behaviour.

To fully understand the behaviour of the BIONICS fill material the wetting primary curve should be obtained first which would help in the understanding of the SWRCs obtained in this work. The study would involve samples that had to be completely dried. This study could prove to be challenging since there are no techniques for accurate measurements of suction that are reliable at extremely low water contents.

Improvement on the field system for continuous measurement of pore water pressure should include the use of TDRs (Time Domain Reflectometer) that measure volumetric water content close or even at the same position as the suction probes, creating the possibility of generating continuous relations of pore water pressure with volumetric water content. This would allow the possibility of observing how the SWRC changes in the field.

References

Al-Khafaf, S. and Hanks, R. J., (1974) *Evaluation of the Filter Paper Method for Estimating Soil Water Potential*, Soil Science, Vol. 117, No. 4, pp. 194–199.

Al Mukhtar, M., Robinet, J. C. and Liu, C. W. (1993). *Hydro-mechanical behaviour of partially saturated low porosity clays*. Engineering fills (eds. B.G. Clarke, C.J.F.P. Jones, and A.I.B. Moffat) Thomas Telford, London, 87-98

Alonso E. E., Gens A. and Josa A. (1990). *A constitutive model for partially saturated soils*. Geotechnique **40**, No. 3, 405-430.

Au, S W C (1998) *Rain-Induced Slope Instability in Hong Kong*, Engineering Geology, Vol. 51, No. 1,pp. 1-36.

Barbour, S. L. (1998). *Nineteenth Canadian Geotechnical Colloquium: the soil–water characteristic curve, a historical perspective*. Can. Geotech. J. **35**, No. 5, 873–894.

Bishop, A. W. and Donald, I. B. (1961). *The experimental study of partly saturated soils in the triaxial apparatus*. Proc. 5th Int. Conf. Soil Mech. Found. Engng, Paris 1, 13–21.

Black D. K. and Lee K. L. (1973), *Saturating Laboratory Samples by Back Pressure*, ASCE Journal Soil Mech. Found. Eng. Div., Vol. 99, SM1, pp. 75-95.

Blatz, J. A. and Graham, J. (2003). *Elastic-plastic modelling of unsaturated soil using results from a new triaxial test with controlled suction*. Geotechnique **53**, No. 1, 113-122

Blight, G. E. (1967). *Effective stress evaluation for unsaturated soils*. ASCE Journal of Soil Mechanics and Foundations Engineering Division, vol. 93, SM2, 25-148.

British Standard Institute (1990), *BS 1377-4: Methods of test for Soils of civil engineering purposes Part 4: Compaction-related tests*, *BSI*, Milton Keynes.

Bulut, R., Leong, E. C. (2008). *Indirect measurement of suction*. Geotech. Geol. Eng. Vol.26, N. 6, pp. 633-644.

Bulut, R., Lytton R. and Wray W. (2001) *Suction measurements by filter paper method*. American Society of Civil Engineers Geotechnical Special Publication No.115 pp 243-261.

Burland, J.B., (1965a). *The yielding and dilation of clay*. Correspondence. Geotechnique, 15, 211-214.

Chandler, R. J., Crilly, M. S., and Montgomery-Smith, G., (1992). *A Low Cost Method of Assessing Clay Desiccation for Low- Rise Buildings*, Proceedings of the Institution of Civil Engineers, Vol. 92, No. 2, pp. 82–89

Chandler, R. J. and Gutierrez, C. I. (1986). *The filter paper method of suction measurement*. Geotechnique, vol. 36, n.2, 265-268

Chatterjea, K (1989) *Observations on the Fluvial and Slope Processes in Singapore and their Impact on the Urban Environment*, PhD Thesis, National University of Singapore.

Chatterjea, K (1994) *Dynamics of Fluvial and Slope Processes in the Changing Geomorphic Environment of Singapore,* Earth Surface Processes and Landforms, Vol. 19, pp. 585-607

Ching, R K H, Sweeney, D J and Fredlund, D G (1984) *Increase in Factor of Safety due to Soil Suction for Two Hong Kong Slopes*, Proc. 4th Int. Symp. on Landslides, Toronto, Vol. 1, pp. 617-623.

Chipp, P N, Henkel, D J, Clare, D G and Pope, R G (1982) *Field Measurement of Suction in Colluvium Covered Slopes in Hong Kong*, Proc. 7th Southeast Asian Geotechnical Conf., Hong Kong, pp. 49-62.

Colmenares-Montanez, J.E., (2002). *Suction and volume changes of compacted sandbentonite mixtures*. PhD thesis, University of London (Imperial College), London, UK.

Croney, D. (1952). *The movement and distribution of water in soils*. Geotechnique, 3(1):1–16.

Cunningham, M. R. (2000). *The mechanical behaviour of a reconstituted, unsaturated soil*. Ph.D. thesis, Imperial College of Science, Technology and Medicine, University of London.

Cui Y. J. and Delage P. (1996). *Yielding and plastic behaviour of an unsaturated compacted silt*. Geotechnique **46**, 291-311.

Cui, Y.J., Tang, A.M., Mantho, A.T. and De Laure, E. (2008). *Monitoring field soil suction using a miniature tensiometer.* Geotechnical Testing Journal 31 (1), 95–100.

Cunningham, M. R., Ridley, A. M., Dineen, K. and Burland, J. J. (2003). *The mechanical behaviour of a reconstituted unsaturated silty clay.* Geotechnique **53**, No. 2, 183–194

Delage P., Romero E.E., Tarantino A. (2008) *Recent developments in the techniques of controlling and measuring suction* in unsaturated soils 1st European Conference on Unsaturated Soils, Durham, UK, 33-52

Dineen K. (1997). *The influence of suction on compressibility and swelling*. Ph.D. thesis, Imperial College of Science, Technology and Medicine, University of London.

Dineen, K. and Burland, J.B. (1995), *A new approach to osmotically controlled oedometer testing*, Unsaturated Soils, Alonso and Delage (eds), **2**, 459-465

Donoghue, A.M. (2006). *The performance effects of suction probe saturation in laboratory testing applications*, MEng. Report, Durham University.

Evangelista A., Nicotera M.V., Papa R. and G. Urciuoli G. (2008) *Field investigation on triggering mechanisms of fast landslides in unsaturated pyroclastic soils*, 1st European Conference on Unsaturated Soils, Durham, UK, 909-915

Fawcett, R.G. and Collis-George, N. (1967). *A filter paper method for determining the moisture characteristics of soil.* Australian Journal of Experimental Agriculture and Animal Husbandry, n.7, 162-167.

Fredlund D. G. and Morgenstern N. R. (1977). *Stress state variables for unsaturated soils*. *J. Geotech. Eng. Div., ASCE* **103**, GT5, 447-466

Fredlund, D. G. and Rahardjo, H. (1993). *Soil mechanics for unsaturated soils*. New York: Wiley.

Futai, M. M. and Almeida, M. S. S. (2005), *An experimental investigation of the mechanical behaviour of an unsaturated gneiss residual soil,* Geotechnique **55**, No. 3, 201-213

Gallipoli, D., Gens, A., Sharma, R. and Vaunat, J. (2003a). *An elasto-plastic model for unsaturated soil incorporating the effects of suction and degree of saturation on mechanical behaviour*, Geotechnique **53**, No. 1, 123–135

Gallipoli, D., Wheeler, S. J. and Karstunen, M. (2003b). *Modelling the variation of degree of saturation in a deformable unsaturated soil.* Geotechnique **53**, No. 2. 105-112

Gardner, R. (1937). *A method of measuring the capillary tension of soil moisture over a wide moisture range.* Soil Science, vol. 43, 277-283.

Gasmo, J M (1997) *Stability of Unsaturated Residual Soil Slopes as Affected by Rainfall*, MEng Thesis, School of Civil and Structural Engineering, Nanyang Technological University.

Geotechnical Control Office (1982) *Mid-levels study: Report on Geology, Hydrology and Soil Properties*, GCO Report, Hong Kong: Geotechnical Control Office.

Google maps, *http://maps.google.co.uk/*

Hamblin, A.P. (1981). *Filter paper method for routine measurements of field water potencial.* Journal of Hydrology, 53, 355-360

Harrison, B. A. and Blight, G. E., (1998) *The Effect of Filter Paper and Psychrometer Calibration Techniques on Soil Suction Measurements*, Proceedings of the Second International Conference on Unsaturated Soils, Vol. 1, International Academic Publishers, Beijing, China, pp. 362–367.

HIGHWAYS AGENCY (1998). *Specification for Highway Works*. The Stationary Office, London.

Hilf, J. W. (1956). *An investigation of pore-water pressure in compacted cohesive soils*. Technical Memorandum 654. Denver: US Bureau of Reclamation.

Hong, Y., Adler, R., and Huffman, G. (2006). *Evaluation of the potential of NASA multi-satellite precipitation analysis in global landslide hazard assessment. Geophysical Research Letters,* 33

Hughes, P. (2005) personal communication.

Hughes, P., Glendinning, S. and Mendes, J. (2007). *Construction Testing and Instrumentation of an infrastructure testing embankment*, Proc. Expert Symposium on Climate Change: Modelling, Impacts and Adaptations, Singapore, pp. 159-166.

Hughes, P.N., Glendinning, S., Mendes, J., Parkin, G., Toll, D.G., Gallipoli, D., Miller, P. (2009). *Full-scale testing to assess climate effects on embankments.* Special Issue of Engineering Sustainability, Institution of Civil Engineers, 162, No. ES2, pp. 67-79.

Hughes, P.N., Glendinning, S, Toll, D.G.(2005) *REPORT ON THE DESIGN AND CONSTRUCTION OF THE BIONICS EMBANKMENT*

Hulme, M., Jenkins, G. J., Lu, X., Turnpenny, J. R., Mitchell, T. D., Jones, R. G., Lowe, J., Murphy, J. M., Hassell, D., Boorman, P., McDonald, R. and Hill, S. (2002) *Climate Change Scenarios for the United Kingdom: The UKCIP02 Scientific Report*. Tyndall Centre for Climate Change Research, School of Environmental Sciences, University of East Anglia, Norwich, UK.

Jotisankasa, A. (2005), *Collapse behaviour of a compacted silty clay*, PhD Thesis, Imperial College.

Karube, D., Kato, S., Hamada, K. and Honda, M., (1995). *The relationship between the mechanical behaviour and the state of pore water in unsaturated soil*. Accepted for publication in JSCE Journal of Geotechnical Engineering.

Lee, H.V., Wray, W.K. (1995). *Techniques to evaluate soil suction – a vital unsaturated soil water variable.* Unsaturated soils, Alonso and Delage (eds) 2, 615-622.

Leong E. C., He L., and Rahardjo H. (2002) *Factors Affecting the Filter Paper Method for Total and Matric Suction Measurements*. J Geotechnical Testing, Vol. 25, No. 3 pp 321-332.

Lim, T T (1995) *Shear Strength Characteristics and Rainfall-Induced Matric Suction Changes in a Residual Soil Slope*, MEng Thesis, School of Civil and Structural Engineering, Nanyang Technological University, Singapore

Lim, T T, Rahardjo, H, Chang, M F and Fredlund, D G (1996) *Effect of Rainfall on Matric Suctions in a Residual Soil Slope*, Canadian Geotechnical Journal, Vol. 33, pp. 618-628.

Lourenço, S.D.N. (2008). *Suction Measurements and Water retention in unsaturated soils*, Phd Dissertation, Durham University

Lourenço, S.D.N., Gallipoli, D., Toll, D.G. and Evans, F. D., (2006*). Development of a commercial tensiometer for triaxial testing of unsaturated soils.* In Fourth International Conference on Unsaturated Soils, Carefree – Arizona – USA, Geotechnical Special Publication No. 14., Reston: ASCE, Vol.2, pp. 1875-1886.

Marinho, F.A.M. (1994). *Medição de sucção com o método do papel fitro*. Proc. X Congresso Brasileiro de Mecanica dos Solos e Engenharia de Fundações. Vol 2, 516522.

McQueen, I. S. and Miller, R. F., (1968b) *Calibration of a Wide-Range Gravimetric Method for Measuring Moisture Stress,* Soil Science, Vol. 106, No. 3, pp. 225–231.

McKeen, R. G., (1980) *Field Studies of Airport Pavements on Expansive Soils*, 4th International Conference on Expansive Soils, pp. 242–261.

Nattrass, W. (2009) personal communication

Noguchi, T. (2009) *Comparison of Major Suction Measurement Techniques Used to Determine the Soil Water Retention Curves*, MEng Final Year Project Report, Durham University.

Oldecop, L.A. and Alonso E.E. (2000*), A model for rockfill compressibility*, Geotechnique **51**, No. 2, 127-139

Papa, R., Evangelista, A., Nicotera, M.V. and Urciuoli, G. (2008). *Mechanical properties of unsaturated pyroclastic soils affected by fast landslide phenomena*. 1st European Conference on Unsaturated Soils, Durham, UK, 917-923

Pitts, J and Cy, S (1987) *Insitu Soil Suction Measurements in Relation to Slope Stability Investigations in Singapore*, Proc. 9th European Conf. on Soil Mechanics and Foundation Engineering (ed. Hanrahan, E T, Orr, T L L and Widdis, T F), Rotterdam: Balkema, Vol. 1, pp. 79-82.

Richards, S.J., (1965). *Soil suction measurements with tensiometers*. In: Methods of Soil Analysis, Monograph No. 9, American Society of Agronomy, Madison, 153-163.

Ridley, A. M., Dineen, K., Burland, J. B. and Vaughan P. R. (2003). *Soil matrix suction: some examples of its measurement and application in geotechnical engineering*. Geotechnique **53**, No. 2, 241–253

Ridley, A.M. and Burland, J.B., (1993). *A new instrument for the measurement of soil moisture suction*. Geotechnique, **43**, No. 2, 321-324.

Ridley, A. M. and Wray, W. K. (1996). *Suction measurement: theory and practice. A state-of-the-art-review*. Proc. 1st Int. Conf. Unsaturated Soils, Paris 3, 1293–1322. Roscoe, K.H. and Burland, J.B., (1968). On the generalised stress-strain behaviour of "wet" clay. *Engineering Plasticity* (Heyman, J. and Leckie F.A., eds.) Cambridge University Press, Cambride, 535-609.

Schofield, A. N. and Wroth, C. P. (1968). *Critical state soil mechanics*, McGraw Hill, London.

Shull, C. A. (1916). *Measurement of the surface forces in soils.* The Botanical gazette, vol. LXII, n.1, 1-31.

Simmon, R. (2007) http://earthobservatory.nasa.gov/Features/LandslideWarning/.

Sivakumar, V. (1993). *A critical state framework for unsaturated soil*. Ph.D. thesis, University of Sheffield, UK.

Skempton, A. W. (1953), *The colloidal activity of clays*, Proc. 3rd ICSMFE, Zurich, 1, 57-61.

SMI Soil Mechanics Instrumentation (2004) Manual for the 12-probe transistor psychrometer. Adelaide, South Australia.

Springman, S.M., Jommi, C., Teysserie, P. (2003). *Instabilities on moraine slopes induced by loss of suction:a case history.* Geotechnique **53**, No. 1, 3-10.

Springman, S.M. and Teysserie, P. (2003). *Artificially induced rainfall instabilities on moraine slopes.* In Kühne M et al (eds), Proceedings of the international conference on landslides, Davos, VGE, Essen, 209-223.

Stenke, F., Toll, D.G., and Gallipoli, D. (2006) *Comparison of suction measurement techniques for three clayey soils*. Proceeding 4th International Conference on Unsaturated Soils, Phoenix, USA, Geotechnical Special Publication No. 14., Reston: ASCE, Vol.2, pp 1451-1461.

Stephenson, I. B. (2008) *Pore water pressures in embankments: soil compaction influencing water infiltration and its effect on pore water pressures,* Msc dissertation, School of Civil Engineering and Geosciences, Newcastle University.

Sweeney, D J (1982) *Some Insitu Soil Suction Measurements in Hong Kong's Residual Soil Slopes*, Proc. 7th Southeast Asian Geotechnical Conf., Hong Kong, pp. 91-106.

Tarantino, A. and Mongiovi, L. (2003) *Calibration of tensiometer for direct measurement of matric suction*. *Geotechnique* **53**, No.1, 137-141

Tarantino, A. and Tombolato, S. (2005) *Coupling of hydraulic and mechanical behaviour in unsaturated compacted clay*. *Geotechnique* **55**, No. 4, 307-317

Toll, D.G. (1999) *A Data acquisition and control system for geotechnical testing*. Computing developments in civil and structural engineering (eds. B. Kumar and B.H.V. Topping), Edinburgh: Civil-Comp Press, pp 237-242.

Toll, D.G. (2001). *Rainfall-induced Landslides in Singapore*, Proc. Institution of Civil Engineers: Geotechnical Engineering, Vol. 149, No. 4, pp. 211–216.

Toll, D. G. and Ong, B. H. (2003). Critical-state parameters for an unsaturated residual sandy clay. *Geotechnique* **53**, No. 1, 93–103.

Tsaparas, I., Rahardjo, H., Toll, D.G., Leong, E. (2003) *Infiltration characteristics of two instrumented residua soil slopes*. Canadian Geotechnical Journal, 40, pp. 1012-1032.

Van Genuchten, M. T. (1980). *A closed-form equation for predicting the hydraulic conductivity of unsaturated soils*. *Soil Sci. Soc. Am. J.,* pp. 892-898.

Vaquero, J.L. (2007) *Soil suction measurement using the pressure plate technique within the MUSE network*, Project report, Durham University.

Vaunat, J., Romero, E. and Jommi, C., (2000). *An elastoplastic hydromechanical model for unsaturated soils.* Proceedings of the International Workshop on Unsaturated Soils, Trento, 121-138.

Wheeler, S. J., Sharma, R. J. and Buisson, M. S. R. (2003). *Coupling of hydraulic hysteresis and stress–strain behaviour in unsaturated soils*. Geotechnique **53**, No 1, 41-54

Wheeler, S. J. and Sivakumar, V. (1995). *An elastoplastic critical state framework for unsaturated soil*. Geotechnique **45**, No. 1, pp. 35-53.

Woodburn, J.A. and Lucas, B. (1995*) New Approaches to the Laboratory and Field Measurement of Soil Suction*, Unsaturated Soils. Alonso, E.E. and Delage, P. (eds) Unsaturated Soils (UNSAT 95) Proc. 1st Int. Conf., Paris, France. Rotterdam: Balkema, Vol. 2, pp 667671.

Zur, B. (1966). *Osmotic control of the matric soil-water potential*. Soil Science. **102**, 394-398.